Initium Sapientiæ Timor Domini

Krebs, Frederik C

Publication date:
2000

Document Version
Publisher's PDF, also known as Version of record

Risø-R-1144(EN)

Initium Sapientiæ Timor Domini

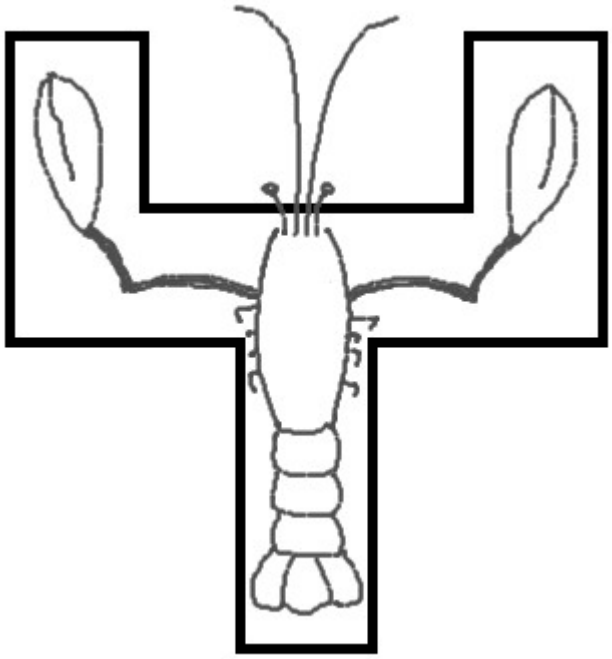

Risø National Laboratory, Roskilde, Denmark
January 2000

Abstract: This Ph.D. Thesis describes the synthesis, structure and properties of a series of organic molecules. The main effort has been placed towards the structural understanding of organic materials and the scattering techniques employed for this purpose has involved conventional X-rays, synchrotron X-rays and neutrons.
The report is divided into four *Chapters*. The first, *Chapter one*, is in three *Parts*. The first *Part* gives a brief but complete introduction to the dielectric properties of organic materials. The second *Part* describes the experimental work on synthesising organic dielectric materials and provides an understanding their structure and properties. The third *Part* describes some work on placing polar organic materials on surfaces under UHV (Ultra High Vacuum) conditions. *Chapter two*, is also in three *Parts* the first being a brief introduction to the subject of molecular liquid crystals with particular emphasis on discotic liquid crystals. The second *Part* describes the structural characterisation pertaining to triphenylene based discotic premesogens and their relation to the structural properties as found in the literature. The final *Part* is a critical discussion of the structure of discotic mesophases as presented in the literature and as implied by the results obtained from this work. *Chapter three* describes the work done on the structural characterisation of a particular type of macromolecule and is in three *Parts*. The first *Part* is a brief introduction to the subject while the second *Part* describes the synthesis and the structural characterisation of the conformational behaviour of these molecules. The third *Part* describes a statistical survey based on the CCD (Cambridge Crystallographic Database). *Chapter four* is the final *Chapter* and is also in three *Parts*. The first *Part* is a statistical survey of *R*-factors as found in the CCD. The second *Part* is a structural study of an atropisomeric organic molecule and the final *Part* describes the synthesis of a perdeuterated polymer for neutron studies.

Resumé: Denne Ph.D. afhandling beskriver syntese, struktur og egenskaber af en serie af organiske molekyler. Hovedvægten har været lagt på en strukturel forståelse af organiske materialer og de anvendte spredningsteknikker har gjort brug af konventionel Røntgen stråling, synkrotron Røntgen stråling og neutroner.
Afhandlingen er delt i fire kapitler. Det første kapitel er i tre dele. Den første af disse giver en kort men præcis introduktion til de dielektriske egenskaber for organiske materialer. Den anden del beskriver det eksperimentelle arbejde med syntesen af organiske dielektriske materialer samt en forståelse for deres struktur og egenskaber. Den tredje del beskriver arbejdet med at placere polære dielektriske materialer på overflader under UHV (Ultra Høj Vakuum) betingelser. Kapitel to omhandler flydende krystaller og er ligeledes i tre dele hvor den første del giver en introduktion til begrebet flydende krystaller med specielt henblik på diskotiske flydende krystaller. Den anden del beskriver den strukturelle karakterisering af triphenylen afledte diskotiske flydende krystaller samt en sammenligning med det i litteraturen fundne. Den sidste del er en kritisk diskussion af diskotiske mesofaser som de er præsenteret i litteraturen samt set i lyset af de resultater der er opnået gennem dette arbejde. Kapitel tre omhandler en speciel type makromolekyler og er i tre dele hvoraf den første er en kort indledning til emnet. Den anden del beskriver syntese, struktur og konformationelle egenskaber af de molekyler der har været studeret gennem dette arbejde. Den tredje del beskriver et statistisk studie omhandlende disse makromolekyler og baseret på CCD (Cambridge struktur databasen). Det sidste kapitel, kapitel fire er i tre dele. Den første del er et statistisk studie baseret på CCD omhandlende R-værdier. Den anden del er et strukturelt studie af et organisk molekyle der udviser atropisomeri og endelig er den sidste del en beskrivelse af syntesen samt neutron sprednings egenskaberne for en lavtemperatur beskyttende olie fremstillet specielt med henblik på neutron studier af følsomme materialer.

ISBN 87-550-2614-1

ISBN 87-550-2633-8 (Internet)

ISSN 0106-2840 Typeset by Word97

Print: Information Service Department, Risø, 1999.

Binding: Majgrens Bogbinderi A/S, Esplanaden 34, 1263 København K, DENMARK.

Frederik Christian Krebs

Date and time of signature: 1st of January year 2000 at 00:00h (i.e. 01/01/2000 00:00)

Preface

This Ph.D. thesis is written in/as partial fulfilment of the Danish Ph.D. degree. The project has the title: “Molecular Dielectric materials”. The work was financed through a Risø National Laboratory/Danish Research Academy grant and was carried out jointly at the Condensed Matter Physics and Chemistry Department (Risø National Laboratory) and at the Department of Chemistry, (Technical University of Denmark) with supervision by Klaus Bechgaard and Niels Thorup. The style of the thesis have been kept to the best of my ability short, succinct and concise. Consequently only the fruitful work is presented and very little unfinished work has been included. The report is a complete collection of what a person of my limited skill, ability and aptitude has created and completed within the time span available which exacts at three years. It would be appropriate to add that I probably have material (unfinished) enough for a report equal to this in size, however, being unpublished this material remains my property until I decide to publish it or forget about it altogether. During this project I have collected crystallographic data on well in excess of 100 crystals and while not all data collections lead to successful structure determinations I still have succeeded in solving just a few more than 100 structures! 61 of which have been published so some are still on their way. To properly justify that I have pursued and adhered to the obligations imposed by the project description authored at the beginning of the projects running period all the work covering the project description has been included. It is perhaps also the proper moment to reflect on what this project is, where it has taken me and how it should be viewed by myself and probably others. The impression the time as a Ph.D. student has left in my mind and probably in the minds of all the people with whom I have had the pleasure to work with is really what should be in this report and it is quite short (as opposed to the report itself). The rest of what you will find in the report is merely the documentation of how I acquired this impression or sense of the past three years. Here goes:

My belief is that it is in the interest of society that people acquire skills and contribute to the advancement of our conception of ourselves and the world we live in. There are many ways to pursue this goal ranging from the supernatural to the humanitarian. Among all these ways is science which I have chosen. It is by no means perfect nor complete it is however powerful when provision is made for the inherent weaknesses. An example of its weakness can be

found in the very foundationalistic nature of science as it relies on knowledge, it thrives on knowledge. Knowledge is something finite beings like humans can not have, we have however the ability to approach the state of knowledge by the acquisition of a methodology on how to know or how to become conditionally knowledgeable. For instance, suppose a human is explained the basic principles of the working and reading time of a clock. If such a human, knowledgeable of time, the clock and how the clock works, is then shown a clock and (for the sake of argument the clock shows that it is twelve noon) asked: ”Do you know what the time is ?”, the answer would be: “Yes I do, it is twelve noon”. Suppose that the clock was broken but accidentally the human read the time at exactly twelve noon, so the answer given: “It is twelve noon” would be correct but the human did not know that is was twelve noon. This is at the heart of the very fallible nature of science, it is thus imperative to have a sense of how to use the science to achieve our common advancement and avoid being mislead by the excruciating limitations inherent in the scientific approach. Thus, from having enjoyed the infinite comfort of a scientific explanation for everything I have come to take pleasure in exploring our inaptitude towards achieving the very foundation of our approach namely knowledge. It would be superfluous to give an example or even examples of the strengths of science, just take a look around !

Contents

Appendix P 199

Appendix S

Introduction

To give in just a few words the complete summary of the work covered in this report would be a difficult task if the expectation is that this report is an account of a concentrated effort towards achieving a single goal. The original project title: ”Molecular Dielectric Materials”, has been adhered to in the sense that all work undertaken during this project is covered by that title. Furthermore all the ideas set out in the project description have been addressed and treated. The results presented have as a common factor that they all involve synthetic organic molecules. Molecules all designed for a purpose, the purpose being either polar dielectric materials, liquid crystals, molecular sensors or the purpose of advancing a technique for studying organic molecules. Henceforth the report is written with four main topics/chapters which are based on 17 out of the 19 papers which have been authored/co-authored during this project. 6 additional papers are in preparation. Since the report is based mainly on the underlying publications the style of the report is general and should be an easy stand-alone read with only key references are given. Should the reader for one reason or another find the need to scrutinise on some particular scientific detail or reference he or she is referred to the *Appendix P* where all the underlying publications are presented with the references and scientific detail required. The first chapter describes the effort towards achieving organic pyroelectric/ferroelectric materials and an understanding of good candidates for that purpose (6 papers). The second chapter describes briefly some characterisation work on a type of molecules known to exhibit liquid crystallinity (3 papers). The third chapter deals with a quite considerable effort towards an understanding and control of the molecular conformation of a particular type of macromolecule (5 papers). The final chapter is of a technical character and describes the results from some analysis made during the project and the development of a new technique (3 papers). The red thread in the report is the structural understanding of organic matter studied by many different methods. The many different scientific methods that have been applied during the course of this project are most significantly scattering techniques using synchrotron X-rays, conventional X-rays and neutrons. A wide range of perhaps more standard analytical techniques have also been employed such as: NMR, GCMS, MALDI-TOF, Rheometry, SEC, HPLC, IR, SIMS, AFM, ESCA, Dielectric spectroscopy, IRAS, UHV-techniques and probably many more that I can not think of right now.

Chapter one

This chapter is divided in three parts. *Part 1.1* is meant as an introduction to the subject of the dielectric properties of materials. *Part 1.2* and *Part 1.3* represents the results obtained during this work. The former on crystalline molecular organic materials and the latter on molecular organic materials deposited on various surfaces.

1.1 Introduction to dielectric materials

In this chapter one of the twins of the electromagnetic properties of matter will be the subject of interest. More specifically the electric part. The formalism and theory for magnetic and electric properties of matter is very similar but magnetic properties will not be dealt with at all. What is more, only the electric properties relating to insulating (or very poorly conducting) molecular organic materials will be addressed. Having said this it may seem that all the interesting and perhaps well known properties of matter have been left out with only the boring parts left. This notion however, untrue bye fact and untrue by nature, is obviously a fallible one as the electric properties of insulating molecular organic materials are amongst the most far reaching. A conscious recognition of the ubiquity of these materials in the world around us by weight, by volume and what is more by necessity and compelling need should make this crystal clear. The electric properties of materials are most often termed the dielectric properties of materials. The reason for this is mostly historical and stems from the fact that an electrically insulating material when placed in an electric field charges (at faces perpendicular to the field with charges of opposite sign at opposite faces and opposing the applied field) and develop an electric polarisation, hence the name *dielectric*.

1.1.1 The dielectric

Even though part of this section is classical textbook material, such material has in general been kept aside from this report. It is only included here and in my own words because of its absolute necessity in defining the concept of a dielectric and the terms used in this chapter. It should further aid in the proper reading and understanding of the scientific papers appropriate to this chapter which are included in *Appendix P1* through *Appendix P6*.

1.1.1.1 The all-in-one textbook illustration

Suppose we were to charge a parallel plate capacitance C with charge Q. An electric voltage ϕ would be required. The voltage ϕ could be read of an electrometer[1]. The introduction of a dielectric sheet between the electrodes of the parallel plate capacitor would, everything else left untouched, result in a decrease of ϕ as measured on the electrometer.

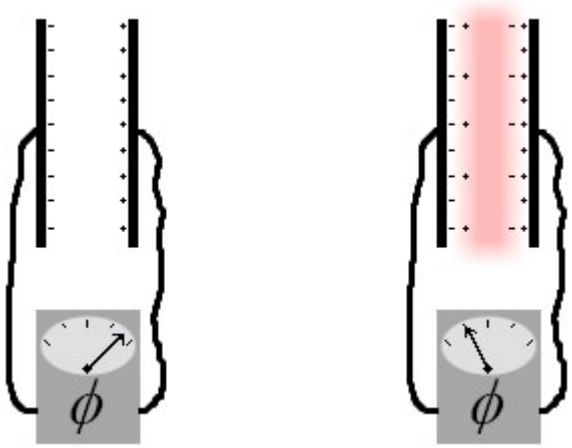

Figure 1.1. The experiment which shows how the voltage across the plates of a charged parallel plate capacitor is lowered when vacuum (or air) as shown to the left is replaced by a dielectric material (red shading) as shown to the right. A schematic drawing of the electrometer with an indication of the magnitude of the voltage ϕ. Larger ϕ values are towards the right.

The observation above can be described in simple terms where the capacitance, C, of the system is related to the measured voltage, ϕ, using the assumption that the charge on the capacitor plates is constant (which it is if ideal electrical insulation and a good (ideal) electrometer is applied).

$$C_o = \frac{Q}{\phi_o} \quad \wedge \quad C = \frac{Q}{\phi} \quad \Rightarrow \quad \frac{C}{C_o} = \frac{\phi_o}{\phi} = const. \tag{1.1}$$

Where the subscripted ϕ_o is the voltage measured across C with vacuum between the capacitor plates, hence designated C_o. For an isotropic material this relation always hold. The constant is a tensor of rank zero (a scalar) and depends upon the material in question. It is referred to as the relative permittivity or the dielectric constant of the material due to its dimensionless nature. The Greek letter *epsilon,* ε_r, is often used to represent the relative permittivity with a

[1] An electrometer is a device that can measure the charge without using any in the process.

subscript, *r*, to specify that it is relative. The permittivity of the material is obtained by multiplication of the relative permittivity with the permittivity of vacuum which has a value of 8.854×10^{-12} F m^{-1}, often referred to as ε_o. The vacuum permittivity is the lowest value of permittivity that can be attained. Most materials have values of permittivity considerably larger than that of vacuum or in terms of relative permittivity values larger than one. Typical values of relative permittivity for molecular organic materials are in the range from three to ten.

1.1.1.2 How the dielectric acquires its ε

While the previous subsection showed the effect of placing a dielectric between the plates of a charged capacitor no explanation for the observation was given. However, careful inspection of the right part of figure 1.1 did leave a clue, namely the appearance of surface charges. The existence of surface charges on the dielectric would explain why the voltage is lowered as the dielectric is introduced because some of the electric field lines between the capacitor plates will terminate on the surface charges and only some of the field lines will penetrate through the dielectric and terminate on the opposing plate of the capacitor. The electric field is lowered and therefore also a lowering of the voltage is seen. The magnitude of ε for the given material thus depends upon the ability of the material to generate surface charges

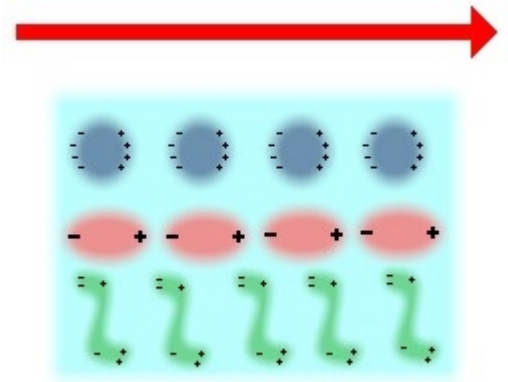

Figure 1.2. An illustration of how an applied electric field (red arrow, pointed end is negative) affects a dielectric (large turquoise coloured rectangle) by inducing dipoles of non-polar molecules (blue spheres) and by reorienting the permanent dipoles of polar molecules (pink ellipses). The inverted *S*-shaped green objects depict locally induced dipoles in large molecules or macromolecules which are thought to reorient further in time. The main point is that negative charges of the dipole species are exposed at one face perpendicular to the direction of the electric field and only positive charges at the opposite face.

What needs to be explained is how a material with no free flowing electrons can generate charges at its surface. To keep this introduction general we can assume that the dielectric is composed of for instance molecules with no particular arrangement. The molecules or substructures of molecules can be polar or non-polar. In the latter case the electric field that exists between the plates of the capacitor can perturb the electron distribution slightly so that the molecules (or part of) acquire a slightly positive end and a slightly negative end thus *inducing* dipoles. In the former case the molecule already has a polarity but will in addition experience an induction of polarisation. In both cases the molecules will tend to align the dipole (induced or permanent) along with the field. The result is that one face of the dielectric (perpendicular to the applied field) will have the negative end of the dipoles exposed whereas the opposing face will have the positive end of the dipoles exposed. In figure 1.2 a few of the possibilities are shown in the same figure. For a typical polymer or for molecules in solution all three of the cases shown would be observed whereas for most crystalline materials only the induced dipoles would be observed to align with the field. On rare occasions both permanent dipoles and induced dipoles could be observed to align with the field in a crystal.

1.1.1.3 The complex nature of ε_r and how it depends on time and reciprocal time

We now advance from the simple picture given so far and consider what happens the moment a static electric field is switched on an initially discharged parallel plate capacitor containing some previously unpolarised dielectric between the plates. We assume that the switching process does not extend in time i.e. a discrete voltage step. The dielectric could be a polymer or a solution. Initially the capacitor charges and in principle we measure ϕ_o as if there was no dielectric between the capacitor plates. Very quickly however the induced dipoles would manifest themselves as the redistribution of the electrons according to the field. This is a very fast process and can take place without any opposition, the time scale involved is of the order of 10^{-14}-10^{-17} s. If the electrometer needle could follow the changes in ϕ that would occur on such a short time scale it would show how much ϕ decreased due to the induced dipoles (electron redistribution). Following on from this electron redistribution, the atomic nuclei of the molecules would distort again leading to a further decrease of ϕ, the time scale here is slower 10^{-11}-10^{-14} s. Later on the permanent dipoles would slowly (compared to the electrons and less slowly compared to the nuclei) start to physically rotate and reorient themselves thereby aligning with the applied electric field. Again our ideal and infinitely fast electrometer

needle would show a further decrease in ϕ due to the reorientation of the permanent dipoles, the time scale involved here would be of the order of 10^{-8}-10^{-11} s for small molecules but in principle anywhere between 10^{5}-10^{-11} s. The limit 10^{5} s is not a rigorous one it could be a lot longer it is just a question of how long one wishes to wait before the final reading is done (10^{5} s is a bit longer than one day). The long time scales are associated with larger molecules like polymers. An illustration suggesting this was included in the lower part of figure 1.2 where one could imagine that the inverted *S*-shaped molecules, assumed to be entangled in some way, would slowly reorient. Thus the relative permittivity seems to increase as time goes by because the dielectric becomes more and more polarised. The important point to make here is that the permittivity is a polarisability phenomenon. The more polarisable a material is the higher the dielectric constant of that material will be. The dielectric constant that is normally quoted is the one obtained after waiting for an infinite period of time before reading ϕ. While the concept of time introduced above was convenient for an understanding of the processes and time scales involved in the polarisability it is better to use the reciprocal of time, namely frequency, as this relates better to how real measurements are made and it introduces the notion of dielectric spectroscopy which covers the entire electromagnetic spectrum. To further emphasise this relationship the term displacement, denoted D, is introduced (in the following section this concept is expanded and explained further).

$$D(t) = \varepsilon(t)E \tag{1.2}$$

The displacement is thus related to the applied field, *E*, through the time dependent dielectric permittivity, $\varepsilon(t)$. As the time dependent dielectric permittivity was appropriate for the time domain so is the frequency dependent dielectric permittivity appropriate for the frequency domain. They bear a fourier relationship.

$$\hat{\varepsilon}(\omega) = \frac{1}{2\pi}\int \varepsilon(t)\exp(-i\omega t)dt \tag{1.3}$$

The dielectric constant, denoted, $\hat{\varepsilon}(\omega)$, thus depends upon the frequency at which it is measured and is often given a superscript indicating the frequency of measurement i.e. ε_r^{120Hz} would refer to the relative permittivity of some compound at a frequency of 120 Hz. The time dependent and the frequency dependent dielectric permittivity can be stated as.

$$\varepsilon(t) = \varepsilon^{\infty Hz} + \left(\varepsilon^{0Hz} - \varepsilon^{\infty Hz}\right)(1 - \Phi(t)) \tag{1.4}$$

$$\hat{\varepsilon}(\omega) = \varepsilon^{\infty Hz} + \left(\varepsilon^{0Hz} - \varepsilon^{\infty Hz}\right)(1 - i\omega\Phi(\omega)) \tag{1.5}$$

In the equation 1.5 last the excitation functions or response functions $\Phi(t)$ and $\Phi(\omega)$ also bear a fourier relationship.

$$\Phi(\omega) = \frac{1}{2\pi}\int_0^{\infty} \Phi(t)\exp(-i\omega t)dt \tag{1.6}$$

The consequence of using a frequency scale (instead of a time scale) is that measurements are done using a sinusoidal voltage instead of a step voltage followed by a steady voltage in the experiment. There are distinct advantages of using the frequency scale and one of them is the natural introduction of the complex nature of the dielectric permittivity. ε_r thus has two components a real part and an imaginary part.

$$\hat{\varepsilon}_r(\omega) = \varepsilon_r'(\omega) - i\varepsilon_r''(\omega) \tag{1.7}$$

Where $\hat{\varepsilon}_r$ is the complex relative permittivity (the hat denotes that it is a complex valued quantity), ε_r' is the real part of the relative permittivity, i is $\sqrt{-1}$ and finally ε_r'' is the complex part of the relative permittivity. The ω included in brackets refers to the angular frequency (i.e. $2\pi f$) and means that the various values depends upon the frequency. The reason for having a negative sign in front of the imaginary part is that we think of our sample as a capacitive reactance. Without being pretentious this is a clever way to think of it (and true) because it makes $\varepsilon_r''(\omega)$ a positive valued quantity. The normal interpretation of ε_r is straight forward and is the polarisability observed after an infinite amount of time. Sometimes it is referred to as the DC dielectric constant or the dielectric permittivity as the frequency approaches 0 Hz. Much like ε_r, $\varepsilon_r'(\omega)$ has the same meaning but the frequency dependence is dispersive, in other words $\varepsilon_r'(\omega)$ exhibits dispersion which generally means that it takes on lower values with increasing frequency. At 0 Hz $\varepsilon_r = \varepsilon_r'(\omega)$. The interpretation of $\varepsilon_r''(\omega)$ is not so uncommon and can be thought of simply as loss, hence a positive value (a negative value would imply a gain or an energy generation *ab nihil*). It is in fact the quantity which is observed, recorded, interpreted and referenced within all branches of absorption spectroscopy. An example of what $\hat{\varepsilon}_r(\omega)$ looks like is perhaps appropriate to achieve a clearer picture of the molecular mechanism by which its components manifest themselves. An illustration of their typical frequency dependence will serve as the basis of discussion. If we have the higher frequencies towards the right and shown along the *x*-axis and the relative magnitude of the components of $\hat{\varepsilon}_r(\omega)$ along the *y*-axis. It is observed that $\varepsilon_r'(\omega)$ has a higher and roughly

constant value at the lower frequency end up until some frequency range where it decreases suddenly to attain a lower and constant value at the higher frequencies. This is an example of the dispersive nature of $\varepsilon_r'(\omega)$. At the same time we observe that $\varepsilon_r''(\omega)$ has a low value at low frequencies. In the same frequency range where $\varepsilon_r'(\omega)$ showed dispersion we find that $\varepsilon_r''(\omega)$ increase to a maximum value and then decrease to a very low value at the higher frequencies. The system is said to relax in this frequency span or said to exhibit dielectric loss.

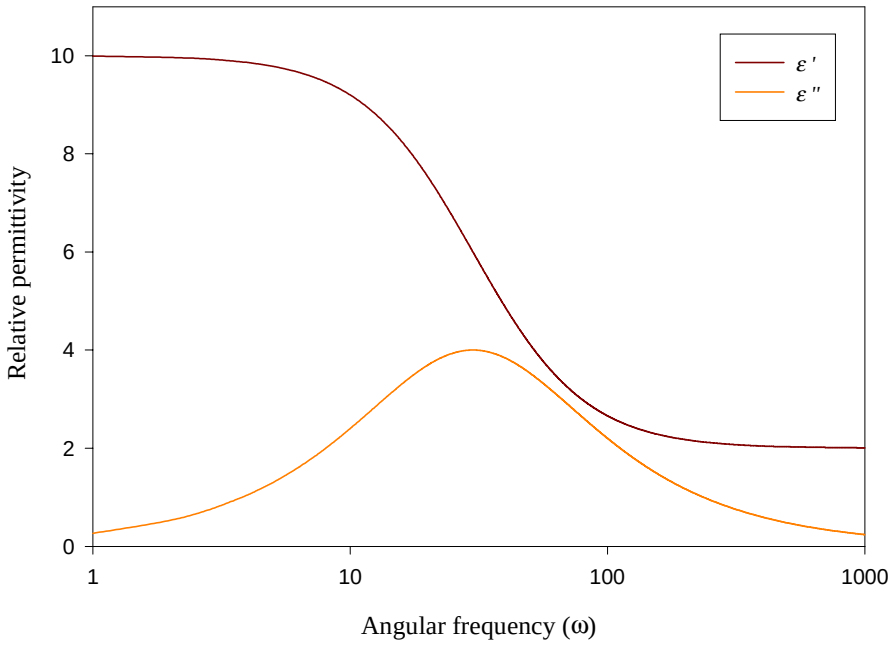

Figure 1.3. A plot of the real and the imaginary part of the relative permittivity as a function of angular frequency. Notice that a logarithmic scale has been used along the *x*-axis. The dielectric phenomenon has a relaxation time of 0.03 s and therefore a maximum (loss) for values of ε_r'' at around 30 s^{-1} in ω. In that same area of ω we see the dispersion of ε_r' i.e. how it decreases from a larger to a smaller value.

Sometimes the reciprocal of the value for ω where ε_r'' is at a maximum (or where ε_r' changes most rapidly) is quoted as the relaxation time, τ, which indicates the time scale at which the process or relaxation phenomenon is taking place. i.e. when,

$$\frac{\partial \varepsilon_r''(\omega)}{\partial \omega} = 0 \quad \wedge \quad \frac{\partial^2 \varepsilon_r'(\omega)}{\partial \omega^2} = 0 \tag{1.8}$$

If for instance the excitation function, $\Phi(t)$, is chosen as an exponential time decay its frequency domain function, $\Phi(\omega)$, can be worked out using equations 1.6 and 1.9.

$$\Phi(t) = \exp\left(-t/\tau\right) \tag{1.9}$$

$$\Phi(\omega) = \int_0^\infty \exp-\left(i\omega t + \frac{t}{\tau}\right)dt = \frac{\tau}{1+i\omega\tau} \tag{1.10}$$

Occasionally the process is referred to as Debye relaxation named after the scientist who fathered the concept of dielectric relaxation. It can be expressed in terms of the complex frequency dependent dielectric permittivity using equations 1.5 and 1.10.

$$\hat{\varepsilon}_r(\omega) = \varepsilon_r^{\infty Hz} + \frac{\varepsilon_r^{0Hz} - \varepsilon_r^{\infty Hz}}{1+i\omega\tau} \tag{1.11}$$

With the complex an real parts as plotted in figure 1.3 given by equation 1.12 and 1.13 as shown below.

$$\varepsilon_r'(\omega) = \varepsilon_r^{\infty Hz} + \frac{\varepsilon_r^{0Hz} - \varepsilon_r^{\infty Hz}}{1+(\omega\tau)^2} \tag{1.12}$$

$$\varepsilon_r''(\omega) = (\omega\tau)\frac{\varepsilon_r^{0Hz} - \varepsilon_r^{\infty Hz}}{1+(\omega\tau)^2} \tag{1.13}$$

With the knowledge built up so far we understand what has happened at the molecular level at the low frequency end and at the high frequency end. What is left is a detailed description of the reason for the changes in the values observed for both $\varepsilon_r'(\omega)$ and $\varepsilon_r''(\omega)$. The time picture given for dielectric polarisation explained the behaviour of $\varepsilon_r'(\omega)$ quite well above and below the transition where $\varepsilon_r'(\omega)$ changes in magnitude. What happens to the molecules in the region of change and why is the loss only observed in this region ? As fate would have it this central question is not well understood. The behaviour of loss phenomena in polymeric systems have been studied and results from these studies have lead to a categorisation procedure whereby the loss peaks observed in the dielectric spectrum can be classified. i.e. according to how they depend on the temperature, pressure, molecular weight etc. The most known relaxation phenomena are the α- and the β-relaxation. The purpose of this introduction is however not to explain these as it would be to specialised and detailed literature exists on

the subject[2]. Instead a pictorial explanation is sought in terms of the concepts already outlined. As an example we can consider the relaxation associated with molecular dipolar rearrangements. In order to contribute to the polarisation of the material the molecular dipoles need to have time to reorient in response to an applied field. The energy available that allows for this reorientation is the thermal energy. We can thus think of the reorientation as a thermally activated process with Arrhenius type behaviour.

$$\frac{1}{\tau} = C \exp\left(-\frac{E_a}{kT} \right) \tag{1.14}$$

Where τ is the relaxation time in s, C is the pre-exponential factor in s^{-1}, E_a is the activation energy for the reorientation of the molecules in J, k is the Boltzmann constant 1.38×10^{-23} J K^{-1} and T is the temperature in K. At a given temperature the number of molecules reorienting per unit time can be calculated by use of equation 1.14. Thus at low frequency (below the relaxation frequency) the thermal reorientations of the molecular dipoles are faster than the applied oscillating field and therefore the polarisation is aligned with the applied field at all time. At frequencies above the relaxation frequency the thermal reorientation of the molecules are much slower than the applied oscillating field. The molecular dipoles do thus not reorient in response to the changing field and thus do not contribute to the polarisation. When the frequency of the applied oscillating electric field is of the same order as the relaxation frequency the thermal reorientation of the molecular dipoles can not sufficiently reorient all the molecules so that they align with the applied field. Therefore only some of them contribute to the polarisation and we observe a lowering of ε_r'. The fact that not all the molecular dipoles reorient also houses an explanation of the sudden appearance of a large ε_r'' since some of the current used to charge the capacitor is lost. When at low frequency the electric field is at a maximum there is no current flowing to or from the capacitor plates since all the molecules have had the time to reorient. When the electric field is at a minimum (i.e. 0) the current flowing to or from the capacitor plates is a maximum since all the polarised dipoles are reorienting and giving up the charge they bound at the electrodes. The oscillating applied electric field and the resulting charging current are exactly out of phase by 90^o (or $\pi/2$). There is thus no current loss i.e. ε_r'' is close to or equal zero. The same argument applies

[2] See general references at the end of this section.

to the high frequencies above the relaxation frequency. When we are close to the relaxation frequency and the applied field is at a maximum some current is still flowing because some of the molecular dipoles are still reorienting in response to the field (they just are not doing it fast enough). When the field is at a minimum the current has not yet reached a maximum as some of the molecular dipoles still have not had time to reorient and give up the charge they cause to bind at the electrodes. The oscillating applied electric field and the resulting charging current are no longer out of phase by 90^o or in other words the polarisation current and the charging current are no longer in phase. The component of the polarisation current which is out of phase with the charging current corresponds to the loss current. This type of loss in dielectric materials is often referred to as polarisation loss.

1.1.1.4 The electric field, displacement, polarisation and the tensorial nature of ε_r

All the treatment above assumed isotropy and therefore the applied field and the polarisation were always collinear. The electric field and the polarisation have not been explicitly written as vectors yet even though they have been referred to as if they were. Now is the time to introduce them as vectors along with a new and practical vector, the displacement (mentioned briefly in equation 1.2). They bear the relationship,

$$\vec{D} = \varepsilon_o \vec{E} + \vec{P} \tag{1.15}$$

Where $\vec{D}$, $\vec{E}$, $\vec{P}$ and ε_o are the displacement, electric field, polarisation and vacuum permittivity respectively. $\vec{D}$ has the same units as $\vec{P}$ namely C m^{-2} and the three vectors need not be parallel. Equation 1.15 can be thought of as expressing the relationship between the total charge given by $\vec{E}$, the amount of free charge given by $\vec{D}$ and the amount of bound charge due to the dielectric given by $\vec{P}$. In terms of Gauss's law it is the flux of the three vectors taken individually and integrating over some surface enclosing one face of the electrode that gives the total, free and induced charge respectively for $\vec{E}$, $\vec{D}$ and $\vec{P}$. $\vec{P}$ is often expressed using the concept of dielectric susceptibility, χ_e, which equals $\varepsilon_r - 1$.

$$\vec{P} = \chi_e \varepsilon_o \vec{E} \tag{1.16}$$

Equation 1.16 relates the polarisation to the electric field inside the dielectric. Even though it may seem superfluous at first we can put it all together.

$$\vec{D} = \varepsilon_o \vec{E} + \vec{P} = \varepsilon_o (1 + \chi_e)\vec{E} = \varepsilon \vec{E} = \varepsilon_o \varepsilon_r \vec{E} \tag{1.17}$$

The derivative of the displacement with respect to the electric field gives us the permittivity and the derivative of the polarisation with respect to the electric field gives us the susceptibility. A further expansion of the concept of the relative permittivity is necessary before we can treat any molecular dielectric material. While the relative permittivity was shown to be a complex property it was assumed that the material was isotropic i.e. the measurement of the relative permittivity, while complex, did not depend on the physical orientation of the sample nor did it depend on the shape as the dielectric was assumed to completely fill the space between the capacitor plates. The treatment of the dielectric permittivity as a complex property is an absolute necessity when dealing with polymeric systems and solutions. With crystalline matter it is in many cases not necessary to treat the relative permittivity as a complex quantity. If there is rotational disorder in the crystal or some other type of dynamic disorder the relative permittivity must be treated as a complex quantity. The difficulty that a arises with crystalline materials is the often high degree of anisotropy associated with crystalline order. The anisotropy causes the permittivity to become a tensor of rank two denoted ε_{ij}. The subscripts refer to the components of the tensor (a three-by-three array of nine numbers) the relation between components depends upon the symmetry of the crystal. If the values of ε_{ij} show a frequency dependence (i.e. dispersion and loss) each component should be treated as complex and denoted $\hat{\varepsilon}_{ij}$. An explanation of the tensor concept and how a tensor of rank two expresses the relationship between two vectors can be given using the now quite familiar vectors $\vec{D}$ and $\vec{E}$. The expression would be,

$$D_i = \varepsilon_{ij} E_j \tag{1.18}$$

Where D_i and E_j are components of the vectors $\vec{D}$ and $\vec{E}$ respectively and ε_{ij} is the permittivity tensor. Equation 1.18 gives the displacement in the *i*-direction when an electric field is applied in the *j*-direction.

$$\begin{pmatrix} D_1 \\ D_2 \\ D_3 \end{pmatrix} = \begin{pmatrix} \varepsilon_{11} & \varepsilon_{12} & \varepsilon_{13} \\ \varepsilon_{21} & \varepsilon_{22} & \varepsilon_{23} \\ \varepsilon_{31} & \varepsilon_{32} & \varepsilon_{33} \end{pmatrix} \begin{pmatrix} E_1 \\ E_2 \\ E_3 \end{pmatrix} \tag{1.19}$$

Or we can express the polarisation with respect to the applied electric field in terms of the susceptibility tensor.

$$P_i = \varepsilon_o \chi_{ij} E_j \tag{1.20}$$

$$\begin{pmatrix} P_1 \\ P_2 \\ P_3 \end{pmatrix} = \varepsilon_o \begin{pmatrix} \chi_{11} & \chi_{12} & \chi_{13} \\ \chi_{21} & \chi_{22} & \chi_{23} \\ \chi_{31} & \chi_{32} & \chi_{33} \end{pmatrix} \begin{pmatrix} E_1 \\ E_2 \\ E_3 \end{pmatrix} \tag{1.21}$$

So if we apply the electric field $\vec{E}$ (E_1,0,0) we get.

$$\vec{P} = \varepsilon_o \begin{pmatrix} \chi_{11} E_1 \\ \chi_{21} E_1 \\ \chi_{31} E_1 \end{pmatrix} \tag{1.21}$$

So unless χ_{21} and χ_{31} are zero $\vec{E}$ and $\vec{P}$ are not collinear. A further and very important point is that the components of tensors with a physical meaning nearly always are symmetric i.e. $T_{ij} = T_{ji}$ the reason being of thermodynamic origin. A further constraint on the components of the tensor is that they do not violate Neumann's principle which states that the components of the tensor has to stay invariant when subjected to the symmetry operations of the crystallographic point group (*vide supra, Subsection 1.1.2.3*). So far we have only considered the cases where an electric field was applied. In reality, we wish to encompass all the cases related to polarisation but where we do not have an applied field i.e. spontaneous polarisation or cases where we get polarisation as a function of some other applied field i.e. mechanical stress.

1.1.2 Polar dielectric materials

1.1.2.1 The permanent dipole moment and its arrangements

The permanent dipole moment is a property molecules or parts of extended systems can have. Most of the discussion given here pertains to molecular materials henceforth the permanent dipole moment will be understood as a molecular property. For any given molecule two possibilities exist. Either the molecule has a permanent dipole moment or the molecule does not have a permanent dipole moment. The supreme reason for a molecule having or not having a permanent dipole moment is that of molecular point group symmetry. Second to this comes the composition of the molecule which governs the attainable magnitude of the dipole moment. It can be argued that for small molecules (i.e. molecules of binary composition) the composition is responsible for the existence of a permanent molecular dipole moment as the molecule with the given composition can not be put together without creating a permanent dipole moment. While true it is still the point group symmetry of the molecule that governs polarity. As for the case of molecules of binary composition it is a combinatorial effect which in essence gives only one option when putting the molecule together. The permanent dipole

moment itself arises due to a displacement of the mean position of electrons orbiting the nuclei with respect to the mean position of the nuclei for the molecule in question. In simple mathematical terms,

$$\vec{\mu} = Nq\left(\langle \vec{r}_p \rangle - \langle \vec{r}_e \rangle\right) \tag{1.22}$$

$$\langle \vec{r}_e \rangle = \frac{\sum_{j=1}^{N} \vec{r}_{e,j}}{N} \quad \wedge \quad \langle \vec{r}_p \rangle = \frac{\sum_{i=1}^{N} \vec{r}_{p,i}}{N} \tag{1.23}$$

Where $\vec{\mu}$ is the molecular dipole moment in C m, $\langle \vec{r}_e \rangle$ and $\langle \vec{r}_p \rangle$ represents the mean position (in an arbitrary frame of reference common for the two) of the N negative and N positive unit charges respectively, q is the unit charge and equals 1.6×10^{-19} C. We assume that the molecules are electrically neutral. The permanent molecular dipole moment is thus measured in units of charge times the distance of separation of the charge. A unit commonly used is the Debye again named after the record breaking scientist Peter Debye (1 Debye = 1 D = 3.336 x 10^{-30} C m). It is quickly realised that the magnitude attainable by typical organic molecules is limited to the range of 0-10 D. It should be mentioned that an induced dipole moment is also a possibility which is not governed by the point group symmetry of the molecule. It is not of interest here and is thus not discussed. While the permanent molecular dipole moment and the studies thereof is greatly appreciated as seen in the previous section its treatment in this context ends and we now turn to the interest of this section namely what happens when dipoles are collected in materials either crystalline, semicrystalline or amorphous in such a way that a permanent polarisation exist in the absence of an applied electric field. As molecular point group symmetry played the key role in obtaining a permanent molecular dipole moment so does the symmetry of assembling molecules in space play the key role. To illustrate the concept of macroscopic dielectric polarisation the possible ways of assembling an extended system using molecular dipoles can be made in two dimensions or planar projection. For the moment symmetry is neglected. Small arrows can be made to indicate the molecular dipole moment and small spheres can be made to indicate molecular entities. There are three distinct ways of packing the molecules (and dipoles) together as shown below. If we choose to consider macroscopic polarisation as a desirable property it is desirable to have all the molecular dipoles aligned in the solid as shown in figure 1.4. The second possibility, the Type II material, is the case where there is still a macroscopic

polarisation but the polarisation is some fraction of the maximum obtainable polarisation for the given molecule.

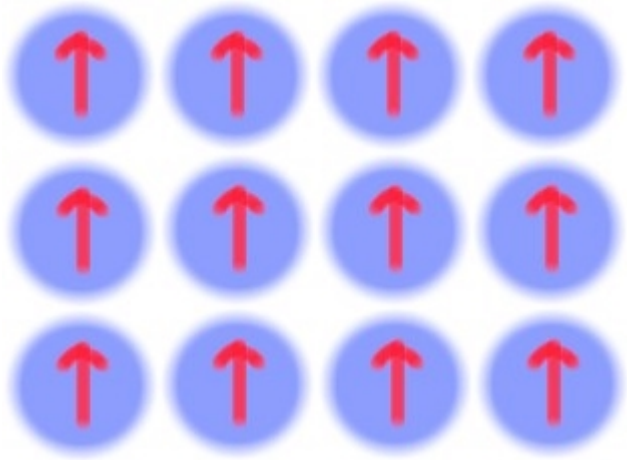

$\vec{P} = \vec{P}_{maximum}$

Type I

Figure 1.4. An illustration of how a complete alignment of the molecular dipoles leads to the maximum possible dielectric polarisation possible for the given molecule with the given packing arrangement. This ordering of dipoles is termed **Type I**. Molecules are shown as blue spheres with their molecular dipole moment vector shown as a red arrow.

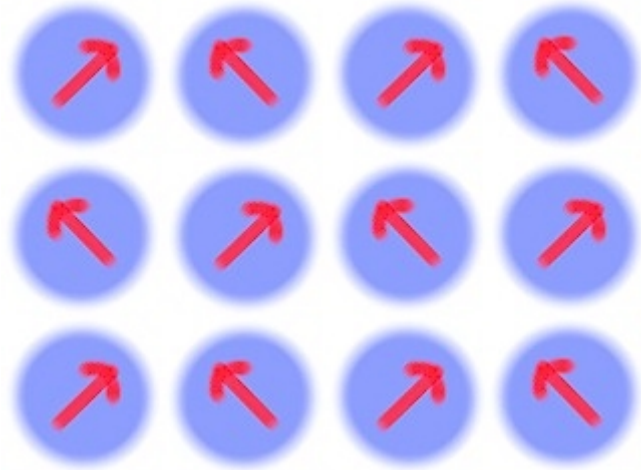

$\vec{P} < \vec{P}_{maximum}$

Type II

Figure 1.5. An illustration of how a partial alignment of the molecular dipoles leads to a dielectric polarisation which is smaller in magnitude than the maximum possible dielectric polarisation for the given molecule with the given packing arrangement. This ordering of dipoles is termed **Type II**. Molecules are shown as blue spheres with their molecular dipole moment vector shown as a red arrow.

While there, in essence, is only one way of realising a Type I material (still neglecting the effects of packing symmetry, crystalline or non-crystalline) there are an infinite number of ways that Type II materials can establish themselves ranging from near maximum dielectric polarisation to near dielectric depolarisation. A stereotypical example of a Type II material is shown in figure 1.5.The third possibility, the Type III material, is the case where there is no macroscopic dielectric polarisation. It may be appropriate to add that there are no other possibilities left thus any material can be categorised according to on of the types I, II or III. The Type III material share with the Type I material the fact that it can only, in essence, be realised in one way. An example is shown in figure 1.6.

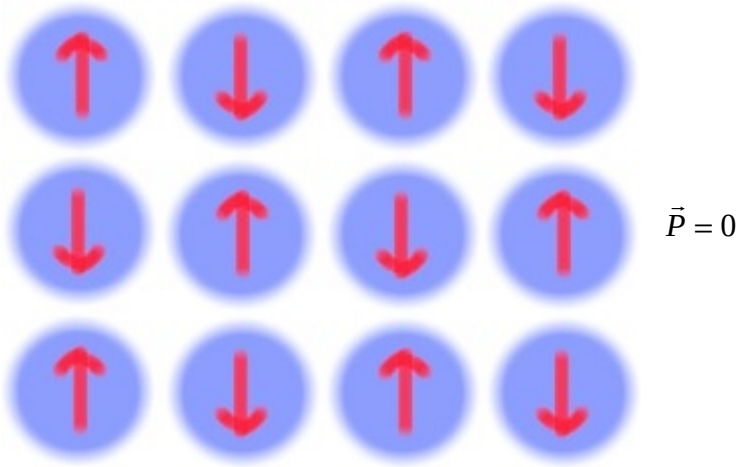

Figure 1.6. An illustration of how a complete anti-alignment of the molecular dipoles leads to a dielectric depolarisation. No macroscopic dielectric polarisation is thus possible. This ordering of dipoles is termed **Type III**. Molecules are shown as blue spheres with their molecular dipole moment vector shown as a red arrow.

As we shall see later, this work has resulted in examples of all three types of materials and without bringing disappointment to the reader most of the new materials that have been made and/or characterised are Type III materials. Part of this treatment is therefore also an attempt to understand this observation.

1.1.2.2 Polarisation as a vector sum

The macroscopic dielectric polarisation is simply given by its definition as the number of dipole moment per volume. Since both the polarisation and the dipole moment are vector

valued quantities a simple expression for the macroscopic dielectric polarisation can be written as the vector sum of the dipoles filling space or alternatively as the sum of the component of the molecular dipole moments along the polar axis, μ_p, in a given unit cell,

$$\vec{P} = \frac{\sum \vec{\mu}}{V} \quad \wedge \quad \vec{P} = \frac{Z\mu_p}{V} \tag{1.24}$$

Where $\vec{P}$ is the resulting macroscopic dielectric polarisation, $\vec{\mu}$ is the molecular dipole moment, Z is the number of dipoles in the volume element V. Whereas the magnitude of $\vec{\mu}$ is often given, Z and V are a matter of choice but are usually chosen as the corresponding crystallographic observables, the number of molecules per unit cell and the unit cell volume respectively.

1.1.2.3 The symmetry of assembly and Neumann's principle

Except for just a few polymeric/amorphous materials most of the materials studied during the course of this work have been crystalline and perhaps it would due to this fact seem most appropriate to deal with the symmetry of assembly as crystallographic symmetry. There are advantages in doing so firstly because it is a very rigid and well proven approach and secondly because the results obtained from a crystal structure solution can be used directly in categorising materials according to their type. The crystallographic symmetry also expand the concept of types as introduced in *section 1.1.2.1* in the sense that for each of the types I, II and III, subtypes given by the crystallographic symmetry can be recognised. To further emphasise this point examples of the crystallographic requirements that needs to be fulfilled in order to obtain each of the given types of materials is given in the following sections. Neumann's principle is essential for an appreciation of the physical properties in crystals and is stated as:

> *The symmetry elements of any physical property of a crystal must include the symmetry elements of the point group of the crystal.*

The statement has to be read carefully as the symmetry elements of a physical property does not have to be the same as that of the crystallographic point group but it has to include the symmetry of the crystallographic point group. Often the physical property has more symmetry elements than the crystallographic point group. There are 32 crystallographic point groups. Eleven of these posses a centre of symmetry and are called centrosymmetric. The remaining

twenty one crystallographic point groups are non-centrosymmetric. The distinction between crystalline and non crystalline materials which exhibit a macroscopic dielectric polarisation is that for the crystalline materials the polarisation is given by the crystal structure and a control of the polar properties for crystalline materials boils down to controlling or understanding crystallisation whereas for non-crystalline materials there is no spontaneous polarisation but by proper treatment the material can be made to exhibit a macroscopic dielectric polarisation.

1.1.2.4 The symmetry of Type I and Type II

A Type I or a Type II material can belong to only some of the twenty one non-centrosymmetric point groups. There are ten of them and they are referred to as the polar point groups or the axial point groups. A Type I or a Type II material thus has to crystallise in one of the following crystallographic point groups: *1, 2, 3, 4, 6, m, mm2, 3m, 4mm, 6mm*. The reason being that the crystallographic point group symmetry has to allow for the existence of a vector quantity namely the polarisation i.e. a vector has to stay invariant when acted upon by the symmetry elements of the particular crystallographic point group. In general nothing can be said about how the point group symmetry or the space group symmetry relates to the molecules in the crystal. There is however a tendency for molecules to make use of the molecular symmetry in the crystal i.e. if the molecule has a C_3-axis it may crystallise such that it is situated on a crystallographic three fold axis with the crystallographic and molecular symmetry elements coinciding. It is thus not possible to rationalise in such a way that given a particular space group it will always lead to a Type I material or a Type II material. It is a matter of the multiplicity in the given case. What can be said however is where the polar axis will be. Except for point groups *1* and *m* the polarisation will always be along the principal symmetry axis. In summary, in point group *1* the polar vector can take any direction with respect to the crystallographic co-ordinate system, in point group *m* the polar vector can take any direction within a crystallographic mirror plane or glide plane, in *2, 3, 4, 6, mm2, 3m, 4mm, 6mm* the polar vector can only take a direction along the principal axis. To give an example which distinguishes a Type I and a Type II material we can take two cases of different dipole moment vectors in the same point group, for instance point group 4. For the Type I material the dipole moment vector would be along the unique axis i.e. the *c*-axis. Our dipole would be $\vec{\mu}(0,0,1)$. The four fold rotation operator around the *c*-axis would be.

$$4^j = \begin{pmatrix} 0 & -1 & 0 \\ 1 & 0 & 0 \\ 0 & 0 & 1 \end{pmatrix} \tag{1.25}$$

The superscript *j* is the order of the symmetry operator which is four in the case of a four fold rotation operator. We have to perform the operation four times to get back where we started. When we operate upon $\vec{\mu}_i$ with 4^1 we get $\vec{\mu}_{i+1}$ and we have to perform the operation on the product for a total of *j* times in order to generate all the symmetry equivalent dipole moment vectors (i.e. $\vec{\mu}_{i+j} = \vec{\mu}_i$) the sum of which gives us the component of the dipole moment that survives. In the above case we get.

$$\vec{\mu}_{i+j} = 4^j \vec{\mu}_i \qquad \Rightarrow \qquad \frac{\sum_{i=1}^{4} 4^i \vec{\mu}_i}{4} = \vec{\mu}_z = \vec{\mu}(0,0,1) \tag{1.26}$$

Thus the *z*-component remains the same and we get maximum polarisation obtainable. For the case of a Type II material in the same point group we would have some component of the dipole which is not parallel to the four fold axis like the dipole moment vector which is along the space diagonal of the unit cell $\vec{\mu}(1,1,1)$. Even though it takes up some space all four symmetry operations have been written out for the sake of clarity.

$$\vec{\mu}_2 = 4^1 \vec{\mu}_1 = \begin{pmatrix} 0 & -1 & 0 \\ 1 & 0 & 0 \\ 0 & 0 & 1 \end{pmatrix} \begin{pmatrix} 1 \\ 1 \\ 1 \end{pmatrix} = \begin{pmatrix} -1 \\ 1 \\ 1 \end{pmatrix} \tag{1.27}$$

$$\vec{\mu}_3 = 4^1 \vec{\mu}_2 = \begin{pmatrix} 0 & -1 & 0 \\ 1 & 0 & 0 \\ 0 & 0 & 1 \end{pmatrix} \begin{pmatrix} -1 \\ 1 \\ 1 \end{pmatrix} = \begin{pmatrix} -1 \\ -1 \\ 1 \end{pmatrix} \tag{1.28}$$

$$\vec{\mu}_4 = 4^1 \vec{\mu}_3 = \begin{pmatrix} 0 & -1 & 0 \\ 1 & 0 & 0 \\ 0 & 0 & 1 \end{pmatrix} \begin{pmatrix} -1 \\ -1 \\ 1 \end{pmatrix} = \begin{pmatrix} 1 \\ -1 \\ 1 \end{pmatrix} \tag{1.29}$$

$$\vec{\mu}_5 = 4^1 \vec{\mu}_4 = \begin{pmatrix} 0 & -1 & 0 \\ 1 & 0 & 0 \\ 0 & 0 & 1 \end{pmatrix} \begin{pmatrix} 1 \\ -1 \\ 1 \end{pmatrix} = \begin{pmatrix} 1 \\ 1 \\ 1 \end{pmatrix} = \vec{\mu}_1 \tag{1.30}$$

We see immediately that only the *z*-component of the dipole moment does not change sign and further that the vector sum of the four vectors $\vec{\mu}_1$ to $\vec{\mu}_4$ gives $\vec{\mu}(0,0,1)$. Therefore we can only have polarisation along the unique axis. To illustrate how a polarisation can exist in the

presence of a mirror plane we can imagine a dipole moment vector $\vec{\mu}(1,1,1)$ it thus extends along the space diagonal of the unit cell. If a mirror plane exists along the *ab*-plane we get.

$$\vec{\mu}_{i+1} = m\vec{\mu}_i = \begin{pmatrix} 1 & 0 & 0 \\ 0 & 1 & 0 \\ 0 & 0 & -1 \end{pmatrix}\begin{pmatrix} 1 \\ 1 \\ 1 \end{pmatrix} = \begin{pmatrix} 1 \\ 1 \\ -1 \end{pmatrix} \quad \Rightarrow \quad \frac{\sum_{i=1}^{N}\vec{\mu}_i}{N} = \begin{pmatrix} 1 \\ 1 \\ 0 \end{pmatrix} \tag{1.31}$$

Therefore the component of the dipole moment vector that is parallel to the mirror plane survives. This would be typical for a Type II material where only some of the available polarisation survives to give rise to a permanent polarisation.

1.1.2.5 The symmetry of Type III

Whereas polarisation a vector valued quantity required one of the ten polar crystallographic point groups a Type III material simply has to belong to one of the remaining twenty two crystallographic point groups. The absence of a permanent polarisation does thus not imply the presence of a centre of symmetry. While obvious that a centre of symmetry cancels any vectorial property it is at first thought not so obvious that a vector valued property should cancel in a non-centrosymmetric crystallographic point group. In the centrosymmetric case the inversion operation is made upon a vector (or a point). To get polarisation in the crystal some component of the vector must survive the symmetry operation so that the vector sum is non zero. Below a polar molecule is placed in a crystal with its dipole moment vector $\vec{\mu}(1,0,0)$.

$$\vec{\mu}_{i+1} = \bar{1}\vec{\mu}_i = \begin{pmatrix} -1 & 0 & 0 \\ 0 & -1 & 0 \\ 0 & 0 & -1 \end{pmatrix}\begin{pmatrix} 1 \\ 0 \\ 0 \end{pmatrix} = \begin{pmatrix} -1 \\ 0 \\ 0 \end{pmatrix} \quad \Rightarrow \quad \sum_i \vec{\mu}_i = 0 \tag{1.32}$$

The dipole moment vector changes to the exact opposite direction and therefore the polarisation would be zero. It has therefore been shown that when the $\bar{1}$ symmetry operation is present no polarity can exist. This would happen no matter how the dipole moment vector was placed in the unit cell. In the non-centrosymmetric case we can take the orthorhombic point group *222* and see what happens to a the dipole moment vector $\vec{\mu}(1,0,0)$ when we use the three distinct and mutually perpendicular two fold rotation symmetry operators. The operators are along the crystallographic axis (i.e. space group P222) and have a superscript that denote their direction with respect to the crystallographic co-ordinate system.

$$2^{[100]} = \begin{pmatrix} 1 & 0 & 0 \\ 0 & -1 & 0 \\ 0 & 0 & -1 \end{pmatrix} \quad \wedge \quad 2^{[010]} = \begin{pmatrix} -1 & 0 & 0 \\ 0 & 1 & 0 \\ 0 & 0 & -1 \end{pmatrix} \quad \wedge \quad 2^{[001]} = \begin{pmatrix} -1 & 0 & 0 \\ 0 & -1 & 0 \\ 0 & 0 & 1 \end{pmatrix} \quad (1.33)$$

When applying these symmetry operations in turn to $\vec{\mu}(1,0,0)$ we find that the first symmetry operation leaves the vector untouched as the symmetry operator and the vector are pointing the same way. The remaining two reverses the direction of the vector and no polarisation is thus possible.

1.1.2.6 Translational symmetry

All of the above symmetry operations changed direction or sign of the vector (or its components) upon which it operated. In crystallography translational symmetry also exist. Translational symmetry however does not interfere with a vector valued property such as polarisation it is left untouched in magnitude and direction by translation. Only the spatial position of the dipole moment vector in the unit cell is affected.

1.1.3 Piezoelectric materials

1.1.3.1 An illustration of the effect

The piezoelectric effect is the observation of a dielectric polarisation as a consequence of the application of a mechanical stress to a crystal which belongs to one of the piezoelectric point groups. The piezoelectric point groups are twenty out of the twenty one non-centrosymmetric point groups. The exception is the cubic non-centrosymmetric point group *432* that though not possessing a centre of symmetry has symmetry operations that balance out the polarising effect of an applied mechanical stress. The mechanical stress can be represented by a tensor of rank two called the stress tensor, σ_{ij}. The components with $i = j$ are called the normal components and the components $i \neq j$ are called the shear components. The sign of the components often leads to confusion but in relation to piezoelectricity a compressive stress is indicated by a positive value. σ_{11} would thus be the force exerted in the *x*-direction to the face of a cube which is perpendicular to the *x*-direction i.e. a compressive stress. σ_{31} would thus be the force exerted in the *z*-direction to the face of a cube which is perpendicular to the *x*-direction i.e. a shear stress. A classic illustration of how the effect manifests itself is shown in figure 1.7.

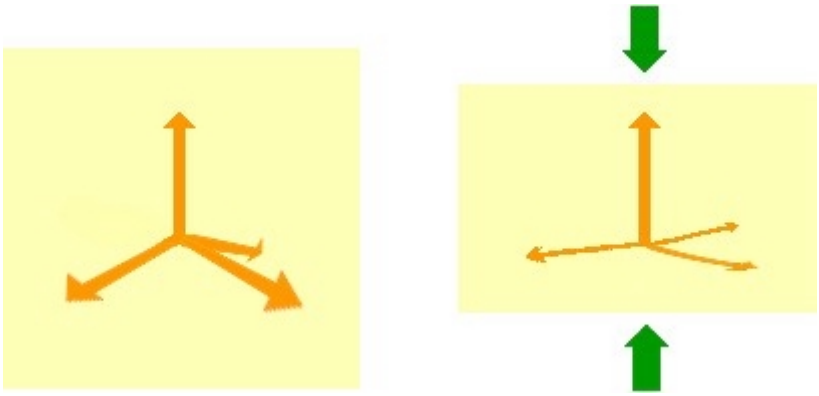

$\vec{F} = 0, \vec{P} = 0$ $\vec{F} \neq 0, \vec{P} \neq 0$

Figure 1.7. An illustration of the piezoelectric effect for a small crystal (yellow shading) containing dipoles connected in a perfect tetrahedral arrangement. To the left no mechanical stress is applied to the crystal and the vector sum of the dipole moment vectors exactly cancel with no resultant polarisation. To the right a compressive mechanical stress, denoted by $\vec{F}$, is applied (indicated by green arrows) leading to a greatly exaggerated strain of the crystal (given by the appropriate strain tensor). The strain breaks the perfect symmetry of the tetrahedron and leads in the illustration to a cancellation of the dipole moment in the directions perpendicular to the direction of the applied stress. In the direction of the applied stress however a polarisation, $\vec{P}$, exists.

The stress tensor is different from the permittivity and susceptibility tensors in that it does not have to conform to the symmetry of the crystal i.e. the force can be applied in any direction to the crystal. The permittivity and the susceptibility tensors are called matter tensors because they depend upon the crystal orientation. The stress tensor (and the related strain tensor) are called field tensors because they depend on some applied field i.e. a mechanical stress field.

1.1.3.2 The tensorial representation of piezoelectricity

To get an expression for the polarisation, represented by the vector $\vec{P}$, obtained by the application of an applied stress, represented by the field tensor σ_{ij}, we need a tensor of rank three which expresses the relationship between a tensor of rank one and a tensor of rank two. The piezoelectric moduli, *d*, are represented by a tensor of rank three. The components of the vector representing polarisation are thus obtained by.

$$P_i = d_{ijk}\sigma_{jk} \tag{1.34}$$

d_{ijk} is thus a collection of twenty seven coefficients. And the characterisation of the piezoelectric properties of a given material is in essence the determination of the individual coefficients of d_{ijk}. The tensor is symmetrical in *jk* and this makes some of the twenty seven coefficients identical therefore only eighteen of the twenty seven coefficients are sufficient to completely represent the tensor. Just like the other matter tensors met so far the piezoelectric tensor has to conform to the symmetry of the crystallographic point group.

1.1.3.3 A reversal of terms

The above (and quite limited) introduction did not reveal the important point that any reversal of cause and effect is allowed and consequent physical phenomena observed. For instance should one apply a tensile stress instead of a compressive stress the piezoelectric effect is observed with a reversal of sign of polarity. Most importantly is however the application of an electric field to a piezoelectric crystal thereby introducing a dielectric polarisation and a resultant stress. This is known as the converse piezoelectric effect and find wide applicability within many fields of science and technology.

1.1.4 Pyroelectric materials

1.1.4.1 How polar crystals acquired the name pyroelectric

Even though *section 1.1.2* treated the phenomenon of permanent dielectric polarisation in great detail nothing was said of the physical properties associated with the state of permanent dielectric polarisation. Such a state implies the presence of a permanent polarisation in the absence of an applied electric field. Since the symmetry constraints imposed upon such a property by the crystal symmetry have been defined in *section 1.1.2* what remains is to explain how it manifests itself. If considered in terms of figure 1 a permanent polarisation would imply that if we placed the pyroelectric between the capacitor plates of an initially discharged parallel plate capacitor we would observe a reading different from zero on our electrometer. This would be in the ideal case and in reality pyroelectric materials are not as spectacular as the above would suggest because the permanent polarisation is exactly balanced out by the appearance of surface charges on the dielectric itself. Therefore such a crystal in mechanical and thermal equilibrium will in time acquire a state of electrical equilibrium which implies the existence of an external electric field due to surface charges that exactly opposes the internal electric field generated by the dipoles in the crystal. These

surface charges originate from conduction through the material (or on its surface) and through charge accumulation in defects. The time it takes for a crystal to reach this electrical equilibrium is quite short even though the material may be a good electrical insulator the fields involved are excruciatingly large and make even an insulator appear as a good conductor. The electrical relaxation times for a crystal (considered as a parallel connection of a resistor and a capacitor) can thus be worked out and is most often found to be on the millisecond scale. The property pertaining to polar crystals has to be found somewhere else and as the name “pyroelectric” would imply the effect is observed upon heating a crystal whereby thermal and mechanical equilibrium can be reached but not electrical equilibrium (initially at least). The effect is thus observed as the apparent generation of charge upon changing the temperature of the crystal. An, in my view, incredibly beautiful property with an enormous technological applicability within the field of thermal sensing and thermal imaging. The reason for the thermal generation of charges can be one of many. There are three well recognised mechanisms and it is questionable whether any further mechanisms would be unique as they would probably be coupled to one of the three by some other known quantity.

1.1.4.2 The pyroelectric coefficient

Just like the piezoelectric moduli gave us the possibility of expressing what polarisation we would get by the application of a given stress we can define a pyroelectric coefficient which expresses the polarisation we get upon changing the temperature. The pyroelectric coefficient is a vector and is given by.

$$\frac{d\vec{P}}{dT} = \vec{p} \tag{1.35}$$

Here the polarisation vector is given by $\vec{P}$, the pyroelectric vector by $\vec{p}$ and the temperature by *T*. Often the polarisation in the material is along the unique axis of the crystal (except in point group *1* and *m*) so only the component of $\vec{p}$ which is along the unique axis is non-zero. In these cases the pyroelectric coefficient is given as p_n where the subscript *n* has a value indicating the unique axis i.e. $n = 3$ if the unique axis is the *c*-axis. $\vec{p}$ is in units of C m^{-2} K^{-1}.

1.1.4.3 A separation of terms

It should be evident that the ten polar point groups which allow for the existence of pyroelectricity are exactly half of the twenty point groups that allow for piezoelectricity. If a

material is pyroelectric it is thus by logical necessity also a piezoelectric but not *vice-versa*. We can then immediately recognise a mechanism of pyroelectricity which is coupled to the piezoelectric properties i.e. the thermally inhomogeneous heating of a crystal will make the crystal subject to stress with an associated piezoelectric effect. This is known as a tertiary pyroelectric effect and is normally sought eliminated in experiments. All materials (less a few) expand upon heating and for pyroelectric materials the thermal strain lead to a change in the polarisation. Illustrated simply by considering the temperature derivative of equation 1.24.

$$\frac{d}{dT}\left(\frac{Z\mu_p}{V(T)}\right)=\vec{p} \tag{1.36}$$

The sign convention is important here. Normally a decrease in the dielectric polarisation is indicated by a negative sign for the pyroelectric vector. A good approximation to the volume-temperature behaviour of a given material is that of linear thermal expansion and if unit cell parameters are available over some temperature span it is possible to completely characterise the pyroelectric properties associated with thermal expansion (or contraction). The volume, V(T), is known along with the number of dipoles, Z, if further the dipole moment is known either from calculation, solution measurements or desirably charge density studies the expression below is complete.

$$\vec{p}(T)=\frac{d}{dT}\left(\frac{Z\mu_p}{V(T)}\right)=-\frac{Z\mu_p}{\left(aT^2+2bT+\frac{b^2}{a}\right)} \tag{1.37}$$

With $V(T) = aT + b$. Normally the pyroelectric coefficient shown in equation 1.36 is a function of temperature and in the case of a linearly expanding material it is slightly decreasing in magnitude. Equation 1.37 expresses what is known as the secondary pyroelectric effect. Since most materials expand upon heating the secondary pyroelectric coefficient normally bears a negative sign. The primary effect has not yet been given mention but it is not so common and is not coupled to the secondary or tertiary pyroelectric effect. When observed it is of a very large magnitude. It is most often observed close to a phase transition in a material passing from either one polar phase to another polar phase or from a polar phase to a non-polar phase. It can also happen that the dipole moments simply decrease or increase in magnitude. Due to the often transitional nature of the primary effect it is rarely observed in a very large temperature span. The primary pyroelectric effect is difficult to measure on its own and normally the experimentally determined pyroelectric coefficient is the

sum of a the contributions from the primary, secondary and tertiary effects. In most experimental determinations of the pyroelectric coefficient the contribution from a tertiary pyroelectric effect is sought eliminated by careful homogenous heating i.e. using some heat transfer media around the crystal. The pyroelectric coefficient thus obtained is often called the stress free pyroelectric coefficient and is denoted by $\vec{p}_n^T$ where again the subscript *n* refers to the polar axis and the superscript *T* refers to the stress free conditions of the experiment i.e. the crystal is free to expand/contract (strain) without stress. Strain free pyroelectric coefficients can also be obtained and they represent the pure primary pyroelectric coefficient denoted by $\vec{p}_n^S$ where *S* indicates the strain free conditions of the experiment.

1.1.5 Ferroelectric materials and analogues

1.1.5.1 The conditions

A ferroelectric is an interesting extension to the concept of pyroelectricity and is the further requirement that the pyroelectric material which belongs to one of the ten polar crystallographic point groups has the added property of reversible polarisation. A ferroelectric is thus piezoelectric, pyroelectric and it can exhibit a polarisation in at least two crystallographically distinct directions at the same temperature. Often the two distinct crystallographic directions are along a unique crystallographic axis as it has to be by symmetry in the point groups *2, 3, 4, 6,mm2, 3m, 4mm, 6mm*. Even though examples of a crystalline ferroelectric material that can exhibit a polarisation in more than two directions or in directions which are not coaxial to my knowledge have never been observed it should be possible to design such a system or for such a system to exist in either of the point groups *1* or *m*.

1.1.5.2 The mechanism of ferroelectricity

The necessary condition for a reversal of polarisation is in essence a reversal of the direction of the dipole moment vector. For rigid molecular materials this is often not possible and therefore crystalline molecular organic ferroelectric materials are a rarity. Within the realm of inorganic chemistry ferroelectric behaviour is not so uncommon and comes about by often tiny displacement of ions leading to a reversal of the polarisation. Materials which exhibit ferroelectricity in a given temperature span often also has the capability of exhibiting paraelectric properties at temperature above a certain temperature threshold (called the Curie

temperature by analogy with magnetic materials) and pure pyroelectricity below a certain temperature threshold. In the paraelectric state the thermal energy of the system is large enough to overcome the barrier for switching between the two directions of polarisation therefore the paraelectric state is non polarised but highly polarisable in close analogy to the discussion in *section 1.1.1*. A classical material with ferroelectric properties is $BaTiO_3$ which as the sum formula may suggest could have the cubic perovskite structure. The perovskite structure is indeed observed above 120 ^oC. Apart from the in terms of ferroelectricity uninteresting cubic high temperature phase it has a series of other phases. For the purpose of this brief introduction the tetragonal phase which appear just below the cubic phase and is stable between 5 ^oC and 120 ^oC will serve as an illustration. The tetragonal phase allow for polar properties. The structure in the cubic phase can be described with barium atoms at the corners, oxygen atoms at the faces and titanium atoms in the middle of the unit cell. The titanium atoms are thus found in an octahedral co-ordination environment surrounded by oxygen atoms. Upon a passage into the tetragonal phase there is no longer room for the titanium ion in the middle of the octahedron and it moves out of the plane defined by four oxygen atoms halving the unit cell in a direction along one of the axis of the unit cell which becomes the polar axis[3].

Figure 1.8. An illustration of the atomic rearrangements that take place for the phase transition from the cubic (left) to the tetragonal phase (right) as a projection onto a plane containing the polar axis. Two of the oxygen atoms have been left out. The colour coding for the atoms is barium (dark blue), oxygen (red) and titanium (green). To the right the titanium moves up towards the upper oxygen atom. The other five oxygen atoms move downwards (only three of which are shown). This leads to an uneven charge distribution and a subsequent dielectric polarisation.

[3] See for instance F. Jona and G. Shirane´s book under general references at the end of this part.

From the illustration in figure 1.8 it should be evident that any of the six unit cell directions in the cubic phase can become the positive tetragonal *c*-axis upon the phase transition. The direction chosen by the crystal is perhaps initiated by chance but is very co-operative and when single crystals of the cubic phase are cooled into the tetragonal phase polycrystallinity as a result is rarely observed. Domains of different direction of dielectric polarisation can be observed but the tetragonal *c*-axis corresponds to only one of the former cubic axis.

1.1.5.3 The characterisation of a ferroelectric

While a crystallographic examination can be used to classify a material as a ferroelectric candidate ferroelectric behaviour can only be established by dielectric measurements. Unlike a pyroelectric where there is a macroscopic spontaneous polarisation and pyroelectric properties a ferroelectric even though it has a spontaneous polarisation it often resides in domains and on a macroscopic scale the sum of the polarisation from the individual domains cancel and it could appear to have no pyroelectric properties. The net polarisation is normally induced by the process of poling whereby the crystal is subjected to a large electric field which will switch the domains so that they all have their polarisation in the same direction. Hereafter the material can be made to exhibit pyroelectric properties. How can the ferroelectric effect be observed ?

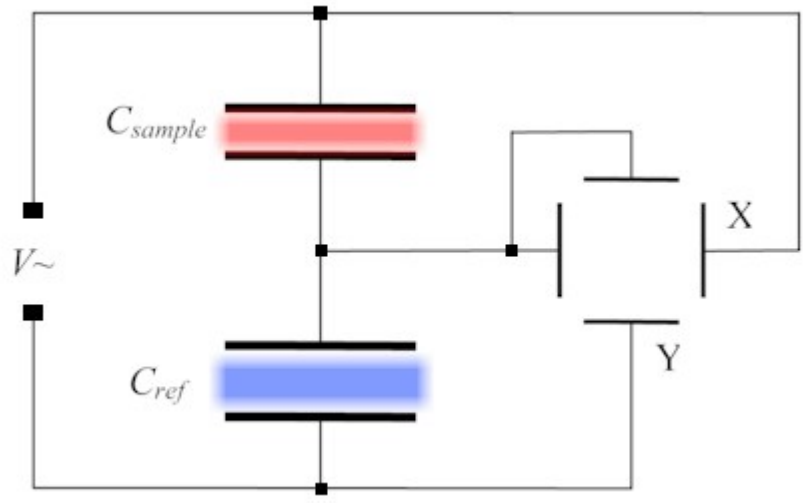

Figure 1.9. The circuit employed for the characterisation of the polarisation and switching behaviour of a ferroelectric. The sample (red shading) and the reference (blue shading) are subjected to an alternating electric field. When the voltages are traced on an oscilloscope screen it is possible to follow the behaviour of the material as the polarisation is given along the Y-axis and the applied electric field is given along the X-axis. The oscilloscope screen is illustrated to the left in the drawing.

The most obvious answer would be to monitor the switching and the polarisation. This is exactly what was done a long time ago by Sawyer and Tower, in 1930 to be historical[4]. The van Braun tube (known today as an oscilloscope) had just been invented and this greatly facilitated the characterisation of the polarisation in terms of the applied field. A simple but clever circuit was devised whereby both parameters could be extracted by the application of a low frequency alternating voltage (typically around 50 Hz) to the sample in the form of a capacitor and a reference capacitor. The clever part of the set-up is that the electric field subjected to the sample is given along the *x*-axis on the oscilloscope if the sample thickness is known (the electric field is given by the measured voltage on the oscilloscope *x*-axis divided by the sample thickness). The polarisation is given along the *y*-axis on the oscilloscope if the sample electrode surface area is known (the polarisation is given as the charge on C_{sample} given by C_{ref} times the voltage measured along the oscilloscope *y*-axis divided by the electrode area).

1.1.5.4 Paraelectrics, pyroelectrics, ferroelectrics and antiferroelectrics

The circuit shown in figure 1.9 thus enables a complete characterisation of a given dielectric material with respect to the field dependent polarisation properties.

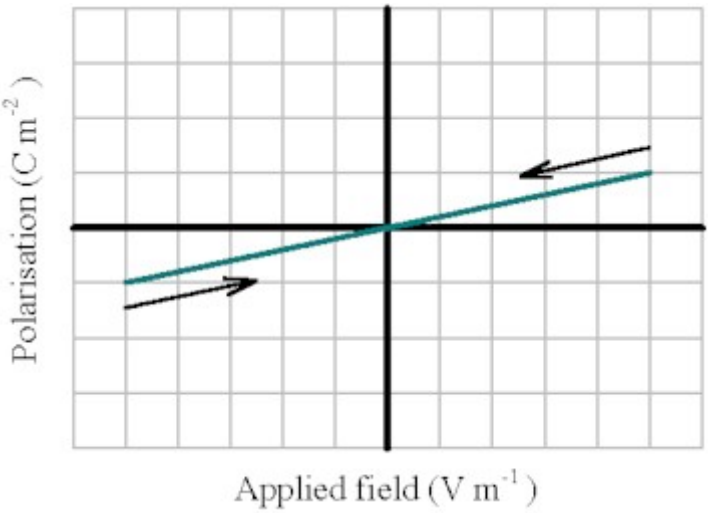

Figure 1.10. Field-polarisation plot for a material in the paraelectric phase. It is characterised by a large polarisability with the applied field (i.e. a steep slope). There is no real distinction between a paraelectric and a dielectric but a dielectric would have a very flat slope.

[4] Sawyer, C. B.; Tower, C. H. *Phys. Rev.* **1930**, *35*, 269-273.

If a material that can switch between directions of polarisation but that has no barrier of switching is subjected to measurements using the circuit described in figure 1.9 we get a response as shown in figure 1.10. The arrows in figure 1.10 indicate the path of the applied field which oscillates back and forth between the endpoints of the sloped line. The slope of the line is related to the relative permittivity ε_r' (under lossless conditions the slope equals ε_r'). Another important finding is that there is no net polarisation at zero applied field.

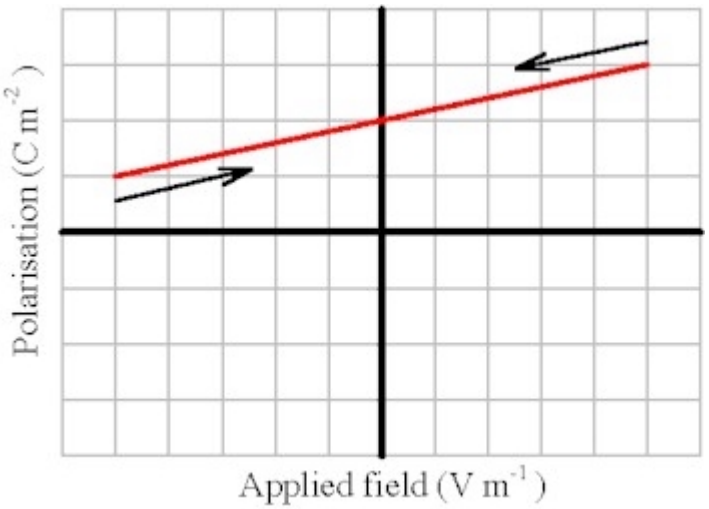

Figure 1.11. Field-polarisation plot for a pyroelectric material. It is noteworthy that there is some polarisation at zero applied field.

If the material under study has pyroelectric properties i.e. a permanent dielectric polarisation. It will appear as in figure 1.11. As for the paraelectric shown in figure 1.10 the slope of the line is related to the relative permittivity but the line no longer crosses the origo. Thus at zero applied field there is a net polarisation and depending upon the orientation of the sample the crossing point with the *y*-axis will be either towards positive or negative values. When a ferroelectric is subjected to the same conditions the behaviour is quite different and switching between polarisation states is seen as a hysteresis curve. In this case the black arrows are important because they indicate the path taken by the field and shows the associated polarisation. What happens is that it behaves like a pyroelectric with a permanent polarisation and a slope related to the dielectric constant. If we start at the upper right corner and trace along the curve the field decreases and we follow a straight sloping line (related to the relative permittivity). When the applied field has reached zero we can read the value for the permanent polarisation, $+\vec{P}$, of the *y*-axis.

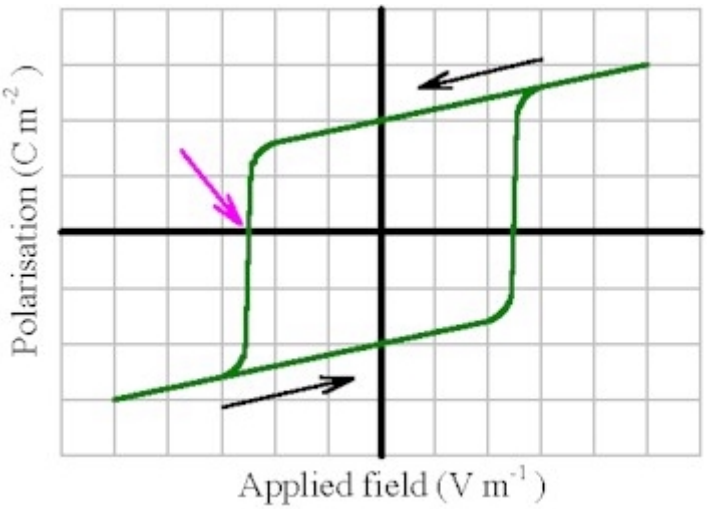

Figure 1.12. Field-polarisation plot for a ferroelectric material. It is characterised by a hysteresis curve. The value for the coercive field is indicated by the pink arrow. It is the field required to exactly cancel the polarisation in the material.

As the applied field starts to increase towards negative values the direction of the induced polarisation (given by the dielectric permittivity) opposes the direction of the permanent polarisation of the material. At a certain point the applied field is strong enough to start reversing the polarisation in some domains (i.e. in $BaTiO_3$ this would make some of the titanium atoms flip) this process continues and can be made to exactly cancel the permanent polarisation of the material. The field required to make this come about is called the coercive field and its value is read off the *x*-axis at a point indicated by the pink arrow in figure 1.12. If the field is increased further towards negative values a complete reversal of polarisation is obtained. The magnitude of the polarisation which is obtained is in generally the same whether obtained at positive or at negative applied field (this need not however be the case). When tracing backwards from the negative field towards zero we follow a straight sloping line which crosses the *y*-axis at $-\vec{P}$. Carrying on further towards positive field values switching and polarisation reversal is observed as before and the system ends up where it started. The value of the coercive field is with respect to some applications sought to have a low value (i.e. in ferroelectric memories where switching must be fast and low fields are required) and in some applications the coercive field is sought to have a high value (i.e. for pyroelectric sensor applications where a large pyroelectric signal could lead to a cancellation of polarisation). It is also possible to have an antipolar system. What happens in such a system

on passing from the paraelectric phase to the antiferroelectric phase can be understood in terms of a coupling of the dipoles such that every dipole has its neighbouring dipoles oppositely polarised. Such a system has no net polarisation at zero applied field.

Figure 1.13. An illustration of the antipolar state and the polar state induced by a sufficiently large applied field. To the left the system is shown at zero field where there is no permanent polarisation. To the right a sufficiently large electric field (indicated by the red arrow) has been applied and the system has switched to the polar state.

The hysteresis curve associated with such a system is shown in figure 1.14 and again the black arrows indicate the path taken upon tracing through different values for the electric field.

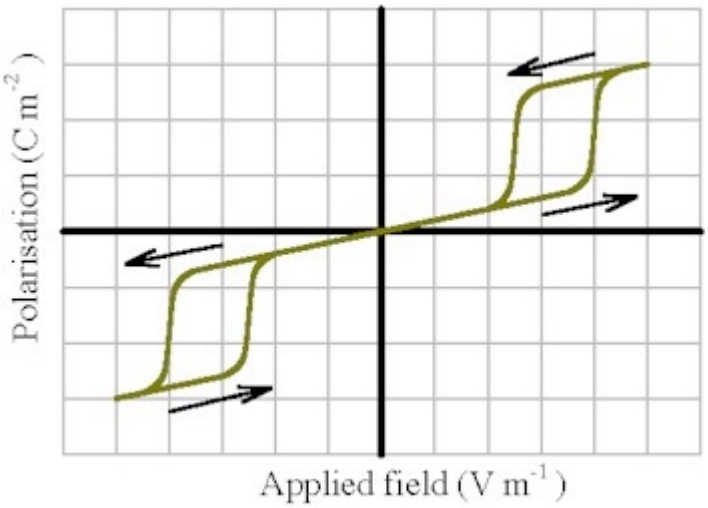

Figure 1.14. Field-polarisation plot for an antiferroelectric material. A dual hysteresis curve is observed with ferroelectric behaviour at high applied field. At low field intensities it behaves as a paraelectric or dielectric with no polarisation at zero applied field.

Starting at high field values in figure 1.14 where the system is in the polar state. When the field decreases the polarisation follows a straight sloping line until it switches into the antipolar state which exists through zero applied field (with an associated polarisation of zero) until a sufficiently negative field is applied and switching to the oppositely polarised state

takes place. A reversal follows the same line of arguments. It should be noted that an antiferroelectric material is obtained only when the energy of the antipolar state is comparable to that of the polar state.

1.1.6 Non-crystalline polar materials

1.1.6.1 The various types

Permanent dielectric polarisation is not a property which is reserved to crystalline materials it can be observed for polymers, amorphous and crystalline (crystalline polymers does not imply perfect crystalline order but merely some order which is rudimentary compared to a single crystal), in solutions of small molecular dipoles in polymers, in amorphous small molecule solids and in some types of liquid crystals and liquid crystalline polymers.

1.1.6.2 Classical polymers

The perhaps best known polymer which has it all is polyvinylidenedifluoride (PVDF). It is ferroelectric, pyroelectric, piezoelectric, a polymer, widely used in the world around us (more than you would think) and very importantly cheap when compared to crystalline materials. It is made by polymerisation of 1,1-difluoroethylene and initially it does not have an appreciable permanent polarisation. It has to be heated above a glass temperature where the polymer chains are mobile, mechanically stretched and placed in a strong electric field whereby the dipoles align with the field, and cooled to below the glass temperature so that the orientation of the dipoles is frozen in a polar state.

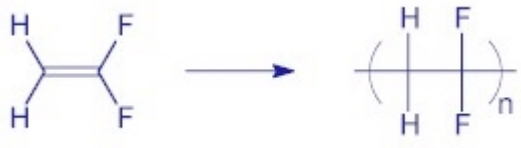

Figure 1.15. A schematic representation of the synthesis of PVDF. The projection to the right is **not** a Fischer projection. The representation is meant to imply that there is no correlation along the chain of the methylene units i.e. the two fluorine atoms could be coming out of the plane of the paper in one repeat unit and be pointing into the plane of the page the next.

The important structural point to make is that along a chain certain dipoles can be defined as shown in figure 1.16 where the dipole is formed between the adjacent difluoromethylene and methylene groups. There are at least four crystalline phases of PVDF known only one of which is interesting from a technological viewpoint.

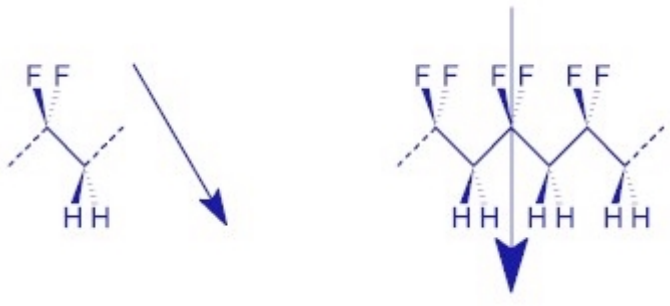

Figure 1.16. To the left one repeat unit of PVDF is shown along with its single isolated dipole indicated by the arrow. To the right a section of a polymer chain which has been subject to poling is shown. All the dipoles now have a component in the same direction the sum of which is the observed macroscopic dielectric polarisation (indicated by the large arrow).

Once poled PVDF exhibits ferroelectric behaviour with the typical hysteresis curve as shown in figure 1.12. If heated above the glass temperature the polarisation is lost and so is some of the order therefore the reappearance of ferroelectric behaviour is not necessarily observed upon cooling down below the glass temperature. Being a ferroelectric PVDF also has both pyroelectric and piezoelectric properties. The values for the pyroelectric coefficient and the piezoelectric moduli vary greatly and this has been subject to a lot of dispute in the literature but has been ascribed to a large dependence on the pre-treatment and preparation of the polymer samples. As examples of other well known types of polymers which can exhibit pyroelectricity are the nylons. The principle of operation is the same as for PVDF except that the dipolar units are the hydrogen bonds observed between the amide groups in the polymer.

1.1.6.3 Polarisation in small molecules and in small molecule/polymer solutions

The mechanism or the nature of the polarisation that can be observed in systems where small molecules are dissolved in a polymer matrix or in systems where small molecules that do not crystallise well form a glass is similar to that outlined in *section 1.1.6.2* for PVDF. What is required is a system that can be heated to a certain temperature where the thermal energy allows for the molecular dipoles to reorient in accordance with an applied electric field. Upon cooling to below a certain temperature the molecular dipoles can no longer reorient and are thus frozen in some polarised state.

1.1.6.4 Polarised liquid crystals

The liquid crystalline state is briefly described a state which does not have the long range translational order characteristic of crystals they do however have some molecular orientational order. The orientational molecular order is highly dependent on the shape of the molecules. Any further discussion on the shape and structure of molecular liquid crystals is deferred until *Chapter two*. Molecular liquid crystals exhibit many different phases with often confusing names. Of interest here is what is known as the nematic phase. The nematic phase is characterised by no long range translational order only orientational order is observed. The molecules involved are often rod shaped i.e. axial. If the individual molecules have a dipole moment along the axis of the molecule it becomes possible to pole the system. It can be considered as a liquid consisting of molecular dipoles with translational freedom but not with orientational freedom i.e. directionally constrained. It is indeed possible to have a permanent dielectric polarisation in such a system as the polarisation as such does not at all depend upon translational order whereas it depends highly upon the orientational order.

1.1.7 General references

Sears, F. W.; Zemansky, M. W.; Young, H. D. *University Physics 6th Edition.* (1982) Addison-Wesley Publishing Company, U.S.A.

Atkins, P. W. *Physical Chemistry 3rd Edition.* (1987) Oxford University Press, UK.

Kittel, C. *Introduction to Solid State Physics 6th Edition.* (1986) John Wiley and Sons, U.S.A.

Nye, J. F. *Physical Properties of Crystals.* (1976) Oxford University Press, UK.

Jona, F.; Shirane, G. *Ferroelectric Crystals.* (1962) Pergamon Press, Germany.

Ashwell, G. J. *Molecular Electronics.* (1992) Research Studies Press, UK.

Giacovazzo, C.; Monaco, H. L.; Viterbo, D.; Scordari, F.; Gilli, G.; Zanotti, G.; Catti, M. *Fundamentals of Crystallography.* (1994) Oxford University Press, UK.

1.2 Organic pyroelectrics and ferroelectrics

This part describes the work aimed at characterising and understanding crystalline molecular organic materials with respect to pyroelectric and possible ferroelectric properties. The entire part relies heavily on the publications appropriate to this part which can be found in *Appendix P1-P6*. Some synthetic work has been done but the main effort has been placed with crystal structure solution and structural characterisation of molecules thought to be interesting. In a few cases dielectric measurements were made or attempted. As should be evident from *Appendix P* some people have made contributions towards the work presented in this chapter most significantly perhaps Georg K. H. Madsen, Jørgen Eskildsen, Bo W. Laursen and André Faldt.

1.2.1 Hat shaped and helical molecules

1.2.1.1 Phosphangulene

The recognition that phosphangulene[5] (**1**) is hat shaped is perhaps not so important but when considering that it is the hat shape that allows for it to form a polar stack and further that the hat shape gives rise to the most desirable of all, a Type I material, with significant pyroelectric properties. A study of hat shaped molecules and their relation to polar space groups or at least non-centrosymmetric space groups was found appropriate.

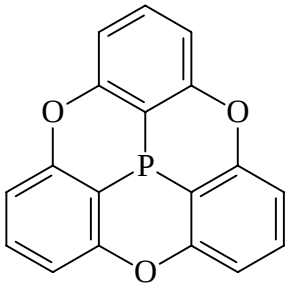

1

Figure 1.17. A molecular drawing of phosphangulene (below). The molecule has C_{3v} Schönflies molecular point group symmetry and crystallises in space group *R*3*m*. Interestingly the molecular point group symmetry is the same as the crystallographic symmetry.

[5] Krebs, F. C.;Larsen, P. S.; Larsen, J. Jacobsen, C. S.; Boutton, C.; Thorup, N. *J. Am. Chem. Soc.* **1997**, 119, *1208-1216*.

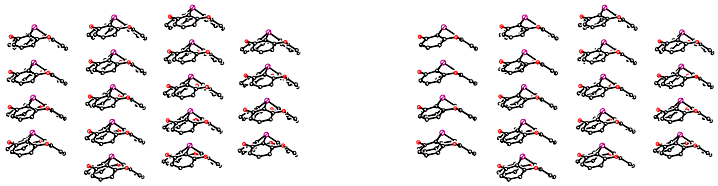

Figure 18. A stereoview of the polar structure of phosphangulene. Notice how the hat shaped molecules stack beautifully and how all the stacks point the same way (the $(a-b)c$-plane is shown (the positive c-direction is upwards). All crystallographically distinct molecules are thus shown.

The next question that arose was what other hats would be interesting and was the three fold axis observed in phosphangulene important for polar stacking.

1.2.1.2 Other hats

The obvious choice when considering new hat shaped candidates was of course molecules related to phosphangulene. The systematic name for molecules with a structural formula like that of phosphangulene but with a carbon atom in the middle is 4,8,12-trioxa-4,8,12,12*c*-tetrahydrydibenzo[*cd*,*mn*]pyrene but it will be referred to as trioxatriangulene. The central atomic position is the 12*c*-position and while many attempts have been made to substitute for different atoms at the 12*c*-position few have been successful and the only known are to this date the one with phosphorous[5] and the one with carbon[6]. The system has attracted a considerable interest and in the literature studies range from synthetic[7,8,9], structural[10,11], macrocyclic[12,13,14] and spectroscopic[15,16] to photophysical[17]. Apart from the hat shape it would also be of interest to perturb the space filling properties of the hat shaped molecule to see how

[6] Martin, J. C.; Smith, R. G. *J. Am. Chem. Soc.* **1964**, *86*, 2252-2256.
[7] Hellwinkel, D.; Melan, M. *Chem. Ber.* **1971**, *104*, 1001-1016.
[8] Hellwinkel, D.; Melan, M. *Chem. Ber.* **1974**, *107*, 616-626.
[9] Hellwinkel, D.; Aulmich, G.; Melan, M. *Chem. Ber.* **1981**, *114*, 86-108.
[10] Faldt, A.; Krebs, F.C.; Thorup, N. *J. Chem. Soc. Perkin Trans. II* **1997**, 2219-2227.
[11] Krebs, F.C.; Laursen, B. W.; Johannsen, I.; Faldt, A.; Bechgaard, K.; Jacobsen, C. S.; Thorup, N.; Boubekeur, K. *Acta Cryst.* **1999**, *B55*, 410-423.
[12] Lofthagen, M.; Siegel, J. S. *J. Org. Chem.* **1995**, *60*, 2885-2890.
[13] Lofthagen, M.; Siegel, J. S.; Chadha, R. *J. Am. Chem. Soc.* **1991**, *113*, 8785-8790.
[14] Lofthagen, M.; Siegel, J. S.; VernonClark, R.; Baldridge, K. K. *J. Org. Chem.* **1992**, *57*, 61-69.
[15] Müller, E.; Moosmeyer, A.; Rieker, A.; Schleffer, K. **1967**, *39*, 3877-3880.
[16] Sabacky, M. J.; Johnson, C. S. Jr.; Smith, R. G.; Gutowsky, H. S.; Martin, J. C. *J. Am. Chem. Soc.* **1967**, *89*, 2054-2058.
[17] Laursen, B. W.; Krebs, F.C.; Nielsen, M. F.; Bechgaard, K.; Christensen, J. B.; Harrit, N. *J. Am. Chem. Soc.* **1998**, *120*, 12255-12263.

this would affect the packing. In order to be able to say just a little general about the structural properties of a given class of compounds (i.e. trioxatriangulenes) several structures are needed for a comparison. The outline of the study could thus be described as the synthesis of related trioxatriangulenes followed by solving their structures and recognising the possibility of dielectric properties with a characterisation of these if applicable. What was known was of course the ideal structure of phosphangulene (space group *R*3*m*) but also the structure of the 12*c*-methylated trioxatriangulene was known (space group $P2_1/c$) and it was found that the molecules do not stack. From this it would appear that stacking and non-centrosymmetric behaviour was sensitive towards substitution at the 12*c*-position for the trioxatriangulene system.

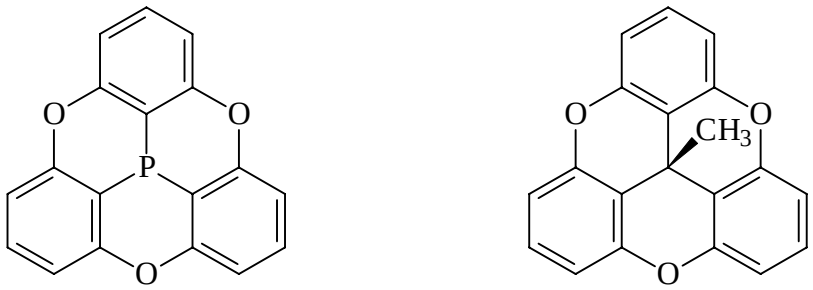

*R*3*m* (**1**) $P2_1/c$ (**2**)

Figure 1.19. Known compounds with known structures at the time the study was begun. Phosphangulene (left) stacks whereas 12*c*-methyltrioxatriangulene does not. The associated space groups are shown.

The reason for the non-stacking observation in the 12*c*-methylated trioxatriangulene did of course not need to have anything to do with the methyl group. The compounds that was chosen for the comparison are shown in figure 1.20. From the data it became clear that the system was very sensitive to the space filling of the substituents but mostly at the 12*c*-position and less so at the periphery (2,6,10-positions). Of the six compounds studied two were centrosymmetric. The remaining four crystallises in non-centrosymmetric space groups and interesting dielectric properties are allowed. The three new compounds with dielectric properties to be characterised are the three non-phosphorous containing compounds in figure 1.20.

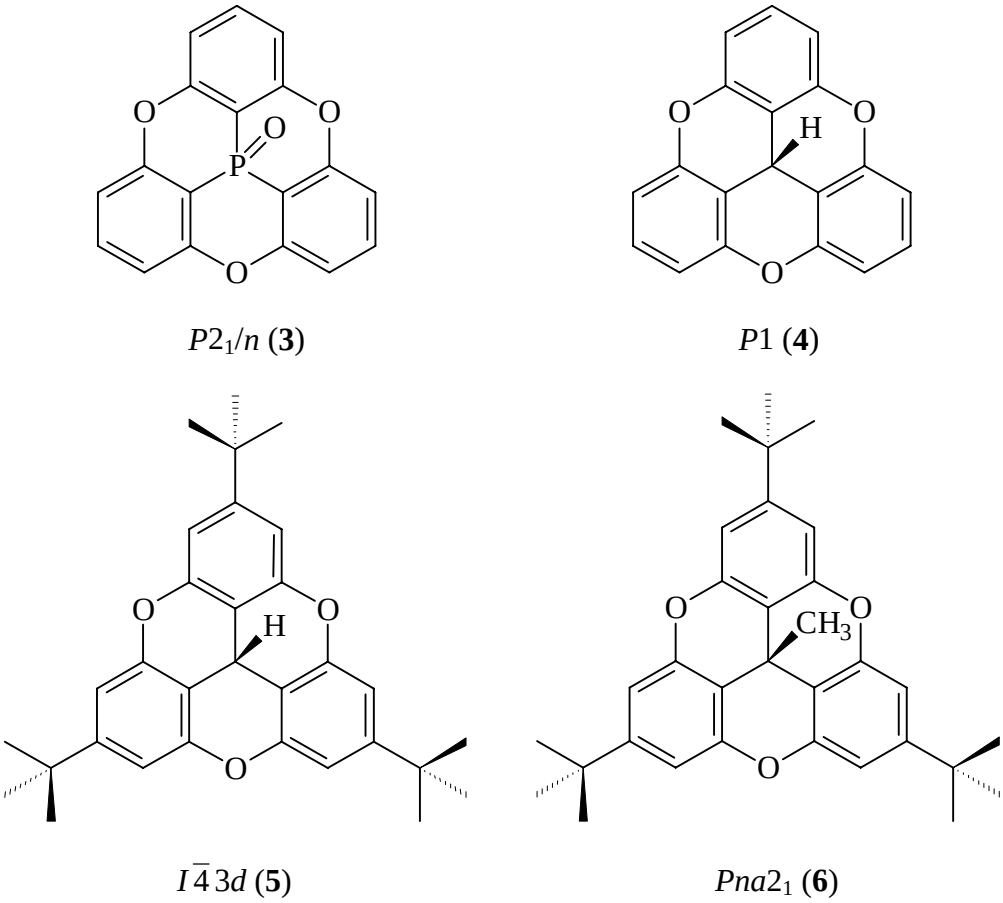

$P2_1/n$ (**3**) $P1$ (**4**)

$I\bar{4}3d$ (**5**) $Pna2_1$ (**6**)

Figure 1.20. The compounds **3**-**6** chosen for the comparison. The space groups are shown.

1.2.1.3 The properties and classification

According to the classification of dielectric materials outlined in the introduction there is in the group of six compounds one Type I material which is **1** itself. There are two Type II materials with potential pyroelectric properties, compounds **4** and **6**. Finally there are three Type III materials two of which are centrosymmetric, compounds **2** and **3**, and one non-centrosymmetric, compound **5**. The latter should in principle have piezoelectric properties.

1.2.1.4 The pyroelectrics

In terms of the exemplification of Type II materials given in the introductory part the results for compound **4** and **6** are interesting as they show the diversity of the polarisation that can be observed in Type II materials. By comparing the molecular structures obtained from the crystallographic data it is evident that compound **1** is a lot more conical than compound **4**.

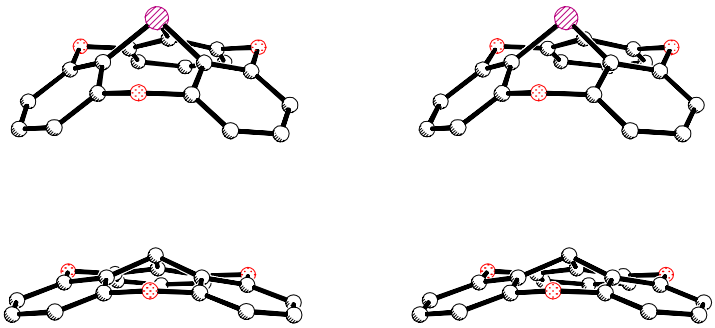

Figure 1.21. Stereoviews of how conical compounds **1** (above) and **4** (below) are. Compound **1** is very conical whereas compound **4** is quite flat. Oxygen atoms are coloured red whereas phosphorous is in a taupe colour.

Based on this the dipole moment is expected to be smaller for **4** than for **1** henceforth the resulting polarisation is expected to be smaller on these grounds alone. Furthermore the hat shaped molecules does not form discrete stack in **4** as observed for **1**. There is a partial cancellation of the dipoles which lie along the molecular C_3 axis. This has been illustrated in figure 1.22.

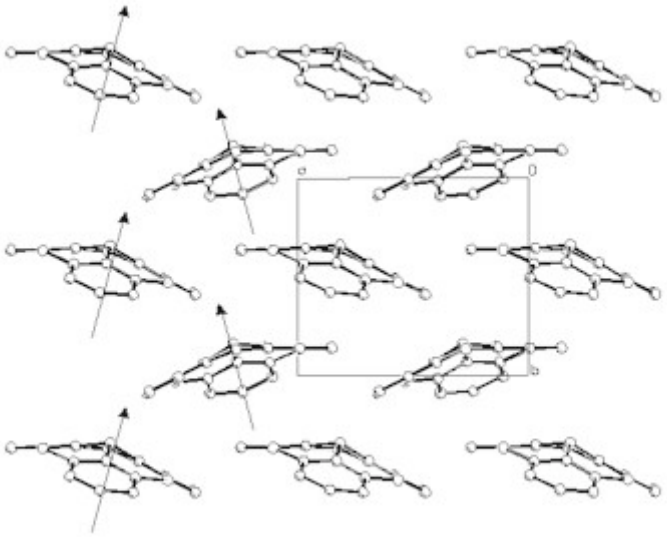

Figure 1.22. The structure of **4** illustrating how the molecular dipoles partially cancel (projection along the *c*-axis). By and large molecular axes do show a remarkable directivity in the packing of the molecules leading to a significant polarisation and pyroelectric properties.

Based on the assumptions of a smaller dipole moment for **4**, partial cancellation of dipoles and similar coefficient of linear expansion the pyroelectric signal for **4** should be significantly smaller than that observed for **1**. This was indeed the case and the pyroelectric coefficient for **4** was determined to be -0.5 μC m^{-2} K^{-1} as opposed to -3 μC m^{-2} K^{-1} for **1** thus a factor of six smaller. The method of measurement employed was the temperature step method first described by Ackermann[18] the main reason being that it was a relatively small signal and large crystals were not easily grown. Fortunately the orientation of the crystal was not complicated by a difficult morphology as the polar axis was found to be along the longest physical dimension of the small needle shaped crystals The experimental set up has been described in ref. 5. For compound **6** no significant or measurable pyroelectric properties were expected. The reason being that even though **6** crystallises in a polar space group the molecular dipoles nearly cancel each other in the crystal. It is thus a Type II material at the other end of the scale from compound **4**.

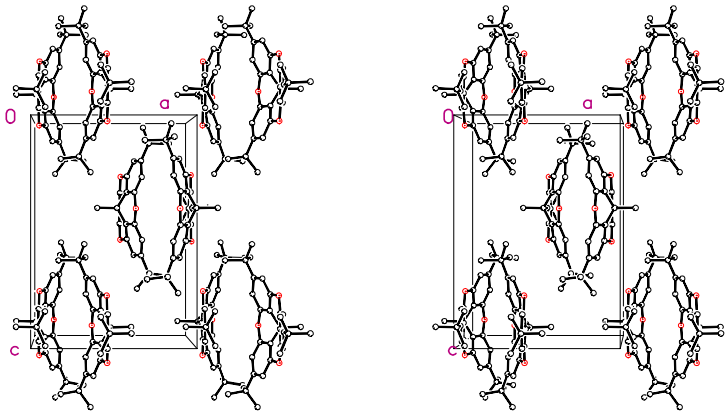

Figure 1.23. The structure of **6** illustrating how the molecular dipoles nearly cancel. There is no significant polarisation in the material.

The molecular dipoles in figure 1.23 are directed along the molecular C_3-axis which is approximately horizontal on the drawing. There is a little net polarisation as the dipole moment vectors are not quite parallel with the *a*-axis (the dipoles form an angle of approximately 0.2^o with the *ab*-plane). The packing is different from **1** and **4** where stacking

[18] Ackermann, W. *Ann. Phys.* **1915**, *46*, 197.

to near stacking was observed. In a sense the packing pattern for **6** resembles the packing of **2** and **3**. A stereoview has been included in figure 1.24.

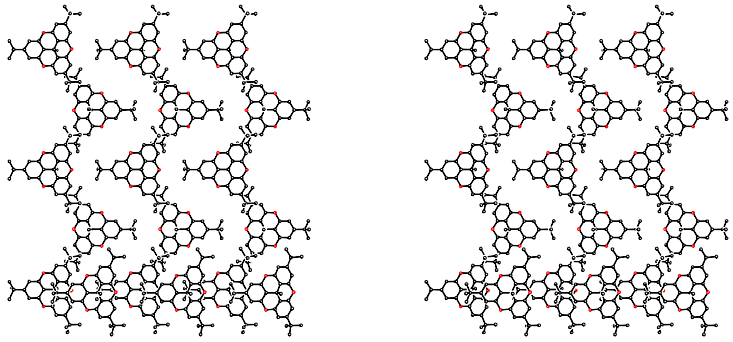

Figure 1.24. The packing of compound **6** in the *ac*-plane. In the lower part of the figure the molecules line up and the *tert*-butyl groups of molecules in one layer fits nicely in the cavity of the trioxatriangulene core from molecules in the adjacent layer.

1.2.1.5 The piezoelectric

Compound **5** crystallises in a very rare space group for organic molecules, the cubic space group $I\bar{4}3d$. This space group or more specifically the crystallographic point group $\bar{4}3m$ does not allow for a permanent polarisation as exemplified for the crystallographic point group *222* in *Subsection 1.1.2.5*. Being non-centrosymmetric it does however allow for piezoelectric properties. Attempts were made to determine the piezoelectric modulus for the compound as there is only one. Returning to the introduction given in *Section 1.1.3* where the expression for the polarisation obtained upon subjecting a piezoelectric crystal to mechanical stress. Normally another and simpler notation is employed (than the on given in *Section 1.1.3*). The advantage is one of simplicity but a severe disadvantage is that the components do not transform as a tensor and therefore great care has to be exercised when for instance transforming the basis. It can be recalled that the piezoelectric tensor was of rank three and thus contained twenty-seven components. Eighteen of these were independent. By creating a new notation for both stress components and the piezoelectric moduli a notation commonly called matrix notation is obtained. The first subscript, *i*, in *d* stays invariant whereas the two following subscripts, *j* and *k*, are compressed into one so that *jk* = 11, 22, 33, 23, 13, 12

become just j = 1, 2, 3, 4, 5, 6 respectively. As for the stress tensor components σ_{jk} the same rule apply.

$$\vec{P} = \begin{pmatrix} d_{11} & d_{12} & d_{13} & d_{14} & d_{15} & d_{16} \\ d_{21} & d_{22} & d_{23} & d_{24} & d_{25} & d_{26} \\ d_{31} & d_{32} & d_{33} & d_{34} & d_{35} & d_{36} \end{pmatrix} \begin{pmatrix} \sigma_1 \\ \sigma_2 \\ \sigma_3 \\ \sigma_4 \\ \sigma_5 \\ \sigma_6 \end{pmatrix} \tag{1.38}$$

Or in general terms if we would like to find the polarisation in a given direction the simpler and compressed expression applies.

$$P_i = d_{ij}\sigma_j \tag{1.39}$$

It should perhaps be mentioned that the way the compressed version of d is defined all the off diagonal components are multiplied by a factor of one half the reason being of simplicity. It has to be remembered when transforming components from matrix notation to tensor notation or *vice-versa*. All this leads to the symmetry of the piezoelectric moduli for compound **5**. Due to the high symmetry of the crystallographic point group $\bar{4}3m$ many of the components are zero and the ones that are non-zero are all equal in magnitude (i.e. it is cubic). The piezoelectric moduli are.

$$d_{ij}^{\bar{4}3m} = \begin{pmatrix} 0 & 0 & 0 & d_{14} & 0 & 0 \\ 0 & 0 & 0 & 0 & d_{14} & 0 \\ 0 & 0 & 0 & 0 & 0 & d_{14} \end{pmatrix} \tag{1.40}$$

This made the task appear quite simple. By determination of just one modulus the entire third rank tensor would be characterised. The tricky point turned out to be that shear force that has to be applied. The determination of d_{14} would require that the polarisation is measured for instance along P_1 while a shear stress (for instance σ_{23}) is applied. Simple at first glance but in reality an arduous task which turned out to be impossible. Even though very nice gem quality diamond like crystals could be grown they were much to small to allow for proper application of electrodes with a surface area large enough to collect sufficient charge for measurements and at the same time have them sustain a shear force around the axis of polarisation. What was achieved was a system that in principle could measure piezoelectric moduli that relies on compressive or tensile mechanical stress. The force could be generated between one (or two) ceramic piezoelectric transducer(s). By the application of a sinusoidally

modulated compressive mechanical stress field derived by excitation of the piezoelectric transducer with a sinusoidal voltage the signal from the crystal could be measured. Even if the signal was very weak a lock in amplifier could be used. The piezoelectric moduli of **5** thus still remains undetermined. All the work described in *Subsection 1.2.1.1* to *1.2.1.5* have been published and can be found in *Appendix P1*.

1.2.1.6 Pyroelectricity and phosphangulene revisited

When phosphangulene was studied and characterised it was found that the experimentally determined direction of the dipole moment and that arrived at by *ab initio* calculations did not agree i.e. the results were exact opposites. Being an experimentalist (which is the only thing humans really can do, see for instance the preface) it was decided that the experiment and reasoning was correct and consequently most of the work relating to calculations was not published. It would of course be nice to have the discrepancy resolved. One way of doing this is by performing a charge density study as set out in the original project description for this thesis. When at the Sandbjerg summer school on synchrotron radiation I had the pleasure to meet some of the experts in this field (Georg K. H. Madsen and Finn K. Larsen at the university of Aarhus). As they seemed eager to engage in this study I grew some crystals and grew some more and finally a large data set were collected at low temperature (10 K) on a crystal of sufficient quality. The potential advantage of this way of attack is that the solid state dipole moment could be obtained in both magnitude and direction. Thus in principle resolving the discrepancy mentioned above and giving a better value for the dipole moment as dipole moments measured in solution or arrived at by calculation are known to differ in magnitude from the dipole moment in the solid state[19,20]. In this way a more reliable prediction of the pyroelectric properties for a given material would be possible. Furthermore since the crystal structure has to be solved in order to evaluate a new and potentially valuable material one may as well get the full monty by also measuring the unit cell parameters at several temperatures (or at least two). In that way the crystal structure, the solid state dipole moment, the direction of the dipole moment with respect to the molecular co-ordinates, the coefficient of thermal expansion (linear or some other description) can be obtained and thereby the polarisation and the pyroelectric properties in just one experiment. It should be emphasised that an experimental determination of the pyroelectric coefficient is still an absolute necessity

[19] Spackman, M. A. *Chem. Rev.* **1992**, *92*, 1769.

(we live in a real world) but the above process can save the precious time of the experimenter and severely speed up the process of selecting good candidates.

1.2.1.7 The direction of the dipole moment and the absolution

The multipolar modelling of the X-ray data turned out to be very sensitive towards the modelling of the hydrogen atoms and it was found necessary to use neutron data to get good positional and vibrational information for the hydrogen atoms. Neutron powder diffraction was found to be the method of choice. A large portion of phosphangulene was needed. As the synthesis had been described and found to work quite well on a 0.5 – 1g scale it was just a matter of scaling up (10 g was needed). There are two types of people some are true believers like myself (but other people are not and they take back ups etc. all the time). I scaled up and realised that the yield was exceptionally poor < 10 %. This obviously was a large scale problem and the culprit turned out to be the *t*-BuOK which is used as a base in the reaction.

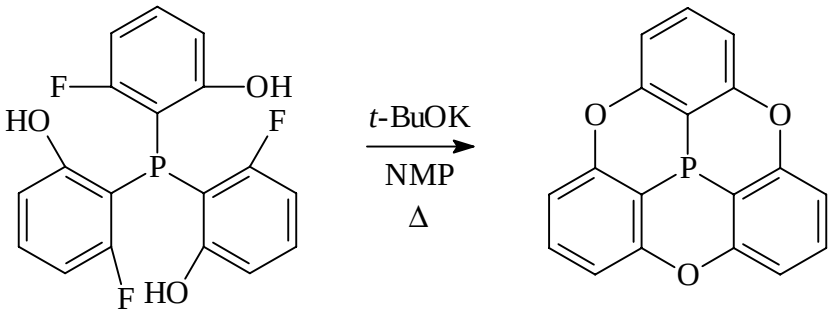

Figure 1.25. The synthesis of phosphangulene in boiling NMP with *t*-BuOK as a base. The internal temperature was found to be crucial when doing large scale synthesis.

The synthesis employs *t*-BuOK as base with NMP (N-methylpyrrolidone) as a high boiling solvent (b.p. ~210 ^{o}C). A little *t*-BuOH obviously evolves during the course of the reaction and on a small scale the low boiling *t*-BuOH probably condenses in the glass ware set-up and the temperature of the reaction can then reach the boiling point of NMP. On a large scale the *t*-BuOH does not just condense somewhere in the glassware and this leads to a considerable lowering of the boiling point for the mixture. After some trials it was realised that for the small scale reaction a temperature of 205 ^{o}C was observed for the boiling mixture whereas in large scale it was as low as 160 ^{o}C. In conclusion phosphangulene only forms at temperatures

[20] Howard, S. T.; Hursthouse, M. B.; Lehmann, C. W.; Frampton, C. S. *J. Chem. Phys.* **1992**, *97*, 5616.

close to the boiling point of NMP. Once this had been realised it was a question of distilling solvent of the reaction flask until an internal temperature of 205 ^{o}C was measured. Hereafter the reaction proceeded smoothly and 14 grams could be made in one go with 80 % yield. Having the large quantity of phosphangulene required for the neutron experiment data were collected at the powder neutron data facility (TAS 3, see *Appendix E5*) at Risø. The data from the experiment allowed for a proper modelling of the parameters for the hydrogen atoms and the numerical value for the solid state dipole moment could be worked out as 4.6 D as opposed to 3.3 D obtained from measurements in solution. The final and important point however was the opposite direction of the dipole moment to the experimentally determined. My original experiment was however bullet proof and checked over and over again in the days of the initial discrepancy between calculation and observation. The only thing that had not been questioned by the devils advocate was the simple straight forward structure solution which was done on a CAD-4 using Cu-radiation. As Cu-radiation had been used and since phosphangulene contains phosphorous then (though it was room temperature data) the determination of the absolute configuration should be an easy task. The only way the world could agree however, was if somehow there was an error in the sign of the absolute configuration from the determination of the absolute configuration. So, I made some new and large crystals and collected data on the SMART diffractometer (using Mo-radiation at 120 K) on three new and different crystals and on the original crystal which had been kept by Niels Thorup. All four structure solutions gave the same result which was different from the original and in agreement with the new data. The absolute crystal morphology is now known.

1.2.1.8 A summary of the phosphangulene story

The story of phosphangulene is now complete and some new data has been added. A wealth of information now exists on this single molecule. To mention a few, at least eight crystal structure determinations using Ag, Mo and Cu-radiation. The absolute configuration for the crystals with respect to the crystal morphology is now known, the pyroelectric properties have been determined experimentally and theoretically and arrived at by means of multipolar modelling of X-ray structure factors, the molecular dipole moment is known in solution and in the crystal, the thermal expansivity tensor is known from 10 K to 473 K and finally its physical-chemical properties are well known (i.e. heat capacity, thermogravimetry etc.).

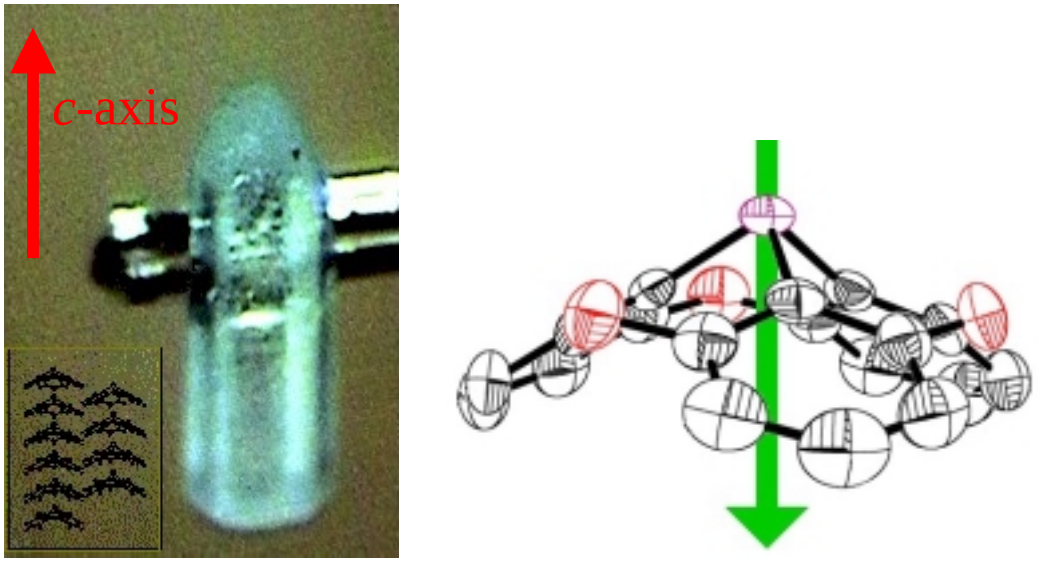

Figure 1.26. A picture of a typical phosphangulene crystal showing the correct crystal morphology along with the how the molecules pack in the crystal and the direction of the positive *c*-axis (left). An ORTEP drawing of phosphangulene along with an arrow indicating the correct direction of the molecular dipole moment (right).

The story of phosphangulene can be read in ref. 5 and the contribution made during this work has been included in *Appendix P2*.

1.2.2 Horseshoe shaped helicenes and V-shaped hats

1.2.2.1 The study

Some time ago my supervisor, Klaus Bechgaard, was quite involved in making helical molecules[21, 22, 23, 24]. The synthetic routes were, albeit beautiful, tedious and time consuming. And since the object of the game was to get helical molecules a simple synthetic route was desired. The interest in helicenes is mainly that they rotate polarised light by as much as 10000^{o} compared to an amino acid which may rotate light by 50^{o} on a good day[25]. Materials with this kind of behaviour are of potential use in fast optical switching devices. In 1940 Dischendorfer[26] published the condensation of 2-naphthol with glyoxal to give a 7*a*,14*c*-

[21] Larsen, J.; Bechgaard, K. *J. Org. Chem.* **1996**, *61*, 1151-1152.
[22] Larsen, J.; Bechgaard, K. *Acta Chem. Scand.* **1996**, *50*, 71-76.
[23] Larsen, J.; Bechgaard, K. *Acta Chem. Scand.* **1996**, *50*, 77-82.
[24] Larsen, J.; Dolbecq, A.; Bechgaard, K. *Acta Chem. Scand.* **1996**, *50*, 83-89.
[25] Wynberg, H. *Acc. Chem. Res.* **1970**, *4*, 65.
[26] Dischemdorfer, O. *Monatsh.* **1940**, *73*, 45.

dihydro-7,8-dioxa[6]helicene. Since then further studies on the condensation have been made[27, 28, 29, 30].

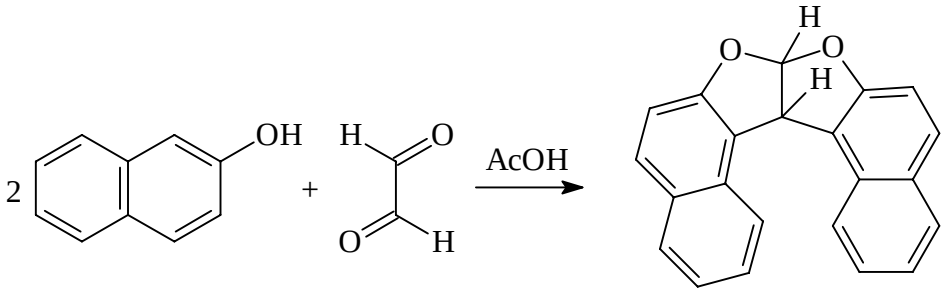

Figure 1.27. The one-step synthesis of 7*a*,14*c*-dihydro-7,8-dioxa[6]helicene starting from 2-naphthol and glyoxal.

The questions that remained to be solved were, firstly, whether the dihydrohelicene shown in figure 1.27 was in a *cis* or a *trans* form i.e. what does the molecular structure look like. Also if it was in the *cis* form it would be a V-shaped molecule that could potentially stack and give rise to dielectric properties. Secondly, could the dihydrohelicene be dehydrogenated to give 7,8-dioxa[6]helicene and would it be helical i.e. what does the molecular structure and the crystal structure look like.

1.2.2.2 The synthesis and structure

This is where André Faldt and myself became involved. André Faldt tried many different ways (S, Se, Pd/C) of dehydrogenating with no success. While I tried to solve the structure of the dihydrohelicene and also I proved unsuccessful as the material forms large long needle shaped crystals but it is highly polycrystalline and scatters X-rays poorly. Then one day the dehydrogenation worked by use of DDQ (dicyanodichlorobenzoquinone). At least the desired hydrogen atoms had been removed as shown by NMR. It turned out to be a mixture and two products could be isolated in very unmentionably poor yield using HPLC. The important point however was that one of the products had the NMR spectrum expected for the helicene while the other did not. Attempts to separate alleged enantiomers using a chiral HPLC column (which had been used to separate chiral helicenes earlier) failed. The two fractions were each

[27] Kito, T.; Yoshinaga, K.; Yamaye, M.; Mizobe, H. *J. Org. Chem.* **1991**, *56*, 3336.
[28] Fan, X.; Yamaye, M.; Kosugi, Y.; Okazaki, H.; Mizobe, H.; Yanai, T.; Kito, T. *J. Chem. Soc. Perkin Trans. II* **1994**, 2001.
[29] Fan, X.; Yanai, T.; Okazaki, H.; Yamaye, M.; Mizobe, H.; Kosugi, Y.; Kito, T. *J. Org. Chem.* **1995**, *60*, 5407.
[30] Coxworth, E. C. M. *Can. J. Chem.* **1967**, *45*, 1777.

put in a sealed tube and crystals were grown. The unknown product was soon identified to have been chlorinated in the 5-position.

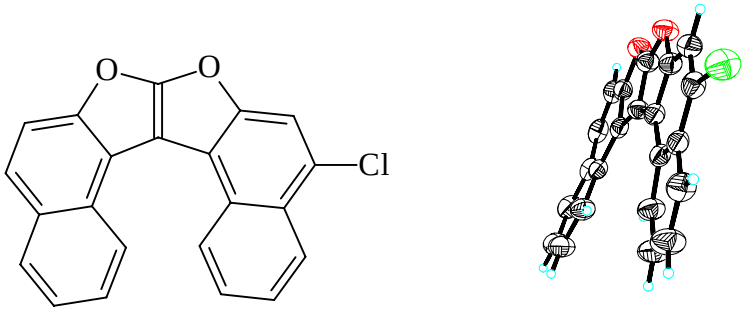

Figure 1.28. The structural formula for the unknown product (left) and an ORTEP drawing clearly showing the helical nature of the molecule (oxygen atoms are red and chlorine atoms are green).

The mechanism by which the product forms is difficult to envisage. It is perhaps not so difficult to see how the 5-position is chlorinated and it most likely proceeds by a radical mechanism but where the chlorine atom comes from and how it enters is questionable. The chlorine could come from the solvent (1,2-dichlorobenzene) or DDQ itself or perhaps from slight amounts of Cl_2 (or HCl) present under the reaction conditions. Since the dehydrogenation most likely proceeds via hydrogen abstraction from the 7*a*-position this radical can rearrange to the 5-position as shown in figure 1.29. It might also be the hydrogen in the 14*c*-position which is abstracted directly by DDQ. In figure 1.29 the two possible radical species obtained upon hydrogen abstraction are indicated to be in some sort of equilibrium. Having answered some questions the molecular structure of the other product obtained needed to be characterised. While nice crystals could be grown the structure turned out to be difficult to solve and the first attempts yielded poor data where the structural model that could be arrived at to account for the data was very poor. Plenty of Weissenberg photographs were recorded by myself and Liselotte Berring to whom I am extraordinarily grateful and it was found that there were some satellite reflections close to the spots (corresponding to a 6 Å axis). It was found that the real space axis would have to be around 46 Å. Bold as I am I collected data in such a cell and solved the superstructure showing eight different helicenes in the asymmetric unit. Each helicene has a different pitch. Six of the molecules in the asymmetric unit are ordered (three *R* and three *S* molecules) and two are disordered. The disorder might extend to higher order i.e. the 46 Å axis is a lot larger than 46 Å maybe 368 Å or even incommensurate. The result obtained from the super structure model

was however very satisfactory because the molecule was helical and it was the molecule we thought it were. Later crystallographic data were collected using synchrotron radiation at HASYLAB in Germany (See *Appendix E4*).

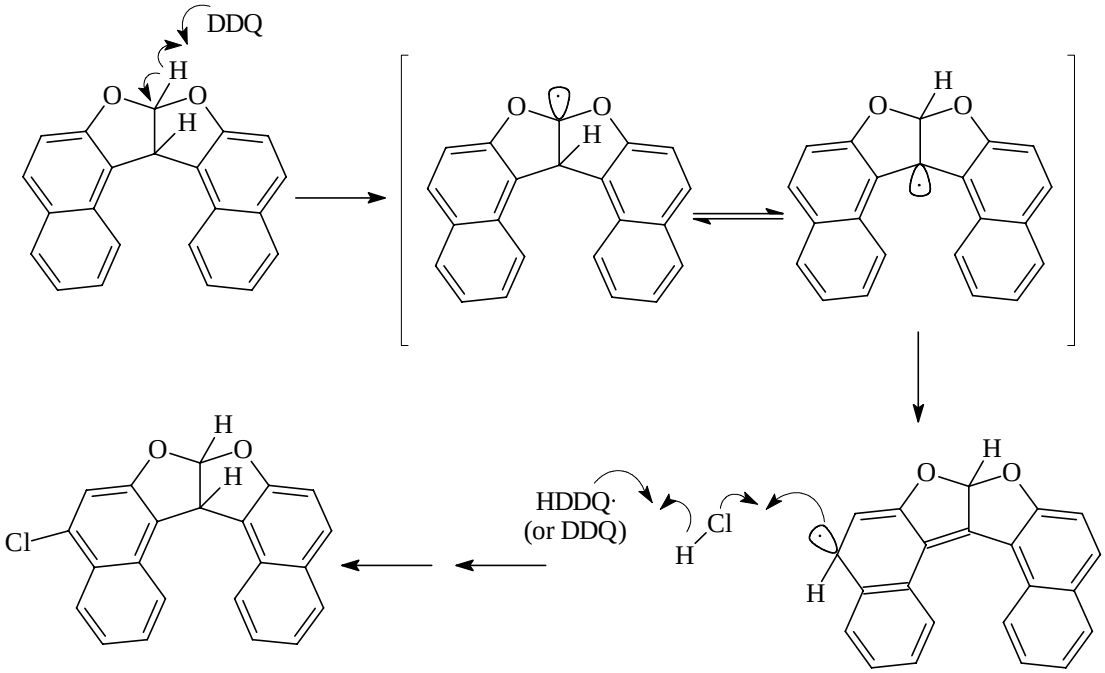

Figure 1.29. A radical chlorination where DDQ acts as oxidant of first the helicene and then HCl which is the source of chlorine.

1.2.2.3 Implications of the results

In terms of dielectric properties both of the helicenes were of interest as they both crystallised in non-centro symmetric space groups. The chlorohelicene crystallises in a polar space group ($Pna2_1$) and should be pyroelectric even though the highly inefficient synthesis probably would prevent it from being a commercially viable product (unless it could be synthesised by the asymmetric coupling as described in *Appendix P3* from readily available starting materials). The polarisation would be along the crystallographic *c*-axis. The polarisation in the structure would be zero or near zero had it not been for the presence of the chlorine atom which makes the direction of the molecular dipole moment form an angle with the molecular C_2-axis of the parent helicene. The helicene crystallises in space group *Cc* and belongs to the crystallographic point group *m*. The polarisation vector can thus lie anywhere in a plane. The plane happens to be perpendicular to the *b*-axis. It is however doubtful whether there is any polarisation in 7,8-dioxa[6]helicene as a the stack of eight molecules that forms the

asymmetric unit has significant dipole moment unless there is enantiomeric excess in the disordered layers.

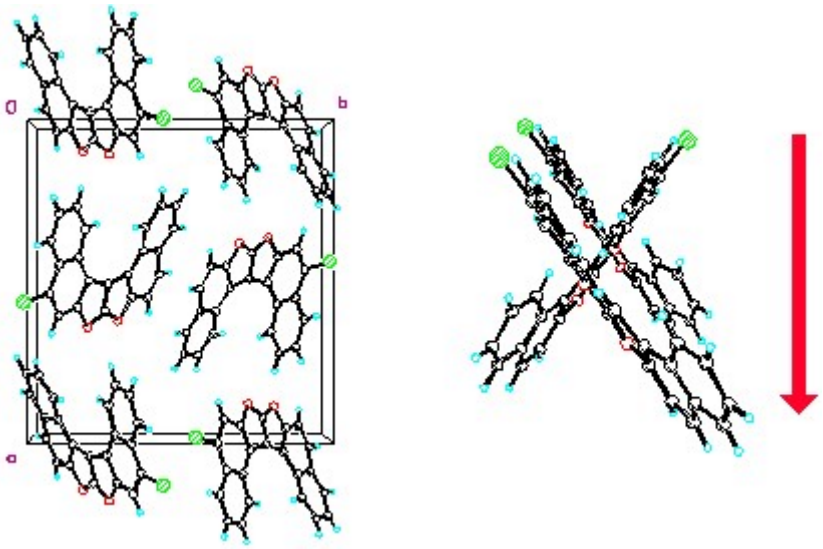

Figure 1.30. The structure of 5-chloro-7,8-dioxa[6]helicene shown to the left as a projection along the polar axis (*c*-axis). Notice how the helicenes pack in lines. To the right a view along such a line is shown (along the *a*-axis) with an indication of the polarisation (red arrow).

In figure 1.31 the asymmetric unit containing eight crystallographically distinct molecules is shown. Notice how the dipole moments of the *R* and the *S* triads cancel (the helicenes that are not disordered).

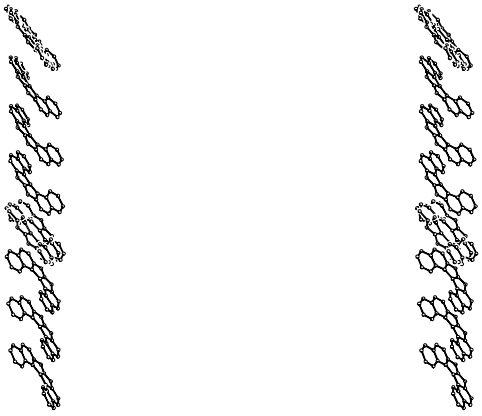

Figure 1.31. The asymmetric unit of 7,8-dioxa[6]helicene. The first and the fourth molecule from the top are disordered. The *R* and the *S* triads are found between these disordered molecules.

It is important to notice that unless there is enantiomeric excess in the disordered layers the asymmetric unit does not have a dipole moment (or an appreciable one at least). This recognition made us reflect upon the fact that if the disorder was dynamic it would be possible to pole the system and thereby get a dielectric polarisation. More importantly however, if the polarisation implied chiral excess we would have an optical switch which could allow for very fast switching (limited by the rate of rotation of the molecules in the crystal and as we know from the introduction this can be very fast maybe the terabit switch is possible). The reason for the cleverness of such an optical switch is the enormous rotation of plane polarised light that would be seen even with slight enantiomeric excess due to the helical nature of the molecules.

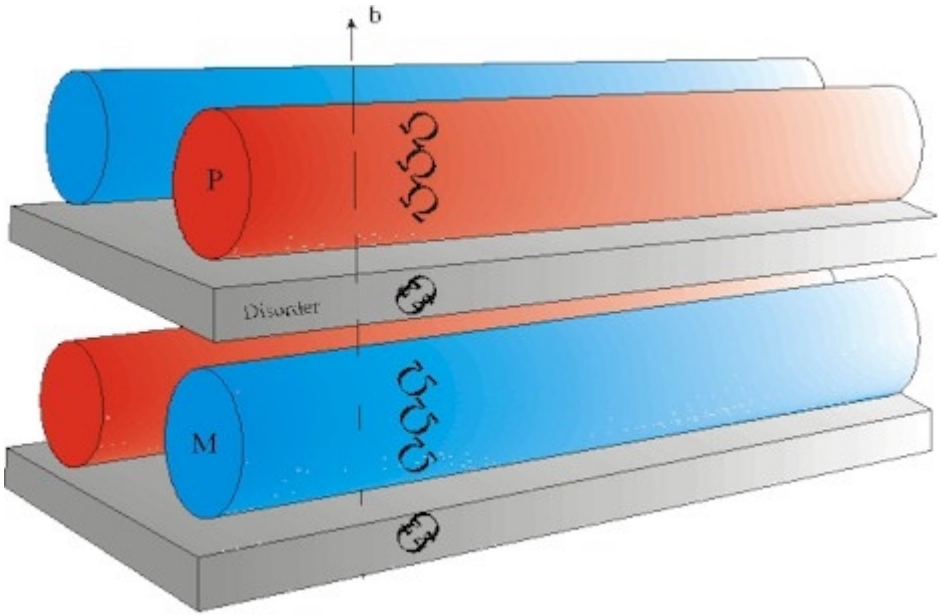

Figure 1.32. A schematic drawing of the structure and the asymmetric unit (molecules shown as omega shaped objects). The structure consists of domains with *R* and *S* molecules coloured blue and red along with disordered domains (Illustration with permission from Klaus Becgaard).

An experiment was set up (with greatly acknowledged help from Lars Lindvold) using a poling apparatus (described later in *Section 1.2.4*) whereby a large field could be applied to a single crystal whilst shining a laser at the crystal and analysing the polarisation of the laser light after passage through the crystal. The experiment unfortunately did not work and this either means that the conditions of the experiments were not correct or that the disorder is not dynamical as is most likely. Even though the disordered molecules were subject to slight

constraints during the crystallographic refinements the positions of the atoms did not seem to be smeared out as would be expected for a plastic phase.

1.2.2.4 The V-shaped hats

The final question that needed answering was whether the 7*a*,14*c*-dihydro-7,8-dioxa[6]helicene was in the *cis* or the *trans* form. A young promising scientist bearing the name Jørgen Eskildsen provided material for answering this question. Before the arrival of Jørgen Eskildsen, Klaus Bechgaard had improved the dehydrogenation procedure in the synthesis of 7,8-dioxa[6]helicene by using NBS (N-bromosuccinimide) in CCl_4. This made the easy and large scale two step synthesis of a helicene a reality. Jørgens mission was to make plenty of derivatives and he did. Amongst them was the 3,12-dibromo-7*a*,14*c*-dihydro-7,8-dioxa[6]helicene shown in figure 1.33 along with its crystal structure which confirms the *cis* form but also that the molecule is slightly helical.

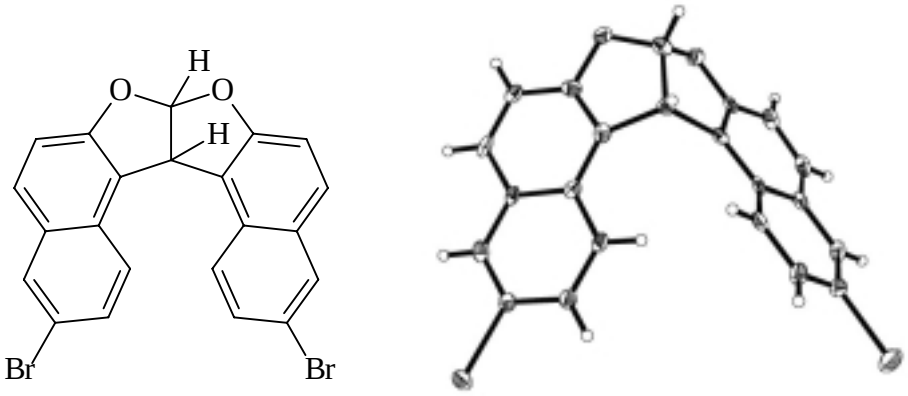

Figure 1.33. The first direct proof of the *cis* form for the 7*a*,14*c*-dihydrohelicenes. A structural drawing to the left and the molecular structure as an ORTEP drawing to the right.

Furthermore the hat shaped molecules form polar stacks and the material is a pyroelectric (space group $Pna2_1$). The measurement of the pyroelectric properties were not attempted due to the extremely thin needle shape morphology of the crystals. Based on the molecular dipole moment (which was calculated by Peter Sommer-Larsen) the polarisation could be worked out. Furthermore the structure was solved at two different temperatures and the unit cell volume determined at several temperatures this allowed us to estimate the value for the secondary pyroelectric coefficient to be of the order of $-1.3\ \mu C\ m^{-2}\ K^{-1}$ which is a moderate value. Interestingly all the helicene derivatives studied and mentioned so far are Type II materials and they exhibit the typical diversity of the Type II materials with respect to

dielectric polarisation. Out of the three polar helicene derivatives 7,8-dioxa[6]helicene has no permanent polarisation (or effectively zero), 5-chloro-7,8-dioxa[6]helicene has partial cancellation but some polarisation whereas the 3,12-dibromo-7*a*,14*c*-dihydro-7,8-dioxa[6]helicene has a very significant polarisation about 75% of what could have been obtained with that molecule had it been a Type I material. In figure 1.34 a projection along the polar axis an the a polar stack is shown.

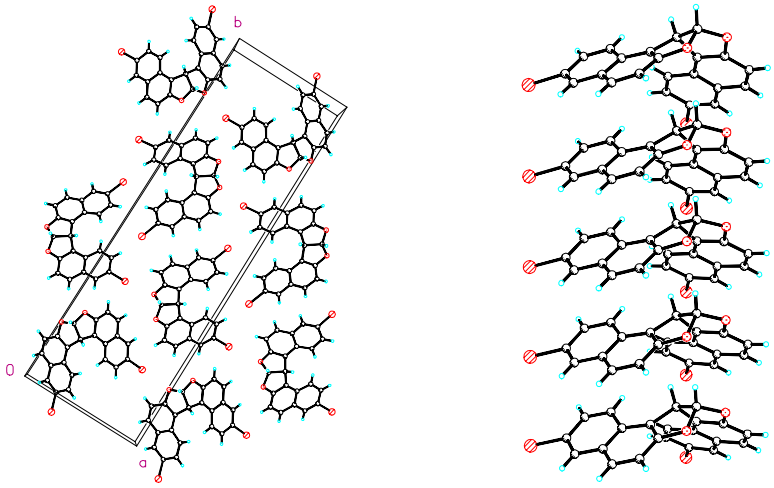

Figure 1.34. The structure of 3,12-dibromo-7*a*,14*c*-dihydro-7,8-dioxa[6]helicene shown as a projection along the polar axis (left) and a polar stack (right).

Even though several attempts were made to grow crystals of all the other derivatives made these molecules in general suffer from an unease towards growth in a nice morphology.

1.2.2.5 The steric effect of stacking in retrospect

The stacking observed for 3,12-dibromo-7*a*,14*c*-dihydro-7,8-dioxa[6]helicene is in spite of the steric effect of the hydrogen atoms in the 7*a* and 14*c* positions. In the case of trioxatriangulene based hats the steric effect of the hydrogen atoms in the 12*c* position was enough to prevent proper stacking. Would stacking still be observed if a large steric demand was placed in the 7*a* and 14*c* positions of the helicene system ? Luckily Jørgen made the 7*a*,14*c*-dibromo-7,8-dioxa[6]helicene (albeit by accident). The steric demand of the two bromine atoms were perfect to provide an answer to this question and as it turned out the molecules do not stack and the most centrosymmetric space group of them all was observed ($P2_1/c$). In figure 1.35 a stereoview of the molecule is seen.

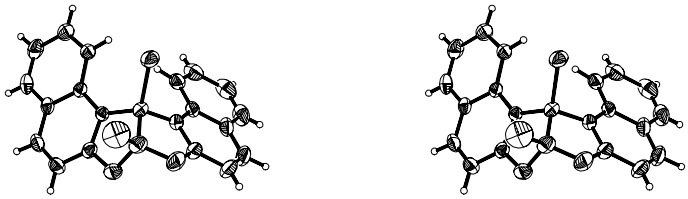

Figure 1.35. A stereoview of 7*a*,14*c*-dibromo-7,8-dioxa[6]helicene. Notice how the steric demand of the bromine atoms makes the molecule quite helical (ORTEP 50% ellipsoids).

It is thus possible to summarise all the information presented in this part of the project and put forward a simple rule of stacking of hat shaped molecules to form polar stacks.

Molecules with a general hat shape that allows for stacking with efficient space filling will form a directed polar stack and crystallise in a polar space group.

This is perhaps in my own words the entire lesson to be learned from all that you have read so far on polar materials. The proposition is not so bold as it would seem as certain geometric requirements have to be fulfilled before the ...*hat shape that allows for stacking*... is observed. The important point is that the interplanar distance of the aromatic part of the hat shaped molecule (if it contains aromatics) is of the order of 3.6 Å. The problem obviously is what to put at the pointed part of the hat where the planes of the aromatic parts meet.

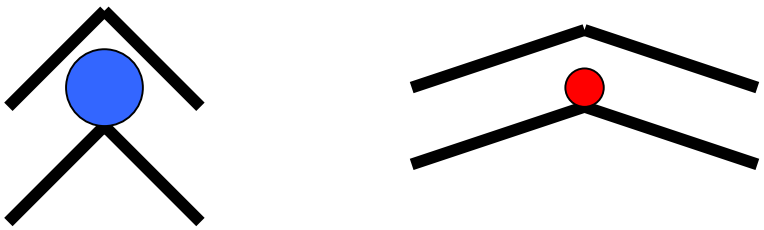

Figure 1.36. An illustration of the steric effect in the stacking of hats. The interplanar distance in the two cases is thought to be identical in the two illustrations. The angle between the planes of the molecules making the hat shape is however different and by a simple geometric argument the space left for a substituent without interfering with polar stacking is a lot smaller for the flat hat than for the high hat, thus wear a high hat!

When choosing what substituent to put where the planes of the hat shaped molecule meet we as chemists can only choose from the periodic table. The only substituents with a small steric

demand for this sort of purpose is the lone pair, hydrogen, (a vacant p-orbital) and perhaps fluorine. As we have seen the lone pair worked well (phosphangulene), hydrogen worked with a high hat like 3,12-dibromo-7*a*,14*c*-dihydro-7,8-dioxa[6]helicene but not so well for a flat hat like 4,8,12-trioxa-4,8,12,12*c*-tetrahydrodibenzo[*cd*,*mn*]pyrene.

1.2.2.6 On the induction of helicity and the largest isotope effect ever seen

The strange structural behaviour of 7,8-dioxa[6]helicene where a varying helical pitch was observed for the different molecules within the asymmetric unit made it obvious that the system exhibits near-helicity i.e. it is somewhat helical but can inter convert between *R* and *S* at room temperature and the degree of helicity can vary according to conditions. What if the atoms (or more appropriately the steric demands of the atoms) in the 1,14-positions were perturbed slightly i.e. what would happen to the structure if they were just smaller than hydrogen or just larger. The smaller version could be a lone pair and the larger version a fluorine atom. But the most subtle change would be deuterium as it is has slightly shorter bond length due to the isotope effect. We would thus expect the helicene to become less helical upon substitution.

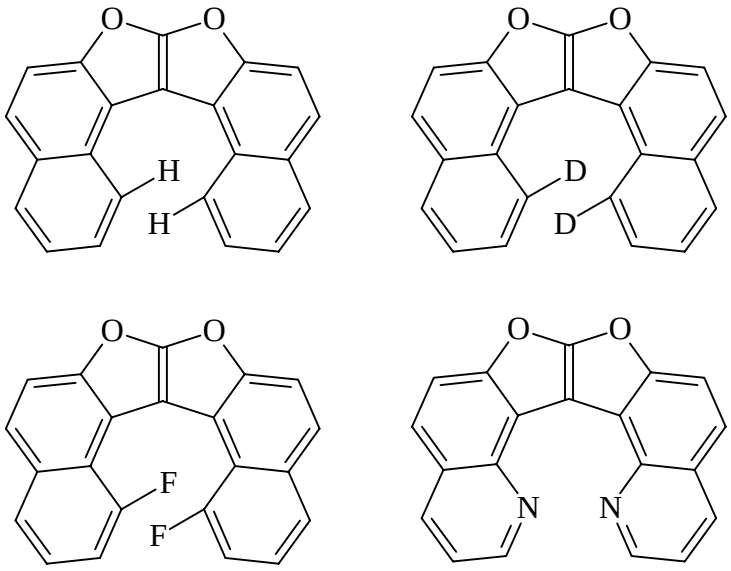

Figure 1.37. The various steric perturbations envisaged. The deuterium substitution turned out to be feasible while the flourinated helicene could not be dehydrogenated. The 7-hydroxy-quinoline did not condense to form the dihydrohelicene, consequently the helicene was never synthesised.

When Jørgen had synthesised the deuterated compound we were ecstatic because the powder diffractograms of the 1,14-hydrogenated and the 1,14-deuterated 7,8-dioxa[6]helicene were different, especially at low angle (2θ) thus making this a potentially large structural isotope effect.

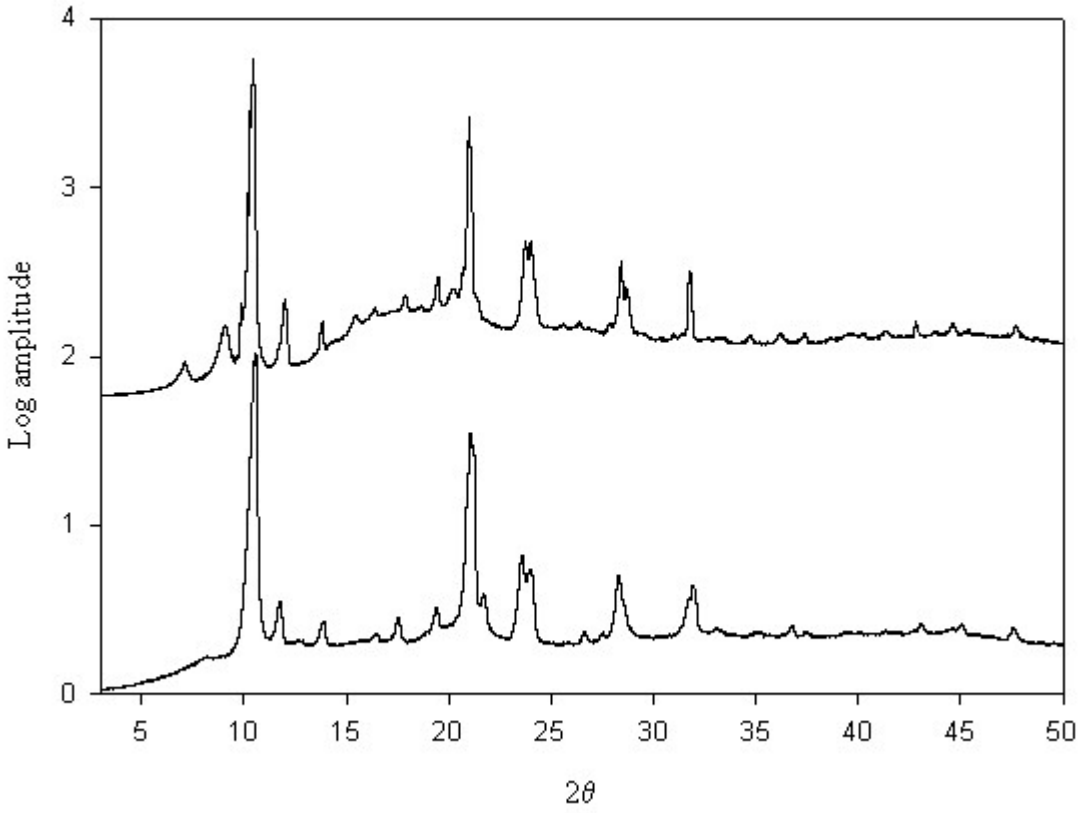

Figure 1.38. Powder diffractograms of the 1,14-hydrogen substituted 7,8-dioxa[6]helicene (above) and the 1,14-deuterium substituted 7,8-dioxa[6]helicene (below). Notice especially the peaks at low 2θ-values for the 1,14-hydrogen substituted 7,8-dioxa[6]helicene.

We found greater difficulty in growing crystals of a quality which would allow for single crystal data collection and when we eventually got there we could not index the crystal in the large unit cell and instead only found the 6 Å axis. Attempts to get a good model at both high and at low temperature failed and what was obtained was essentially the average of the asymmetric unit observed for the superstructure of the 1,14-hydrogen substituted 7,8-dioxa[6]helicene. As we paused for reflection Liselotte Berring recorded a Weisenberg photograph with a very long exposure time. At normal exposure time the superstructure reflections did not show. But at long exposure times they were visible. So in conclusion the deuterated compound somehow exhibited the same superstructure but with a lesser degree of

correlation. The experimental procedure was scrutinised and the differences between the two synthesis were sought eliminated. The synthetic procedure for the deuterium compound had been slightly more elaborate than for the hydrogen compound. The main reason being that 2-naphthol comes in kilos and therefore more sloppy procedures are allowed than for 8-deutero-2-naphthol which comes only in grams and after weeks of hard work. Two parallel synthesis were run identical in every aspect. This gave a new form of the hydrogen compound identical to the deuterium compound with respect to the powder diffractogram. So even though there may be a difference between the structural properties of the two compounds it was not as spectacular as thought at first. We finally found that it was the condition of crystallisation that gave rise to the highly correlated superstructure for the hydrogen containing compound. All the work pertaining to the helicenes have been published and can be found in *Appendix P3* and *P4*.

1.2.3 Pancake shaped molecules as candidates for an organic ferroelectric

1.2.3.1 The molecular system

There is another and interesting story to tell about the 4,8,12-trixoa-4,8,12,12*c*-tetrahydrodibenzo[*cd*,*mn*]pyrene system as it forms carbenium ions of exceptional stability and what is more the carbenium ions are planar, large pancake shaped cationic organic molecules.

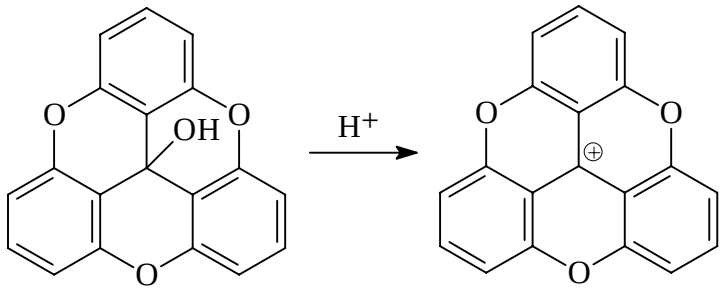

Figure 1.39. The formation of the planar pancake shaped stable carbenium ion under acidic conditions.

The planarity of these carbenium was established quite some time ago by Ib Johannsen and Kamal Boubekeur the results were never published however. At a later stage I became interested in the potential use of these systems as polar dielectric materials. While Type I or Type II molecular materials will nearly always be pyroelectrics and not ferroelectrics these ionic systems could, provided that one of the ions are in a double potential (in this case

assumed to be the anion), exhibit switching behaviour and therefore have ferroelectric properties.

1.2.3.2 The salts

From the study of the hat shaped molecules the starting materials (4,8,12-trioxa-12*c*-hydroxy-4,8,12,12*c*-tetrahydrodibenzo[*cd*,*mn*]pyrene and 2,6,10-tri(*tert*-butyl)-4,8,12-trioxa-12*c*-hydroxy-4,8,12,12*c*-tetrahydrodibenzo[*cd*,*mn*]pyrene) were readily available. Bo W. Laursen had crystals of some salts and I made some more salts until a total of eleven salts were in our hands. The structures were solved and characterised and every single one of them crystallised in centrosymmetric space groups (for a structural discussion see *Appendix P5*). At first however it was thought that the PF_6^- salt actually was non-centrosymmetric i.e. that it was in space group *R*3*c* instead of space group $R\bar{3}c$. This led to data collection and structure solution at many temperatures. The interest was that it seemed to interact preferentially with neighbouring carbenium ions to one side (see the lower part of figure 1.40) and not the other i.e. a double potential with the possibility of switching.

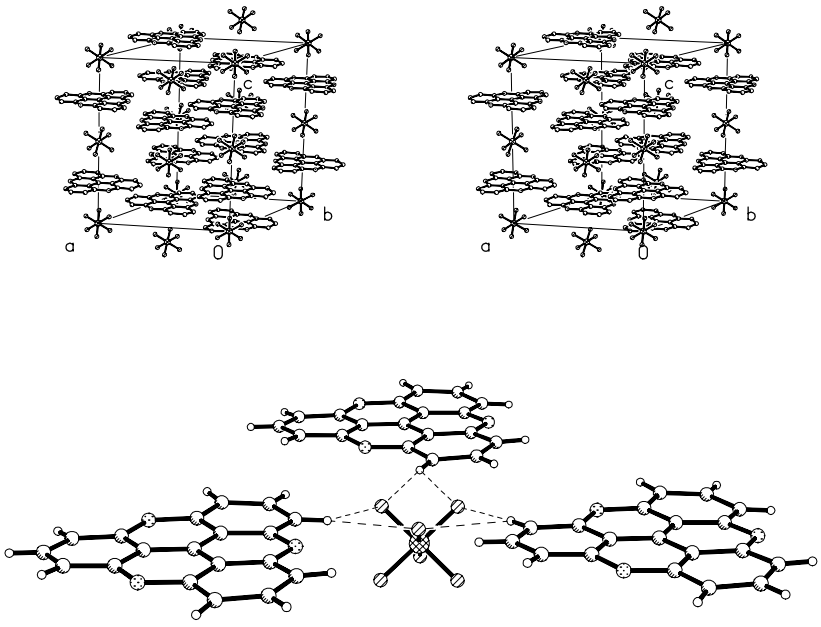

Figure 1.40. A stereoview of the unit cell of the PF_6^- salt showing the PF_6^- ions sandwiched between two carbenium ions and the two layers of surrounding triad carbenium ions (above). A triad of carbenium ions interacting with the PF_6^- ion (below).

Furthermore structure solutions at many temperatures (ten in total) would give the anion movement as a function of temperature thus enabling one to look for the temperature regime where the largest pyroelectric signal could be observed. Intense effort was made to characterise this system as it was thought to be non-centrosymmetric.

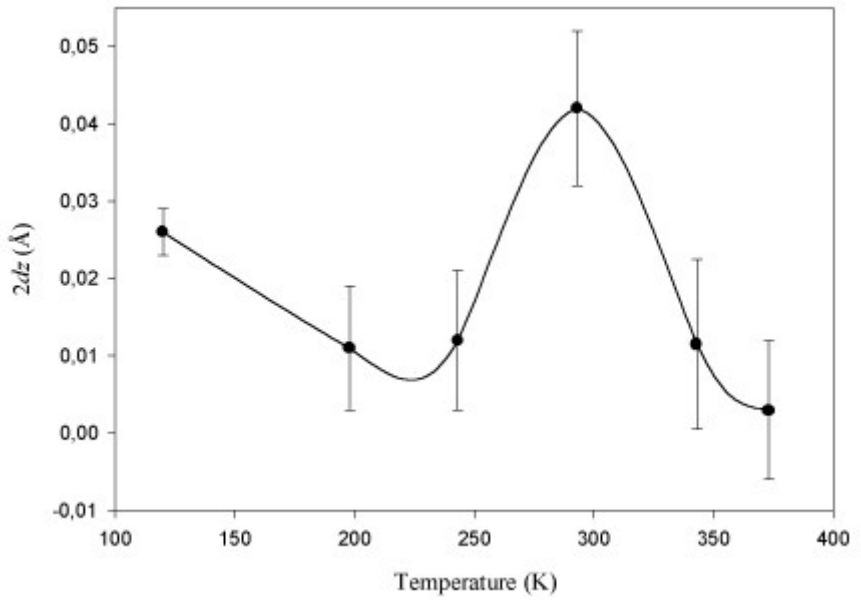

Figure 1.41. A plot of the PF_6^- ion displacement (*dz* represents the displacement of the PF_6^- ion from the central position between two carbenium ions) as a function of temperature when the structure was solved in space group R3c.

From the plot (in figure 1.41) it would seem that a large pyroelectric coefficient should be observed just above and just below room temperature i.e. a large anion movement and thus a large polarisation change. The dielectric permittivity tensor was determined at 35 GHz and attempts were made to pole the material in an electric field at elevated temperature followed by pyroelectric measurements. In spite of severe dedication and intense work I never managed to get a single pyroelectric electron out of crystals of this material. And another problem was the absolute configuration which could not be determined accurately suggesting either racemic twinning or a centrosymmetric space group. Consequently a data set using Cu-radiation was collected (thanks to Flemming Hansen and Henning O. Sørensen at HCØ as there were no inclination to change from an Mo-tube to a Cu-tube at DTU to resolve the problem). The copper data gave the same result and I finally gave in to the fact that the material is centrosymmetric. While a large structural diversity was exhibited by these salts it

was still a possibility to maybe replace the centrosymmetric PF_6^- ions with an anion that had no centre of symmetry and that had the same (or nearly) steric requirements. Everything else being equal this would result in a permanent polarisation. The choice was the trifluoromethansulphonate anion. This ion placed at the same site as the PF_6^- ion in the same structure as the PF_6^- salt would have the negative charge displaced with respect to the centre between the two carbenium ions and therefore a permanent dielectric polarisation. As it turned out however the trifluoromethansulphonate salt crystallised in an entirely different and centrosymmetric manner. As a conclusion to *Section 1.2.3* it is difficult to get non-centrosymmetry when having an ionic system as the system has a larger degree of freedom and the cations and anions can always adopt a centrosymmetric arrangement. Unless one of the ions is chiral and in this case it would have to be the anion. Attempts were made to make salts with a chiral sulphonic acid but no suitable crystals were obtained which is quite puzzling as these salts have a large propensity towards forming large and well shaped crystals. The work presented here on the salts has been published and can be found in *Appendix P5* and *P6*.

1.2.4 Poling of ferroelectrics

1.2.4.1 The principles

The advantage of crystalline Type I or Type II materials is that they crystallise with a given *de facto* polarisation i.e. the polarisation is spontaneous and "as is". Provided that the crystal morphology is known all that is needed for the proper function (i.e. as a detector material) is the correct orientation of the material. With some materials however where there is no spontaneous polarisation to start with but where the polarisation can be introduced by proper treatment the process of poling is employed. After poling the material can be made to exhibit for instance pyroelectric properties as is the case for PVDF which needs such treatment as mentioned in *Section 1.1.6*.

1.2.4.2 The poling procedure

If the material is amorphous i.e. glassy or polymeric a typical poling procedure involves either the deposition of the material onto a suitable substrate followed by the application of electrodes or if mechanical stretching is required (i.e. to reorient polymer chains) the material has to be stretched between electrodes. The process then employs a heating of the material

with the simultaneous application of a large electric field (i.e. of the order of 0.1-10 MV m^{-1}). Upon cooling down in the large electric field the polarisation induced in the material due to molecular reorientations are frozen and the material is polar and will unless heated above a temperature that permits reorientation remain polarised indefinitely.

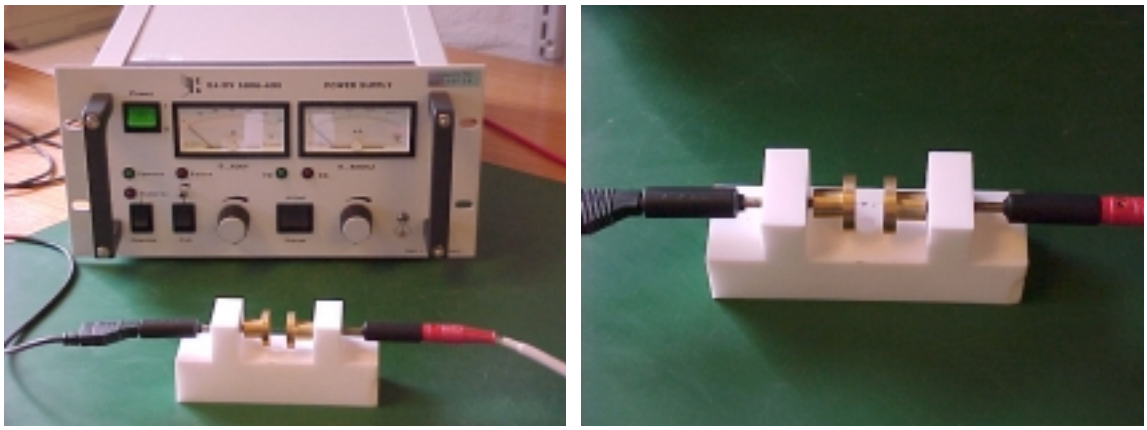

Figure 1.42. A picture of the set-up employed for poling of materials (left). And a close-up of the sample holder right). It is possible to stretch a material between the electrocdes and adjust their proximity and also mount small crystals on a silver wire insert as is just visible to the right.

The set-up shown in figure 1.42 was used in the attempted poling of the carbenium ion salt described in *Section 1.2.3*. The intensity of the field could be adjusted both by varying the distance between the electrodes and the voltage applied. The block is made of Teflon and the electrodes are made of brass. The same set-up was used in the experiment where the 7,8-dioxa[6]helicene was subjected to an applied electric field whilst analysing the polarisation of transmitted laser light as mentioned in *Subsection 1.2.2.3*.

1.2.5 Adamantane type molecules dispersed in polymers as candidates for a ferroelectric

1.2.5.1 The adamantane based molecules

Some small nearly spherical organic molecules are known to rotate in the crystal and form so-called plastic phases. Classical examples are C_{60}, camphor and one phase of HMTA (hexamethylenetetramine). If is was possible to have a near spherical molecule in the solid state that could be made to rotate at high temperature it might be poled. Also if it could be made to rotate it might also be a possibility that it could be made to have two or more preferred orientations i.e. ferroelectric behaviour. A good candidate was thought to be adamantane based molecules which somehow were made dipolar. The reduction of 1,3,5-

trihydroxybenzene using Raney-nickel gives amongst other products the all *cis* 1,3,5-trihydroxycyclohexane[31]. And a condensation of this molecule with triethylorthoformiate gives the now dipolar adamantane derivative trioxaadamantane[32].

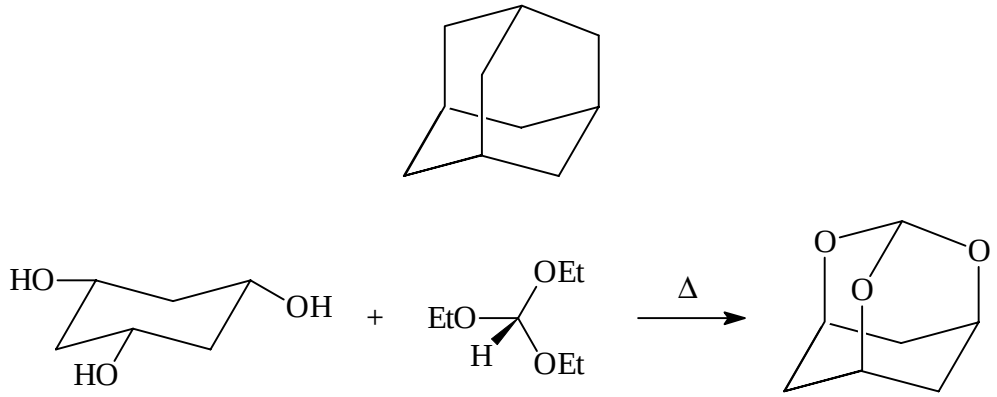

Figure 1.43. Adamantane (above) and the synthesis of the dipolar trioxa-adamantane derivative (below).

Many of the adamantane derivatives based on all *cis* 1,3,5-trihydroxycyclohexane are known and they were all made a long time ago.

1.2.5.2 Trioxaadamantane dispersed in polystyrene

The obvious way of answering the question whether these molecules would rotate if dispersed in a polymer matrix was by means of dielectric spectroscopy at high frequency. The process of answering the question was considered an experimental exercise and was used in conjunction with a course held by Peter Sommer-Larsen on Dielectric spectroscopy. The method of choice was for me to decide and I chose the microwave cavity perturbation method. The cavity perturbation method relies on resonance in a cavity. Resonance imply a very narrow frequency range and to fulfil the term spectroscopy a clever design had to be made so that the complex permittivity could be determined at several frequencies. The dispersion of the real part of the permittivity would give information on any relaxation phenomena taking place in the frequency interval covered and the complex part would give information on the loss associated with the relaxation. Since dielectric relaxation phenomena as mentioned during the introductory part normally cover a very large frequency span it was not possible to rely on any relaxation phenomena but instead prepare two polystyrene samples

[31] Stetter, H.; Steinacker, K. H. *Chem. Ber.* **1952**, *85*, 451.
[32] Stetter, H.; Steinacker, K. H. *Chem. Ber.* **1953**, *86*, 790.

one with and one without trioxaadamantane. A comparison of the results would give information on the contribution towards the polarisability made by trioxaadamantane. The cavity was thus designed to in principle cover nearly a decade (8 GHz from 8.5 to 16.4 GHz) but in reality reliable measurements could only be made at four different frequencies and covering only 5.6 GHz (from 9 to 14.6 GHz). The frequency span covered was however enough to justify usage of the term spectroscopy. The way of achieving this range was by making a multi-resonant cavity which has been shown in figure 1.44.

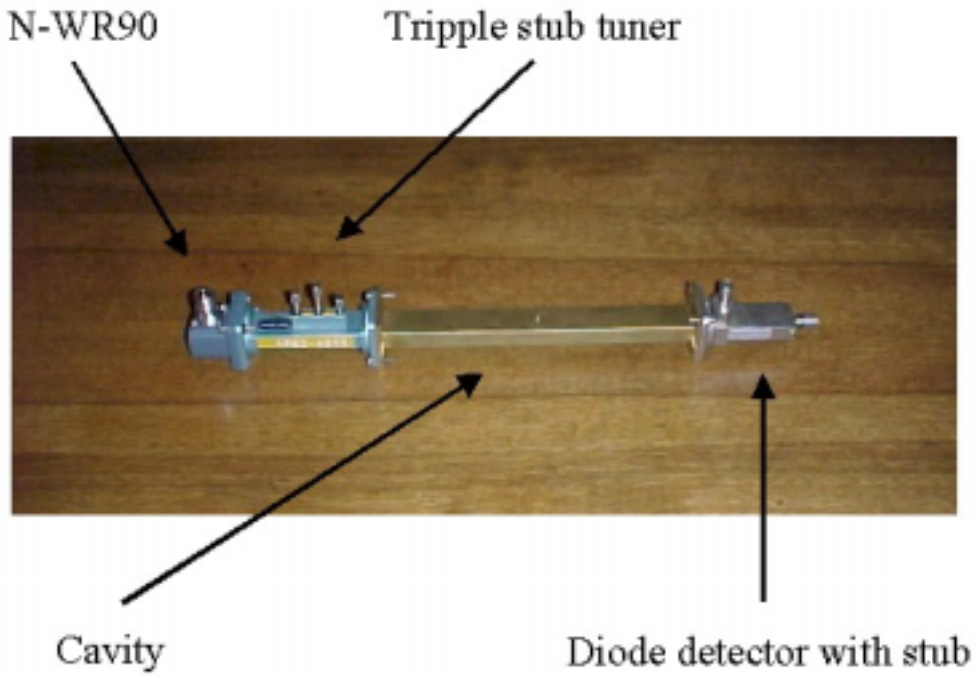

Figure 1.44. A picture of the X-band microwave cavity used for the determination of the complex dielectric constant of trioxaadamantane dispersed in a polymer matrix. The tiny hole where the sample is inserted can just be seen towards the middle of the cavity section.

The polymer matrix chosen was as mentioned polystyrene and the reasons for the choice were several. Firstly polystyrene does not have excessive loss in that frequency range, secondly it is readily radical polymerised by using ionising radiation thus not introducing impurities as would be done using a chemical initiator and thirdly it can me machined afterwards to precision although it is quite brittle.

1.2.5.3 The samples and the results

Two types of samples were prepared by making a solution of polystyrene in styrene. Using that solution in the polymerisation reaction on its own or with trioxaadamantane yielded the

two different samples used in this study. It was found that the best way to prepare the samples were by polymerising the mixture in closed syringes. This circumvented the well known problem of polymerisation shrinkage which was reduced by using the polystyrene/styrene solution as a prepolymer. After the polymerisation the syringes with the polymer could be fastened in a lathe and the desired sample shape could be made. Small rod shaped samples (3 mm in diameter) were thus made and measurements performed. Excruciating care was taken in preparing the samples in an identical manner i.e. they were polymerised very close to each other to avoid them getting different radiation doses and they were mechanically identical with a precision better than 0.05 mm. The only thing not known was whether trioxaadamantane was subject to radiation damage. The microwave measurements were repeated several times and were quite consistent even though an explanation for the odd dispersion behaviour can not be given the results show that the addition of trioxaadamantane increases the value of both the real part and the complex part of the permittivity which means that it either couples in some way to polymer rotation or that it most likely rotates in itself.

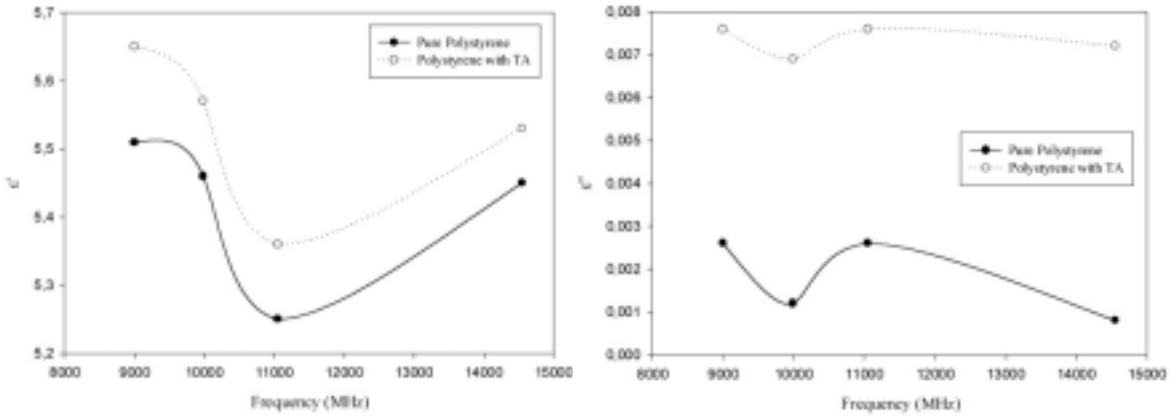

Figure 1.45. The real part and the complex part of the permittivity determined using the X-band multi resonant cavity designed for the purpose of this experiment for samples of polystyrene and polystyrene containing trioxa-adamantane.

This concludes the section on adamantane based molecules and their dielectric properties and behaviour.

1.3 Pyroelectrics on surfaces

The first part of the chapter described the machinery, the second part described the materials and this third and final part describes the attempt to produce! Many people have been involved and have aided greatly to this part of the project most significantly perhaps Torben Kjær, Niels B. Larsen, Lene Hubert and Robert Feidenhans'l but also the people in Leeds Adam Robertson and Rasmita Raval.

1.3.1 The deposition of molecules onto surfaces

1.3.1.1 The idea

While many ferroelectric materials are used in detector systems they require poling and often a careful control of the temperature. If a molecular Type I material could be used so that advantage was taken of the ability of the material to always give the maximum possible polarisation without the need for poling then some technological problems would have been solved. Since the material would be molecular then a miniaturisation would be possible provided that the material could somehow be self assembled in place. For instance a pyroelectric material generates an electric field when its temperature is changed if it could somehow be self assembled into a device which is sensitive to an electric field then a miniature detector could be obtained that did not require any difficult treatment i.e. the tedious growth of high quality crystals followed by the cutting of the crystals perpendicular to a given crystallographic axis, poling, mounting etc. or the complicated mechanical treatment of a polymer with heating, stretching and poling followed by a delicate incorporation of the polymer into the device. A device sensitive to an electric field is well known and it is called a FET or field effect transistor. It relies on the electric field that is set up between the so-called GATE and SOURCE for amplification (i.e. detection) as opposed to a typical bipolar transistor where it is a small current which is amplified. In *Part 1.1* it was made clear that the pyroelectric response was transient and that relatively little charge was generated. If one had to rely on the field it would have to be a high impedance system so that the pyroelectric charge stays for as long as possible or desirable. Such a device also exists it is the so-called MOSFET from metal oxide semiconductor field effect transistor. It relies on a thin layer of SiO_2 on the GATE structure making it a very high impedance device thus ideal for our purpose. The aim was then to be able to deposit a molecular pyroelectric material on the surface of a MOSFET GATE. Since it was not practical for experimental purposes to use the

GATE of a MOSFET for the studies a model system resembling the MOSFET GATE surface was employed so that success with the model system would be likely to also succeed with a real MOSFET GATE. The model system was simply a thin SiO_2 layer grown on a *p*-doped silicon wafer backed with aluminium (provided by O. Hansen at MIC). A deposition onto the surface would thus allow for a surface characterisation and for pyroelectric measurements. It all relied on getting the material to grow on the surface with the polar axis perpendicular to the surface otherwise it would not work as a detector. There were of course other potential problems such as even growth of the pyroelectric on the surface and single phase formation i.e. the polarisation would be directional with respect to the surface as it would not be possible to reverse the polarisation once the material had been deposited onto the surface. It would have to be a case of a spontaneously self assembled highly directional polar material with the polar axis normal to the surface or at least a significant component of the polarisation normal to the surface.

1.3.1.2 The conditions of deposition

To be useful in the event of further development the choice of conditions for the deposition had to match the conditions under which semiconductors are normally handled. This involves the use of UHV (ultra high vacuum) techniques. Even though the principles of the idea outlined above are simple there were a lot of questions that needed answering before an evaluation of the possibility of the use of a molecular organic material could be used in a MOSFET based detector system. In this respect it was fortunate that I was awarded a small sum of money for the purpose of carrying out some research abroad (Emil Herborgs Legat) and I chose to spend the money on a trip to Leeds with Rasmita Raval and Adam Robertson to attempt the deposition of a molecular pyroelectric material under UHV conditions and at the same time make use of their expertise within the field of IRAS (infrared reflection absorption spectroscopy) to quantify the deposition process and perhaps even get some surface structural information. The choice of deposition strategy was to sublime the material from a capillary and form a molecular beam. By the proper placement of the target surface in the molecular beam one could envisage growth of the material on the surface. This is thus where the story starts.

1.3.2 Phosphangulene on surfaces

1.3.2.1 The choice of material and the IRAS experiment

The material would have to be a Type I material and preferably a stable material that sublimes well. If it further was a good pyroelectric and a structurally simple molecule this could be an advantage at a later characterisation stage. The obvious choice of material was of course phosphangulene and the first step was to be the establishment of whether it could be deposited onto a surfaces under UHV conditions. The target surface was a Ni(111) crystal which has a hexagonal arrangement of the atoms exposed at the surface. The experimental set-up and the run of the experiment should just be mentioned. The UHV chamber had been baked just before the experiment was started (the baking procedure consists of heating the entire UHV chamber to between 150 and 200 ^{o}C for at least one day while pumping thus effectively degassing the species adsorbed on the inside of the chamber. A good UHV can then be achieved which lasts for as long as the introduction of impurities is kept to a minimum. During the course of experiments however impurities are introduced and the baking procedure has to be repeated now and again). The phosphangulene was placed in a small capillary that could be heated. The opening of the capillary was made to point at the Ni(111) single crystal which had been heated sputtered and annealed to give a clean surface. The idea is then to reflect the IR-beam of the Ni(111) crystal surface at near grazing incidence. For various physical reasons that would be too involved to mention here only the vibrational modes of the molecules with a component normal to the surface are seen in the IR spectrum. Furthermore the IR absorption bands are normally red or blue shifted with respect to the bulk IR absorption bands giving important information on the orientation of the molecule with respect to the surface and the mechanism by which it attaches to the surface. A normal procedure is thus to slowly dose the molecules onto the surface and if they adsorb then any coverage dependence in the adsorption process can be monitored by recording multiple spectra which can give important hints on the nature of the molecules on the surface. In brief it was the ideal way to test whether phosphangulene at all adsorbs under UHV conditions as the IR spectrum of the adsorbate is obtained and since some structural information can under favourable conditions be obtained it was the method of choice. Another important technique which was also available was LEED (low energy electron diffraction). In this technique an electron beam is fired at the surface and the back scattered electrons are monitored on a fluorescent screen. The technique gives information on the periodic distribution of molecules or atoms on the surface

and it is very surface sensitive probing only the structure of the outermost layers. It is also of use before the deposition experiment is started as it can be tested whether it really is a Ni(111) surface that one is looking at. Once the material has been deposited it is possible to see the periodicity of the material if applicable.

1.3.2.2 IRAS and LEED results

It was mentioned that a baking procedure was necessary to clean the chamber and obtain a good vacuum. This procedure is problematic when dealing with materials like phosphangulene that sublimes significantly at temperatures below 100 ^{o}C and considerable above 100 ^{o}C. In Leeds the problem had been solved by having a gate valve where the sample assembly could be attached at a later stage after baking. After baking when the molecular dosing assembly was attached and pumped down it could be partially baked leaving the sample compartment at room temperature. Afterwards the deposition assembly could be introduced into the main chamber by opening the gate valve. In figure 1.46 the bulk IR spectrum is shown along with the IRAS data. It is noteworthy and highly unusual that the IRAS spectrum closely matches the bulk IR spectrum. Furthermore there seemed to be no spectral evolution or coverage dependence of the IRAS spectra. The LEED experiments did not yield any Bragg scattering and the Ni(111) underlying layer was observed at first but then gradually as coverage increased the discrete scattering disappeared. While this first experiment was pleasing in that phosphangulene could be deposited under high vacuum conditions (onto Ni(111) at least) there were some facts that could not be explained i.e. why is only the bulk IR spectrum observed and why could LEED scattering from the underlying Ni(111) surface be seen for quite a while during dosing. It was decided based on this result to carry on with the *phosphangulene on surfaces* project.

1.3.2.3 Modifications to the MBE chamber at Risø

At home (Risø) we have a rather well equipped UHV chamber but at the time this work was initiated there were no facility which permitted the deposition of organic species onto surfaces in the chamber. So one had to be constructed, and in constructing, a few salient features had to be encompassed. Baking had to be possible with subsequent introduction of the deposition assembly, translation of the deposition assembly would be an advantage such that the sample

to substrate distance could be chosen at will, easy access and the possibility of applying several different samples (not at the same time but in sequence).

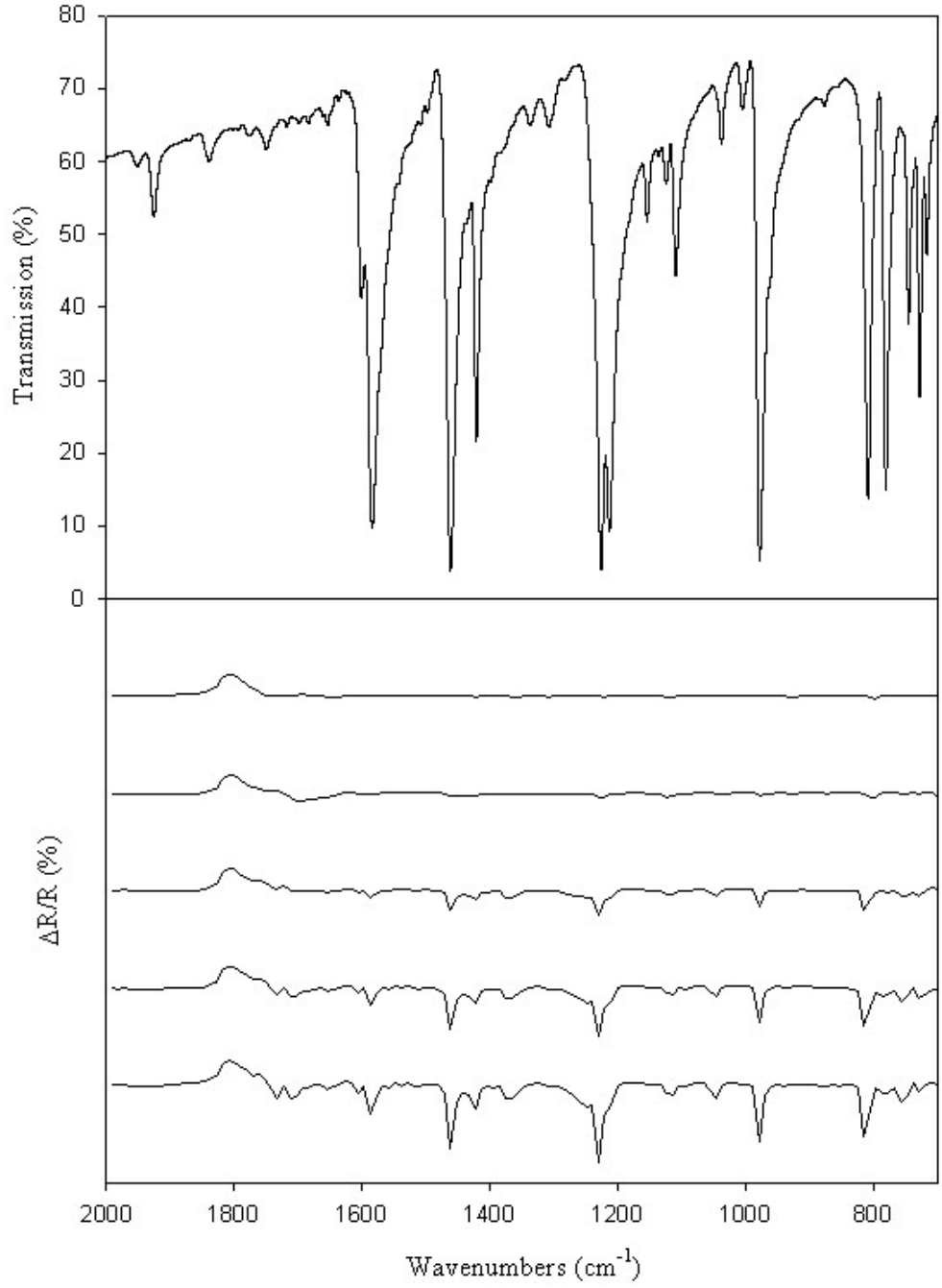

Figure 1.46. The bulk IR spectrum of phosphangulene recorded in a KBr disc (above) and the IRAS data. The spectra were recorded at times of 0.75, 5, 15, 25, 35 min. after the deposition was started (starting from above).

With supervision by Torben Kjær I constructed an organic molecule deposition assembly which is shown on the following photographs.

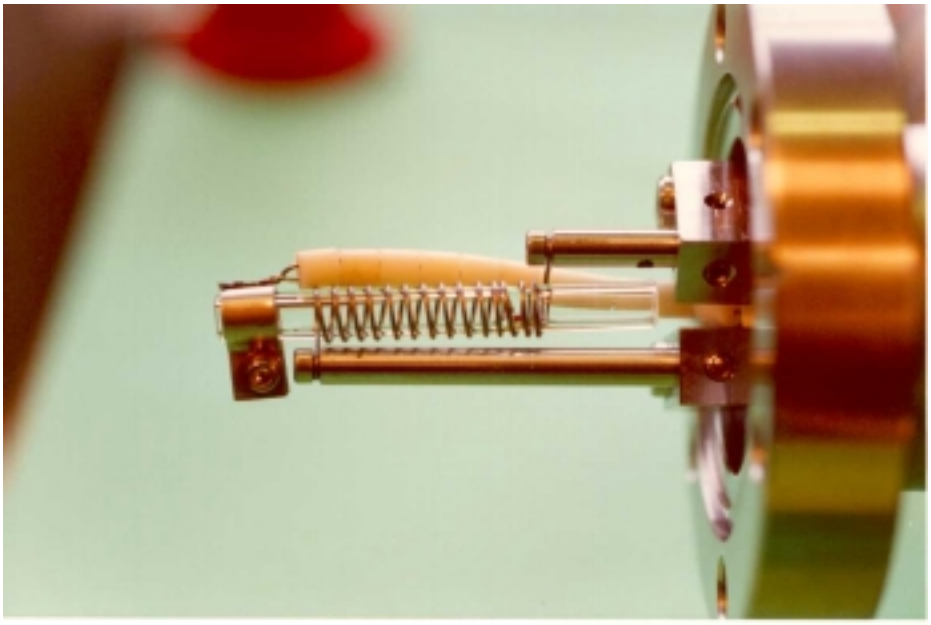

Figure 1.47. A close-up picture of the sample holder. The quartz capillary holds the sample to be deposited. The capillary can be heated by the surrounding spiral (tungsten wire). The temperature is measured at the opening of the capillary (the white porcelain insulators guide the thermocouple.

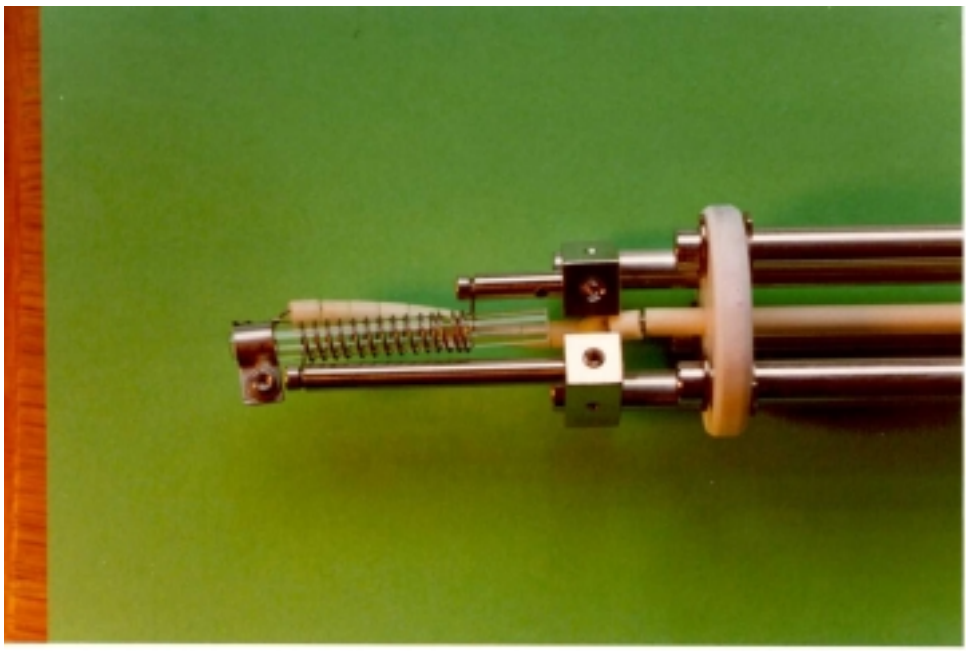

Figure 1.48. A picture showing the mounting of the sample holder. The stainless steel rods are kept in place by the large white disc which is also an electric insulator two of the support rods conduct the current for the heater.

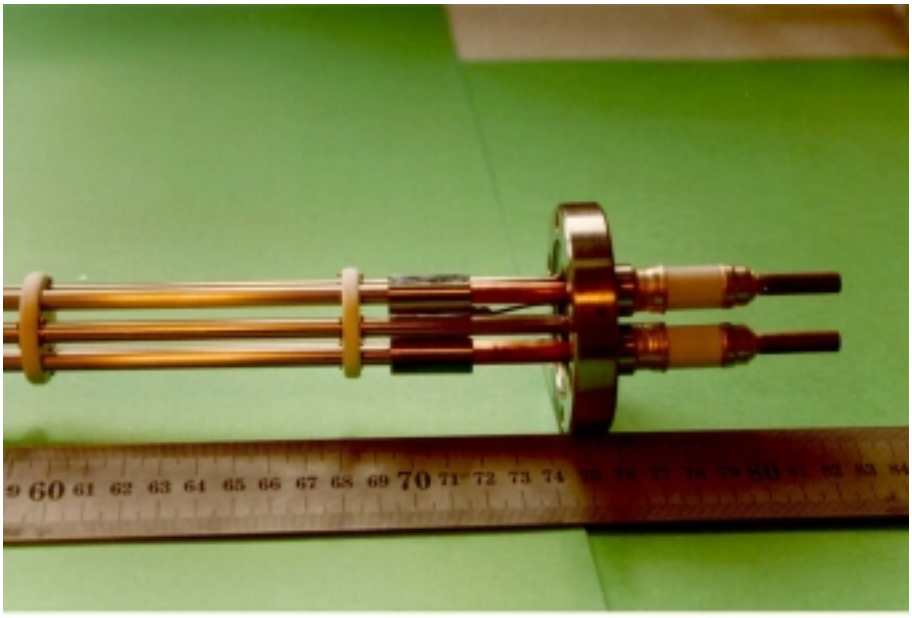

Figure 1.49. The flange end of the assembly. The high vacuum flange with the feed through for the heating current and thermocouple is shown.

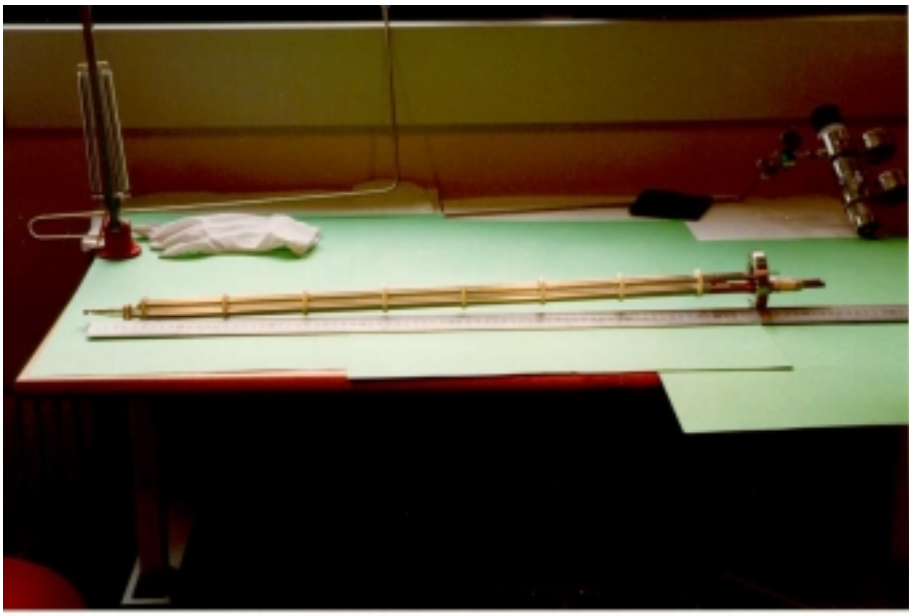

Figure 1.50. A picture of the entire sample holder that goes inside the translation and general assembly.

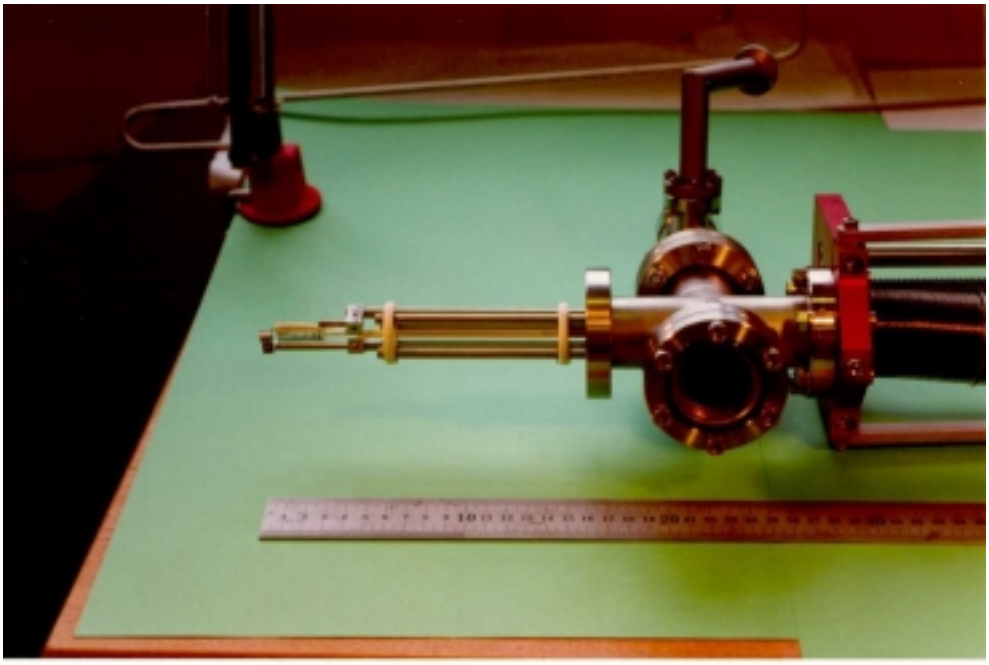

Figure 1.51. A picture of the deposition assembly mounted in its housing and high vacuum translation .

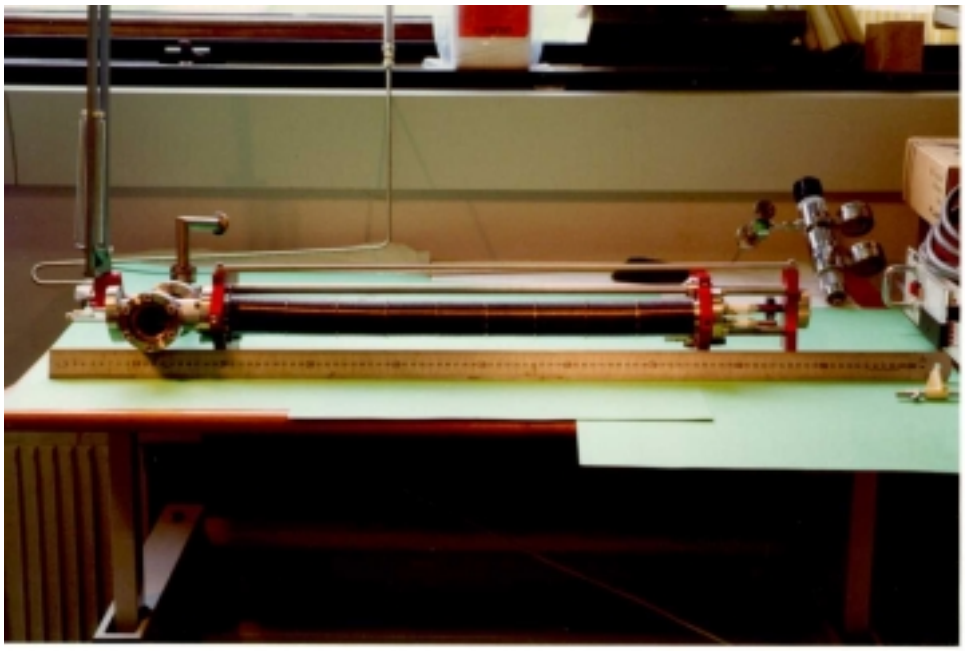

Figure 1.52. The entire assembly and housing with the long translation.

Figure 1.53. The entire assembly mounted on the UHV chamber. Notice the hose attached for separate pumping.

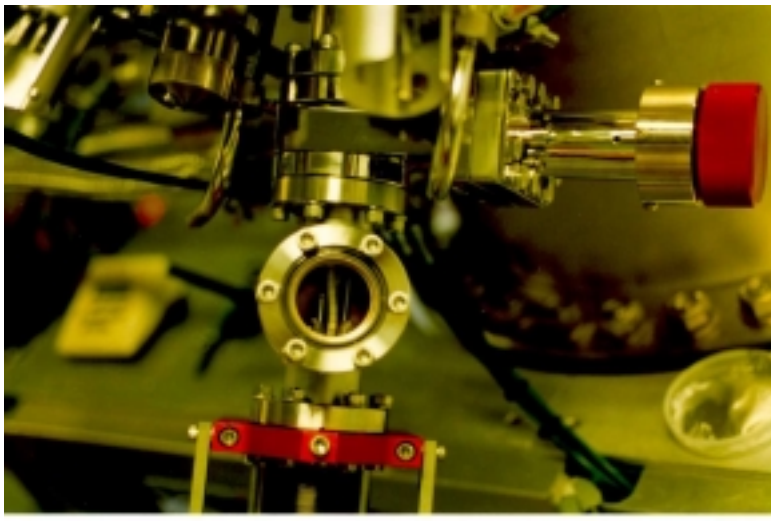

Figure 1.54. A close-up of the mounted set-up. It is possible to inspect the sample before (and after) introduction into the chamber. The large valve (upper part with large red knob in the upper right corner) opens and closes between the set-up and the main UHV chamber.

With the set-up outlined in the photographs above it was made possible to deposit phosphangulene onto the surface of choice.

1.3.2.4 Studying the deposit with SEM, ESCA and AFM

Following on from this grand scale deposition of phosphangulene onto various surfaces was commenced. To mention the initial lot: Au(111), Au(111) with a self assembled monolayer of dodecyl-1-thiol, Al_2O_3(100), and SiO_2. By using SEM (scanning electron microscopy) it was quickly realised why the IRAS experiments gave the results obtained and that regardless of choice substrate surface (or at least regardless of the choices we made) the same surface structure was observed. A representative is shown in figure 1.55.

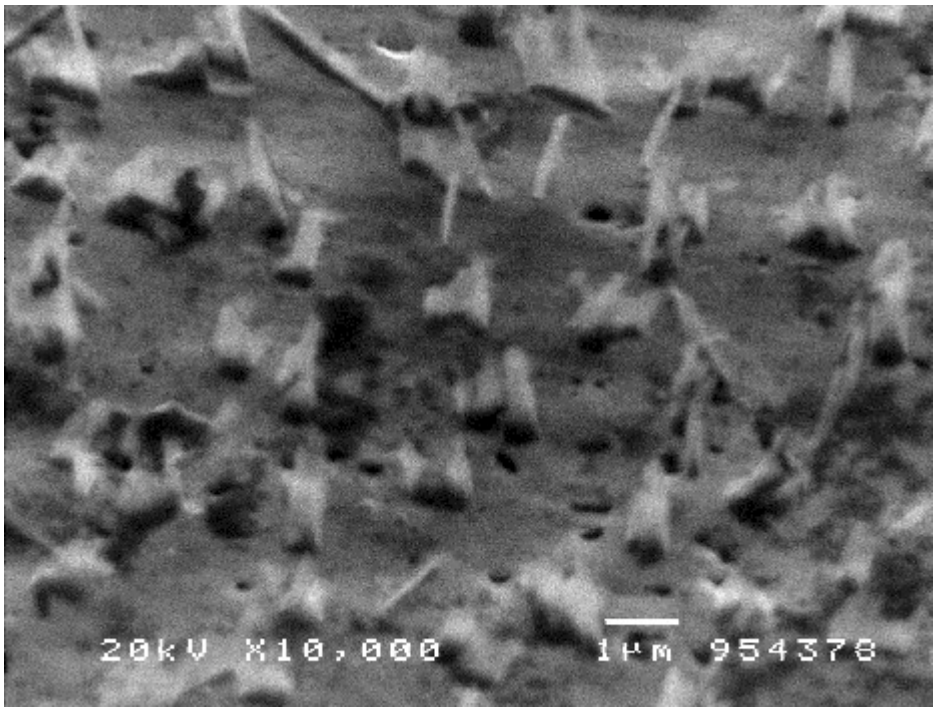

Figure 1.55. A SEM image of the deposit on Au(111). Notice the crystallites that are formed leaving the Au(111) surface partially exposed.

The formation of crystallites explains why the IRAS spectra corresponded to the bulk IR spectra as most of the molecules on the surface effectively are bulk and very few molecules are truly adsorbed. To further analyse the deposit on the surface ESCA (electron spectroscopy for chemical analysis) was used to characterise freshly prepared samples. An added feature of the MBE chamber at Risø is that the samples prepared can be transferred to a transporting container so that the substrate with the sample could be taken to the ESCA without the

unnecessary introduction of impurities from the atmosphere. With the experiments on Au(111) surfaces it was found that the phosphorous content as indicated by the ESCA analysis was very low compared to what was expected for phosphangulene. At low coverage (few crystallites) very little phosphorous could be quantified. At the same time a large signal from gold was observed consistent with the idea that there were areas of the Au(111) surface that were exposed and areas that were covered with crystallites. When the surface was the SiO_2 semiconductor model surface a much better agreement between the phosphorous and the carbon content was obtained thus consistent with the idea that phosphangulene was the adsorbate. Silicon was however also observed even at large coverage so the crystallites still left some of the substrate surface exposed. The choice of method to finally prove that growth of an even layer of phosphangulene was not possible was AFM (atomic force microscopy).

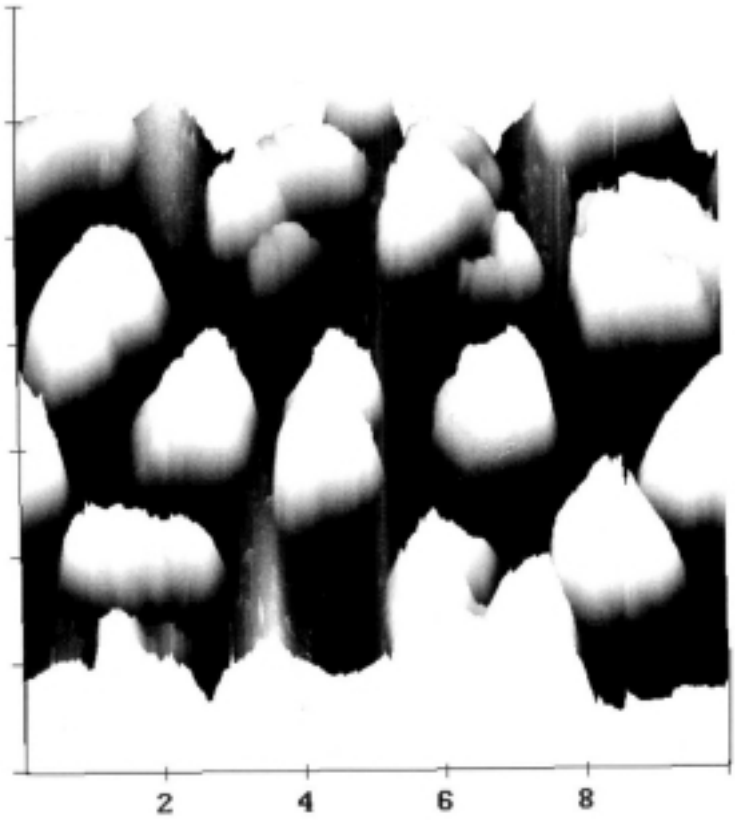

Figure 1.56. An AFM image of phosphangulene on SiO_2. Notice the distinct island formation and that the aspect ratio of the image makes the islands look taller then they are (xy-scale = 2 μm/div, z-scale = 730 nm/div). The Q-balance reading gave en equivalent phosphangulene layer thickness of 800Å for this experiment.

From AFM it was again clear that the layer was not even but the concept of crystallites changed a little and perhaps islands of phosphangulene instead of crystallites would be a more appropriate term. The layers grown with phosphangulene on surfaces were nevertheless not even regardless of how the layers were characterised. Another point is the thickness of the deposited layer. There is a Q-balance in the UHV chamber which in brief is an oscillating quartz crystal exposed to the inside of the chamber. If placed in the molecular beam molecules will deposit on the surface of the oscillating crystal thereby altering its resonant frequency which can be related to the thickness of the layer provided that it is even and that its Z-ratio is known (the Z-ratio is a dimensionless number which relates the shear constants of the deposited material to that of quartz). In all experiments the Z-ratio was set equal to one as it is not known for the materials used in this study. If the Q-balance is then placed where the substrate will be placed during deposition it is possible to monitor the flux of the molecules to be deposited i.e in units of Å s^{-1}. In this way one can get a good idea of the exposure time required to get a layer of a given thickness. The only constant that need experimental determination (i.e. by means of AFM) is the constant that relates the Q-balance thickness reading to the actual thickness of the layer which is not necessarily related to the Z-ratio although it should be under ideal conditions. It is also a bit difficult to give a layer thickness for phosphangulene as it grows in crystallites and nothing is known about how the crystallites ripen in time i.e. the crystallites could grow quickly to a height of 1 μm and then upon continuing the deposition grow in volume but not in height which makes the concept of layer thickness meaningless. What could perhaps be measured is the weight of material deposited for a given area and then with a detailed knowledge of the growth/time properties it would possible to say something about the state of the surface given the weight of material deposited in a given time.

1.3.2.5 Pyroelectric measurements

Even though the layers were highly irregular and polycrystalline it could be that the crystallites or islands were all growing directionally. One way to test this would be pyroelectric measurements. If the crystallites were oriented at random no pyroelectric signal would be observed. The same applies if the growth is directional but with an even amount of crystallites with the positive and negative *c*-direction perpendicular to the surface. However if there is a tendency for crystallites to grow in a directional manner from the surface (i.e. if all

the phosphorous atoms are pointing towards the surface) then there is hope in spite of the unevenness of the layer. An advantage in this case is that a large electrode area can be employed in principle allowing for the measurement of a pyroelectric signal up to two orders of magnitude weaker than for bulk phosphangulene. Furthermore since the polarity of the signal is measured it would be possible to determine which orientation of the molecules that is predominant. For this purpose various electrodes were deposited on top of the phosphangulene layer. Several metals were attempted (Au, Cu, Al and Ag) and silver turned out to be best as it evaporates at a relatively low temperature and it is quickly deposited. The problem with the deposition is that a Knudsen cell is used which is very hot (approx. 1000 ^{o}C). During the deposition of the metal on top of the relatively volatile phosphangulene heat is radiated from the Knudsen cell thus heating up the substrate and in a few instances the heat simply made the phosphangulene evaporate from the substrate surface before the electrode had been deposited. In the actual pyroelectric measurements a circular 2500Å silver electrode with a diameter of 2 mm were deposited on 800Å phosphangulene layers (i.e. 800Å indicated layer thickness). The surfaces will have looked like the AFM image shown in figure 1.56. Subsequent measurements with a parallel capacitor of 150 pF gave signal voltages of around 8 mV showing some decrease with the number of thermal cycles performed. On heating or cooling 45 degrees a pyroelectric coefficient of 0.01 $\mu C\ m^{-2}\ K^{-1}$ was obtained thus less than a percent of what would have been obtained with a phosphangulene single crystal. These data have to be considered with some care as there are many unknown sources of error i.e what is the true or effective surface area of the electrodes, how much has the process of evaporation influenced the structure of the surface layer and most importantly what is the angle between the polar axis and the surface. What can however be concluded is that there is a pyroelectric response from the surface and importantly that the signal is negative when heating (with respect to the semiconductor side of the construct).

Figure 1.57. The orientation (or at least predominant) of phosphangulene on the surface of SiO_2 as determined by pyroelectric measurements.

This means that the orientation of the molecules with respect to the surface is with the phosphorous pointing away from the surface or at least that there are more molecules with phosphorous pointing away from the surface than against the surface (in obtaining this particular direction of the molecules the direction of the molecular dipole moment given in *Appendix P2* has been utilised). This conclusion may hold some of the explanation for the polycrystallite formation as it would be expected that a phosphangulene molecule placed as above would be mobile on the surface as has been shown earlier for similar albeit a bit larger systems[33]. The molecules when impacting with the surface could then move around until they reach a crystallite which has somehow nucleated and attach there thus increasing the size of the crystallite and causing preferential growth in localised areas rather than growth on the entire surface in an even layer. Since the time scale of the crystallite formation is not known it could be an electrostatic effect from the polarised material if for instance the growth process was quicker than the discharging of the newly grown polar crystallites the oncoming molecules would sense the powerful electric field generated by the crystallites and orient with respect to the crystallite generated electric field thus preventing growth in the vicinity of one crystallite. This could also explain the relatively even distribution of crystallites.

1.3.3 Thiophosphangulene and homogenous layers

1.3.3.1 The stratagem

The problem of the growth of uneven layers had to be solved or at least a solution had to be sought. If this part of the project employing phosphangulene should have any chance of success even layers would have to be grown. The question of how to make phosphangulene (which obviously prefers to grow unevenly) grow in an even fashion could be attempted answered by preparing the substrate surface so that it mimics or looks like the surface of a giant phosphangulene crystal to the oncoming phosphangulene molecules. The idea of using the SAM on the gold surface was an idea along these lines but it had to look more like phosphangulene itself i.e. it had to be hat shaped. The concept would be to synthesise long chain compound with a hat shaped molecule at one end and a thiol at the other. In that way a SAM could be made that would expose the bottom of a hat shape at the surface. To overcome

[33] Gimzewski, J. K.; Joachim, C.; Schlittler, R. R.; Langlais, V.; Tang, H.; Johannsen, I. *Science*, **1998**, *281*, 531-532.

the voids created due to the differently sized end groups an auxiliary thiol without the hat end group could be added to fill in the gaps.

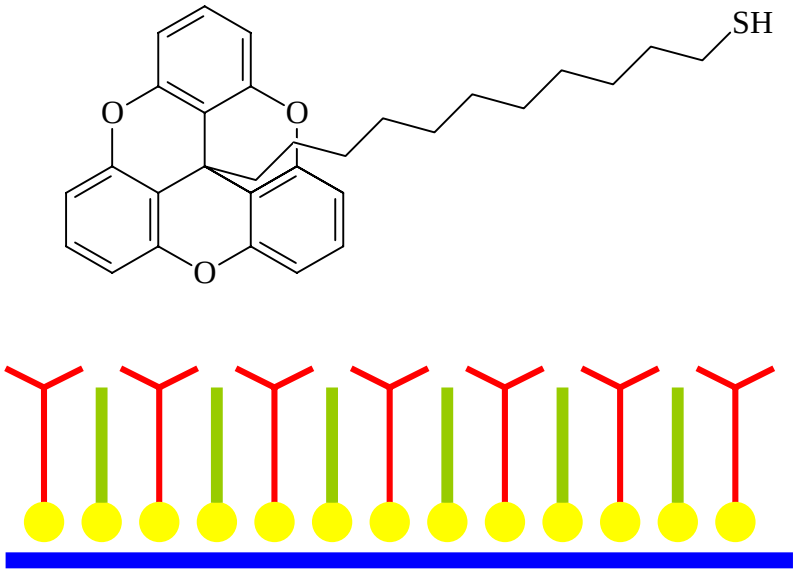

Figure 1.58. A proposed hat shaped surface reshaping agent (above). Provided that a SAM could be made perhaps with dodecyl-1-thiol as auxiliary the surface would appear like a large crystal of hat shaped molecules. Schematic drawing shown below with the surface reshaping agent (red) auxiliary (green), gold surface (blue) and attachments (yellow) i.e. sulphur.

There are many reasons as to why the proposition outlined above could turn out a failure. Firstly the synthesis would not be as easy as it might seem, secondly the idea of having a mixed SAM would rely on some yet unknown and unexplored properties of mixtures of thiol based SAM's on surfaces i.e. would the two different thiols mix etc. thirdly the trioxatriangulene based hat is a lot less hat shaped then phosphangulene so phosphangulene itself might miss the point and not like the surface.

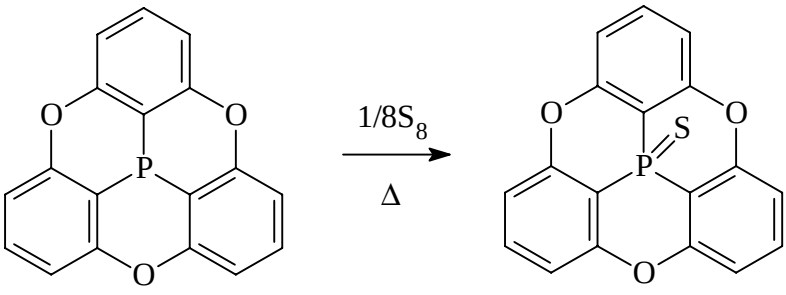

Figure 1.59. The sulphur containing phosphangulene based surface reshaping agent. The synthesis is simple and yields beautiful crystals when phosphangulene and sulphur in equimolar amounts are heated at 200 ^{o}C in a sealed tube.

It was therefore decided to make a less fantastic alternative based on phosphangulene itself and containing sulphur. While the molecule outlined above is not as elegant as the mixed SAM approach (in my eyes anyway) it does have advantage of ease of preparation, greater similarity to phosphangulene and simpler conceptually.

1.3.3.2 The P-sulphide

The 4,8,12-trioxa-12*c*-thiaphospha-4,8,12,12*c*-tetrahydrodibenzo[*cd*,*mn*]pyrene molecule was easily prepared and the crystal structure was solved. It was found to crystallise in the centrosymmetric space group *Pbca* as expected from the discussion of the perturbation of steric demands on hat shaped molecules given in *Part 1.2* and in *Appendix P1*. It is noteworthy that the P-sulphide compound differs from the P-oxide with respect to space group and packing arrangement they are however similar.

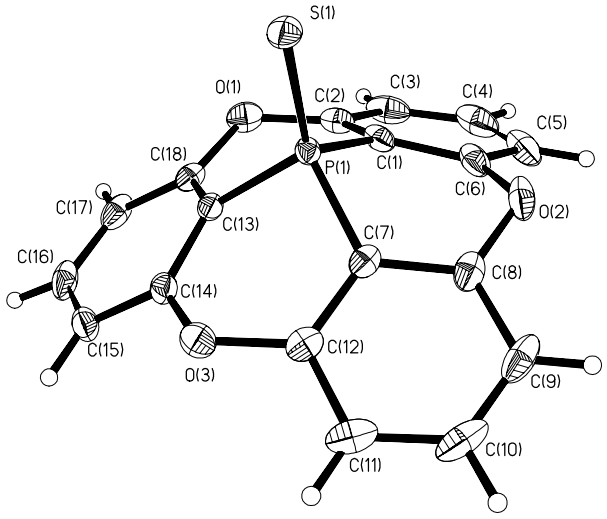

Figure 1.60. An ORTEP drawing (50% ellipsoids) of 4,8,12-trioxa-12*c*-thiaphospha-4,8,12,12*c*-tetrahydrodibenzo[*cd*,*mn*]pyrene.

1.3.3.3 The P-sulphide on surfaces

The deposition of the P-sulphide onto surfaces was first attempted with a polycrystalline gold surface using the classical methodology for preparing thiol based SAM's on gold by submerging the gold substrate in an ethanol solution of the P-sulphide. It however proved unsuccessful and instead UHV deposition was attempted and it worked. More importantly

even layers were obtained that completely covered the surface. The layers were even judging from AFM, SEM images and also by visual inspection.

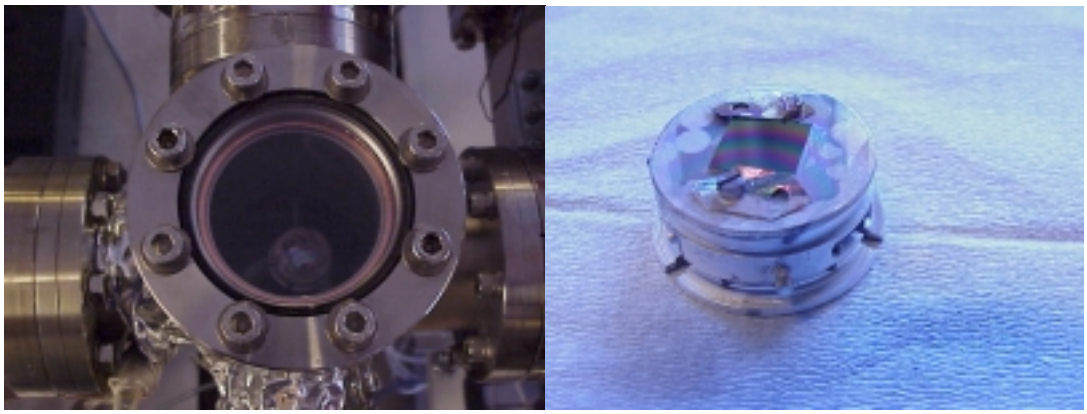

Figure 1.61. Pictures of thiophosphangulene on SiO_2 mounted on the substrate holder. On the left the substrate holder is seen in the UHV chamber before transfer to the load lock. On the right a close-up picture of the substrate with a layer thiophosphangulene is seen. Notice the distinct rainbow colouring (the substrate measures 10 mm by 10 mm).

In some cases on SiO_2 the layer thickness could be seen as a rainbow colouring under the right light conditions. The different colours are due to a differing thickness of the layer. It is noticeable that the coloured bands are circular which is due to the nature of the molecular beam and it gives an indication of the narrowness of the molecular beam. The layer thickness of the sample shown in figure 1.61 was shown by AFM to be 250 nm and with a very even surface ±4 nm.

1.3.4 Bilayers

1.3.4.1 Layer upon layer

While phosphangulene did not give rise to even layers when deposited under UHV conditions thiophosphangulene does give rise to an even layer when deposited under UHV conditions. Even though no structural information on thiophosphangulene on the SiO_2 surface was revealed by the characterisation experiments made it was decided to try and deposit a layer of thiophosphangulene first followed by and overlaid layer of phosphangulene. The hope was of course that the growth of the overlaid phosphangulene layer would be even due to an influence by the similar and underlying thiophosphangulene. The influence of the underlying layer was not the major issue in this highly empirical approach which leans against the spirit of the engineer who will try an idea and if it works it deserves attention if it does not work it

does not deserve attention. The reason for this desperate approach was that the aim of the game was to make a phosphangulene based MOSFET detector system and not unnecessary involvement in the surface science of phosphangulene unless of course it served the purpose of promising development.

1.3.4.2 The SIMS experiments and AFM

The SIMS (secondary ion mass spectrometry) instrument is clever in that a detailed image of the surface is obtained where the amplitude information in the image is given in molecular mass. For instance if part of a surface have had a molecule deposited then a SIMS image, with one mass range corresponding to say the substrate mass in one colour (i.e. blue) and another mass range corresponding to the molecule which have been deposited in another colour (i.e. green), would show a blue colour in regions where the mass corresponding to the substrate was observed and green in regions where the molecular mass was observed. This is achieved by firing ionised argon atoms in short pulses at the surface followed by time of flight mass spectral analysis. Some experiments were made where thiophosphangulene was first deposited on SiO_2 followed by phosphangulene. An analysis in the region towards the edge where the substrate had been clamped allowed for the observation of all three surfaces namely the substrate, thiophosphangulene and phosphangulene.

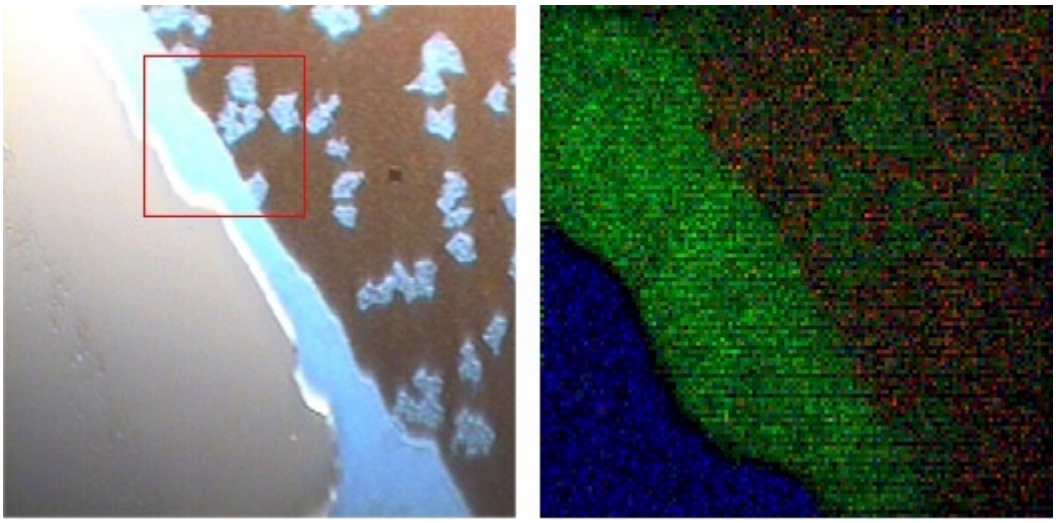

Figure 1.62. A SIMS image of the region where all three layers can be seen. The left picture is an optical image of the surface with the SiO_2 surface to the left on the image (650 μm x 650 μm). The red box is the part which is subjected to the SIMS analysis the result of which is shown on the right (210 μm x 210 μm). The colouring is blue = Si, green = thiophosphangulene and red = diphosphangulene.

From the optical image (and the SIMS image) it would seem that the white areas to the right in the optical image are actually holes in an otherwise smooth phosphangulene surface layer. So based on these results it would seem that we have solved the problem and filling the holes would just be a question of depositing some more phosphangulene. AFM experiments however gave a different picture which are in agreement with the SIMS experiment except that again the phosphangulene layer is not even.

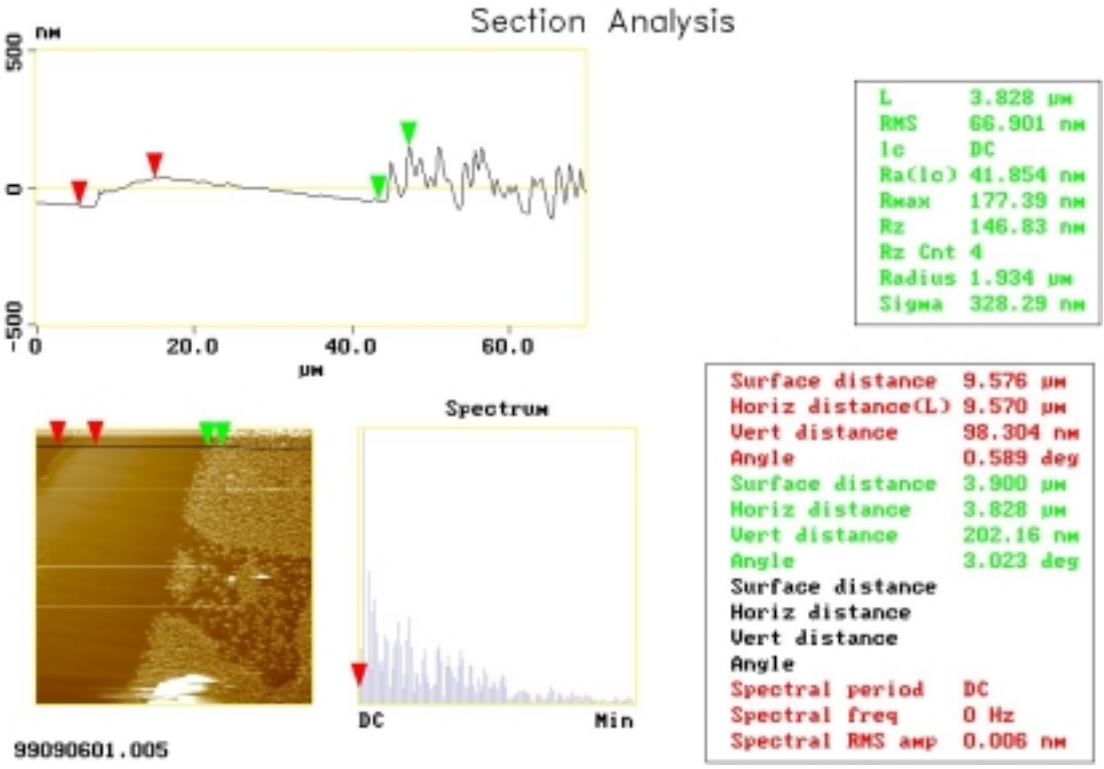

Figure 1.63. A capture of the AFM section analysis. In the lower left part of the illustration the AFM image shows all three transitions with the upper right corner being a small area of SiO_2, the middle part is the thiphosphangulene and the right part is the phosphangulene layer. In the upper left part of the illustration the height profile along the black trace is shown and it can be seen that the thiophosphangulene layer is 100 nm thick and the phosphagulene crystallites are 200 nm in height.

The phosphangulene layer which seemed even in the optical part of the SIMS experiment is thus not when examined in close detail by AFM. The regions in the phosphangulene layer where there seemed to be holes could be explained by areas like the open part of the AFM image.

1.3.4.3 Knudsen cell deposited electrodes probably impairs the surface layer

The silver electrodes were given a little attention as an evaporated electrode might not be the best electrode to use. AFM images of the area close to the edge of the electrode showed small holes in the surface and attempts to create images of the electrode surface itself failed due to an excessive irregularity of the surface. Also by visual inspection the silver electrodes seemed greyish and not shiny and reflective like metallic silver suggesting sizes of irregularities well in excess of several optical wavelengths. Using SIMS images of the area around the edge of the silver electrode revealed small silver particles and a roughness as observed in AFM and by visual inspection (also in a microscope).

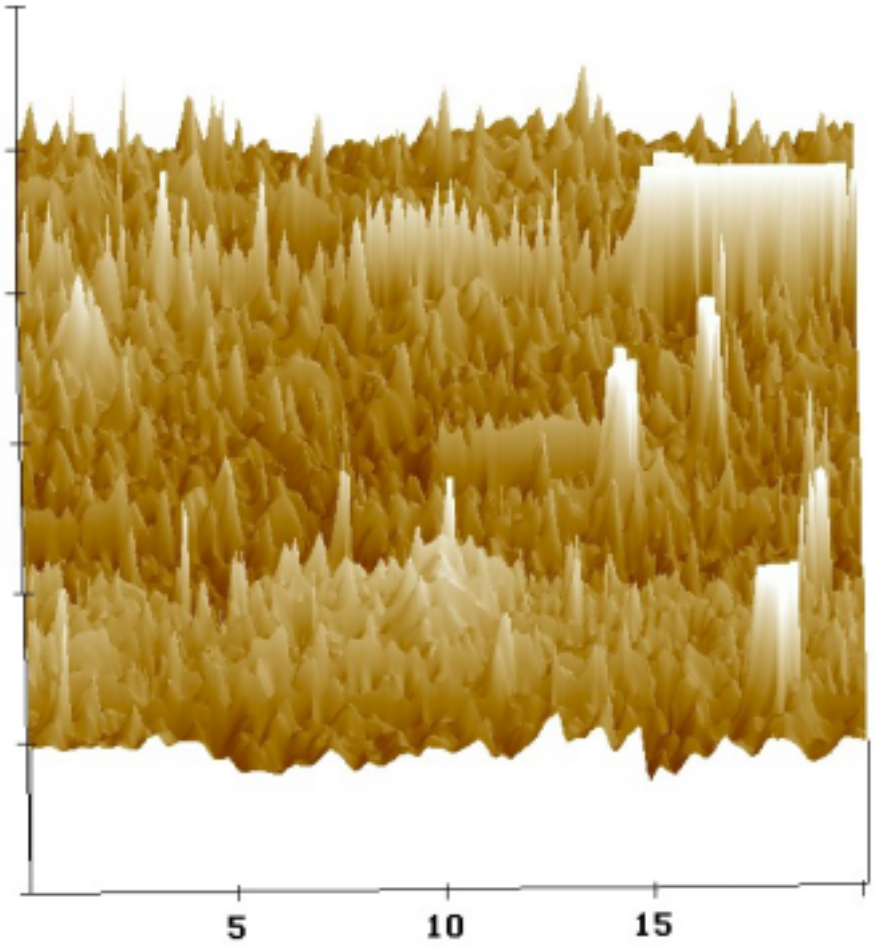

Figure 1.64. An AFM image of the region surrounding the silver electrode. The very large peaks and streaking is believed to be the silver particles (xy-scale = 5 μm/div, z-scale = 100 nm/div).

As an alternative the use of electrode silver epoxy was attempted as electrode material and subsequent pyroelectric measurements gave signals which were equal in magnitude to the signals observed for phosphangulene on SiO_2 but the sign was different.

1.3.4.4 The molecules maybe oriented oppositely

Since the sign of the pyroelectric signal had changed this would imply that the net orientation of the phosphangulene molecules had changed and the large proportion of the molecules have their phosphorous atoms pointing towards the surface. However the amplitude of the pyroelectric signal had not changed significantly and therefore the bilayer approach have not changed the way of the world in terms of efficiency. The very heart of the problem still remains to be the achievement of an even layer and perhaps by other means finding out how the *c*-axis (polar axis) is oriented with respect to the surface.

1.3.5 Conclusions to *Part 1.3*

What may have been uncovered here is the tendency of polar molecular materials to grow on surfaces in a directional fashion (which is wanted) but also due to the directionality unevenly (which is not wanted). The results thus seem to indicate that,

> *Growth of even molecular layers on surfaces cannot be achieved if the material has a polarity and a predisposition to grow in a directional manner.*

1.3.6 Personal conclusions to *Part 1.3*

This entire part is in my eyes a complete an utter fiasco (and my fault). Perhaps not disqualifying me as a scientist but more as an example of a project where all the tools etc. are available but the fundamental understanding of nature is not and therefore the way to success is long and tiresome. It also underscores the necessity for scientists to be able abandon an idea if it keeps being uphill not at too early a stage but not at too late a stage either. It is a fine balance between on the one hand being weak and giving up and on the other hand continuing for too long with blatant stupidity. In my own words: I wish I had not argued so hard for this time consuming, tiresome and stillborn project to start with and that I had given up a lot earlier. I however find comfort in the fact that no one can claim that I did not continue to the

bitter end and until my life reaches a singularity I will hold the claim that pyroelectrics in surface science are fools gold.

1.3.7 Experimental

Since the entire *Part 1.3* has not given rise to any published material with associated experimental detail it is found appropriate to give a parsimonious portion of experimental detail here since none can be found elsewhere.

1.3.7.1 Synthesis and Structural detail

4,8,12-Trioxa-12c-thiophospha-4,8,12,12c-tetrahydrodibenzo[*cd*,*mn*]pyrene (thiophosphangulene) was synthesised by mixing phosphangulene (0.1224 g, 0.402 mmol) and elemental sulphur (0.0129 g, 0.402 mmol) in a tube followed by sealing it at a pressure of 10^{-5} bar. The tube was heated to 200 ^{o}C in an oven. The materials sublime in the tube. After 5 days large round colourless multifaceted crystals were isolated. Yield: 120 mg (96%).

X-ray crystallographic data were collected on one of the crystals and the structure was solved. Orthorhombic space group P*bca*, a = 14.757(3) Å, b = 13.099(3) Å, c = 14.970(3) Å, $\alpha = \beta = \gamma = 90$ ^{o}, V = 2893.7(10) Å^3, Z = 8, T = 120 K, ρ = 1.544, μ = 0.346, MoKα = 0.71073 Å, total reflections = 28663, Unique reflections ($I > 2\sigma$) = 2770, R_{int} = 0.0224, R_{sigma} = 0.0113, reflections/restraints/parameters = 2958/0/208, R = 0.0341, $wR(F^2)$ = 0.912.

1.3.7.2 IRAS experiments and IR

The powder IR spectrum of phosphangulene was recorded on a Bruker FT-IR spectrometer. IRAS experiments were carried out at the IRAS facility within the Leverhulme Research Center in Leeds. The set-up is comprised of a home designed UHV chamber with UHV quality KBr windows for the IR path running through the instrument impeding at grazing angle on a Ni(111) crystal. The IR instrument was a MATTSON Galaxy 6021 FT-IR spectrometer.

1.3.7.3 Sample preparation and MBE detail

The substrate was normally washed in 99% ethanol and blown dry with nitrogen. Mounted on the sample holder using tantalum sheet and molybdenum screws (see the left picture in figure 1.61). Normally at least one hour of pumping was performed before entering the sample to the

main chamber. The position of the molecular beam was first mapped by scanning the Q-balance across the beam thus finding the maximum. Generally the beam was found to be quite narrow. For instance with the sample as far in the chamber as possible (~ 20 cm sample-to-substrate distance) the FWHM was approximately 20 mm (a Gaussian section was normally observed). For phosphangulene sublimation or dosing was performed with a sample exit temperature of 75 ^{o}C (~1.2V on the heating coil) and fluxes obtained at maximum were of the order of 20 Å min^{-1}. Using the density from the X-ray data and a Z-ratio of one. For thiophosphangulene the sample exit temperature for deposition was 145 ^{o}C (~3.1V on the heating coil). The flux for thiophosphangulene was similar to that observed for phosphangulene. In most cases the substrate used was aluminium backed *p*-doped silicon with a 10 nm SiO_2 layer grown at the surface. From the AFM analysis of the layers it was possible to deduce what the actual thickness of the layer obtained was as compared with the layer thickness indicated by the Q-balance. In the experiment shown in figure 1.63 the layer thickness for the two layers as indicated by the Q-balance was 300 Å. From the AFM analysis the layer thickness was in the case of thiophosphangulene found to be 1000 Å and for phosphangulene 2000 Å. In the case of phosphangulene the thickness was measured at the top of the crystallites or crystalline islands and therefore the mean thickness is a lot smaller.

1.3.7.4 Analytical detail AFM, ESCA and SIMS

ESCA analysis was carried out on a *Sage 100* from *SPECS* and usually with over night counting times. AFM analysis was carried out on a *Dimension 3000 AFM* from *Digital Instruments*. TOF-SIMS analysis was carried out on a *TOF-SIMS IV* from *CAMECA*.

Chapter two

In this chapter a brief introduction to the field of liquid crystals is given followed by an account of the results obtained from this work and how it relates to the understanding which can be obtained from a study of the literature. Some people other than myself have been involved in obtaining these results most significantly perhaps Thomas L. Andrésen but also my supervisors Klaus Bechgaard and Niels Thorup.

2.1 Introduction to triphenylenes and liquid crystals

In order to gain an appreciation for this field the concept of a liquid crystal will have to be defined so as to form the basis of a proper discussion. Whereas the liquid crystalline state and the experimental basis for the establishment of a particular state of organic matter as being a liquid crystalline state has been known for some time, the molecular structure of the liquid crystalline state have evaded conscious recognition by the scientists studying this liquid crystalline state. In particular for a specific series of liquid crystals termed discotic liquid crystals where only a few of the myriad of structural studies that have been published are absolute and not relying on some picture of what the structure must look like and therefore heavily biasing the interpretation of often very scarce data. As a result a careful reading of the literature pertaining to the subject leaves the mind of the reader in a state of frustration with respect to the structural properties of these phases. At first glance the structures of the discotic liquid crystalline phases are well known and well referenced. When confronting these alleged structural articles further reference is given and eventually one is at the beginning of time still left with no structural answer. To explain this a conspiracy theory is needed where seemingly many scientists have decided to agree on the structural nature of these phases completely overhearing the few contradicting (and the most well founded) studies. Here a complete answer will not be given but another good solid brick will be placed on that long and tiresome foundationalistic road leading towards the state of conditional knowledge.

2.1.1 The categories of liquid crystals in brief

The above prelude was not meant to put the field asunder or in disregard because as it is a field of confusion it is charming and challenging so challenging that we have to imagine, still

however within the limits of experimental evidence. For instance it is an area that like so many other areas of science suffers from the discovery in reverse order i.e phase 2 is discovered before phase 1 and phase 2 is therefore accidentally called phase 1. This have led to several publications trying to redefine the in my eyes charming but illogical naming conventions thus causing more confusion than the sought after logical terminology.

2.1.1.1 The liquid crystal

A liquid crystalline phase or a mesophase is only observed for some compounds. The first type of materials found to exhibit liquid crystalline behaviour dates back to year 1888 thus quite some time ago[34]. These molecules were termed calamitic or rod like liquid crystals and were typically esters of cholesterol. For normal molecular organic materials (that have a melting point) the following happens upon heating.

$$\mathbf{K} \rightarrow \mathbf{I}$$

Where **K** implies a truly crystalline state with long range order (**K** is used instead of **C** because this is the terminology found in the literature, helpful for German or Danish speaking individuals but probably not for English speaking individuals), the arrow indicates that it is a phase transition and the directionality indicates the direction of the temperature change i.e. an increase (sometimes the phase transitions are denoted with an indication of temperature above the arrow signifying the temperature at which the transition takes place) and finally **I** implies a truly liquid state which is isotropic with no long nor short range order. It is the simple phase transition from crystal to melt i.e. the melting process. For the liquid crystalline phases there is something in-between.

$$\mathbf{K} \rightarrow [\text{mesophase}] \rightarrow \mathbf{I}$$

So, in leaving the crystalline state there is a mesophase *in limbo* before the isotropic or liquid state is reached at a higher temperature. The in-between, the mesophase, can be more than just one phase and often several phases are observed. The liquid crystalline state is thus a state of some order, not crystalline (or perfect) order and not complete disorder but some order.

2.1.1.2 The order and the classification

We now concentrate on the liquid crystalline state where generally for a given compound less and less order in the different phases are observed as the temperature is increased. This gives

[34] Reinitzer, F. *Monatch. Chem.* **1888**, *9*, 421.

a picture of the liquid crystalline state as a lengthened melting process with thermodynamic nuances and several stops before chaos is reached in the liquid state. These stops as it were have different classifications and for the calamitic liquid crystals which are the best known and the most well characterised names have been given to the different phases like smectic and nematic (smectic meaning soapy and nematic meaning thread, both from the corresponding Greek words) where the smectic phase is the most ordered phase in which the rod like molecules are arranged in layers with some long range order and the nematic phase is a state where there is no arrangement in layers and only the directionality of the rods is retained. So the sequence of transitions would typically be[35].

$$\mathbf{K} \rightarrow \mathbf{S} \rightarrow \mathbf{N} \rightarrow \mathbf{I}$$

Where **S** denotes a smectic and **N** denotes a nematic liquid crystalline state. So-called cholesteric phases also exist in which molecules are arranged in layers with the long axis of the rod shaped molecules forming an angle with respect to the normal of the sheet and the angle being different between layers (normally denoted by a superscripted star i.e. $\mathbf{N}^{*}$). Typical features of liquid crystals are that they do not support a shear force i.e. they exhibit viscous flow. Furthermore they show optical, electrical and magnetic anisotropy. Different smectic and nematic phases exist and they are normally denoted by a subscript i.e. $\mathbf{S_a}$ or $\mathbf{S_c}$. To treat in detail each of the phases denoted by their individual subscripts would perhaps be to involved and instead we cut to the chase.

2.1.1.3 The discotic liquid crystals

The discotic liquid crystals are newcomers to the field as opposed to the calamitic or rod-like liquid crystals. The idea of discotic liquid crystals was first conceived of in 1965[36] and later[37,38] but the existence was not definitely shown for a well characterised molecular system until the late 1970s with hexa-substituted benzenes[39] and triphenylenes[40,41,42]. It is based on the shape of the mesogenic core molecules evident that the calamitic and discotic based liquid crystals

[35] On rare occasion the nematic phase is observed at a lower and at a higher temperature than the smectic phase. In such instances the phase behaviour is termed reentrant.
[36] Brooks, J. D.; Taylor, G. H. *Carbon* **1965**, *3*, 185.
[37] Zimmer, J. E.; White, J. L. *Mol. Cryst. Liq.Cryst.* **1970**, *38*, 177.
[38] White , J. L.; Zimmer, J. E. *Carbon* **1978**, *16*, 469.
[39] Chandrasekhar, S.; Shadashiva, B. K.; Suresh, K. A. *Pramana* **1977**, *9*, 471.
[40] Nguyen Huu Tinh; Dubois, J. C.; Malthete, J.; Destrade, C. R. *Acad. Sci.* **1978**, *286C*, 463.
[41] Billard, J.; Dubois, J. C.; Nguyen Huu Tinh; Zann, A. *Nouv. J. de Chimie* **1978**, *2*, 535.

have highly anisotropic diamagnetic, dielectric and birefringence properties and that they complement each other i.e. the calamitic mesogen is highly polarisable along the length of the rod shape whereas the discotic mesogen is highly polarisable in the plane of the disc. The shape leads to another way of distinguishing the different mesogens namely the director of the molecules. For the calamitic mesogens the director is along the axis of the rod shaped molecule and for the discotic mesogens the director is perpendicular to the plane of the disc shaped molecule. The director is sometimes shown as a small arrow or a vector. This complementary relationship is partly reflected in the phases that they are known to exhibit.

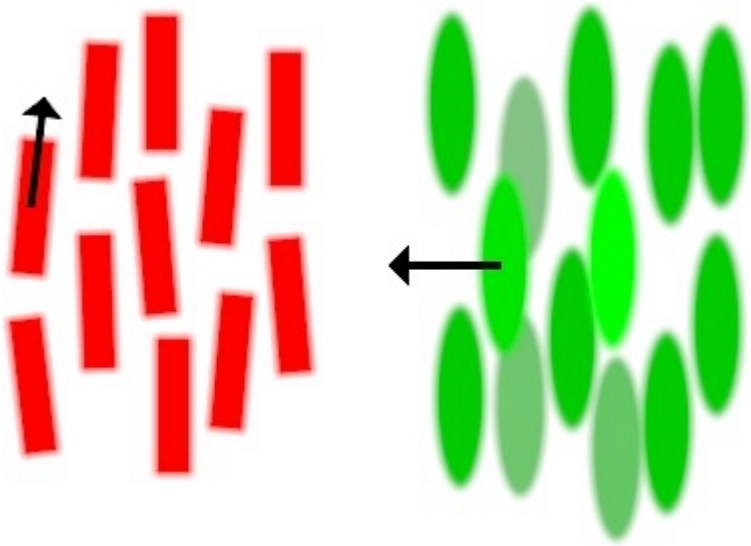

Figure 2.1. An illustration of nematic calamitic liquid crystals **N** (left) and nematic discotic liquid crystals $\mathbf{N_D}$ (right). The arrow shown is the director of the molecules.

Thus it is possible to have both a calamitic nematic phase (denoted **N**) and a discotic nematic phase (denoted $\mathbf{N_D}$). The letter **D** is always used do indicate that it is a discotic mesogen that is involved. And also the nematic cholesteric phases are known to exist denoted $\mathbf{N^*}$ and $\mathbf{N_D^*}$ respectively for the calamitic and discotic phases (sometimes these latter phases are referred to as twisted phases). The contrast here is that while both calamitic and discotic nematic phases have a low viscosity their respective directors are at right angles to each other. The discotic mesogens are also known to exhibit a different type of phase behaviour namely the columnar discotic phases the concept of which are as young as the discotic mesogens themselves. Several structurally different columnar discotic phases are recognised but perhaps not so well understood. Common to them all is that the disc like molecules are arranged in

[42] Destrade, C.; Mondon, M. C.; Malthete, J. *J. Phys.* **1979**, *40-C3*, 17.

columnar stacks with varying degrees of order along the stacks and stacks in-between. The structural properties of the columnar discotic mesophases will serve as the main subject of discussion in *Part 2.2* and *Part 2.3*.

2.1.1.4 The use of liquid crystals in brief

There would not have been such an intense research effort within the field of liquid crystalline materials had it not been for some technological significance of the these materials. While liquid crystals find use within only a narrow part of the *state-of-the-art* technology it is of exceptionally wide application. They are found in displays, LCD-displays, one simple application but used with digital watches, mobile phones, portable PC's, Flat screen televisions, on microwave ovens etc. it would perhaps not be an overstatement to say that every person has five personal LCD's somewhere. It all relies on the ability of the liquid crystalline molecules to reorient in response to an applied field thus altering the refractive properties. This subsection should underscore the widespread use and importance of these materials. It should be pointed out that most of the liquid crystals that are actually used are calamitic type mesogens and while different and interesting properties of the discotic phases have been demonstrated they have not yet given rise to any widespread applicability.

2.1.2 The discotic mesogens and triphenylene

Molecules that exhibit discotic liquid crystallinity are flat and round molecules of varying size. They always have a rigid mesogenic core and flexible corona.

2.1.2.1 The mesogen core

Typical mesogenic core molecules are large extended aromatic systems but as have been mentioned above even benzene may serve as a mesogenic core. A few of the known core molecule structures that have gained appreciation are shown on the following page. Some other mesogenic cores are known[43,44] the latter having only four substituents and while both exhibit a thermotropic phase they are not well characterised. The ones given here are just a few but all known to give rise to columnar liquid crystalline phases. All the molecules in the illustration are planar and it is evident that the size of the disc shaped core range from small as

[43] Giroud-Godquin, A. M.; Billard, J. *Mol. Cryst. Liq. Cryst.* **1981**, *66*, 147.
[44] Fugnitto, R.; Strzelecka, H.; Zann, A.; Dubois, J. C.; Billard, J. *Chem. Commun.* **1980**, 271.

for benzene[45], anthrachinone[46] and triphenylene to the larger truxene[47] and phthalocyanine[48] derivatives (from left to right in the upper and lower row respectively).

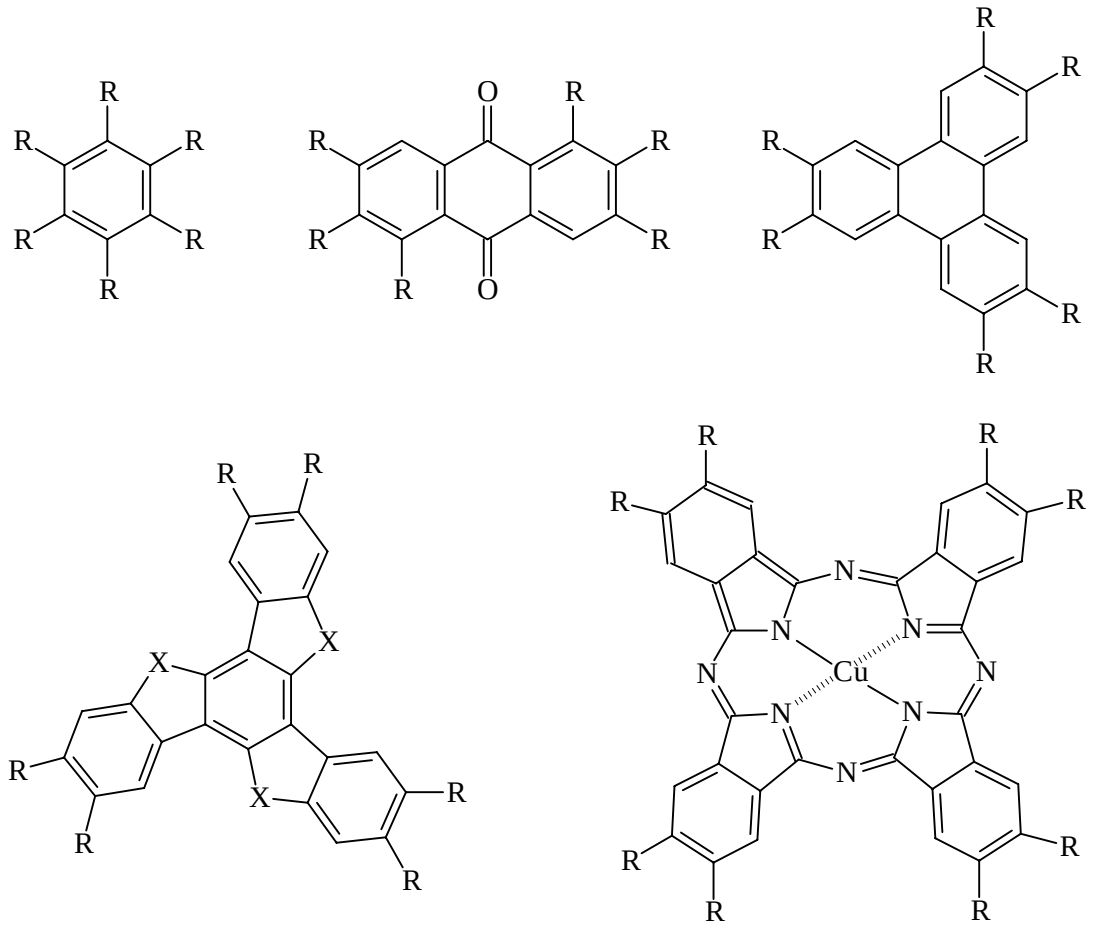

Figure 2.2. Some typical discotic mesogens. R means some substituent and X can be oxygen or CH_2.

The symmetry of the mesogenic core is not important as long as the substituents are distributed around the circumference of the core molecule.

2.1.2.2 The mesogen corona

While the core was rigid the corona or the outer part of the mesogen is flexible and even floppy. It is most often long alkyl chains attached to the mesogen core via ether linkages or

[45] Binder, S. M.; Lord, N. W. *J. Chem. Phys.* **1961**, *36*, 540.
[46] Parthenopoulus, D. A.; Rentzepis, P. M. *Science* **1989**, *245*, 843.
[47] Foucher, P.; Destrade, C.; Nguyen Huu Tinh; Malthete, J.; Levelut, A.M. *Mol. Cryst. Liq. Cryst.* **1984**, *108*, 219-229.
[48] Piechocky, C.; Simon, J.; Skoulios, A.; Guillon, D.; Weber, P. *J. Am. Chem. Soc.* **1982**, *104*, 5245.

long chain alkanoates attached to the mesogen core via ester linkages. Benzoates carrying long chains have also been reported[49]. The condition that needs fulfilment before columnar phases can be obtained seems to be linked to the number of substituent chains and it is commonly accepted that at least six substituent chains are needed[50].

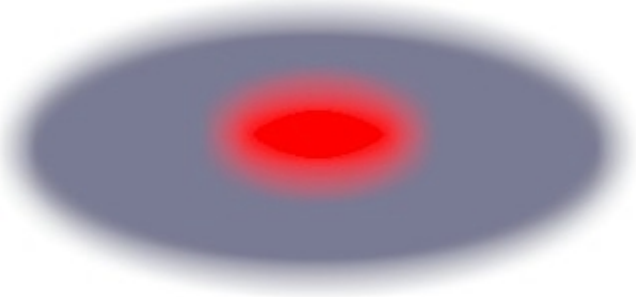

Figure 2.3. An illustration of a discotic mesogen the floppy outer part (blue) is the corona and the rigid inner part (red) is the core.

We can thus draw a picture of the complete discotic mesogen as a disc with different inner and outer texture.

2.1.2.3 Significance of triphenylenes to the field of liquid crystals

Triphenylene is a beautifully symmetric molecule and it is shaped like a disc perhaps only surpassed in disc shape by coronene and hexa-benzocoronene. The parent molecule has been known for some time since the synthesis by trimerisation of benzyne is well known. This is also reflected in the documentation available i.e. the structure of triphenylene itself have been solved by X-ray[51], neutron[52] and electron diffraction[53]. The structure of triphenylene exhibit the typical stacking observed for large aromatic molecules i.e. slipped stacks of molecules packed in a herring bone pattern. Triphenylene molecules with oxygen atoms at the periphery have not been known for very long and the first known was 2,3,6,7,10,11-hexamethoxytriphenylene and actually isolated from the pigment in some spores of *Ustilago Maydis*[54]. Later it was synthesised by Marquardt[55] and my old friend Oliver Charles

[49] Nguyen Huu Tinh; Destrade, C.; Gasparoux, H. *Phys. Lett.* **1979**, *72A*, 251.
[50] Destrade, C.; Foucher, P.; Gasparoux, H.; Nguyen Huu Tinh; Levelut, A. M.; Malthete, J. *Mol. Cryst. Liq. Cryst.* **1984**, *106*, 121-146.
[51] Ahmed, F. R.; Trotter, J. *Acta Cryst.* **1963**, *16*, 603.
[52] Ferraris, G.; Jones, D. W.; Yerkess, J. *Z. Krist.* **1973**, *138*, 113.
[53] Dorset, D. L.; McCourt, M. P.; Gao, L.; Voigt-Martin, I. G. *J. Appl. Cryst.* **1998**, *31*, 544-553.
[54] Piattelli, M.; Fattorusso, E.; Nicolaus, R. A.; Magno, S. *Tetrahedron* **1965**, *21*, 3229.
[55] Marquardt, F.-H. *J. Chem. Soc.* **1965**, 1517.

Musgrave[56]. On occasion I have asked myself whether they knew what they started when discovering the making of these molecules. At first there was silence for 10-15 years and then suddenly intense effort set in which serves to illustrate that most science, if not all, will at one point become of use. The time span from discovery to an appreciation of the importance however, can be anywhere from immediate to a latency extending beyond the life span of a human or several generations. Following on from this, intense research started where many triphenylene derivatives were synthesised and studied with respect to discotic liquid crystalline behaviour. In retrospect the triphenylenes are amongst the most studied discotic mesogens if not the most studied.

2.1.2.4 Synthesis of symmetric and asymmetric triphenylenes

The most easily accessible starting material for the synthesis of triphenylene based discotic mesogens is probably 2,3,6,7,10,11-hexamethoxy-triphenylene obtained by trimerisation of veratrole with an oxidant which typically is DDQ, $FeCl_3$, $MoCl_5$ or $FeCl_3(aq)/H_2SO_4$. The most efficient is perhaps the one of Naarmann *et al.*[57]. An important point to note is that triphenylene is not the sole product and some naphthacenequinones are also formed as demonstrated by Musgrave *et al.*[23,58]. These by-products are difficult to separate and distinguish from the desired triphenylene. A method whereby the naphthacenequinones are efficiently removed has been devised[59].

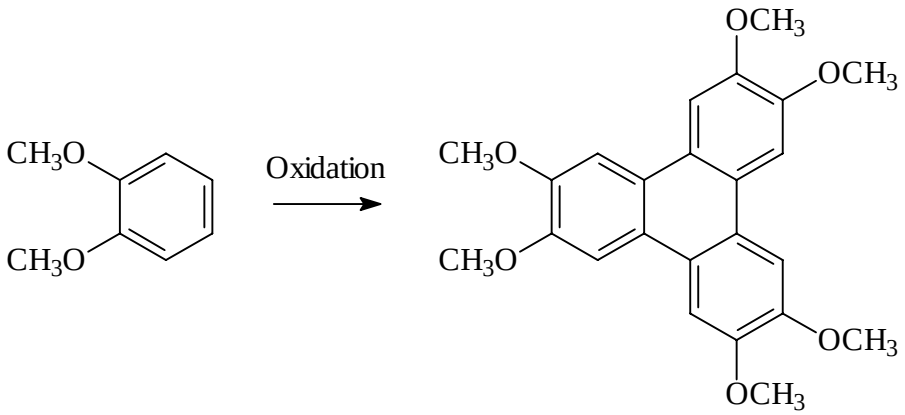

Figure 2.4. The synthesis of 2,3,6,7,10,11-hexamethoxytriphenylene from readily available veratrole using an oxidant.

[56] Musgrave, O. C.; Webster, C. J. *J. Chem. Soc. (C)* **1971**, 1397.
[57] Naarmann, H.; Hanack, M.; Mattmer, R. *Synthesis* **1994**, 477.
[58] Musgrave, O. C.; Webster, C. J. *J. Chem. Soc. (C)* **1971**, 1393.
[59] Krebs, F. C.; Schiødt, N. C.; Batsberg, W.; Bechgaard, K. *Synthesis* **1997**, 1285.

Demethylation of 2,3,6,7,10,11-hexamethoxytriphenylene affords 2,3,6,7,10,11-hexahydroxytriphenylene which is the true starting material for the preparation of discotic mesogens. While the intention is normally to make all the substituents identical clever synthetic procedures have been devised where for instance one or two of the oxygens can be substituted differently from the remaining four or five[60].

2.1.3 Proposed phases of triphenylene based liquid crystals

This section will present the concept of the discotic liquid crystalline phases (mainly triphenylene based) as found in the literature whereas a critical discussion of the structures has been deferred to *Part 2.2* and *Part 2.3*.

2.1.3.1 The ways to distinguish phases

It was mentioned earlier that the nematic discotic phase existed and that the viscosity of this type of phase was different from the columnar phase. Viscosity measurements are useful in distinguishing phases from one another. Also a light microscope with an optical polariser and a hot stage is useful. Further DSC (differential scanning calorimetry) can provide very important information on the heat exchange involved in phase transitions as well as helping in observing the individual phase transitions. The refractive indices of the phases are important parameters and give the optical sign and nature of the director (for the calamitic liquid crystals the optical sign is positive i.e. the refractive index along the director is larger than the refractive index perpendicular to the director. For discotic liquid crystals the optical sign is negative). The final and most exact way is probably X-ray measurements on phases which have been ordered by shearing or in a magnetic field. What is observed in the X-ray measurements is the scattering from the ordered part of the structure which is often limited to diffuse spots but nevertheless highly characteristic patterns are obtained for individual phases.

2.1.3.2 Known columnar phases

Two of the phases that have been mentioned to exist for the discotic mesogens were the nematic, $\mathbf{N_D}$, and the cholesteric nematic or twisted nematic, $\mathbf{N_D^*}$. Most often however discotic mesogens give rise to columnar phases denoted **D**. Many of these have been observed and have been given individual names most often shown as a subscript. The basis for the

[60] Goodby, J. W.; Hird, M.; Toyne, K.; Watson, T. *J. Chem. Soc. Chem. Commun.* **1994**, 1701.

distinction between these sub-phases of the columnar discotic phase have been optical, DSC and X-ray measurements[61]. Normally two subscripts are given and the first refers to the order that exists between the columns i.e. **h** for hexagonal, **r** for rectangular and **ob** for oblique.

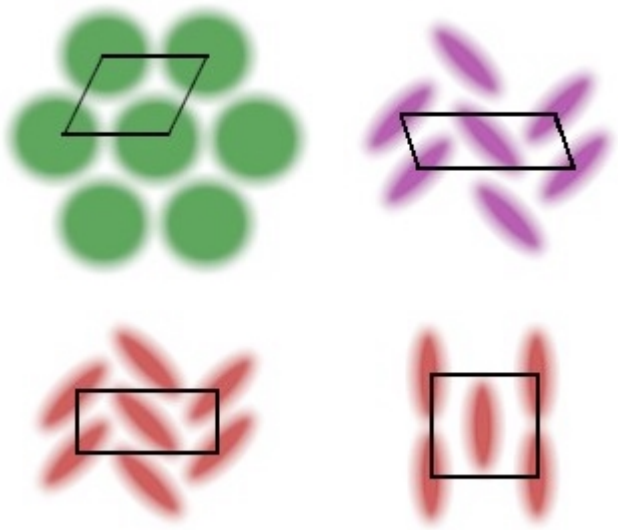

Figure 2.5. An illustration of the most common order of the columns (as seen from above). Above left the hexagonal arrangement, subscript **h** (green). Above right the oblique order subscript **ob** (lilac) the ellipsoids indicate that the director forms an angle with the stacking direction. Below two of the most common rectangular cells subscript **r** (taupe).

A second subscript is often also given and it refers to the order observed between the molecules in the individual stacks i.e. **o** for ordered and **d** for disordered.

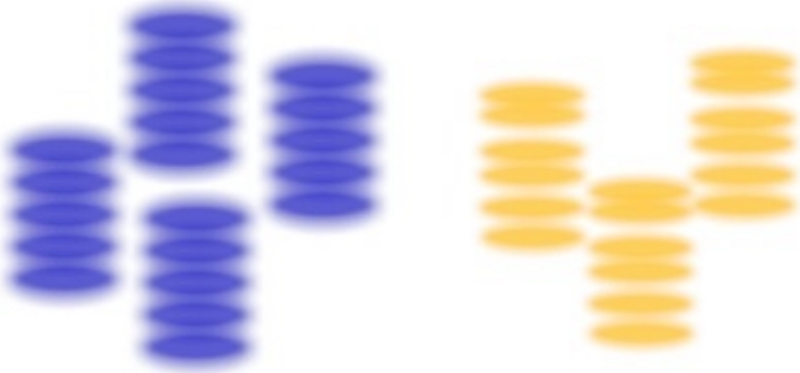

Figure 2.6. The correlation between molecules in the stack. To the left the ordered situation, subscript **o** (blue) and to the right the disordered situation, subscript **d** (yellow). This is a schematic drawing which illustrates the correlation between molecules and nothing is said about the orientation of the molecules in the stack i.e. the director and the column need not be parallel.

[61] Destrade, C.; Gasparoux, H.; Babeau, A.; Tinh, N. H.; Malthete, J. *Mol. Cryst. Liq. Cryst.* **1981**, *67*, 37-48.

It is at this point perhaps appropriate to note that while these X-ray experiments can reveal what the inter columnar arrangement is nothing can really be said about the symmetry.

2.1.3.3 Phase diagrams of pure compounds and binary mixtures

The phase diagrams of the pure compounds are typically represented by schemes as explained in *Section 2.1.1.1* thus for the discotic liquid crystalline material 2,3,6,7,10,11-hexakis(nonanoyloxy)triphenylene the following phase behaviour is observed[62].

$$\mathbf{K} \xrightarrow{68} \mathbf{N_D} \xrightarrow{86} \mathbf{D_{rd}} \xrightarrow{138} \mathbf{D_{ho}} \xrightarrow{280} \mathbf{I}$$

The material thus passes from the crystalline state to a nematic discotic phase. It then enters a more viscous discotic rectangular and disordered phase followed by a discotic hexagonal and ordered phase before finally melting into an isotropic liquid. It should at this point be said that the alkanoyloxy triphenylenes often give rise to disorder in the stacks and that the hexagonal phases nearly always occur just before melting. The latter point is significant in the later structural discussion. Several similar examples of the above pure phase behaviour have been reported for the triphenylenes[63,64,65] and for trioxatruxenes[66]. When two different discotic mesogens are mixed in varying mole fractions a binary phase diagram can be constructed. For instance triphenylene based mesogens with two different chain lengths in the corona or side groups. Several different situations can take place and quite a few of them have been outlined[64]. If the sizes of the mesogens are too different this leads to imiscibility as is the case for mixtures of for instance hexahexyloxytriphenylene and hexadecyloxytriphenylene. On the other hand hexaoctyloxytriphenylene is miscible with either of the above so as long as the mesogens are not too dissimilar mixed phases are possible. While some new phase behaviour is observed at times the main purpose of these phase diagrams is to establish whether phases for the same mesogenic core but with a differing length of side groups are of similar structure. Furthermore it has been shown[64] that different mesogens rarely mix. The mixing of different mesogens also serves the purpose of comparing the stability of the discotic phases that they

[62] Destrade, C.; Nguyen Huu Tinh; Malthete, J.; Levelut, A. M. *J. physique* **1983**, *44*, 597-602.
[63] Nguyen Huu Tinh; Malthete, J.; Destrade, C. *Mol. Cryst. Liq. Cryst.* **1981**, *64*, 291-298.
[64] Destrade, C.; Nguyen Huu Tinh; Gasparoux, H.; Malthete, J.; Levelut, A. M. *Mol. Cryst. Liq. Cryst.* **1981**, *71*, 111-135.
[65] Nguyen Huu Tinh; Gasparoux, H.; Destrade, C. *Mol. Cryst. Liq. Cryst.* **1981**, *68*, 101-111.
[66] Mamlok, L.; Malthete, J.; Nguyen Huu Tinh; Destrade, C.; Levelut, A. M. *J. Physique* **1982**, *43*, L641-L647.

form individually. For instance the mesophases formed by hexaalkyloxytriphenylenes are less stable than the hexalkanoyloxytriphenylenes.

2.1.4 Properties of triphenylenes and properties of columnar phases

The properties of a given molecular material is given by the interplay between two factors. The properties of the constituent molecules and the properties of the structure in which they take part.

2.1.4.1 Properties of the triphenylene core

One of the appealing properties of triphenylene is as mentioned the molecular symmetry which in Schönflies notation is D_{3h}. This implies for instance that it can have a triplet ground state (for the dication)[67,68]. The triphenylene core itself and many derivatives have strong fluorescence properties[69] finally some semiconductors have been prepared from doped hexaalkoxytriphenylenes[70,71]. Further some charge transfer salts have been prepared involving triphenylene and hexamethoxytriphenylene[72]. It is obvious that with such a variety of molecular properties many new properties will emerge as a consequence of placing triphenylenes in a liquid crystal and further a knowledge of the molecular properties can be used to probe our understanding of the columnar liquid crystalline phases.

2.1.4.2 Properties specific to the columnar discotic phase

The concept of columnar discotic phases as being one dimensional columnar stacks of the discotic molecules would imply that the interaction of the molecular functionalities could be explored as a one dimensional ensemble. Evidence in support of a columnar structure are while not exclusive the observation of highly anisotropic conductivity[31] and photophysical energy migration along the columnar structure have been reported (both triplet[73] and singlet[74]). This type of energy migration has also been observed for phthalocyanine based

[67] Bechgaard, K.; Parker, V. D. *J. Am. Chem. Soc.* **1972**, *94*, 4749.
[68] Chiang, L. Y.; Thomann, H. J.; *J. Chem. Soc. Chem. Commun.* **1987**, 172.
[69] Braitbard, O.; Sasson, R.; Weinreb, A. *Mol. Cryst. Liq. Cryst.* **1988**, *159*, 233-242.
[70] Boden, N.; Bushby, R. J.; Clements, J.; Jesudason, M. V.; Knowles, P. F.; Williams, G. *Chem. Phys. Lett.* **1988**, *152*, 94.
[71] van Keulen, J.; Warmerdam, T. W.; Nolte, R. J. M.; Drenth, W. *Rec. Trav. Chim. Pays-Bas* **1987**, *106*, 534.
[72] Andresen, T. L.; Krebs, F. C.; Larsen, M.; Thorup, N. *Acta Chem. Scand.* **1999**, *53*, 410-416.
[73] Markovitsi, D.; Rigaut, F.; Mouallem, M.; Malthete, J. *Chem. Phys. Lett.* **1987**, *135*, 236.
[74] Markovitsi, D.; Lécuyer, I.; Lianos, P.; Malthete, J. *J. Chem. Soc. Faraday Trans.* **1991**, *87*, 1785-1790.

columnar discotic liquid crystals[75]. An example of how an electron acceptor can downgrade the columnar discotic phase ($\mathbf{D_{ho}}$) by mixing to a nematic discotic phase ($\mathbf{N_D}$) thus also downgrading the order of the mesophase have also been reported[76]. While these observations can not be explained without the concept of a columnar phase nothing can from these experiments be inferred upon the molecular orientation within the columns. The synthetic work and charge transfer salts pertaining to this work has been published and can be found in *Appendix P7* and *P8*.

2.2 The development of the discotic premesogen

The terminology is in place now and this section deals explicitly with the question of the structures of the mesogenic core and premesogenic molecules. Many of the results from this section have been published and can be found in *Appendix P9*.

2.2.1 The short chain compounds

While many studies of the structural nature of the mesophases have been carried out (as we shall see in *Part 2.3*) and even involved structural studies attempting a resolution at the atomic level have been undertaken. No structural information is found on the mesogenic core on searching the literature and the CCD.

2.2.1.1 Hexahydroxytriphenylene and hexamethoxytriphenylene

As mentioned already the structure of triphenylene has been solved by several widely differing methods while the structures of the two most common starting materials for the preparation of triphenylene based discotic liquid crystals have not been solved or reported while an erroneous molecular structure for hexamethoxytriphenylene which is based on calculation has been published[77]. It would perhaps be expected that these triphenylene derivatives would have different structural properties from the parent compound triphenylene and further that the hydroxy derivative which was known to contain crystal water would somehow be influenced by this. The notion however that there would be significant π-π aromatic overlap and stacking of the large planar disc shaped molecules proved to be

[75] Markovitsi, D.; Lécuyer, I.; Simon, J. *J. Phys. Chem.* **1991**, *95*, 3620-3626.
[76] Bengs, H.; Karthaus, O.; Ringsdorf, H.; Baehr, C.; Ebert, M.; Wendorff, J. H. *Liq. Cryst.* **1991**, *10*, 161-168.
[77] Etchegoin, P. *Phys. Rev. E.* **1997**, *56*, 538-548.

incorrect as the molecules are arranged in layers with a little aromatic overlap in hexahydroxy compound (ascribed to the specific hydrogen interactions) and no aromatic overlap at all in the hexamethoxy compound.

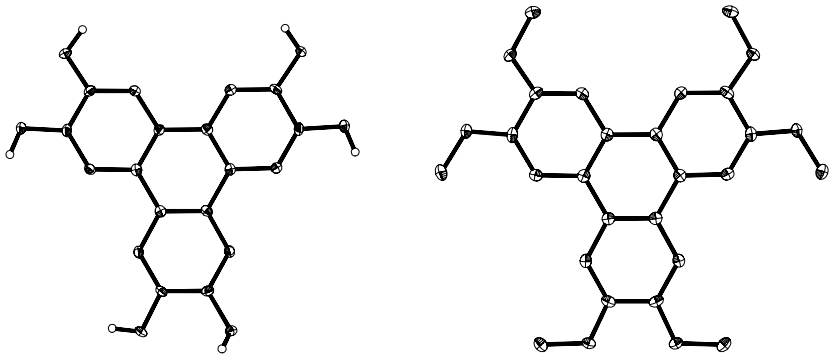

Figure 2.7. The molecular structures of 2,3,6,7,10,11-hexahydroxytriphenylene (left) and 2,3,6,7,10,11-hexamethoxytriphenylene (right) shown as ORTEP drawings (50% ellipsoids).

It is noticeable the substituents point away from each other but remain in the plane of the molecule (in hexahydroxytriphenylene one hydoxy group points at near right angles to the plane of the molecule due to interaction with the crystal water molecule which is not shown). The nature of the specific hydrogen interactions were analysed and can be found in *Appendix P9*.

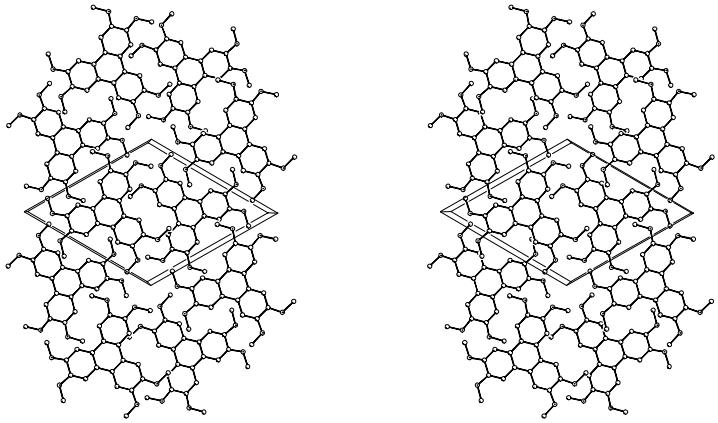

Figure 2.8. A stereoview of the structure of 2,3,6,7,10,11-hexamethoxytriphenylene shown as a projection along the *c*-axis of the hexagonal unit cell. It is noteworthy that the aromatic part of the molecules do not overlap at all.

2.2.1.2 Hexaethoxytriphenylene

Hexaethoxytriphenylene is the next logical step towards the known mesogens the substituents are now beginning to look like chains. Interestingly the structure is isostructural with that of hexamethoxytriphenylene at room temperature and down to 180K.

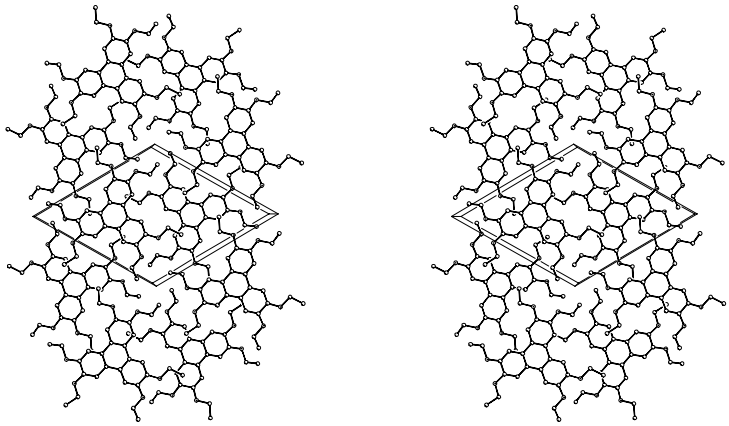

Figure 2.9. A stereoview of the structure of 2,3,6,7,10,11-hexaethoxytriphenylene shown as a projection along the *c*-axis of the hexagonal unit cell. The structure is very similar to that of 2,3,6,7,10,11-hexamethoxytriphenylene and again the aromatic part of the molecules do not overlap.

While the chains need to be considerably longer before a discotic mesophase can be observed the consequence of the results so far is that the molecules do not wish to stack and even though the structure in the mesophase could be very different from the structure in the crystalline phase the above structures are more prototypical of the nematic discotic phase than of a columnar discotic phase.

2.2.1.3 The disorder

It is interesting to examine the above two structures in terms of the rationality of efficient space filling. The alkyl chains have a diameter of 4.6 Å whereas efficient packing of the triphenylene core with say columns of triphenylenes having the director of the molecules parallel would have a thicknes of 3.3-3.4 Å (about the closest aromatic-aromatic distance that can be obtained). This mismatch makes the columnar structure unattractive and instead efficient packing is obtained by mixing the two regions. This works when the alkyl chains

occupy a smaller projected area than the triphenylene core. This is the case for the methoxy compound and the exthoxy compound down to 180K. Below 180K the structure could be solved only with great difficulty and not below 175K. An analysis of the thermal ellipsoids suggest that it is perhaps an order disorder transition which takes place.

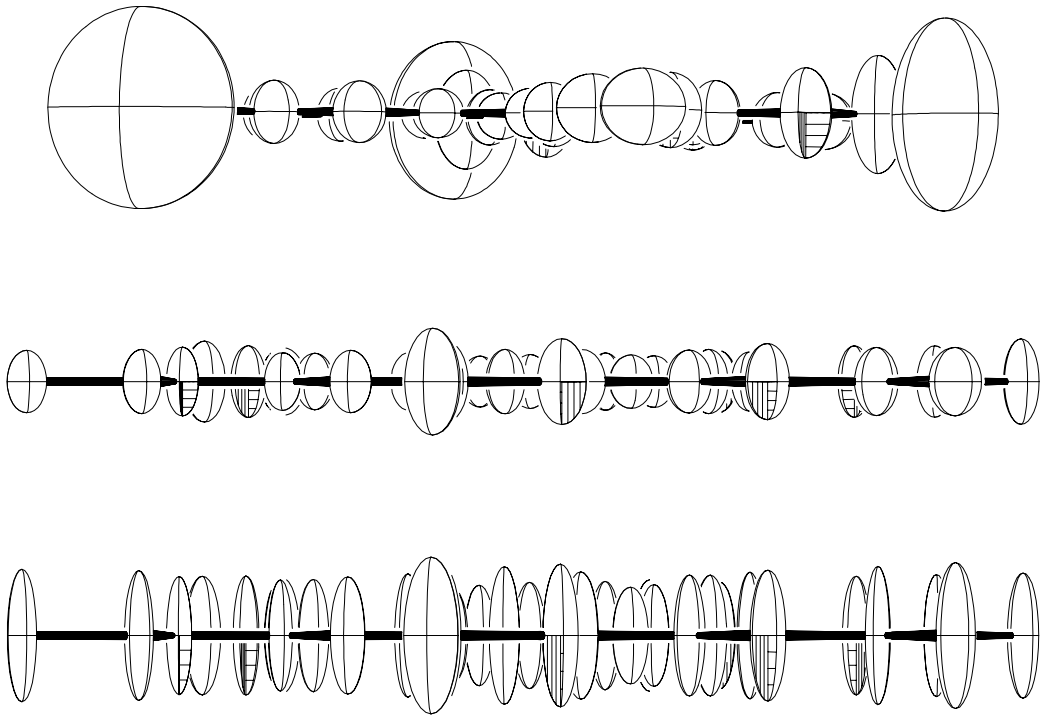

Figure 2.10. The structures of 2,3,6,7,10,11-hexaethoxytriphenylene. The molecules as seen from the side as ORTEP drawings. Above at 294K, middle 180K and below at 175K (50% ellipsoids, by courtesy of Niels Thorup who fathered the illustration which has been altered for the purpose of this text).

At room temperature the ellipsoids are rather large but quite isotropic especially for the methyl groups. At 180K the thermal motion of the atoms is quite well behaved and obviously the ellipsoids have decreased in size. On decreasing the temperature just 5 degrees the thermal ellipsoids become highly anisotropic in a direction perpendicular to the plane of the molecules which is suggestive of some disorder rather than a thermal process. An explanation could be that any further shrinking of the structure would not leave enough room for the ethoxy groups and we thus observe a disordering of the otherwise regular structure. Several attempts were made to collect data and solve the structure at lower temperatures and all these attempts failed

down to 120K which rules out the possibility of an ordinary phase transition. It was found impossible to index the reflections at these lower temperatures. Upon heating the crystal regains its order so it is a reversible order disorder transition and probably linked to the methyl groups of the ethoxy substituents.

2.2.2 The medium chain compounds

The next compound in the series is the propoxy compound which based on the results obtained so far should differ significantly from the isostructural pair, 2,3,6,7,10,11-hexamethoxytriphenylene and 2,3,6,7,10,11-hexaethoxytriphenylene.

2.2.2.1 Hexapropoxytriphenylene

The structure of 2,3,6,7,10,11-hexapropoxytriphenylene also turned out very differently in fact no stacking was observed nor was the molecules observed to be arranged in planer layers. All the molecular planes were found to be at near right angles to one another in a cubic arrangement. The space group number is 228 and the space group is $Fd\bar{3}c$ and there are 32 molecules in the very large unit cell. While this numerical data may seem out of place it serves to illustrate that the molecules find trouble arranging their hairy legs in a rational structure.

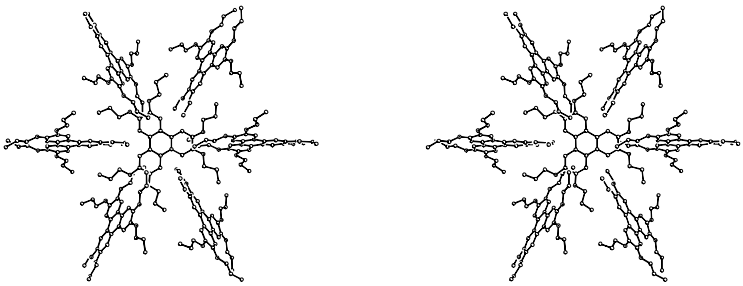

Figure 2.11. A stereoview that illustrates the non-coplanar arrangement of the molecules and how the scissors shape of two adjacent propoxy groups pack with a contiguous molecule.

It should be mentioned that in hexapropoxytriphenylene the number of alkyl chain carbon atoms exactly matches the number of aromatic carbon atoms. It would thus seem that the

alkyl chains have a dominating influence on the structure and that the aromatic core has less influence on the outcome of the structure.

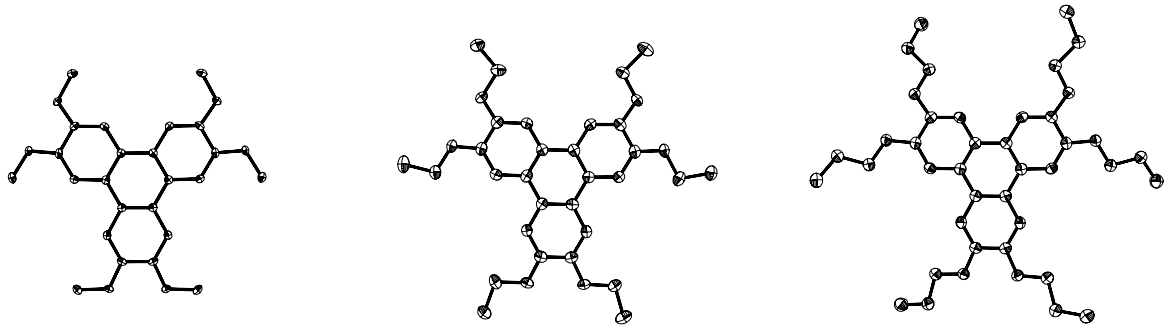

Figure 2.12. ORTEP drawings of the three alkylated derivatives. It should be noticed that the alkyl chains grow from the core in an identical manner (50% ellipsoids)

An attempt to the extend the chain by just one carbon atom more while a synthetic possibility did not give rise to crystals of a suitable quality for single crystal work. This went for the butyl, pentyl and hexyl derivatives for which attempts were made. Powder diffraction data were collected for all three compounds proving the crystallinity of the samples. They do not, however, scatter to very high angle ($< 30^{o}$ 2θ) which is in accordance with the literature where data for the pentyl derivative have been given[78].

2.2.2.2 Other medium chain compounds

The only other triphenylene based medium chain compounds for which studies of a crystallographic character has been initiated are the hexaalkanoyloxytriphenylenes[79]. Further various theoretical studies on the order disorder transitions[80] and the conformations[81] of these systems have been carried out. Single crystal work was attempted with little success and certainly with little conclusive evidence for a stacking in a columnar fashion. Of the compounds studied which were the butanoyl, valeroyl and caproyl derivatives only the first of these compounds allowed for a data collection to be carried out which seen in the light of the size of the structure and the number of reflections collected was rather incomplete. For the remaining two compounds only unit cell data could be obtained. It should be pointed out that

[78] Wang, T.; Donghang, Y.; Luo, J.; Zhou, E.; Karthaus, O.; Ringsdorf, H. *Liq. Cryst.* **1997**, *23*, 869-878.
[79] Cortrait, M.; Marsau, P.; Destrade, C.; Malthete, J. *J. Phys.* **1979**, *40*, L519-L522.
[80] Sun, Y. F.; Swift, J. *Phys. Rev. A* **1986**, *33*, 2735.
[81] Pesquer, M.; Cotrait, M.; Marsau, P.; Volpilhac, V. *J. Phys.* **1980**, *41*, 1039-1043.

the hexaalkanoyloxytriphenylenes are known to give rise to columnar phases where there is a disorder or a density modulation along the stack of molecules in the column. The most common columnar phases for these compounds are the $\mathbf{D_{rd}}$ and $\mathbf{D_{hd}}$ and the pronounced tendency to disorder seems to be linked to the steric demand of the carbonyl groups which results in the chains being out of plane with the molecules thus efficiently preventing extended aromatic π-π stacking. Indeed these compounds are also believed to form dimers within each column with a varying degree of correlation between dimeric species.

2.2.3 The long chain compounds

As mentioned above little work has been initiated on the careful structural characterisation of the short chain and medium chain compounds. The same is true of the long chain compounds perhaps due to an increasing experimental difficulty with increasing chain length

2.2.3.1 The structures of a liquid crystal

The first hexaalkyloxytriphenylene known to exhibit liquid crystallinity is the pentyl derivative. The incentive to achieve structural resolution at the atomic or near atomic level for a material known to exhibit liquid crystallinity bore fruit when using electron diffraction techniques for the crystallographic data collection thereby eliminating the need for a single crystal as only crystalline domains several orders of magnitudes smaller than the size of crystals for single crystal X-ray diffraction are required[45,82]. These structures revealed that the columnar arrangement of molecules did not have extensive aromatic π-π stacking but rather slipped or tilted stacks.

2.2.3.2 The only long chain compound

In spite of the fact that the long chain compounds are the ones forming the largest proportion of known liquid crystalline phases no work on the detailed structural resolution of these compounds have been reported as yet. One structure with an alkyl-like side chain has been reported[83]. While the nature of the chain corresponds to a heptyl side chain in length. It is a water soluble derivative with the side chains being diethyleneglycolmonomethylether. In line with the slipped stacks observed for the pentyl compound a near identical columnar

[82] Voigt-Martin, I. G.; Garbella, R. W.; Schumacher, M. *Macromolecules* **1992**, *25*, 961-971.
[83] Boden, N.; Bushby, R. J.; Jesudason, M. V.; Sheldrick, B. *J. Chem. Soc. Chem. Comm.* **1988**, 1342-1343.

arrangement is observed but while four of the side chains are extended two of them bend significantly out of the molecular plane. One interesting aspect of the water soluble discotic mesogen is the columnar aggregates that are formed in water solution[84,85]. Various interactions between the side chains and the surroundings were thus evaluated i.e. interaction with water and ions.

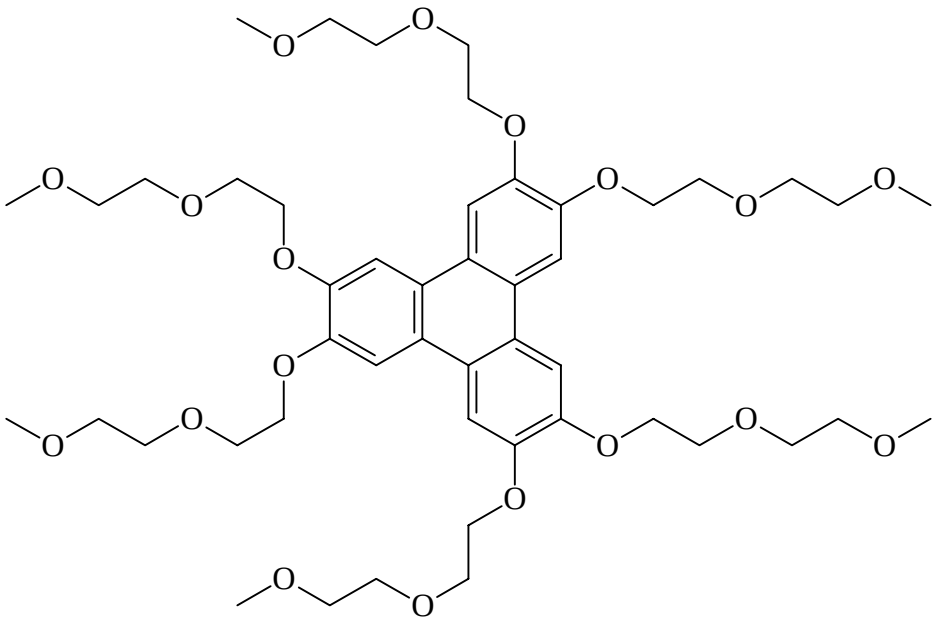

Figure 2.13. The molecular structure of the amphiphilic discotic mesogen. Also the only long chain triphenylene discotic mesogen for which the crystal structure is known.

It would appear that that the crystal structure of the columnar phase was quite invariant with the water content thus allowing for significant water uptake without any alteration of lattice parameters while the aggregation state (i.e. degree of correlation) in solution was highly dependent upon ionic strength.

2.3 The structure of the discotic phase

The concept of a liquid crystal has been defined along with a detailed presentation of what is known on columnar discotic liquid crystals. In this final part a critical discussion of the structure of the columnar discotic liquid crystals as conceptualised in the literature is given. In particular as seen in the light of the findings from this work and some of the important and

[84] Boden, N.; Bushby, R. J.; Hardy, C.; Sixl, F. *Chem. Phys. Lett.* **1986**, *123*, 359-364.
[85] Boden, N.; Bushby, R. J.; Jolley, K. W.; Holmes, M. C. *Mol. Cryst. Liq. Cryst.* **1987**, *152*, 37-55.

seemingly overseen literature findings. The treatment pertains to mainly triphenylene based mesogens but also some of the larger mesogenic core systems are included as they are needed for an acknowledgement of the requirements for a discotic phase.

2.3.1 The molecular conformation in the column

There is no doubt that the columnar arrangements of discotic liquid crystals exist in the crystalline phases and in the mesophase. There is however good reason to disbelieve some of the models proposed for the molecular conformation in the columns in the liquid crystalline state. The main purpose of this entire chapter as a whole and these last three sections in particular is to prove the following argument (discussion and justification will follow).

> ***Columnar discotic mesophases in which the director of the discotic mesogens taken individually and the axis of the mesophasic columns are co-directional do not exist for discotic mesogenic core molecules with a diameter of less than 12Å.***

It should be pointed out that very few of the known mesogenic core molecules actually fulfil the requirements implied by this statement or rule, and certainly, triphenylene is **not** one of the few.

2.3.1.1 The proposed molecular orientation in a columnar discotic mesophase

The columnar structures as the main characteristic of the discotic liquid crystals are well established. The molecular conformations and orientations within the columns are not however. The most plausible way of conceptualising the arrangements is like a pile of plates in a cupboard. While understandable and logically pleasing more scrutiny should have been exercised before so boldly proposing this model as it has since become adopted and shown over and over again albeit as an illustrative and suggestive schematic. A simple concept is good because it allows one to encompass complicated concepts and draw rational conclusions on complex matter with simple means. A wrong schematic planted in ones mind and in the minds of others can severely lead to erroneous results and require a scientific explanation for results that are correct in their own right but that cannot be unified with the unknown-to-be-wrong-but-wrong concept.

Figure 2.14. The stacking of discotic core mesogens in the liquid crystal. To the left, the conceptual orientation which is shown over and over again in the literature for both large and small discotic core mesogens. To the right, the orientation which is the only well documented orientation for the small discotic core mesogens.

To resolve any doubt as to the usage of size descriptions of discotic core mesogens the word small in this context refers to all discotic core molecules with a diameter of less than 12 Å while the word large refers to all discotic core molecules with a diameter of 12 Å or more.

2.3.1.2 The molecular interactions

Of prime importance are the intra molecular interactions. They govern the conformation of the molecule and thereby the possible ways of packing the molecules in space. The intermolecular interactions govern the arrangement of the molecules in an extended system i.e. the choice between the different possible structures given by molecular conformation. As mentioned a discotic mesogen consist of a rigid core and a flexible corona. For all columnar discotic mesogens the amount of atoms in the corona exceeds the amount of atoms in the core by a factor of two or more. Furthermore the corona constituents have a greater thickness than the core. While π-π interaction would be an efficient way of packing the discs it has to be remembered that this sort of interaction is mainly repulsive and only efficient in terms of space filling. It would thus be naive to think or even imply that a grossly under populated proportion of the molecules offering only a repulsive interaction should make the director of the mesogen co-directional with the columnar axis. It is my belief that it is the corona that determines the structure as this is indicated by the studies of the premesogens (*Appendix P9*) and as indicated by the observed structures as mentioned previously. There are thus two ways

of accommodating the discs in columns one is slipped or tilted stacking as shown in figure 2.14 or an incommensurate density modulation arising from the co-directional arrangement and along the columnar stack where on the one hand efficient packing of the core leads to inefficient packing of the corona and *vice-versa* as noted by de Gennes[86].

2.3.1.3 Crystal versus liquid crystal

The point which has not been addressed so far is that most of the studies and conclusions drawn has been on data derived from the crystalline state. What we wish to address is of course the liquid crystalline state. However, the structure of the liquid crystalline state must somehow be derived from the structure of the crystalline state. One study has been carried out assuming this exact strategy where the structure in the crystalline state was first determined using electron diffraction[88]. The result showed the crystalline state to consist of columns of slipped or tilted stacks with an angle of 53^{o} with respect to the columnar axis. While the interplanar distance for the aromatic units was found to be 3.4 Å the distance between the molecules along the column axis was 5 Å. In the liquid crystalline state most high order reflections are lost and the model used to model the liquid crystalline data was a highly constrained model corresponding to the model from the crystalline state. The claim was a hexagonal array of columnar structures with molecules lying flat with rotational disorder. Even though their conclusion is understandable I disagree and will discuss it further in the following section (*Section 2.3.2*).

2.3.1.4 The slipped stacks in the crystal and in the liquid crystal

While it should be unquestionable that the director and the columnar axis are not co-directional for mesogens based on a small mesogenic core in the crystalline state it still need to be proven that slipped stacking is possible in the liquid crystalline state while still in full agreement with the experimental results which have been published but perhaps misinterpreted. An excellent study of triphenylene liquid crystalline material using synchrotron radiation on small strands of the material which could be grown and made stable for days has been pubslished[87]. It was basically shown that the tilt of the molecules with respect to the columnar axis (i.e. the absence of co-directionality of the director and the

[86] de Gennes, P. G. *J. Phys.* **1983**, *44*, L657-L664.
[87] Safinya, C. R.; Liang, K. S.; Varady, W. A.; Clark, N. A.; Andersson, G. *Phys. Rev. Lett.* **1984**, *53*, 1172-1175.

column axis) remained in both rectangular and hexagonal columnar liquid crystalline phases. The explanation for the misinterpretations has to be found with the arrangements of the columns as a function of the mesophases.

2.3.2 The columnar arrangements

We have one piece of solid evidence[87] that the tilt of the molecules in the stacks exist even in the mesophase. All that is needed to unify this with the rest of the knowledge on the mesophases, namely the inter-columnar arrangements.

2.3.2.1 The arrangements of columns

The typical arrangement of columns observed in discotic liquid crystalline materials have been published[88] (on several occasions) and was also shown briefly in figure 2.5. While it is easy to accommodate the concept of tilted or slipped stacking in the rectangular and oblique arrangements of the columns the hexagonal arrangements of the columns observed in the hexagonal liquid crystalline phases does not immediately conform with the tilted or slipped stack concept. The obvious conclusion is of course to assume that the tilt disappears and that the director and the column axis become co-directional. A perfectly understandable conclusion. Someone once said that a theory is only a good theory for as long as it solves or explains more problems than it creates. I will now list a series of reasons as to why the co-directional arrangement of the director and the column axis is not possible for the small mesogenic core molecules or at least there is no experimental evidence that is truly in favour of the co-directional arrangement as opposed to the slipped arrangement. There is however several pieces of experimental evidence in favour of the slipped arrangement as opposed to the co-directional arrangement. The accommodation of the slipped stacking in the hexagonal mesophases becomes very convincing when considering that they are the least ordered phases and with few exceptions always observed at the higher temperatures just before melting. This means that the molecules have thermal energy to move and are in fact rotating which has been verified by NMR experiments[89,90]. If the entire molecules are rotating this means that on the average the entire column take up a volume as if it were rotating thus satisfying the hexagonal requirement and still allowing for tilted rotating molecules. Of course the entire column could

[88] Levelut, A. M. *J. Chim. Phys.* **1983**, *80*, 149-161.
[89] Kranig, W.; Boeffet, C.; Spiess, H. W.; Karthaus, O.; Ringsdorf, H.; Wusterfeld, R. *Liq. Cryst.* **1990**, *8*, 375.
[90] Kranig, W.; Boeffet, C.; Spiess, H. W. *macromolecules* **1990**, *23*, 4061.

also be rotating. It should further be pointed out that while the arrangement of the columns is hexagonal the symmetry is not and further support of the rotating slipped stack column theory is also given[82]. Further there is experimental support of slipped stacks in the hexagonal phase[87]. Evidence against the co-directional arrangement is the inefficient filling of space with a subsequent lengthening of the distance between the planes of the aromatic molecules and in essence resulting in equal favour of the nematic discotic and the columnar discotic arrangement. It is also very likely that it is the difference in thickness between the core and the corona which is the main reason for the observation of the columnar arrangement as an equal thickness would favour the nematic arrangement as observed for instance for some of the hexabenzoyloxy substituted triphenylenes which show nematic/columnar polymorphism[65].

2.3.2.2 Conclusions

The results from this work and the careful study of the literature have provided a clearer picture of the columnar discotic phases with respect to the molecular arrangements within the columnar stacks. In particular all columnar discotic mesophases phases with mesogenic core molecules having a molecular diameter of less than 12 Å consists of slipped stacks of molecules. And argument for the choice of 12Å as the threshold will follow.

2.3.3 The requirements for a co-directional columnar discotic

The above treatment showed (with all due likelihood) that the most commonly encountered discotic mesogens have a core molecule too small in diameter to allow for a columnar arrangement with co-directional director and column axis. An interesting question to ask is whether such a system could be designed and if so what the requirements would be.

2.3.3.1 The difference in thickness for the core and the corona

It has been mentioned a few times now that the closest packing of typical corona constituents (i.e. alkyl chains) leads to a thickness of 4.6 Å (or mean diameter of the chain) whereas the thickness of typical core constituents (i.e. planar aromatics) leads to a thickness of 3.4 Å. One way to accommodate these differences in thickness when constructing a columnar stack is by tilting the planes of the thin constituent with respect to the stacking axis. Another way of doing it which avoids the tilting is by having sufficiently spaced side chains such that a

staggered arrangement of the discotic molecules allow for efficient space filling. In this way the side chains do not collide when attempting to bring the core molecules close together.

Figure 2.15. An illustration of how staggering can allow for a co-directional arrangement. The lower molecule (green) and the upper molecule (red) have their core molecules close together and their alkyl chains sufficiently spaced around the perimeter of the core molecule to allow for efficient packing of both parts.

From the illustration of figure 2.15 it is evident that a certain diameter of the core molecule along with a sufficient spacing of alkyl side chains is required for the staggered arrangement and co-directionality of the columnar axis and the director.

2.3.3.2 The required size of the core

From this simple picture a rule-of-thumb can be drawn. While of course the required size of the core molecules depends upon the substitution pattern columnar discotic mesogens in general needs side chains more or less equally distributed around the perimeter. In assuming the above the core molecules can be thought of as a discs with an interplanar spacing, *d*, and the side chains can be thought of as cylinders with a diameter, *D*. The distance between the side chains along the perimeter of the core molecule for a given interplanar spacing is given by the length, *l*. The required radius, *r*, of the core molecule is thus given by the number of side chains, *n*. There are of course some problems in defining where the core region ends and the corona region begins but it is still only a rule of thumb and certainly capable of ruling out unlikely candidates. It is based on a simple geometric consideration and it can be seen that for typical interplanar distances, alkyl chains and the number of side chains (which normally is in

the range of six to eight i.e. molecules with (two-,) three-, four- or six-fold molecular point group symmetry) the value of *r* ends up in the vicinity of 6 Å i.e. a disc diameter of around 12 Å.

$$r = \frac{nl}{\pi} = \frac{n}{\pi}\sqrt{D^2 - d^2}$$

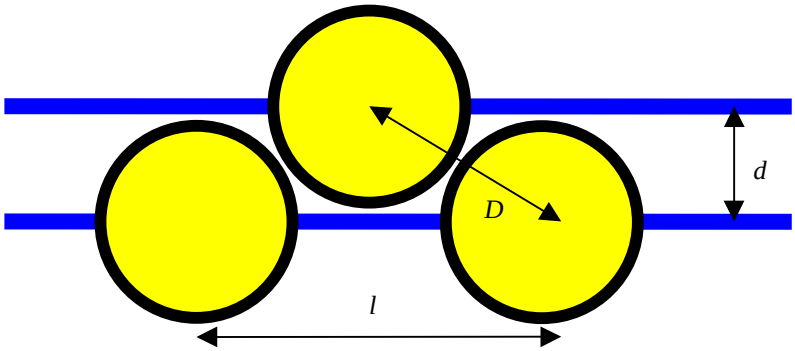

Figure 2.16. A view from the side of the simple geometry which is the basis of the 12 Å rule. It has to be imagined that the perimeter of the mesogen has been rolled onto a plane. The planes of the aromatic cores (blue) have a separation *d*. The diameter of the side chains (black circles with a yellow filling) *D* is also the closest they can be brought together. Finally the distance between two side chains, *l*, on the same core molecules which is required for an interplanar stacking of *d*.

For triphenylene a disc diameter of 9.5 Å is obtained including the oxygen atoms thus considerably less than 12 Å and further the spacing between adjacent alkyl groups (on the same molecule) is not large enough to allow for staggered packing.

2.3.3.3 Existing candidates for the co-directional arrangement

With this new picture at hand it is possible to examine the known discotic mesogenic core molecules and say which of them that can give rise to a staggered arrangement of discotic molecules in a columnar mesophase with co-directional director and column axis. Of the molecules given in figure 2.2 only the phthalocyanine and the truxene derivatives have a diameter larger than triphenylene and while some experimental results have been obtained which seem to indicate the presence of the desired co-directionality they are not conclusive. An experiment needs to be designed whereby the proper angle between the director and the column axis can be measured properly. For instance in the $\mathbf{D_{ho}}$ mesophases where fast rotation of the columns make it appear that there is co-directionality even though there is not. A good

candidate would be hexabenzocoronene for which some NMR data was published recently[91] on a mesophase. In this system it is likely that the diameter of the disc is large enough to allow for a staggered stacking of the discotic molecules in a columnar arrangement.

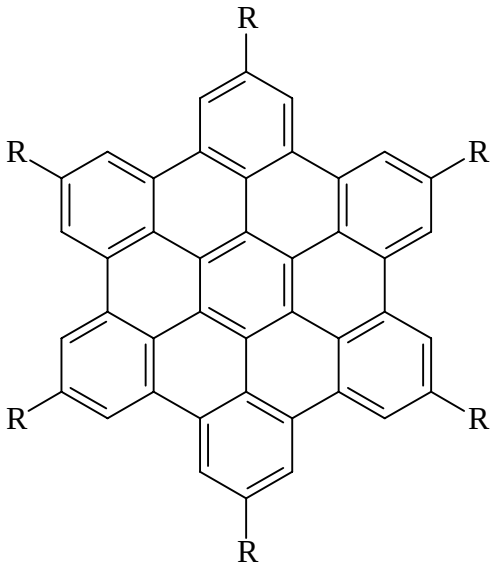

Figure 2.17. Hexabenzocoronene based mesogen. Here the spacing of the alkyl chains (R) and the diameter of the core molecule is sufficient to obtain the co-directional arrangement.

Interestingly the synthesis of the hexabenzocoronene based mesogens is elegant and in only two steps! (from the corresponding tolanes). I would be surprised if these molecules do not hold promise for the future of columnar discotic liquid crystals.

[91] Brown. S. P.;Schnell, I.; Brand, J. D.; Müllen, K.; Spiess, H. W. *J. Am. Chem. Soc.* **1999**, *121*, 6712.

Chapter three

There were three people Mogens Larsen, Mikkel Jørgensen and myself. A dynamic trio that managed to produce a large amount of work on calixarenes in a relatively short time span. I would like to express deep respect, gratitude and thank them both for what I would call the most productive and constructive environment I have ever worked in. Some people other than the dynamic trio have also contributed to this chapter namely Pernille R. Jensen, Mia Bielecki, André Faldt and Kjeld Schaumburg.

3.1 Introduction to calixarenes

The calixarenes have a long history, unfortunately most of the time it was not known that it was the calixarenes that were responsible for writing the history. They are examples of bright peoples discovery, but also examples of a discovery at a stage to early for them to be properly characterised and thus they have, while their existence was granted, suffered for many years as an elusive series of compounds.

3.1.1 A brief history and definition of calixarenes

The bright people had impressive names like Johann Friedrich Wilhelm Adolph von Baeyer, Leo Hendrik Baekeland and Alois Zinke and many others that fathered great ideas and took on problems that by today's measures would seem of moderate difficulty but by the measures of the past their skill, ability and inclination towards an understanding of the insurmountable problem they themselves had posed deserves no less than absolute respect.

3.1.1.1 The condensate

About one hundred and thirty years ago Johann Friedrich Wilhelm Adolph von Baeyer mixed phenols and aldehydes under acidic conditions to get a cement-like substance. This was the beginning of the phenol aldehyde chemistry that is the basis for obtaining molecules like calixarenes. Some thirty years later Leo Hendrik Baekeland took on the job of investigating how phenoles reacted with formaldehyde for some of the 1.000.000 $ that he earned from a patent on photographic paper. The incentive was to make use of the condensate as an item of commerce and in this way he founded the plastic age that we all live in today. It took another

forty years before Alois Zinke while studying some properties of the condensate managed to isolate crystals. From the condensate he isolated a molecular material that could be recrystallised and had a high melting point. At the time an idea of a cyclic tetrameric structure rumoured and Alois Zinke thought of this as well. Even though he had determined the molecular weight by cryoscopy to be around 1725 g mol^{-1} for the acetylated product which was more indicative of an octameric product it was by the standards of the past a proposition that no one would even dare to utter.

3.1.1.2 The molecular weight

The discrepancy in molecular weight was soon resolved, partially, at least when making another derivative that had the right molecular weight for a tetrameric structure. While the tetrameric nature seemed a fact work on elucidating the structure was done by the stepwise synthesis of the cyclic tetramer and finding that it was identical to the product obtained by the condensation reaction. It was not until much later that an absolute confirmation of the molecular structure was provided by X-ray crystallographic means in the end of the 1970's. This also serves to illustrate that while X-ray crystallography is a powerful tool unsurpassed in many ways it will never even come close in matching the impressive feat of these peoples pure and condensed intellectual horsepower.

3.1.2 The synthesis of calixarenes

While the synthesis of the crystalline products had been known for more than a century there were still the problem of controlling the synthesis. The synthesis and the entire basis for the calixarene chemistry of today is due to mainly one man, C. D. Gutsche, who has written an excellent book on the subject which is very well referenced. Little reference is given here as it can all be found in Gutsche's book[92].

3.1.2.1 The precursor

The synthesis of calixarenes is a simple mixing of for instance *p-tert*-Butylphenol, 37% fomaldehyde and an amount of base. The base is important as the cation plays an important role to the product obtained and so does the concentration of the base. But if the right

[92] Gutsche, C. D. *Calixarenes,* Monographs in supramolecular chemistry, Stoddart, J. F. Ed., Royal Society of Chemistry, Cambridge, 1989.

conditions are adhered to then good yields of the desired calixarene is obtained. When heating the mixture a thick meringue like substance is obtained which is called the precursor (at least when making the tetramer and the hexamer). The calixarene product is not obtained until the meringue like precursor is cracked in a high boiling solvent like diphenylether or xylene. Again the nature of the solvent depends on the particular calixarene. But otherwise the cracking procedure simply involves boiling the precursor in the solvent for a few hours. For the synthesis of calix[4]arene *p-tert*-butylphenol, 37 % formaldehyde and 0.045 equivalents of NaOH is used for the precursor and diphenyl ether for the cracking procedure, for the synthesis of calix[6]arene *p-tert*-butylphenol, 37 % formaldehyde and 0.34 equivalents of KOH is used for the precursor and xylene is used for the cracking. For the synthesis of calix[8]arene no precursor is made and instead the *p-tert*-butylphenol, 37 % formaldehyde and 0.03 equivalents of NaOH is mixed in xylene and refluxed directly.

3.1.2.2 The cyclic oligomers

So far no mention have been given of what the actual molecules look like. The calix[*n*]arenes where *n* indicate the number of aromatic rings involved in the metacyclophane have the general molecular structure as that shown in figure 3.1. The name calix comes from the Greek word for vase or chalice.

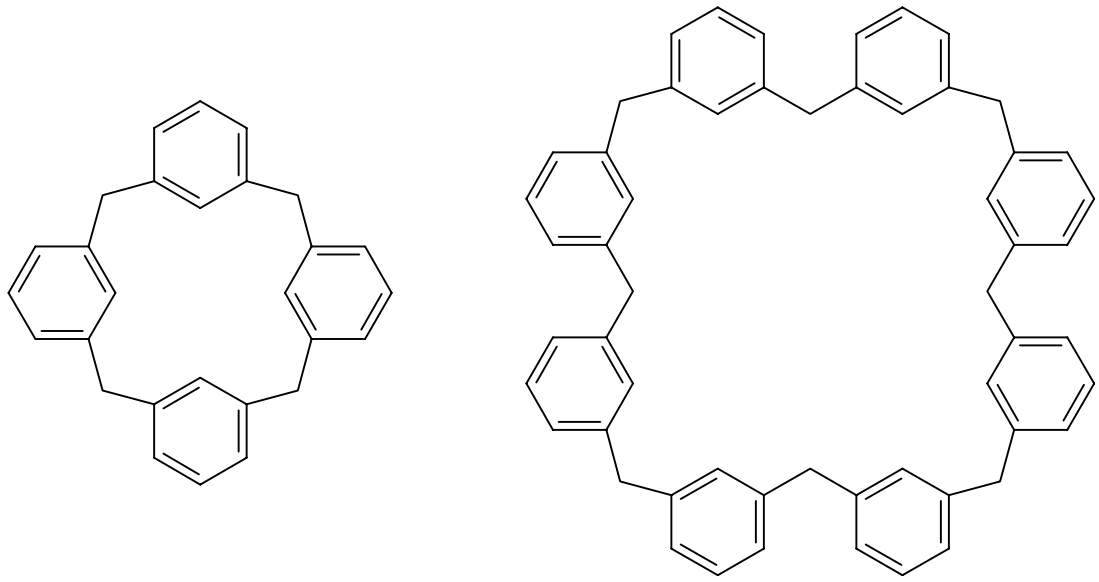

Figure 3.1. The molecular structure of calix[4]arene and calix[8]arene. The phenolic groups have been omitted.

The name calix was chosen because the molecules were thought to resemble a vase in shape or a basket. Calix[*n*]arenes are readily available with *n* equal to 4, 6 and 8 and less readily with *n* equal to 5 and 7. Further more a large series of calixarenes with hetero atoms, different substituents and arenes different from benzene exist. The large interest in calixarenes was spurred by the recognition of enzyme structure and enzyme reaction mechanism which opted for simpler synthetic molecules that could host one or two molecules and perhaps be made to exhibit catalytic activity. Calixarenes was a natural choice to some chemists and this suddenly gave rise to an enormous research effort within the field of what was to become recognised as calixarene chemistry, an area of chemistry which has expanded immensely in just thirty years.

3.1.3 Host-guest chemistry of calixarenes

The host guest chemistry of calixarenes is perhaps the most characteristic feature of calixarenes as a whole and the discovery of the clathrates and inclusion compounds they give rise to confirmed the idea of them as being good platforms for synthetic enzyme studies.

3.1.3.1 The simple inclusion compounds

The bowl shaped *p-tert*-calix[*n*]arenes form complexes with various small solvent molecules like chloroform, benzene, toluene, xylene, anisole, isopropyl alcohol and acetone. The slight differences in the size of the cavity for the different calixarenes makes them selective of the solvent molecules they include. The strength of binding depends on the size of the calixarene. Even though the calixarene molecules appear large there is surprisingly little room inside the cavity even for the largest of the calixarenes. For instance the cavity of calix[4]arene has a size that can just hold a methyl group. Two *p-tert*-calix[4]arenes combined can just hold an anisole molecule when joining forces. Obviously some means of enlarging the cavity is needed so that larger molecules can be held if of course the calixarenes are to bind functional molecules.

3.1.3.2 The binding of metal ions

Fortunately the calixarenes have another functionality than just the cavity. The hydroxy groups of the calixarenes based on the *p*-alkylphenols (if not alkylated) form a ring of specific hydrogen interactions that lock the calixarene in the bowl shaped conformation. These hydroxy functionalities can also bind various cations but not in the traditional sense as

observed for the crown ethers. The calixarenes are particularly efficient in binding and transporting cations of group I elements of the periodic table across a non-aqueous membrane. While the annuli of the calixarene mono anions are in most instances significantly smaller than the ions they are transporting some other mechanism might be operating and an *endo* complex has been suggested in the case of caesium. The ability to efficiently transport cations across a membrane and not only transport them but selectively transport one ion from a mixture across a membrane has led to intense research in making ion selective electrodes etc. and furthermore the chemistry of the hydroxy groups have been modified so as to better bind ions. The distinction between *endo* and *exo* complexes are that for the *exo* complexes the guest molecule can be bound anywhere outside the cavity formed by the arenes whereas for the *endo* complexes the guest has to be bound inside the cavity.

3.1.4 Using calixarenes

All these preliminary recognitions on the simple calixarenes made the design of more specific calixarene molecules imminent.

3.1.4.1 World perspective

A versatile platform like the calixarene molecules have made them become tested for use in very diverse areas of application. Some areas of application have made use of calixarenes on a large scale i.e. the breaking of crude oil emulsions. Furthermore speculations on their potential use in extracting uranium from the worlds sea water and have led to actual experiments which have shown them to be an amazingly efficient and also an appealing way of mining the upper crust of the earth for uranium but the findings also hold prospect for other minerals. The selective transport and binding of ions have given rise to ion selective electrodes, selective for particular mono valent cations and completely undisturbed by the presence of divalent cations. More advanced designs would be the use of calixarenes as catalysts, biomimics or even physiological compounds.

3.1.4.2 Actual sensor design

It must be remembered that the calixarene itself is not specific for any complex organic molecule and has instead to be considered as the platform onto which the specificity has to be engineered. A lot of the way a deep understanding of the calixarene skeleton and

conformational behaviour can pave the way for the engineering approach. The purpose of this study was thus to understand the molecular conformational behaviour of differently substituted calixarene molecules so that a sensor could be designed. It proved to be a difficult task to make a specific sensor but based on the solid piece of characterisation work presented here a sensor specific for the biological molecule ephedrine was arrived at.

3.1.5 The calixarenes used in this study

While a myriad of different calixarenes exist and have been subject to intense research the calixarenes used in this study have been limited to just one type of calixarenes.

3.1.5.1 Calix[4]arenes

There are several reasons that make calix[4]arenes an attractive choice as the chemical platform for synthetic design. Most importantly the fact that they are the least flexible of the series.

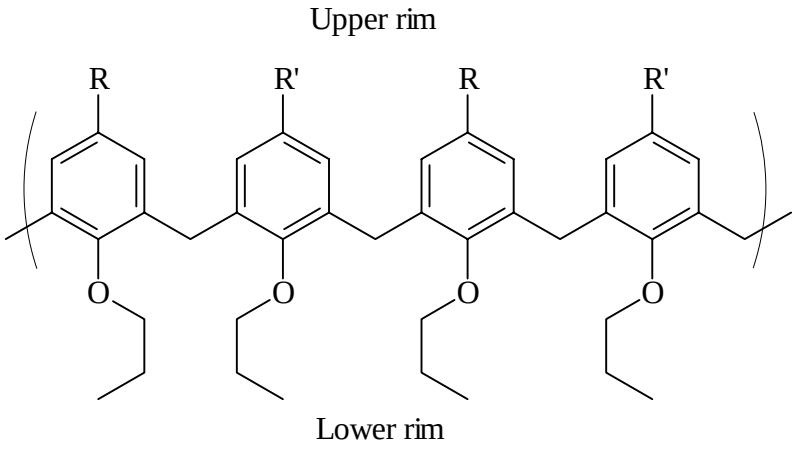

Figure 3.2. An illustration the calix[4]arenes used in this study. The upper rim substituents (R and R') varied but the lower rim was in all instances substituted with propoxy groups.

Molecules of the general form shown in figure 3.2 were the choice. The reason for having propoxy groups at the lower rim will be discussed later but as a brief explanation they serve to lock the conformation.

3.1.5.2 The R-groups

Since the substituents on the lower rim have been chosen as propoxy groups. The upper rim was the place where the engineering of the tetra-propoxy-calix[4]arene were to be carried out.

The starting material was the tetrabromotetrapropoxycalix[4]arene (where R = R' = Br) in all instances and further derivatives were made by bromine-lithium exchange on this compound as a very efficient method had been developed by Mogens Larsen[93]. This method enables one to make R and R' different.

3.2 Controlling the conformation of calix[4]arenes

While NMR is a very useful tool for characterising the conformation of the calixarene molecules in solution X-ray crystallography proved to be a very useful technique in understanding the conformation behaviour as a function of an altering of the substitution pattern.

3.2.1 Known calix[4]arene conformational behaviour

Before presenting the specific results and conclusions from the work on tetrapropoxy-calix[4]arenes it is appropriate to give some detail on what is known regarding the conformational behaviour of calix[4]arenes.

3.2.1.1 Rotational freedom

The simple calix[4]arene as shown in figure 3.1 can exist in one of four conformations. The definition of the individual conformations can be determined as follows. A vector can be defined for each aryl group. Furthermore a molecular axis can be defined passing through the molecule.

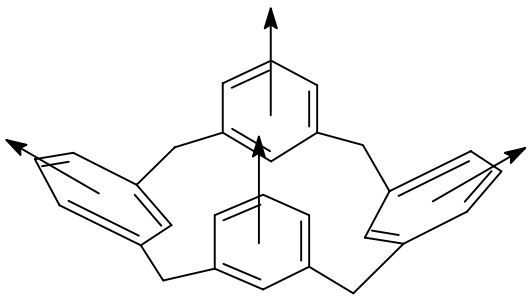

Figure 3.3. An illustration of the vectors used to define the conformation of the calix[4]arene molecule.

[93] Larsen, M.; Jørgensen, M. *J. Org. Chem.* **1996**, *61*, 6651-6655.

The conformation is then determined by the component of each vector along the molecular axis (*z*-axis). A total of four possible conformers are possible as shown in figure 3.4. The conformer which has attracted most attention is the *cone* conformer with all four vectors having a *z*-component with the same sign. The 1,3-alternate conformer is the only other conformer which has attracted some attention in terms of research effort. Judging by the amount of structures found in the CCD the number of structures found are respectively *cone*/*partial cone*/*not cone*:317/25/58.

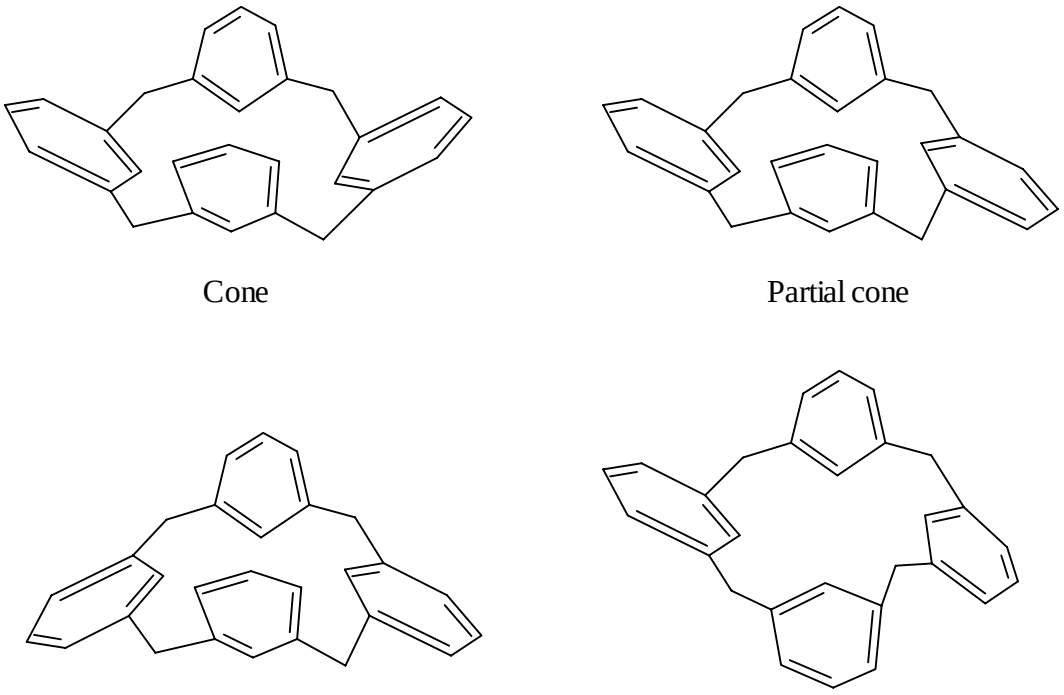

Figure 3.4. The four possible conformations of the calix[4]arene prototype. All four conformers exist for the simple molecule as shown.

There are also some borderline cases where for instance it is difficult to judge whether it is a *cone* or a *partial cone* conformer as the aryl group half way in between (or the *z*-component of the aryl group defined above is zero).

3.2.1.2 The cone conformer and its symmetry

While it has been shown that the 25,26,27,28-tetrahydroxy-calix[4]arene exists in the *cone* conformation and has exact C_{4v} molecular point group symmetry a conformational complication arises when these hydroxy groups are alkylated. The alkylation with for instance propyl groups (as is the case for all the calixarenes studied in this project) serves the very

important purpose of locking the conformation so that the aryl groups can not rotate around the methylene bridges and through the ring so as to convert to one of the other conformers. This action however disrupts the specific hydrogen interacting network that stabilises the exact C_{4v} point group symmetry of the *cone* conformer. What is then observed is a rapid equilibrium between two so-called *pinched cone* conformers which have C_{2v} point group symmetry. The equilibrium between the two conformers is rapid in solution at room temperature but at lower temperatures the inter conversion stops.

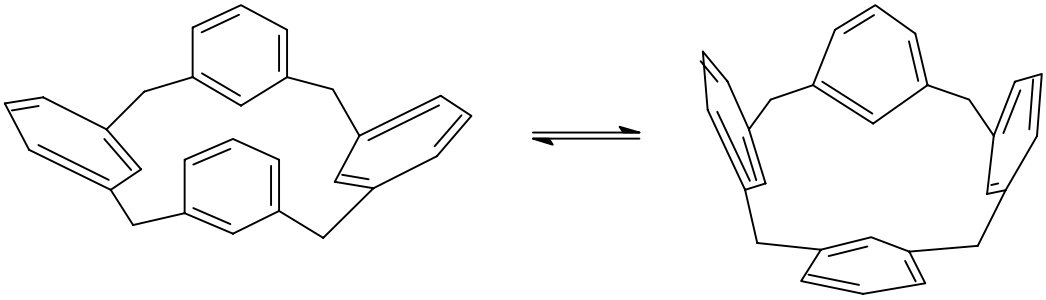

Figure 3.5. An illustration of the inter conversion between the two C_{2v} *cone* conformers for a simple calix[4]arene ground system.

To some extent the equilibrium depicted in figure 3.5 can be affected by the nature of the substituents present at both the upper and the lower rim.

3.2.2 Use of substituents on the upper rim to control the conformation

We now turn to a treatment of the conformational properties relevant to this project and from now on it is assumed that there are propoxy groups attached to the lower rim and the effect of the substituents at the upper rim is explored.

3.2.2.1 Four alike substituents

As shown in figure 3.2 the chemistry available allowed easy access to calixarenes of a general type with either two or four substituents the same. The question as to what happens to the molecular structure if the calixarene is substituted at the upper rim with four non interacting substituents was sought answered by the synthesis of a tetra phenyl derivative followed by solving the crystal structure. The calixarenes are large flexible molecules that sometimes form crystals of a poor quality for X-ray crystallographic analysis. Most of the time however nice crystals can be grown from mixtures of solvents like chloroform and acetonitrile. During this

work 27 crystal structures of calixarene molecules were solved and 17 of them crystallised with solvent (22 of the structures have been published). Even though this is not enough for a thorough statistical analysis it does indicate that a large proportion (maybe 65%) of the calixarenes crystallise with solvent. When solvent molecules are included in the crystal this makes the handling of the crystal and the crystallographic data collection more delicate than for standard small molecule crystals.

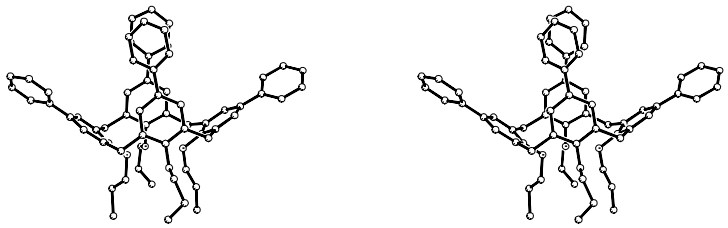

Figure 3.6. A stereoview of the molecular conformation of a tetra substituted calixarene, 5,11,17,23-tetraphenyl-25,26,27,28-tetrapropoxycalix[4]arene.

The tetra phenyl derivative had an approximate C_{2v} molecular point group symmetry as expected and a pinched *cone* conformation. This fact of course implies that two of the substituents are splayed outwards (pointing away from the centre of the molecule) and the other two substituents are pinched together. It is noteworthy that the planes of the two phenyl rings that are pinched together actually are coplanar and have an interplanar distance of around 3.5Å which indicates close contact.

3.2.2.2 Two alike substituents

The next question was then whether the interaction between the two pinched phenyl rings was a favourable interaction or whether it was coincidental. To get a hint the diphenyl derivative was synthesised and the structure was solved for comparison. As seen when comparing the two stereoviews for the two compounds the di substituted compound does not crystallise with the phenyl rings pinched together. The way to interpret this fact is that the interaction energy between two pinched phenyl rings is weak if anything much weaker than the packing forces involved in packing molecules into a crystal.

Figure 3.7. A stereoview of the molecular conformation of a di substituted calixarene, 5,17-diphenyl-25,26,27,28-tetrapropoxycalix[4]arene.

Another similar study was undertaken with a different substituent and the exact same result was obtained.

3.2.3 Large stiff aromatic substituents

In the quest for conformational knowledge a series of calixarenes with two stilbene substituents attached to the upper rim were synthesised and their structures solved for comparison.

3.2.3.1 The compounds

There were three positions that could be substituted and crystals readily obtained. All but one of the molecules contain bromine atoms which are a great advantage with respect to the quality of the crystallographic data. Generally the crystallographic data that could be obtained for the calixarenes involved in this study ranged from average to poor i.e. The internal *R*-factors for the particular data sets ranged from 0.03 – 0.2 in general. Obviously this sets a limit in some instances to what kind of information that can be extracted from the crystallographic data and the detail of the model. In the worst cases only the conformation of the molecules, the connectivity and the packing arrangements could be established safely and any detailed discussion of bond lengths etc. would have been unjustified. The information should however not be neglected as it is very valuable even though it might be unacceptable in a traditional crystallographic sense. Generally the larger the structure the poorer the data and it must be remembered that the structures are large.

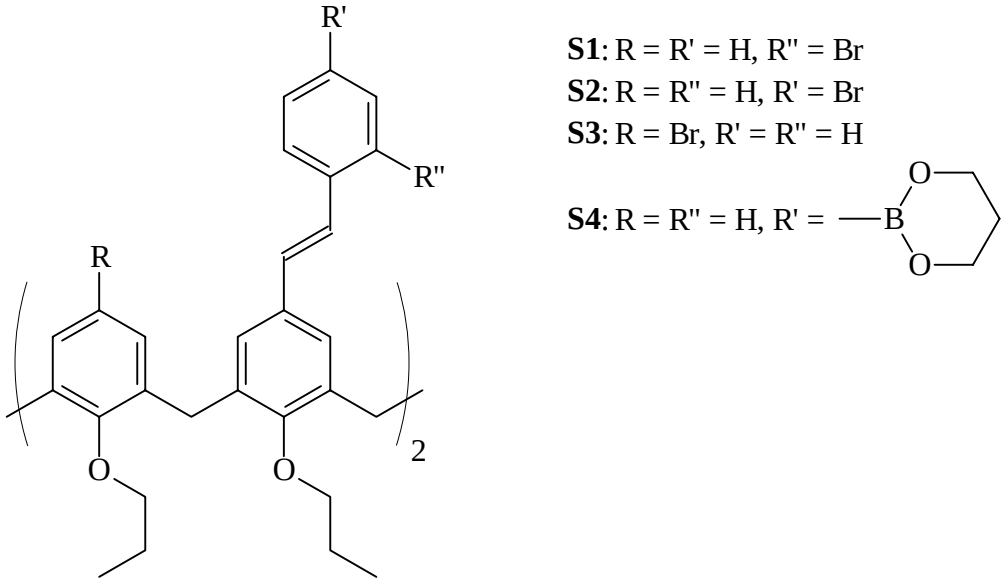

Figure 3.8. The stilbene substituted calixarenes for which the structures were solved and their structures compared.

In some instances up to more than 350 independent atoms were in the final model. In such a case an internal *R*-factor of 0.09 and a *wR*-factor of 0.11 for the final model is perhaps not surprising (see *Chapter 4* for a further discussion of *R*-factors and large molecules).

3.2.3.2 The shape of the substituent

A bromine atom has quite a considerable steric demand much like that of a methyl group. It was therefore of interest to see how the molecular structure and the crystal structure reacted to the placement of a bromine atom as in compound **S1** and **S2**. The stilbene substituent was splayed outwards in both instances but the methyl group had a significant influence on the molecular structure and on the crystal structure when placed as in compound **S1**.

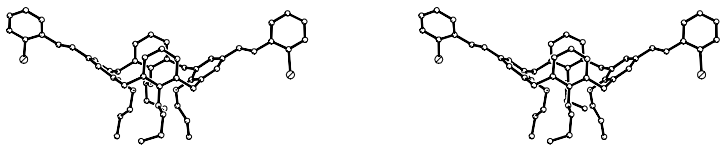

Figure 3.9. A stereoview of the molecular conformation for the compound **S1** described in figure 3.8.

It was noticeable that the stilbene units were not planar but twisted as shown in figure 3.9. The splay angle was also significantly larger than for the other three compounds compared in this section. For compound **S2** the stilbene units were planar unlike the stilbene units of **S1**. The packing arrangements in the crystal were similar for all molecules in this section but again compound **S1** did show some slight differences. The general packing motif simply involves a stacking of the V-shaped molecules. The structure can in this way accomodate nearly any size of substituent.

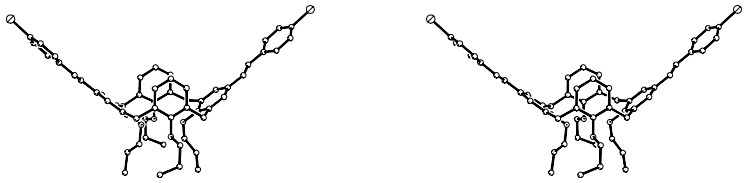

Figure 3.10. A stereoview of the molecular conformation of compound **S2** it is possible to see how the splay angle of this molecule is smaller than for **S2**.

The slight difference in the packing of **S1** is that the substituents do not interdigitate in the same manner due to the twist of the substituent aryl ring. This may account for the larger splay angle observed in compound **S1** so that it efficiently fills out space.

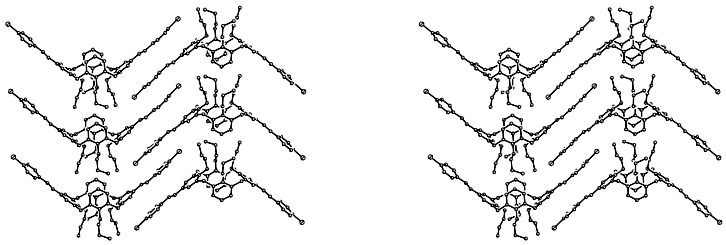

Figure 3.11. The stacking observed in the structure of compound **S2**. The interdigitating substituents allows this type of structure to accommodate any size of substituent.

As a note it should be mentioned that there are two molecules in the asymmetric unit of **S1** and that there are distinct differences between their conformations. It is the most taut of the

molecules that is shown here. Furthermore compound **S1** does not crystallise with a solvent molecule as does compound **S2**.

3.2.3.3 The length of the substituent

While evident that the in structures with two large substituents a preference for having the larger substituents splayed outwards is observed the next question could be to significantly extend the length of the substituent and see if this had any effect. The boronic acid cyclic ester as in **S4** makes the substituent much longer than the unsubstituted molecule **S3**.

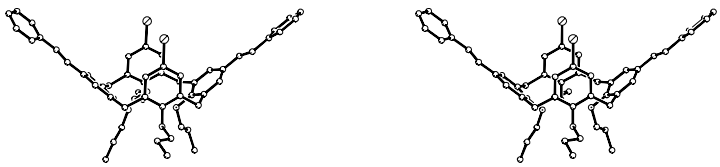

Figure 3.12. A stereoview of the molecular conformation for the compound **S3**.

The molecular conformation of compound **S3** much like that of compound **S2** but it is the compound of the series with the smallest splay angle. A good explanation for this is the steric effect of the bromine atoms that makes the distance between the stacking molecules slightly longer 9.5 Å versus 9.3 Å in compounds **S2** and **S4**.

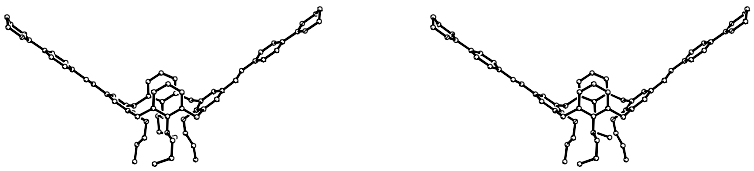

Figure 3.13. A stereoview of the molecular conformation for the compound **S4**.

The molecular conformation and the packing in the crystal of compound **S4** is similar to the other three molecules. In summary all compounds are very similar but slight differences could be observed by the structural perturbations that the small series present. **S2**, **S3** and **S4** are very similar whereas **S1** is a bit different with respect to both the molecular conformation and

the packing in the crystal. Of the compounds **S1, S2**, **S3** and **S4** the stacking distance is similar for **S2** and **S4** while only the **S3** has a longer and **S1** has a shorter stacking length.

3.2.3.4 The properties of the stilbenes

It should perhaps be mentioned that the original motive for the preparation and study of the stilbenes was to establish whether the fluorescent properties of the stilbene moiety could be used to monitor the presence or absence of a guest molecule i.e. a sugar molecule. Seen in the light of the results obtained from the crystal structures and the results obtained in solution by NMR this was a rather still-born approach. Much was however learned from this study and in my eyes this piece of work has been very fruitful in that some of the structural properties of the calix[4]arenes have been uncovered. A comprehension of the molecular conformational behaviour of these molecules had begun and it only spurred more interest in controlling these conformationally wild molecules. Part of this work has been published and can be found in *Appendix P10*.

3.2.4 Intramolecular π-π interactions

Having recognised the conformational behaviour of disubstituted calixarenes as being in favour of a splayed conformation but also having recognised that in the tetra substituted case the pinched substituents did interact. This section seeks to determine how large the substituents of the disubstituted calixarenes should be before a pinched rather than a splayed conformation was observed.

3.2.4.1 One aromatic ring substituent and perturbations

In *Section 3.2.2* we already saw how the diphenyl calixarene behaved with the phenyl substituents splayed outwards. To further substantiate this the structure of the bis-(3-bromophenyl)-calixarene was solved and in this way probing both the structural variance and the molecular conformation with a steric perturbation. The two compounds are isostructural and have like many of the calixarenes in this series a tendency to crystallise in space group C2/c. The molecular conformations observed were also very similar the steric effect of the bromine atom being visible as a larger torsion angle between the aryl group of the calixarene and the aryl group of the substituent.

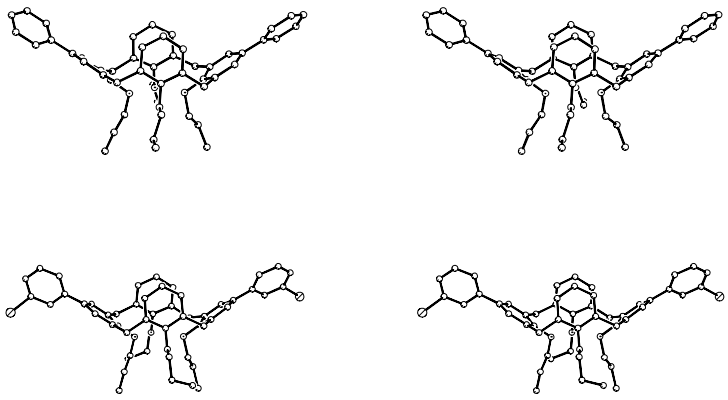

Figure 3.14. A comparison of the two phenyl substituted molecules shown here as a stereoview. The upper compound was shown also in figure 3.7.

The packing arrangement for these molecules is similar to that of compound **S1** of the previous section where the molecules form stacks but the substituents between adjacent stacks do not interdigitate because of the torsion angle between the substituent and the calixarene as mentioned above.

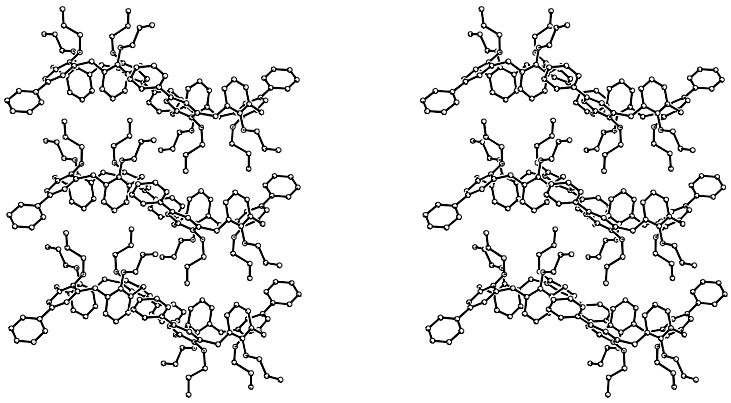

Figure 3.15. A representative packing plot of the diphenyl substituted calixarenes showing both the stacking and the inter stack arrangement. Shown as a stereoview.

It is interesting to compare the packing of the V-shaped disubstituted calixarenes with the packing observed for the smaller V-shaped molecules discussed in *Chapter 1* (*Subsection 1.2.2.5*). While the disubstituted calixarenes have a V-shape and show a pronounced tendency to stack the direction of adjacent stacks is anti parallel. While in at first glance in violation of

the statement made in *Subsection 1.2.2.5* it is not on second thought. While the calixarenes are V-shaped molecules that form stacks, the kink region (i.e. the entire calixarene) is large and does give rise to problems concerning efficient space filling of the voids formed between the substituents. The system accommodates this in two ways. The stacking length is of the order of 9 - 9.5 Å thus considerably larger than 3.3 - 3.6 Å. One way is by tilting the planes of the substituent with respect to the stacking axis analogous to the discussion of the stacking of triphenylenes in *Chapter 2* but still limited by the conformational space of the calixarene. The second and most important way is by making the stacks interdigitate which however implies an antiparallel interstack arrangement.

3.2.4.2 Two and three aromatic ring substituents

How large should the aromatic substituent be before the pinched conformation of the disubstituted calixarenes were to be observed. The answer was given by having a naphthyl group as the substituent (a substituent with two aromatic rings). Naphthalene proved to be large enough to alter the conformation so that the substituents were pinched together in the solid state.

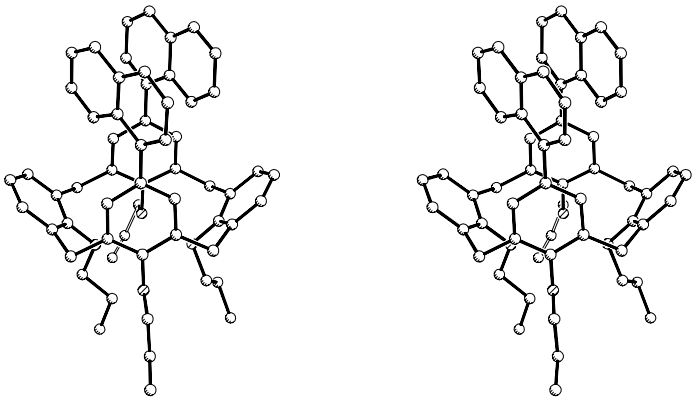

Figure 3.16. A stereoview of the bis-naphthylcalixarene which has the naphthalene substituents pinched together.

While one has to be cautious with the conclusions drawn on molecular conformational behaviour based on the solid state structure these results were confirmed by NMR in solution (in $CDCl_3$) where the naphthalene groups do not become splayed outwards until at higher

temperature which in effect means that there is a definite π-π interaction which controls the molecular conformation of the calixarene which is an observation with large implications on our understanding of the conformational behaviour of the disubstituted calixarenes. To further substantiate these findings a substituent with three aromatic rings was employed and the structure was solved.

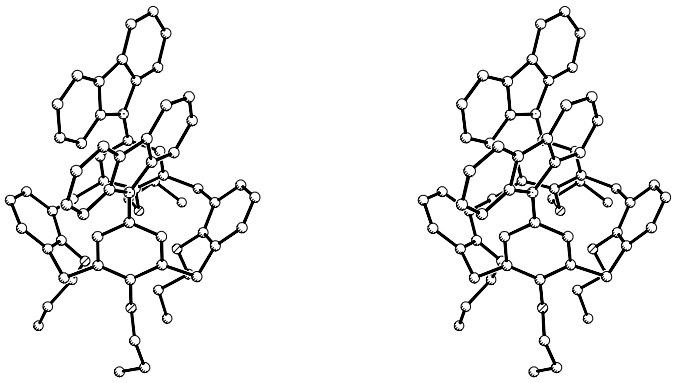

Figure 3.17. A stereoview of the dicarbazolylcalixarene again showing the pinched conformation of the substituent carbazolyl substituents.

It was the dicarbazolyl derivative which in essence can provide the same overlap as the naphthalene group but because it extends to both sides of where it is attached it provides a better interaction with respect to rotation around the substituent bond.

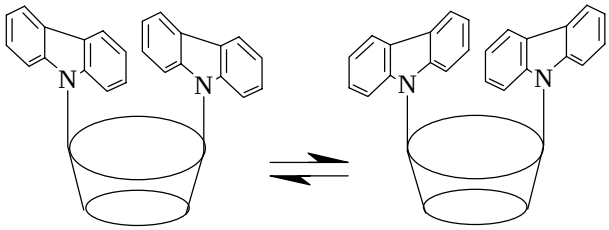

Figure 3.18. An illustration of the rocking motion of the carbazolyl substituents believed to be the reason for not observing free rotation of the substituents.

Again in solution the pinched conformation was preferred. But unlike the naphthalene substituent the carbazolyl substituents stayed pinched together in solution at all the temperatures accessible in the experiment. It can be imagined that rotation around the

carbazolyl substituent bond results in a rocking motion where the carbazolyl substituents rocks back and forth between two conformations one as shown in figure 3.18 and the other its mirror image. In terms of structure the naphthalene and the carbazolyl derivatives are isostructural and both crystallise in $P\bar{1}$ packing head-to-head and tail-to-tail in the structure with slightly interdigitating substituents.

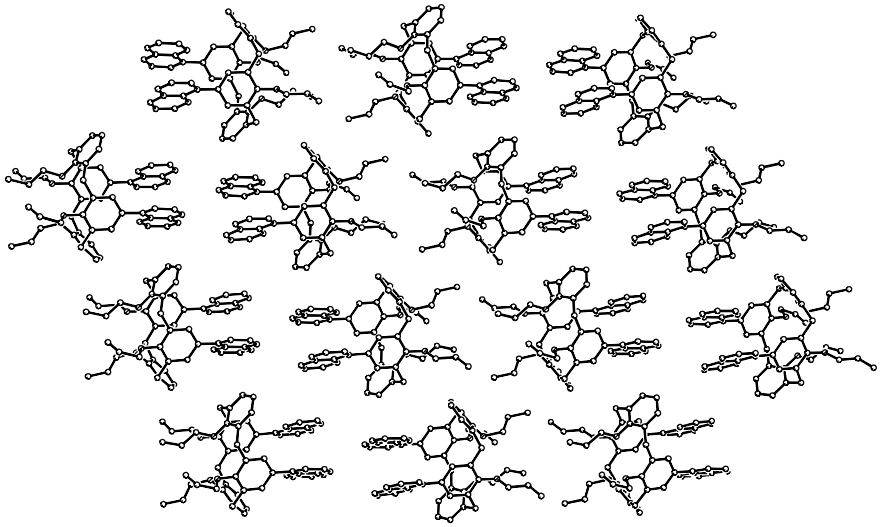

Figure 3.19. A packing plot of the dinaphthyl derivative showing a sheet of molecules and how the naphthalene groups interdigitate slightly.

Interestingly the naphthalene derivative crystallises with a solvent molecule whereas the carbazolyl derivative does not. To further illustrate the alleged π-π interactions planar projections of the interacting aromatics can be made and is shown in figure 3.20 for the naphthyl and carbazolyl substituents.

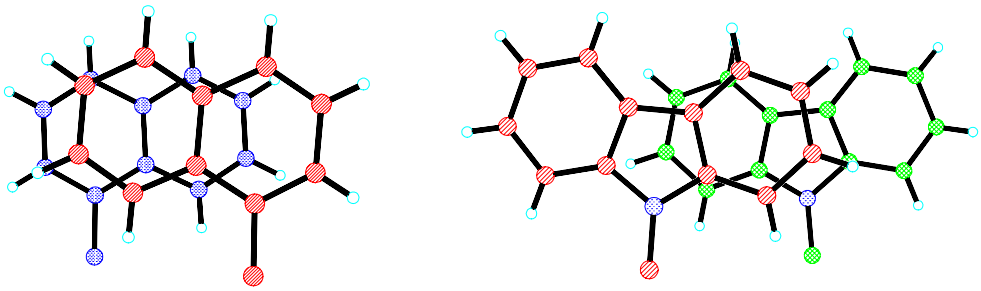

Figure 3.20. Planar projections of two interacting aromatic substituents with the red substituent being above the other. Naphthyl (left) carbazolyl (right).

Most of the work concerning intramolecular π-π interactions has been published and can be found in *Appendix P11*.

3.2.5 Intermolecular π-π interactions

In the previous section the effect of intramolecular π-π interactions was demonstrated. Would it be possible by proper substitution to direct the π-π interaction to be between molecules instead of within the same molecule.

3.2.5.1 Intermolecular π-π interactions in the crystal

A molecule similar to the carbazolyl derivative of the previous section was prepared by André Faldt. The difference between the two being that the plane of the fluorenyl substituent can not be co-planar with the plane of the aryl group of the calixarene (onto which it is attached).

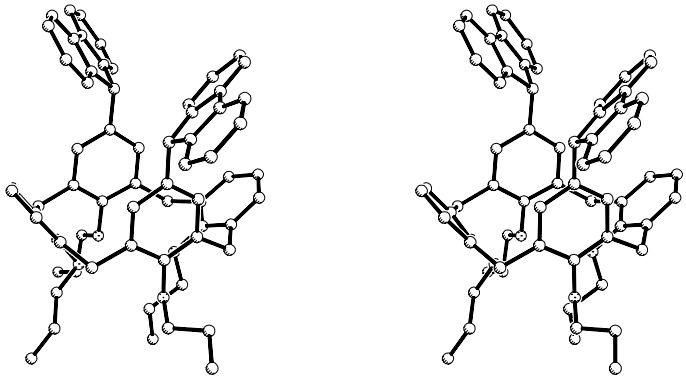

Figure 3.21. A stereoview of the molecular conformation of the difluorenylcalixarene as observed in the crystal.

This would force the substituents to interact with each other but between molecules and not with a substituent on the same molecule. The structure of the bis-1-fluorenyl-calixarene does exhibit intermolecular π-π interactions in the crystal but the molecular conformation is still with the substituents pinched together. This latter observation can only be explained as a crystal packing effect as there is no reason for the substituents to be pinched together. Also NMR measurements of the molecule in solution does indicate that the fluorenyl groups are

splayed outwards with rotation of the fluorenyl substituent around the bond to the calixarene though the experimental evidence is not conclusive.

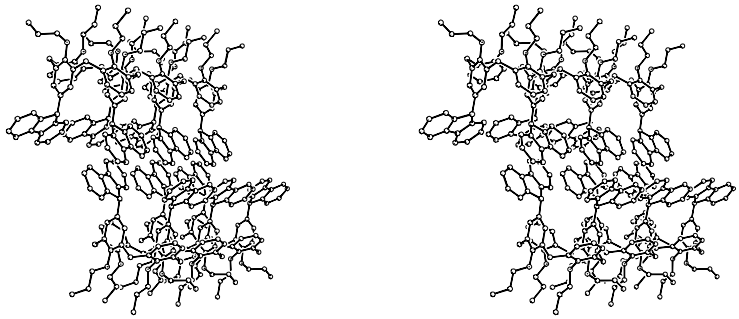

Figure 3.22. A stereoview showing how the fluorenyl moieties interact in the crystal. A line of molecules is shown.

The problem is of course the C_{2v} molecular point group symmetry that forces the molecules to be in either of the two conformations.

3.2.5.2 Assemblage using two conformational effects

All the calixarenes studied during the course of this project had C_{2v} molecular point group symmetry less one (C_{2v} molecular point group symmetry should be understood for the calixarene ground system less the substituents). This odd case, as it were, presents a significant result in terms of the understanding of tetrapropoxycalixarene conformational chemistry but needs to be studied by further examples to substantiate the finding. Where the other examples so far has only involved the effect of the substituent this particular case involves at least two factors that both influence the molecular conformation. The crystals were arrived at by coincidence by André Faldt. It was mentioned in the introduction to this chapter that ions could be bound at the lower rim of the calixarene moiety but also that this was most pronounced for the hydroxy compounds and thus not the alkylated species. In this instance however a lithium was found to be bound between the four oxygen atoms of the calixarene thus forcing it into a C_{4v} molecular point group symmetry. This forces the substituents somewhat outwards and permit them to attain some intermolecular π-π interaction. These two factors are believed to be governing but the inclusion of a solvent toluene molecule seems to stabilise the assembly.

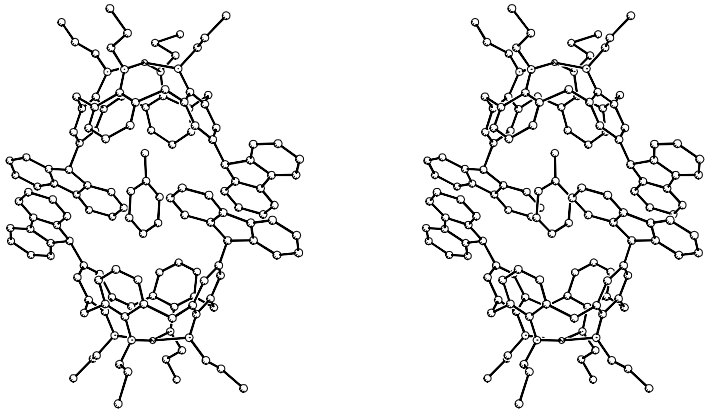

Figure 3.23. A stereoview of the assembly with all the forces believed to be responsible for the observations illustrated. The π-π interaction between the fluorenyl moieties, the lithium ions between the propoxy groups (counter ion not shown) and the included toluene solvent molecule.

While the structure is very large with three solvent molecules surrounding the aggregate consisting of two calixarenes including solvent molecule furthermore there are the counter ions to the lithium ions. These are some rather exotic anions consisting of a zirconium atom which coordinates five chlorine atoms and one tetrahydrofuran molecule (pentachloro-tetrahydrofuryl-zirconate). The space group is *P*1 and while there is an indication of a centre of symmetry a careful checking shows that the space group is *P*1. The structure simply consists of these egg shaped assemblies packed together.

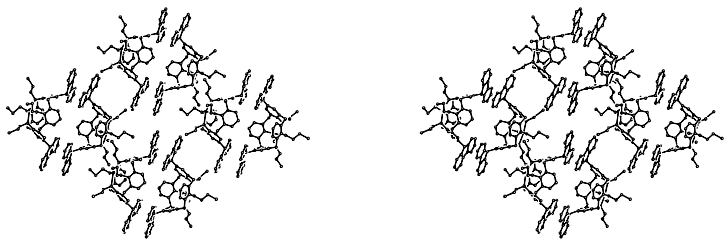

Figure 3.24. A stereoview showing the packing of the egg shaped assemblies. The solvent molecules and the anions have been omitted.

As for the intramolecular π-π interactions planar projections of the interacting substituents can be made for the two cases just presented.

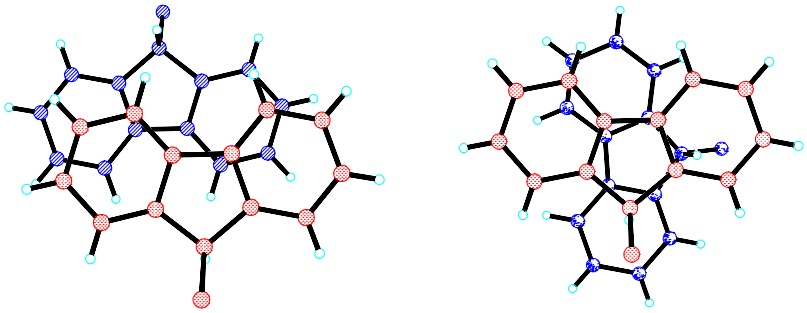

Figure 3.25. Planar projections of two interacting aromatic substituents with the red substituent being above the other. In both cases the substituent is the 9-fluorenyl group. The neutral compound is shown to the left whereas the lithium ion binding structure is shown to the right.

The work pertaining to the intermolecular interactions have been published and can be found in *Appendix P12*.

3.2.5.3 Conclusions to π-π interactions

In the past three sections the conformational behaviour of the calixarene has been studied with disubstituted extended and polyaromatic substituents. As a conclusion to the effect these substituents have on the conformation it can be said that planar aromatic substituents with more than two aromatic rings do give rise to a dominant influence on the conformation.

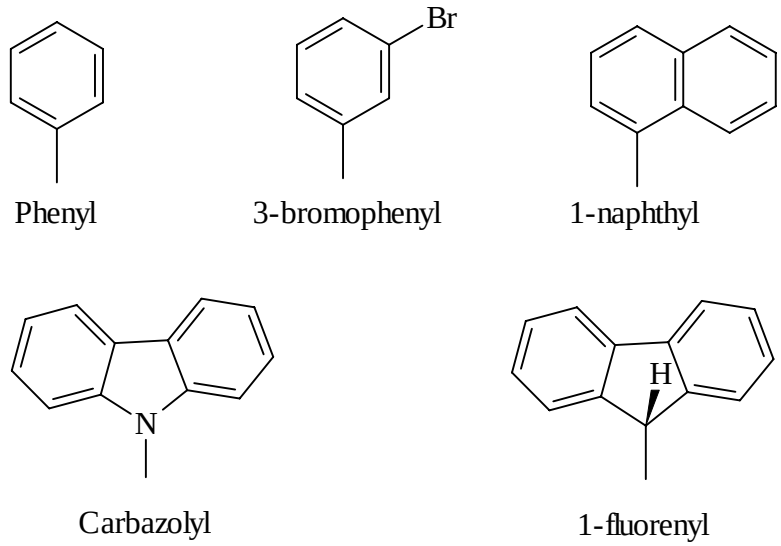

Figure 3.26. An overview of the substituents employed for the molecules studies in *Section 3.2.4* and *Section 3.2.5*.

For simple benzene derived substituents and extended systems like the stilbenes a splayed conformation is observed with the substituents pointing outwards in both the solid state and in solution. As a final remark it was shown that the molecules can be made to interact inter molecularly although this phenomenon has not been studied properly yet. But an interesting aspect is the interplay between several conformational effects such as both intermolecular π-π interactions, the binding of a lithium ion at the lower rim and at the same time forming a large clathrate with the inclusion of a solvent molecule. This holds some promise for the construction of a system that exhibits a co-operative effect.For instance that molecule A is only bound if molecule B (or ion B) is present. The argument can of course be taken further to include more factors. Although this phenomenon has been demonstrated it is at the time of writing too complex for development based on our rudimentary understanding of the calixarene conformational behaviour. Certainly however it should be an aim for the future calixarene chemist prodigy.

3.2.6 N-methyl effect

This section is very interesting because it was initiated by coincidence rather than concerted action and it led (much to our disappointment) to the rediscovery of a very noticeable substituent effect.

3.2.5.1 The rediscovery

Mogens Larsen had synthesised the simple amide formed between N-methylaniline and 5,17-dibromo-11,23-dicarboxy-25,26,27,28-tetrapropoxy-calix[4]arene and good crystals could be grown. This was the first calixarene structure that I solved even though several attempts had been made earlier that had all failed either due to poor crystal quality or most likely due to loosely bound crystal solvent and my (at that point) inaptitude towards handling these sensitive crystals. The structure showed the molecular conformation to be very different from the expected but offering an explanation for the 1H NMR spectrum where some of the signals from the protons had been shifted by a large amount (due to shielding). This conformation was found to be a bit odd and an answer as to why the substituents were found to point towards the cavity was needed. It was however recognised as an interesting aspect of calixarene conformational chemistry as the idea of making a sensor implies the ability to

direct the host-guest interacting substituents towards the cavity which are to hold the guest, in principle at least.

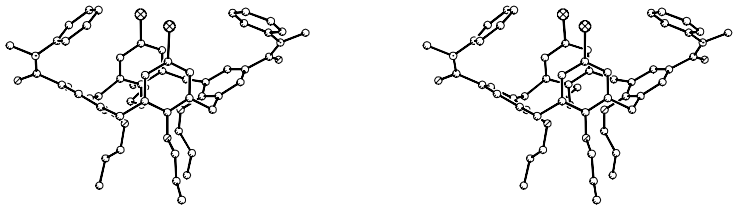

Figure 3.27. A stereoview of the molecular conformation of the simple N-methylated aryl-amide. The solvent molecule has been omitted but is situated just above the centre of the molecule as shown.

Further more the N-methylated diarylamide functionality was immediately recognised as a potentially useful structure generator. Alas, a search in the CCD revealed that the effect had been documented just six years earlier on much simpler systems by a series of papers some in high ranging periodicals much to our dismay. No report of this N-methyl effect could be found in the context of calixarenes so we decided to characterise the N-methyl effect in the context of calixarenes.

3.2.5.2 The N-H amides

When the calixarenes bear a carboxylic acid functionality and when further this acid functionality has been converted to an aryl-amide the conformational chemistry becomes highly solvent dependent as shown by Mikkel Jørgensen[94]. Where the aryl-amide substituents can be either pinched together in chloroform or splayed outwards in dimethylsulphoxide as established by NMR studies. A crystal structure of the N-H arylamide substituted calixarenes was desirable so as to firmly establish the uniqueness of the N-methyl effect. This however proved very difficult because the amides generally were found to form very poor crystals with an extreme needle like morphology. Several derivatives were tried and none of them yielded any crystals. Some crystals of the N-H arylamide corresponding to the compound shown in figure 3.27 were obtained. While data could be collected and the structure solved the data was

[94] Jørgensen, M.; Larsen, M.; Sommer-Larsen, P.; Petersen, W. B.; Eggert, H. *J. Chem. Soc. Perkin Trans. I* **1997**, 2851-2855.

very poor and even though the best crystals were not all that small and contained bromine they were scattering the X-rays with an extreme weakness. Later data were collected using synchrotron radiation (see *Appendix E4*) which improved the data quality somewhat but still the data obtained was poor. Sufficient however to show what was of interest namely the molecular conformation.

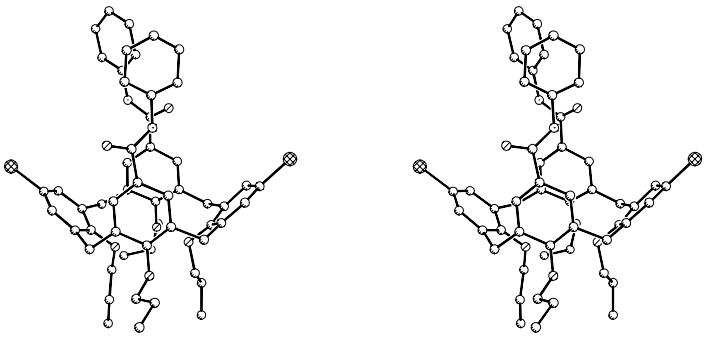

Figure 3.28. A stereoview of the molecular structure of the only N-H amide for which a structure was obtained.

The structure had two molecules in the asymmetric unit and one of them had a water molecule co-ordinating to one of the amide linkages. The two molecules had a very different conformation although they were both pinched together and in a conformation as shown in figure 3.28.

3.2.5.3 The N-Me amides

The dramatic conformational change observed upon simple N-methylation prompted for a detailed study and a series of derivatives were made where the size of the aryl group was altered in size also the steric effect of bromine atoms in the 5,17-position on the calixarene skeleton was investigated.

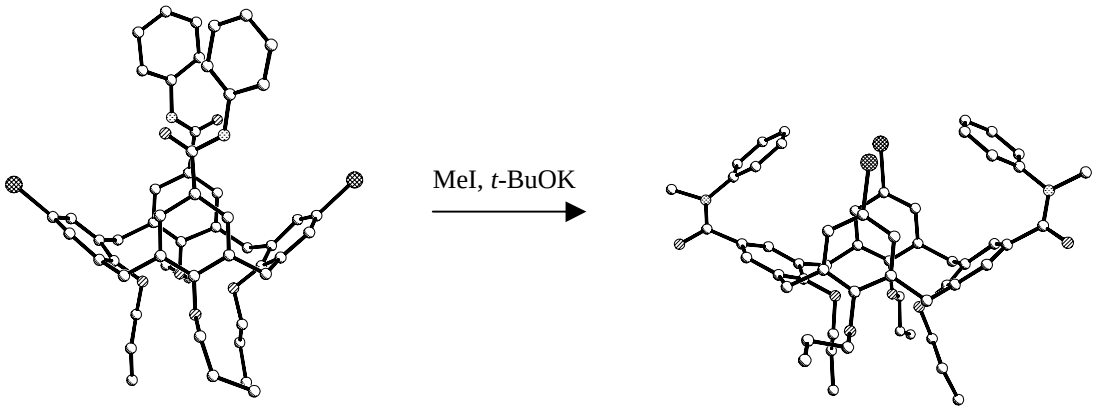

Figure 3.29. An illustration of the effect of the N-methylation. A drastic conformational change in the calixarene is observed.

The conformational behaviour was shown to be invariant in the solid state and in solution with no noticeable solvent dependence.

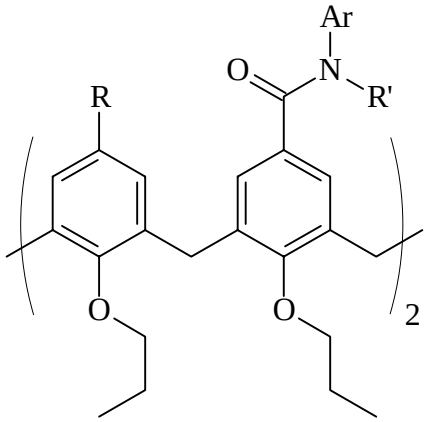

Figure 3.30. The structural formula for the molecules employed in the study. R was either H or Br, R’ was either H or Me and Ar was phenyl, 4-bromophenyl, 4-(pyrrolidin-1-yl)phenyl, 1-naphthyl, 1-pyrenyl. Not all the possible combinations of R, R’ and Ar were studied.

A summary of the effect is shown in figure 3.29 where the massive conformational change is evident and I must add as a personal comment that I have as yet not grown tired from watching figure 3.29. Four structures of the N-methylated compounds were solved and all were identical with respect to the molecular conformation.

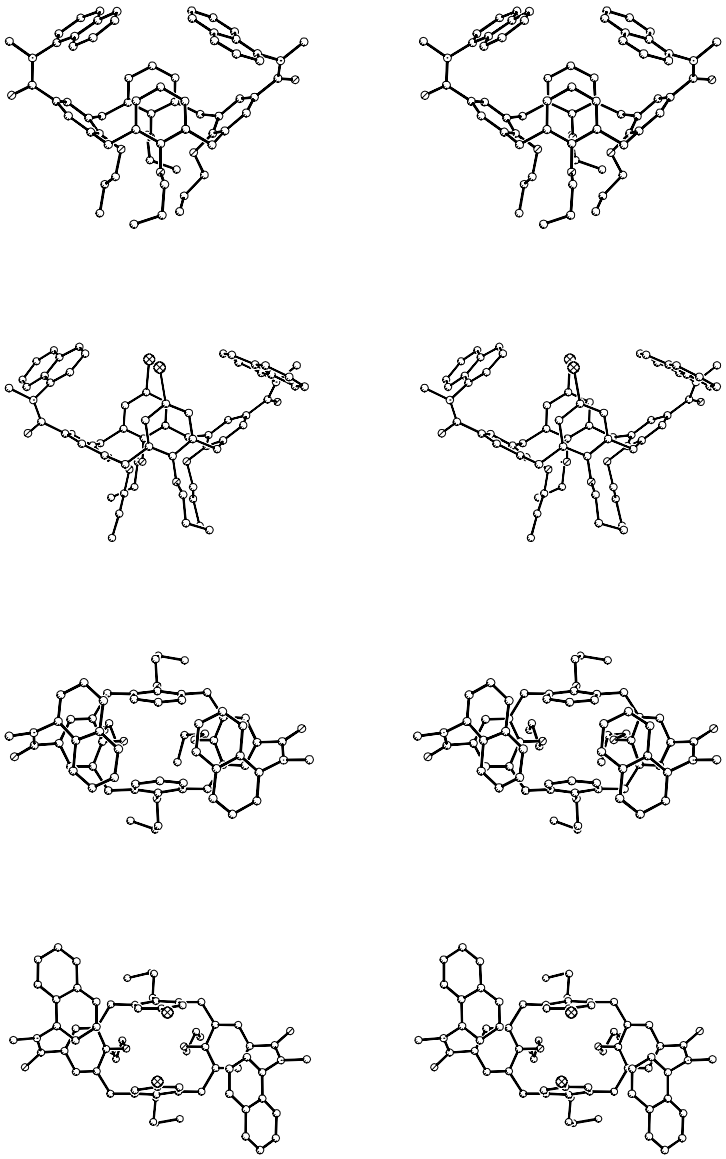

Figure 3.31. Stereoviews from the side (upper pair) and from above (lower pair) of the 1-naphthyl derivatives illustrating the steric effect of the bromine atoms.

The steric effect of the bromine atom is noticeable and is seen as an increased splay and less pinching of the molecular conformation. Further the substituents are forced away from the cavity[95]. A good illustration of the steric effect of bromine is seen by comparing the brominated and unbrominated calixarene with N-methylated 1-naphthyl carboxamide substituents. It is clearly seen that the naphthyl substituents can only lie above the cavity of

[95] Since this work was published an additional four structures have been solved and all four show the exact same features as observed in this work.

the calixarene when no bromine atoms are present. The steric effect of the bromine atoms forces the naphthyl substituents away from the cavity as a close inspection of figure 3.31 will show. It would form this be expected that the larger pyrenyl substituents would also be forced away from the cavity even in the absence of bromine atoms as the pyrenyl substituents would otherwise collide. More interesting however was whether the molecule would still adopt the same conformation as the other representatives.

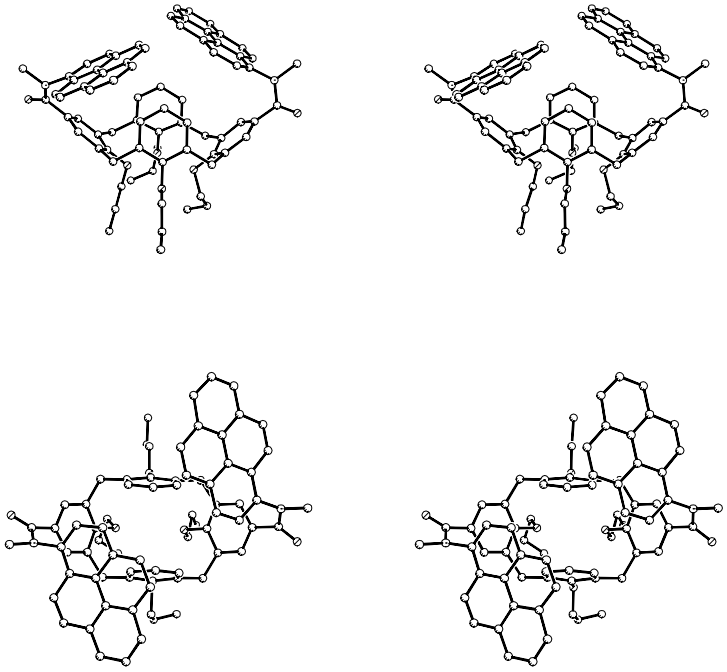

Figure 3.32. The molecular structure of the 1-pyrenyl derivative still showing the generally observed conformation behaviour.

The 1-pyrenyl group is an amazingly large substituent and still the conformational effect is observed and invariant. It would seem that this N-methyl effect is a very strong structure generator in the context of calixarene chemistry but it is noticeable that the substituents are forced in over the cavity. One could ask the question as to why the large groups do not point away from the cavity of the calixarene i.e. by a rotation of 180^{o} around the aryl-carbonyl bond. An answer could be that the products obtained are the kinetic products and that the conformation obtained is the only conformation accessible during the synthesis of the compounds. Further the absolute rigidity was substantiated by an NMR experiment which

focussed on the rotation of the 1-naphthyl substituents around the N-naphthyl bond. It showed that while rotation was possible it took place at higher temperatures.

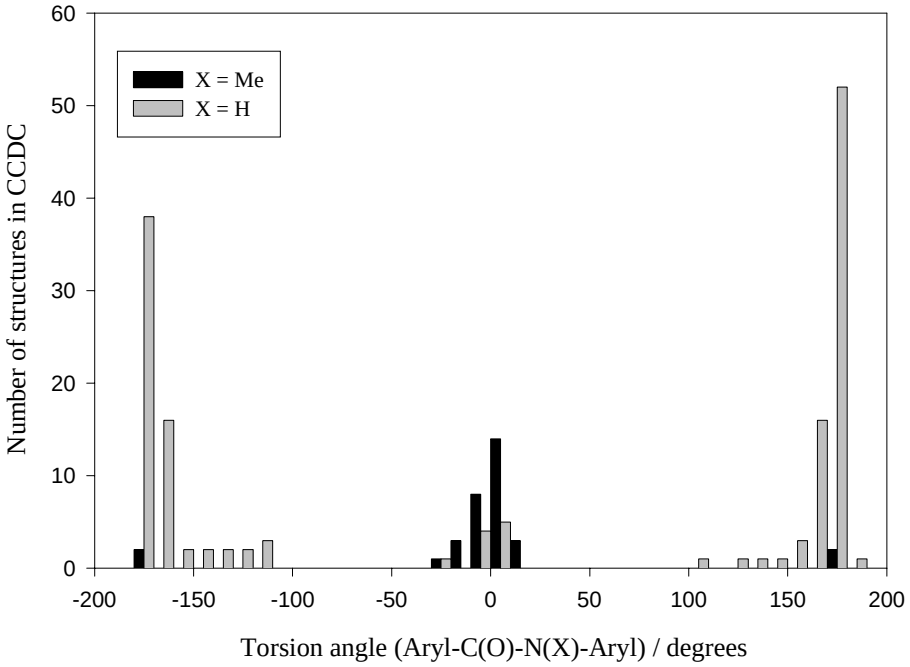

Figure 3.33. VISTA plot of the torsion angle for all the aryl-C(O)-N(H)-aryl and aryl-C(O)-N(CH_3)-aryl found in the CCD. Nearly all the N-H amides are in the *trans* conformation (± 170^o - 180^o) except for a few cases where the stereochemistry does not permit the N-H amides to adopt the *trans* conformation. Nearly all the N-Me amides are in the *cis* conformation (± 0^o - 5^o) except for a few cases where the stereochemistry does permit the N-Me amides to adopt the *cis* conformation.

To substantiate the findings a survey of the CCD was made with respect to the conformation around the amide bond in aryl-aryl N-H and N-Me amides. The result is a VISTA plot shown in figure 3.33. It is clear that N-methylated amides prefer the *cis* conformation whereas the N-H amides prefer the *trans* conformation. There are a few exceptions to the rule but a closer examination of these cases showed that the reason for i.e. a N-H amide adopting a *cis* conformation could be rationalised in terms of the conformational chemistry of the molecule in question as not permitting the *trans* conformation. Likewise for the N-methylated amides.

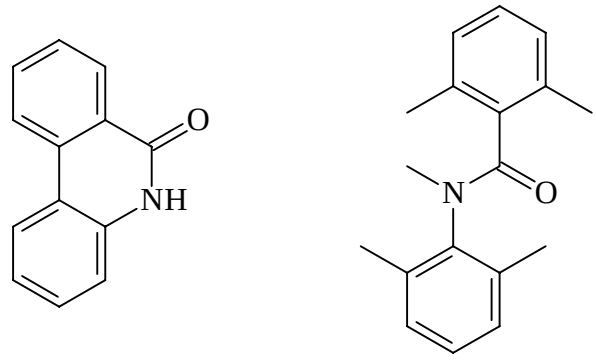

Figure 3.34. Illustration of the structural formula for molecules that do not obey the rules of N-H and N-methyl conformational behaviour. In both instances the molecular connectivity implies a conformation different from the naturally preferred.

The number of structures of N-H amides in the CCD far exceed the number of N-Methylated amide structures found. With our findings however (including the unpublished) the structural knowledge on N-methyl amides as found in the CCD has been increased by 20 %.

3.2.5.4 The impact of the N-Me effect on calix[4]arenes

So far only a recognition of the N-methyl effect in the context of calixarene conformational chemistry has been made. It has been shown that it is of a general nature and invariant with a large range of structural perturbations. The next step would obviously be to make use of the result made here in a design of a sensor as it has the rare property of directing the substituent towards the cavity and not as we have seen for most of the other substituents which point away from the cavity. Since the cavity is where the action is going to be it seems only natural that the substituent should be directed towards the cavity of the calixarene molecule. All the work presented here has been published and can be found in *Appendix P13*.

3.2.7 Specific hydrogen interactions and salt bridges

The studies on calixarene conformational behaviour has so far been limited to making molecules, solving their structures and rationalising the results and while a potential application was envisaged in some of the cases it was without success. This part is concerned with the making of a sensor for ephedrine. The understanding of the calixarene conformational behaviour provided thus far made it possible to make a sensor and some

further aspects of calixarene conformational behaviour in terms of specific hydrogen interactions and salt bridging were uncovered.

3.2.7.1 The simple acid

While it has been known that calix[4]arenes with carboxylic acid functionalities in the 5,17-positions form a dimer in solution it has only in one case been shown by X-ray crystallography. It is probably a very general structural motif for these molecules as we have observed this feature as well for two compounds.

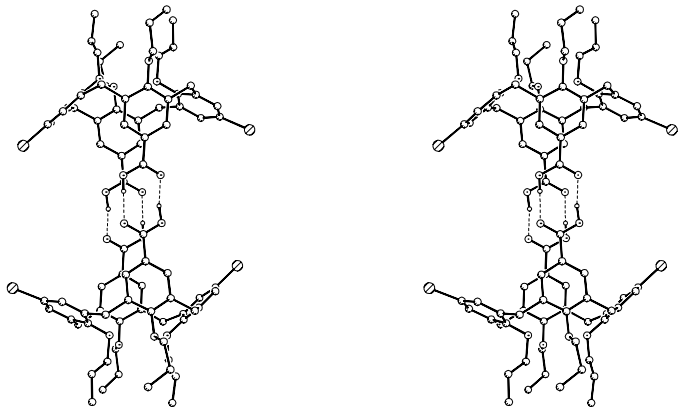

Figure 3.35. A stereoview of the dimeric structure observed for 11,23-dibromo-25,26,27,28-tetrapropoxy-calix[4]arene-5,17-dicarboxylic acid as observed in the crystal and in aprotic solvents.

The conformation of the calixarene is very pinched and it crystallises without any solvent molecules. From figure 3.35 it can be seen that the acid functionalities bend towards the cavity of the calixarene thus filling out space efficiently. The structure of the calixarene diacids have been subject to some dispute and propositions have been made claiming the intramolecular interaction of the acid functionalities across the cavity of the calixarene. This however seemed unreasonable and a statistical argument was made using the CCD. While such an argument does not prove the fallibility of a proposition it can certainly give an indication of whether the proposition is likely to be true or untrue simply based on the average behaviour of a given system. The intramolecular interaction would require the torsion angle between the acid group and the aryl group to be of the order of 90^{o}. A comprehensive search

of the CCD for aryl carboxy occurrences (both acids and acid salts but not esters) was undertaken.

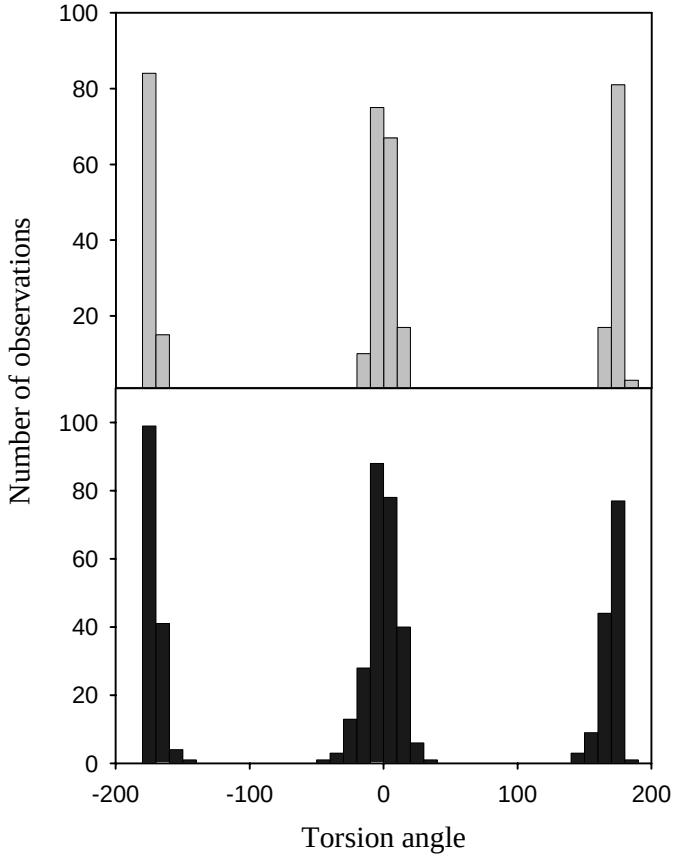

Figure 3.36. *VISTA* plots of the torsion angle between the aryl and the carboxy functionality for the benzoic acids (above) and benzoic acid salts (below) found in the CCD.

The plot of the torsional angle formed between the phenyl ring and the carboxy group (see figure 3.36) clearly shows that carboxy/aryl assembly prefer a very near coplanar arrangement. In no instances were torsion angles of 90 ^{o} or even close found further substantiating the dimer arrangement as being preferred. This result also has an important bearing on the discussion later for some of the salts. The dimer arrangement is clearly due to the specific hydrogen interactions well known for carboxylic acids. Only one type of specific interaction is involved and a unitary graph set descriptive of the dimer motif can be assigned

as $R_2^2(8)$ using graph set theory[96,97,98,99]. A further piece of evidence for a dimeric structure as being the preferred one for the calixarene diacids was obtained by solving the structure of a larger acid namely 11,23-bis-phenylazo-calix[4]arene 5,17-dicarboxylic acid. Again the dimeric structure was observed. The quality of the data for this structure was very poor but nevertheless sufficient to show the geometric features, the conformation and the packing arrangement.

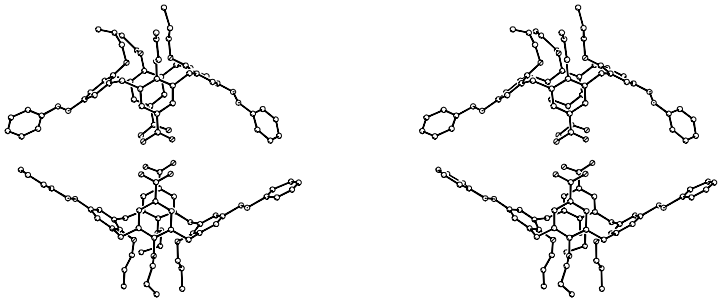

Figure 3.37. A stereoview of the dimeric structure for 11,23-bis-phenylazo-calix[4]arene 5,17-dicarboxylic acid.

It would seem meaningless to discuss specific hydrogen interactions for such a poorly determined structure but seen in the light of the other evidence presented here it is the only fact that could account for the structural behaviour observed.

3.2.7.2 Salts with primary amines

Seen in light of the interactions observed for the pure acid molecules it was found of interest to see how they interacted with simple amines. While many salts were formed between the simple bromo acid and primary amines and studied by NMR in solution only one gave crystals of a quality sufficient for X-ray work. It was the benzylamine salt which gives rise to a complicated dimeric structure. Two distinct specific hydrogen interactions or motifs can be recognised and the system can be described with the unitary level graph set

[96] Etter, M. C. *Isr. J. Chem.* 1985, **25**, 312.
[97] Etter, M. C. *Acc. Chem. Res.* 1990, **23**, 120.
[98] Etter, M. C. *J. Phys. Chem.* 1991, **95**, 4601.
[99] Etter, M. C.; MacDonald, J. C.; Bernstein, J. *Acta Cryst.* 1990, **B46**, 256.

$N_1 = R_1^2(4)R_4^4(12)$ more descriptive however is probably the secondary level graph set which involves both motifs and is given as $N_2 = R_4^2(8)$. Both the graph set for the acids and the salt is well known and has been observed an recognised in many instances. The dimeric structure of the benzylamine salt is shown in figure 3.38 notice how the assembly has the shape of propeller.

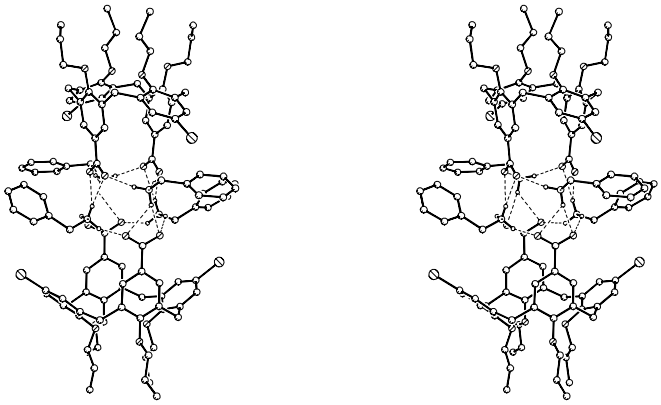

Figure 3.38. A stereoview of the complex dimeric structure with four benzylamine molecules complexing with the acid functionalities in a complicated arrangement.

Many attempts were made to obtain crystals of the ephedrine salt but they all failed. The structure of the benzylamine salt however helped to explain some of the features observed in solution by NMR. It would seem that the structure observed for benzylamine is general for primary amines.

3.2.7.3 Salts with secondary amines

The next step is to use secondary amines and since they have one less hydrogen to interact with the interaction and the structural outcome was expected to be quite different from the primary amine case. Still a certain level of elaboration was expected as several different specific hydrogen interactions are possible. The complexity was however much more involved than first anticipated and in fact the same system was observed to exhibit structural diversity or a sort of temporal pseudo polymorphism. If for instance the diethylamine salt of the simple dibromo calixarene diacid is made the crystal morphology is at first plate like. In time (a few days) however they change to a more needle like morphology. It was decided to

try and collect data on both crystals if their unit cells were different. The unit cells were different and data were collected and the two different structures solved. It was later shown that the late growth phase was pure by powder diffraction. So definitely some sort of ripening with subsequent structural rearrangement takes place.

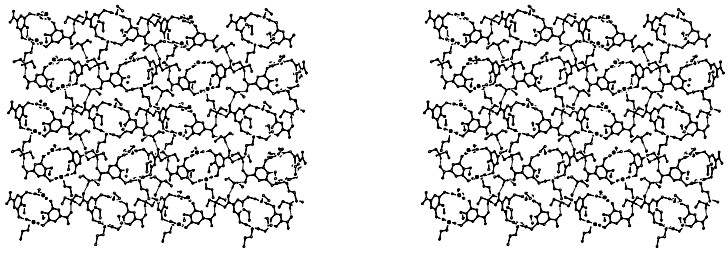

Figure 3.39. A stereoview of the orthorhombic early growth phase. It is a polymeric two dimensional buckled sheet type structure.

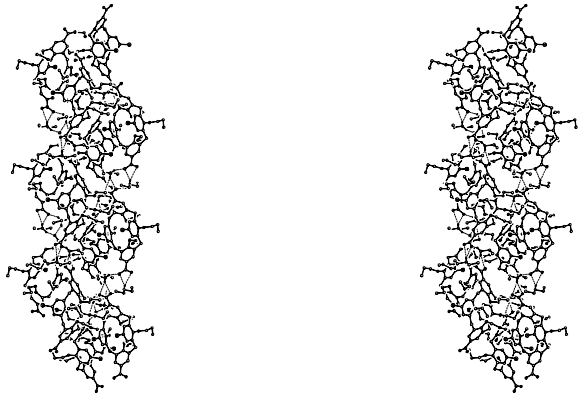

Figure 3.40. A stereoview of the tetragonal late growth phase. It is a polymeric helical one dimensional structure.

It is noticeable that the conformation of the calixarene has changed with the acid functionalities splayed outwards in contrary to the pure acids and the primary amine salt. Graph set theory was used to compare and contrast the two different structures. The data obtained for the orthorhombic structure was quite poor and no true evidence of specific hydrogen interactions could be produced. Seen in the light of the tetragonal structure however, it seems reasonable to present a discussion here on these grounds.

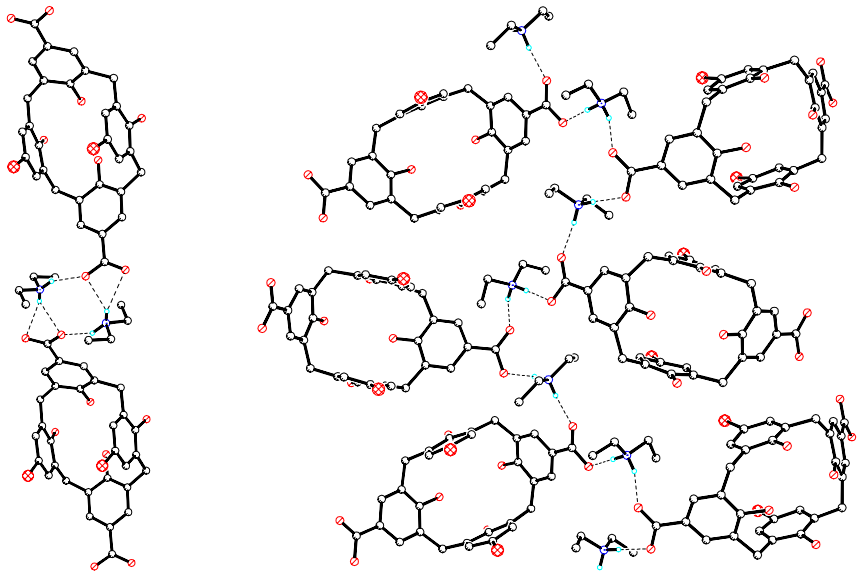

Figure 3.41. The very different specific hydrogen interactions observed for the two diethyl amine salts. The tetragonal structure on the left and the orthorhombic structure on the right.

From figure 3.41 it is evident that the late growth phase (tetragonal) present a closed network of specific hydrogen interactions identical to the one observed for the benzylamine salt with two different interactions. It can be described by the secondary level graph set $N_2 = R_4^2(8)$. In the early growth phase (orthorhombic) four different interactions can be identified. Unlike the previous these give rise to linear chains of specific hydrogen interactions. This network can be described by a quaternary level graph set namely $N_4 = C_4^4(12)$. Seemingly a smaller secondary level graph set, $N_2 = C_2^2(6)$, could apply but would indicate the presence of only two distinct specific hydrogen interactions. A close examination of the specific hydrogen interactions involved confirms that there are four distinct specific hydrogen interactions. As seen to the left in figure 3.41 these can be identified as two different types between molecules on the same side of the chain and two different types between molecules on opposite sides of the chain.

3.2.7.4 Salts with tertiary amines

Finally the tertiary amine salts were investigated with the expectation that they would give rise to simple networks since only one specific hydrogen interaction is possible. The problem

that arose was that most of the salts made formed very poor crystals and the only salts obtained that were crystalline was the salts made from DABCO (1,4-diaza-bicyclo[2.2.2]octane) which was unfortunate in the sense that DABCO is a divalent tertiary amine and in this way the molecule can make more than one specific interaction with hydrogen as indeed observed. The first example was the salt formed between DABCO and the simple calixarene diacid.

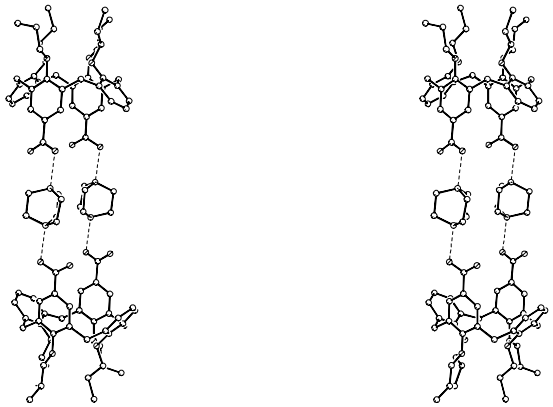

Figure 3.42. A stereoview of the dimer formed between for 25,26,27,28-tetrapropoxy-calix[4]arene-5,17-dicarboxylic acid and DABCO.

The graph set describing such a network is simply *D*. Alternatively a very large ring could be defined extending through the entire dimer arrangement but such a choice would not seem rational. A second DABCO salt with a different diacid was prepared and the structure was solved. The diacid was 11,23-Bis-(E)-(2-phenyl-ethen-1-yl)-25,26,27,28-tetrapropoxy-calix[4]arene-5,17-dicarboxylic acid an analogue of the diazophenylcalixarene diacid. Though the molecular structure for the two acids is similar it is surprising that the bis-stilbenecalixarene diacid does not crystallise well at all and not under the conditions of crystallisation for the diazophenylcalixarene diacid. The molecular structure of the DABCO salt of the bis-stilbenecalixarene diacid was found to be very different to the structure of the corresponding salt for the calixarene diacid. First of all no dimer aggregates are formed and secondly there is one DABCO molecule for each acid functionality. These last findings are rather difficult to explain unless an electrostatic argument is used where the anionic carboxylates repel each other and force the calixarene into the observed conformation with the acid functionalities splayed outwards. In the case of the dimer arrangement for the simple

calixarene only partial deprotonisation is observed so there would have to be less electrostatic repulsion and a dimeric structure is possible with the acid functionalities pinched together.

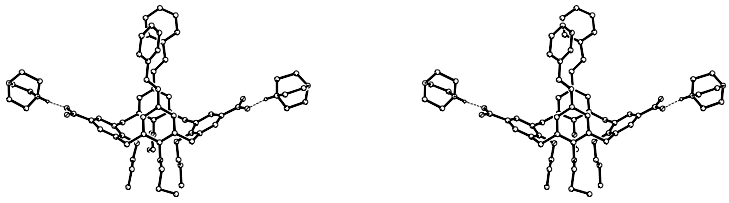

Figure 3.43. A stereoview of the structure of the DABCO salt of the bis-stilbenecalixarene diacid. There are two DABCO molecules per calixarene molecule as opposed to the dimer structure observed for the simple calixarene diacid with one DABCO molecule per calixarene molecule.

An analysis of the N-O distances between the DABCO and the carboxylic acid in the two cases showed no real difference and the C-O bond lengths of the carboxylic acid functionalities did not show spectacular differences although there is a slightly more pronounced carboxylate tendency for the DABCO salt of the bis-stilbenecalixarene diacid i.e. different C-O bond lengths indicating a double bond for one C-O bond and single bond character for one C-O bond. It would thus seem to be a question of structural stability that determines which form that crystallises since the acidities of the different acids involved here are assumed to be very similar and fully deprotonised in solution. Also if both acid groups of the calixarene in the dimeric DABCO salt were fully deprotonised it would imply that the DABCO molecules were in the doubly protonised state which seems unreasonable since the two amine functionalities of DABCO have different basicities.

3.2.7.5 The ephedrine sensor

Some binding studies were performed by Mikkel Jørgensen using NMR in chloroform solution. The pure acids generally had a conformation with the acid functionalities pinched together. Upon addition of a tertiary amine like DABCO it could be shown that the conformation changed so that the carboxy groups became splayed outwards (also in the case of the simple acid which forms dimers in chloroform solution). Thus consistent with the idea of electrostatic repulsion being responsible for splaying the carboxylate functionalities apart. With primary and secondary amines no changes in conformation were observed upon addition of the amine. This could be explained if aggregates as the ones observed in the crystal

structures are formed with specific hydrogen interactions holding the assembly together. The interesting point is that ephedrine is bound very firmly which could be due to a co-operative effect of both salt formation of the amine and specific hydrogen interactions of the hydroxy group of ephedrine.

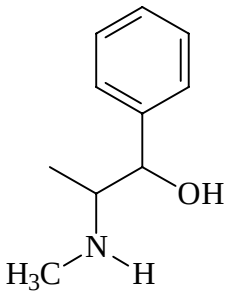

Figure 3.44. The structural formula for ephedrine. It is possible to envisage interaction of the secondary amine functionality in a fashion similar to diethylamine and furter interaction with the hydroxy group thus strengthening the binding to the calixarene.

A crystal structure would have been very informative as it might give a more detailed explanation for the strong binding of ephedrine as opposed to nicotine and N-methylethanolamine.

3.2.7.6 Conclusions

In this entire part the experimental results pertaining to calix[4]arenes have been presented. The work started out as being a mapping of calix[4]arene conformational space using different substituents and ended up with the design of an actual sensor for a biological molecule. It is however clear that the conformational behaviour of disubstituted tetrapropoxycalixarenes is exceptionally complicated if the desire is to fully comprehend and be able to predict molecular behaviour in terms of different substituents or simply in terms of the presence of a weakly or strongly complexing molecule. I am sure that this subject is still pretty juvenile at least if viewed with the eyes of someone anticipating an application that is of benefit to society i.e. a commercially viable sensor. Seen in the eyes of a scientist who is satisfied with a lot less the work presented here certainly can be used as an aid in the further design of a more elaborate and specific molecule. The work presented in this last section has been published and can be found in *Appendix P14*.

3.3 Conformational analysis of calix[4]arenes

As we saw in the previous part the conformational behaviour of the calixarenes though known in rough detail is essential if a sensor system or an application of the calixarene skeleton for a specific purpose is to be obtained. The individual system has to be studied cautiously before any directed approach can be envisaged. Granted all the information that was obtained during this work still more is needed to become an expert.

3.3.1 The structural chemistry of calix[4]arenes based on the literature

While the simple conformational behaviour of the calix[4]arene skeleton has been recognised and known for some time it really does not enable one to draw conclusions to a more elaborate systems as we have just seen.

3.3.1.1 The maxima and the minima

It was soon realised that the calix[4]arene skeleton while rigid in some ways had quite a bit of flexibility. If fixed in the *cone* conformation as is of most interest in this context the conformational energy maxima and minima can be calculated. The results from such a calculation has been published and show that pinched *cone* forms with C_{2v} molecular point group symmetry have the lowest energy and the *cone* with C_{4v} molecular point group symmetry present a small local energy maxima separating the two C_{2v} minima. To convert from one pinched *cone* conformer to the other the calixarene has to pass through the C_{4v} conformation. As we have seen all the structures presented here were in a C_{2v} pinched *cone* conformation except one. The pinched *cone* conformer is preferred in accordance with the conformational energy calculations. If some ion is co-ordinated to the oxygen atoms at the lower rim the C_{4v} conformation (or pseudo C_{4v} conformation) can become the more stable form.

3.3.1.2 Using the CCD to map the conformational space

The CCD is an obvious place to search for information on the conformations for the calix[4]arenes as in excess of three hundred structures of these molecules have been deposited. This forms a basis for a statistical analysis.

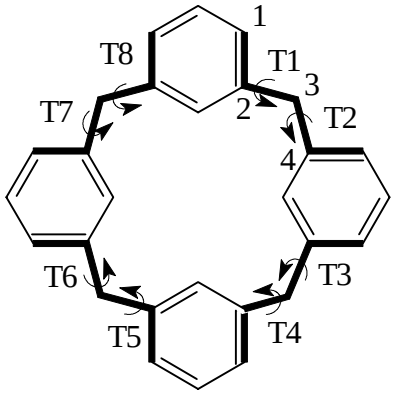

Figure 3.45. The calixarene skeleton along with a definition of the eight torsion angles used to distinguish the possible conformers. The selection of the atoms for the torsion angle was always from the benzene ring towards the methylene bridge.

What could be extracted from the CCD was the torsion angles of the calixarene as shown in figure 3.45. The torsion angles are characteristic of the particular conformation of the calixarene. All eight torsion angles defined as above for the calix[4]arenes could thus be extracted from the CCD.

3.3.2 Basis for a conformational analysis

To analyse how the torsion angles for calix[4]arenes varied with different conformations a model study was made. It is self evident that for any C_{4v} symmetric molecule the numerical value for all the eight torsion angles would be the same even though the magnitude could differ from calix[4]arene to calix[4]arene.

3.3.2.1 The conformers and their torsion angles

A simple energy minimisation for each of the four possible conformations of 25,26,27,28-tetramethoxy-calix[4]arene was made using molecular mechanics in the program *Insight II*. The torsion angles for the C_{4v} *cone* conformer would as mentioned be identical in magnitude but not in sign (as defined the sign would alternate between pairs *vide supra*). The numerical however value would be around 85^{o}. An energy minimisation of 25,26,27,28-tetrahydroxy-calix[4]arene which takes into account the hydrogen bonds does not yield an entirely C_{4v} symmetric molecule but nearly. For the conformers the values could be worked out and are presented in table 3.1.

Table 3.1 Torsion angles for the non-C_{4v} conformers of 25,26,27,28-tetramethoxy-calix[4]arene and for the pseudo C_{4v}-conformer of 25,26,27,28-tetrahydroxy-calix[4]arene.

Torsion angle ^{o}	*cone*	*partial cone*	*distal*	*proximal*	C_{4v}
T1	-118.08	+122.41	-125.37	+137.21	-91.13
T2	+63.49	-66.94	-126.54	+138.25	+82.89
T3	-61.65	+112.24	+125.64	-86.16	-82.95
T4	+113.50	+119.64	+125.41	+75.85	+90.93
T5	-115.13	-119.65	-125.45	-129.39	-91.13
T6	+63.77	-112.03	-125.11	-129.99	+82.89
T7	-62.10	+66.81	+125.18	+76.07	-82.95
T8	+116.62	-122.44	+125.28	-84.78	+90.93

It is noteworthy that there are distinct differences between the torsion angles for the different conformers i.e. for the distal conformation the numerical value for all the torsion angles are near identical whereas for the other three this is not the case. Even though it was decided how to define the torsion angles in figure 3.45 there is the problem of where to start in the ring and further which way to move around the ring.

3.3.2.2 Getting rid of the ambiguity

If the torsion angles for the different conformers are to be compared there has to be some way of accommodating the discrepancy of where the labelling of the torsion angles is started and which way one moves around the ring. There is further the problem of how the data is retrieved from the CCD and this in essence makes it impossible to do anything rational. Of course each structure could be taken out of the database and analysed individually but this would seem pointless and of little general value. Instead it has to be recognised that the in the way the labelling has been done some of the angles are pair wise comparable i.e. as written all the even numbered torsion angles and all the odd numbered torsion angles can be grouped together in pairs. In this way T1 & T2 form a pair so does T3 & T4, T5 & T6 and T7 & T8.

This way of grouping the torsion angles gets rid of some of the ambiguity and allows a simple presentation to be made.

3.3.3 The Ramachandran plot of calix[4]arenes as found in the CCD

A long time ago the famous crystallographer G. N. Ramachandran (some people claim that he is a biochemist and while probably inclined towards both disciplines he is for the purpose of this text a crystallographer) discovered a way to distinguish the different conformations of polypeptides by plotting two torsion angles against each other.

3.3.3.1 The principle

The idea is simply that if one has two different torsion angles being part of a rigid system they can be plotted against each other. One torsion angle along one axis and the other torsion angle along an axis perpendicular to the first (originally these were labelled Φ and Ψ). Since torsion angles can only take on values in a certain interval the surface onto which the values are plotted is closed (i.e. $+180^{o} > \Phi \geq -180^{o}$ and $+180^{o} > \Psi \geq -180^{o}$). Originally this was done for amino acids that are chiral and thus the entire angular space is unique. In the case of calix[4]arenes there is the ambiguity mentioned above which means that a given point is not unique i.e. it could become reflected in a mirror plane due to the choice of labelling of the torsion angles. Therefore unless some rigid standard is set up and each particular calixarene analysed accordingly the entire angular space of the Ramachandran plot will for calix[4]arenes not be unique and as we shall see only an eighth of the angular space can be used and is unique. Unfortunately some of the distinctive features are lost and are instead folded into one eighth of the angular space. It is interesting to speculate on how the chirality of the amino acids completely solves this problem. For the calix[4]arenes which can be chiral or prochiral (if chiral they are in general never resolved) but most often both enantiomers will be present in the structure and the actual enantiomer found in the crystallographic data is then a matter of coincidence.

3.3.3.2 The data and the general plot

The CCD was searched for all calix[4]arenes, tetraalkoxy-calix[4]arenes, *cone* conformers and *non-cone* conformers. The reason for not distinguishing the *non-cone* conformers is that there are not that many.

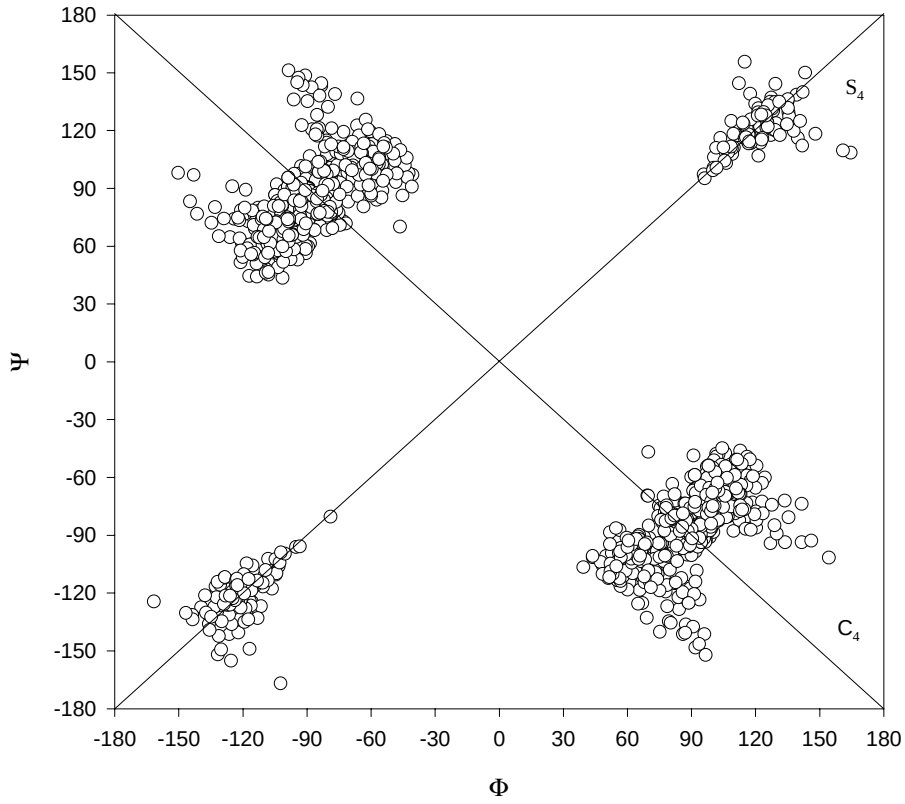

Figure 3.46. A Ramachandran plot of the torsion angle pairs for all the calix[4]arenes found in CCD. The axis along which *C4* and *S4* molecular point groups symmetry exist has been labelled.

It is also noteworthy that all the calix[4]arenes will in the Ramachandran plot give rise to up to four data points each corresponding to one of the distinct torsion angle pairs. The entire Ramachandran plot is shown for all the calix[4]arenes found in the CCD. It is also noteworthy that there is a considerable amount of symmetry as described above. The symmetry axis can be defined as being along the diagonals of the plot. The two diagonals differ in that one is a true *C4* symmetry axis and the other is a true *S4* symmetry axis. By reflection through first $\Phi = 0$ and thereafter $\Psi = 0$ the entire plot can be reflected into the first quadrant which is the most useful way of representing the plot for calix[4]arenes even though there is still some redundancy in the plot. The *C4* and the *S4* axis have now been folded together and are co-linear.

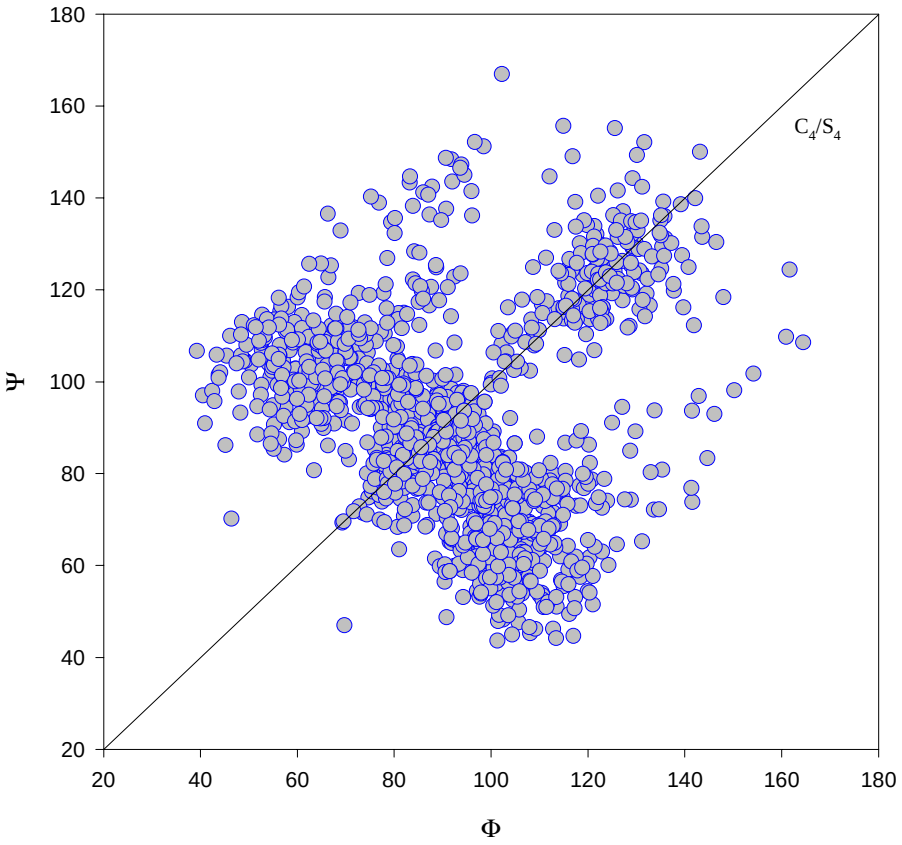

Figure 3.47. The Ramachandran plot folded into the first quadrant. There is still an ambiguity around the combined C_4/S_4 axis.

To make the representation unique a final reflection through the diagonal of the first quadrant should be made. For the purpose of discussion and plotting it is however more useful to present the entire (albeit redundant) first quadrant bearing in mind the symmetry around the combined C_4/S_4 axis. There are thus three factors that the reduce the useable angular space of the Ramachandran plot. First of all the lack of control of chirality, then the direction of moving around the ring structure and finally the choice of the starting torsion angle. By being consistent in the choice of starting torsion angle points will appear on both sides of the combined C_4/S_4 axis at distinct places. By the opposite choice each would end up on the opposite side and in reality it is best to think of the plot as being symmetric.

3.3.3.3 The distinction

It is then possible to plot out the ideal calculated values for the different conformations on top of the entire set of data and in that way identify the conformational behaviour of the calix[4]arenes falling in the general ranges.

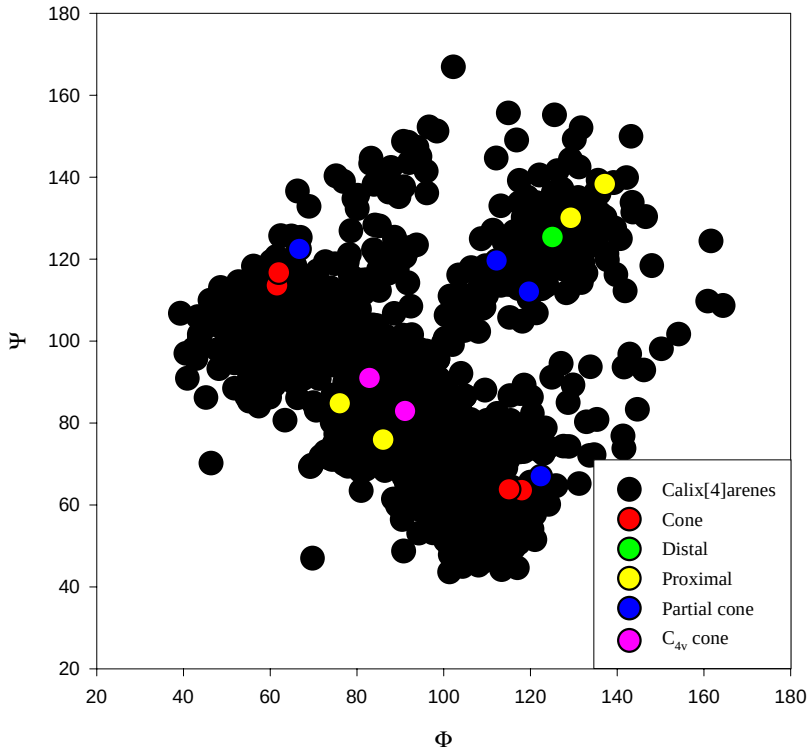

Figure 3.48. A Ramachandran plot of all the calix[4]arenes found in the CCD (black) along with the calculated values for the torsion angles for the different conformers listed in table 3.1.

It is interesting to distinguish the different regions of the plot. Three conformers fall in one region only (if the combined C_4/S_4 axis is included). That is the C_{4v} *cone*, the *cone* and the *distal* conformers. The *proximal* and the *partial cone* fall in two different regions each. With one of their individual regions close to one another. It is then possible to state what conformation a given calixarene has just by plotting it on the graph. More importantly outliers can easily be identified using this plot.

3.3.3.4 The results

With all this knowledge at hand the entire calix[4]arene set from the CCD was split (manually!) into groups of *cone*, not *cone*, alkoxy *cone*, our own data and finally *partial cone* conformers. The results fit very well with what was expected from the above theoretical analysis.

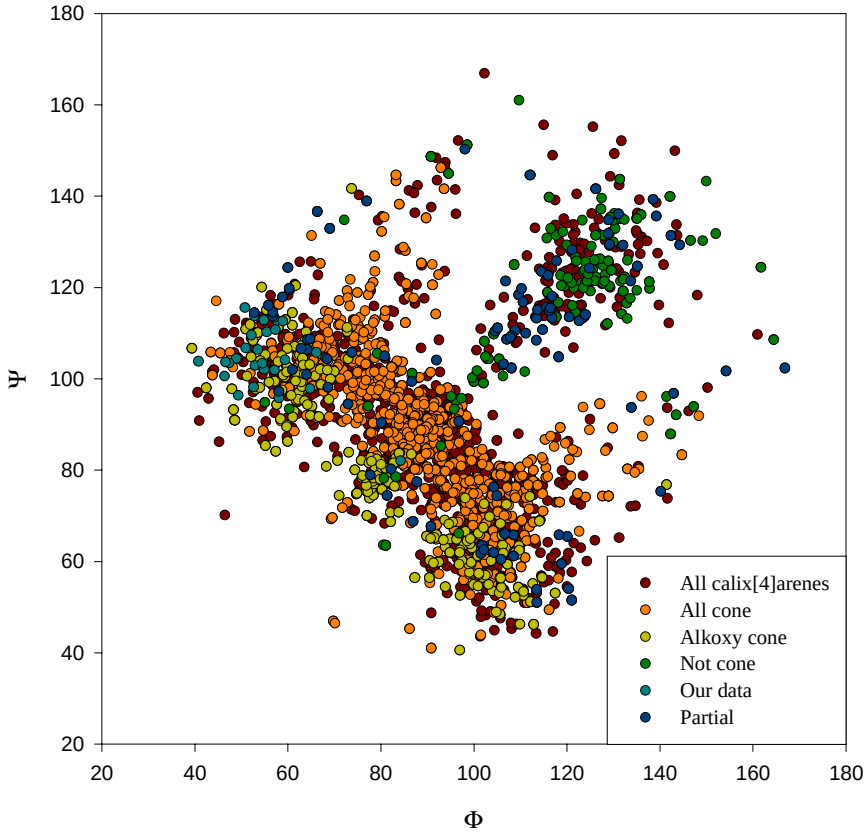

Figure 3.49. A Ramachandran plot of all the calix[4]arenes in the CCD in the background along with identified subsets on top and in a different colouring.

From the analysis it became clear that only a few structures of *distal* and *proximal* conformers existed in the CCD and they were grouped under the *not cone* conformers. It is clear that there is two distinct and separated regions of the plot. One belongs exclusively to the *not cone* and *partial cone* conformers and the other belongs mainly to the *cone* conformers but mix with the *partial cone* and some of the *not cone* conformers. Most importantly is that the *alkoxy cone* conformers generally are displaced towards the lower values in both Ψ and Φ. This fact

is ascribed to the steric demand of the alkoxy groups. Generally the very pinched *cone* conformers were found towards the lowest Ψ and Φ values. Still of course in the C_{2v} regions of the plot which implies that $60^o > \Psi \geq 40^o$ and $120^o > \Phi \geq 90^o$ or *vice versa*.

3.3.3.5 Impact on our conception of the structural chemistry of calix[4]arenes

All the results can the be shown in a generalised form where the different regions are identified.

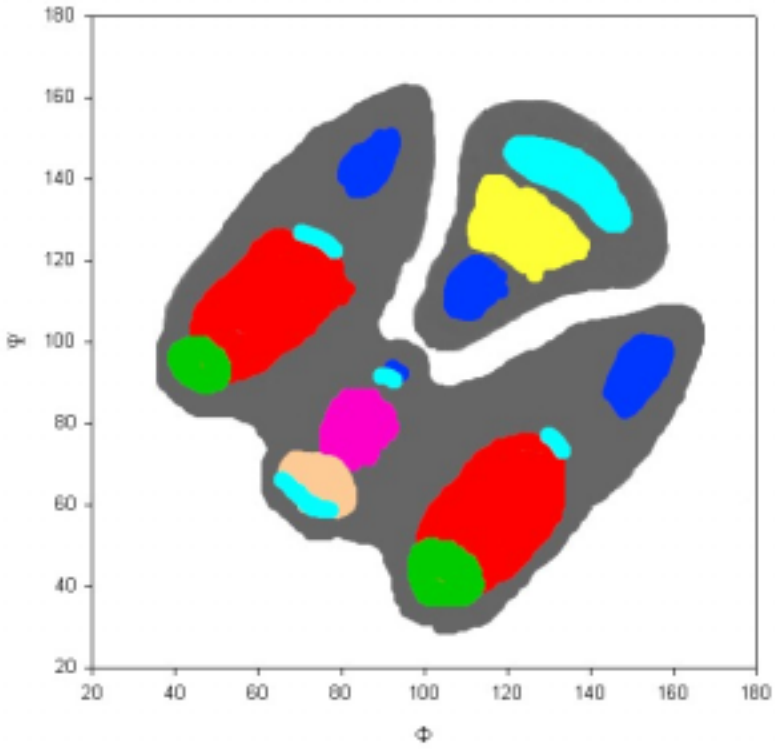

Figure 3.50. A schematic Ramachandran plot for calix[4]arenes. The grey region is the entire range of Φ and Ψ values where calix[4]arenes can be expected to fall. The red and pink coloured regions are C_{2v} and C_{4v} *cone* conformers respectively. Green and peach coloured regions are C_{2v} and C_{4v} *alkoxy cone* conformers respectively. The blue coloured regions are the *partial cone* conformers. Light blue coloured regions are the *proximal* conformers and finally the yellow coloured region is the *distal* conformers.

By surveying some of the outliers it was found that they were most often cases of a conformation in-between two conformers. Particularly observed for the *partial cone* conformer and the few proximal conformers that exist. While this plot is perhaps self evident it does show very nicely the conformational space available to the calix[4]arenes and it is probably correlated with the conformational energies for calix[4]arenes. Attempts were made

to calculate the conformational energy space and place it on top of the Ramachandran plot. While not in disagreement with the results presented here there were some problems in actually calculating the energies in some areas making the results difficult to present. This concludes the conformational analysis of calix[4]arenes. The results presented here are while interesting not complete but by the time this report reaches a broad readership the concepts presented in this last part will have been submitted to and internationally recognised journal.

Chapter four

In this final chapter three small studies of a crystallographic character are presented. This crystallographic trilogy consists of one study of a theoretical nature, one study of an applied nature and finally one study of a technical nature. As with all the previous chapters I have not been alone and must acknowledge the involvement of some people. Most significantly Mikkel Jørgensen and Mogens Larsen but also Kristoffer Almdal, Walther Batsberg, Bente Lebech and Lotte Nielsen.

4.1 Analysis of R-factors using the CCD

The *R*-factor is probably the crystallographic parameter which is best known to everyone, crystallographers and the scientific community as a whole. And since a vast number of structures have been solved and their data deposited in a database, the Cambridge Crystallographic Data Centre database (CCD for short), a simple database project using these data was possible.

4.1.1 Why study *R*-factors

The incentive to undertake this study came mainly from my involvement with the large molecule structures as seen for the calixarenes in *Chapter 3* and the problems often encountered in conforming with the standard set by *Acta Crystallographica* for what an acceptable *R*-factor is.

4.1.1.1 X-ray crystallography in brief

Since a considerable portion of this Ph.D. project is based on structural data obtained by crystallographic means it would be appropriate to briefly regurgitate the experimental procedure and the theoretical background for X-ray crystallography (which in principle applies to neutron and electron crystallography as well). This will not be a *de novo* treatment of crystallography and familiarity with reciprocal space and Sir William Lawrence Bragg's rule is assumed. In simple principle the scattering of an incoming X-ray wave front by the lattice planes or reciprocal lattice points gives rise to a diffracted beam the intensity of which

can be recorded. The physical basis for the scattering of X-rays by a crystal is the periodic distribution of the molecules and their constituent electrons which are the species that scatter the X-rays by a resonant phenomenon. While the intensity can be measured in the experiment the phase of the diffracted wave however is normally said to be lost which is partially untrue. It should read, we can as yet not measure the phase and have to arrive at it by other means. The structure factor which is proportional to the measured intensity of the diffracted wave (i.e. $|F_h| \propto I_h$, I_h being the measured intensity) is given by.

$$F_h = \sum_j f_j \exp(2\pi i(h \cdot r)) \tag{4.1}$$

Where F is the structure factor, the subscript h is the reciprocal space vector, r is the direct space vector and f_j is the atomic scattering factor of the jth atom in the unit cell. If instead of looking at the structure factor as a sum of the scattering from each of the atoms in the unit cell it is looked upon as arising from scattering by an electron density $\rho(x,y,z) = \rho(r)$ at the direct space location x,y,z or given by the direct space vector r. Then the structure factor can more rationally be looked upon as the integral of the electron density over the volume of the unit cell.

$$F_h = \int_v \rho(r) \exp(2\pi i(h \cdot r)) dv \tag{4.2}$$

Now the F's we can measure (or partially at least) but it is the $\rho(r)$ that we would like to determine because if we know where the electrons are then we know where the atoms are and therefore we know the structure. The F's and the ρ's bear a reciprocal relationship one is in reciprocal space the other is in direct space. We can convert from one to the other by the use of a Fourier transform and thus from the F's determine the ρ's. While the equation is given as an integral the F's and the ρ's are discrete quantities and in reality the integral sign is replaced by a summation.

$$\rho(r) = \frac{1}{V} \sum_h F_h \exp(-2\pi i(h \cdot r)) \tag{4.3}$$

Having done these calculations the structure is known. The snatch is the missing phase of the structure factors which has to be arrived at by other means, it has to be solved or the structure has to be solved as it is said. Structure solution thus consists of finding the phase angles for the measured magnitudes of the structure factors. Several methods are commonly employed and direct methods have been the method I have used for all the structure solutions which

have been carried out during this project. It should perhaps be added that the methods available today for crystal structure determination are quite well evolved and mostly it is routine work that does not require any skill or intellectual involvement. We now turn to the quality of the experimental measurements, the ways of quantifying it and expectations that one can have for a given compound or class of compounds.

4.1.1.2 The model

There is a myriad of crystallographic assessment factors that considered individually can give a hint as to flaws or errors in a newly acquired crystallographic data set some that are given based on the data alone. Once satisfied with the quality of the data and having solved the structure additional assessment factors exist that expresses the agreement between the data and the crystallographic model that we believe to be representative of the nature of the molecules in the crystal. The point to make here is that we experimentally measure a series of structure factors (*F*'s) and solve the structure to find the phases of the structure factors. We then have an electron density distribution in the unit cell given by *Equation 4.3* and based on this we propose a model. The model is a collection of atoms in the unit cell placed of course at the right positions in the unit cell. Two different sets of structure factors can then be obtained. The experimentally determined (often termed observed structure factors or F_o) and some calculated (often termed calculated structure factors or F_c) based on the model we have and simply worked out using *Equation 4.1* or *Equation 4.2*. If each observed and corresponding calculated structure factor match well we can say the we have a good model for the electron density distribution arrived at from the experimentally determined structure factors.

4.1.1.3 The R-factor

The way to assess how well the experiment and the model fit is by use the *R*-factor or classically at least. Several other weighted *R*-factors exist and refinements today are actually not made against the *R*-factor but most often against a weighted *R*-factor based on the square of the structure factor which eliminates problems encountered with negative structure factors etc. The refinement procedure is thus a way of accounting for all the electron density in the unit cell and the way of minimising the residual electron density is by minimising the difference between the observed and calculated structure factors. For historical reasons the

classical *R*-factor is always quoted and still used by crystallographers, scientists and by referees to evaluate the quality of a given structural model refined against some experimentally obtained crystallographic data. The classical *R*-factor is given by.

$$R = \frac{\sum \left\| F_{observed} \right| - \left| F_{calculated} \right\|}{\sum \left| F_{observed} \right|} \tag{4.4}$$

It is evident that the better the agreement between model and experiment the smaller the *R*-factor. Classically a value of the *R*-factor which indicates a good model description is of the order of 0.05 or 5% (Editors of *Acta Crystallographica* have a right to reject crystal structure determinations with *R*-factors larger than 0.07 regardless of the size of the structure!). Often this (these) criterion (criteria) has been used as a threshold for ruling a structure determination good or bad and I am convinced that many interesting crystallographic results have not been published because of this by no means complete assessment factor.

4.1.2 R-factors as found in the CCD

Of the order of two hundred thousand structures of molecular organic materials have been included in the CCD. This vast number allows one to make good statistical analysis of some crystallographically determined parameter that is of particular interest. Typical studies are bond lengths, bond angles, torsion angles, co-ordination geometry etc.

4.1.2.1 The CCD data file

The advantage of the CCD is that a search criterion can be entered and the database searched against these criteria. The retrieved sub-set can then be analysed in a particular way and graphic and statistical tools exist within the CCD software package. Also it is possible to decide which parameters to retrieve from each successful hit that matches the search criteria. The parameters are then put in a file which can be accessed at a later stage using in most instances *Vista*.

4.1.2.2 The retrieval

While many search possibilities are available and many parameters can be selected and retrieved in a clever way it was not possible for me to retrieve the *R*-factor and some other parameter. As it turned out I had to retrieve the full information on the entire database without

any criteria for selection, simply the lot. Then I wrote some programs (in C) for the retrieval of the parameters that were to be analysed. In this way full data for every single structure determination ever carried out was retrieved. It was found to be the best solution as further selection or filtering could be done on the entire set at a later stage. The data was in a single file about 300 MB in size which is nothing to be scared of by today's standards. The filtering done thereafter was a selection of only the deposited data sets which had been obtained in year 1972 or later, using a proper diffractometer with proper intensity measurements (i.e. no data sets where the intensity of individual spots had been read by eye) and finally only error free data. This reduced the amount of structures to a little more than hundred and fifty thousand. The error flag needs mention. In each entry in the data file there is an error flag which can be set. It basically means that if an error have been found or reported for a particular data set at a later stage than deposition the flag is set. If a data entry has the error flag set it can not be considered reliable and therefore the data sets retained after filtering was the closest one could get to a collection of reliable structural data sets. This is of course not to say that none of the retained data sets contained an error but to the best of my ability error free data and reliable data were retained as a whole. These were then used for the analysis.

4.1.3 Larger molecules and their R-factors

A large number of reliable structure determinations had now been obtained and now needed analysis. Many different studies could have been done with this information limited only by imagination. Here only one subject was to be addressed.

4.1.3.1 The reason for the study

When solving the structures of small organic molecules the criterion of a particular *R*-factor threshold is perhaps justified but while the size of crystal structures by no means is a fixed quantity why should the *R*-factor threshold be of fixed value ? The new instrumentation which has become available (i.e. area detection) allows for the collection of a lot of data in short time and thus makes accessible a new area of structural chemistry. While the experimental techniques available to small molecule crystallographers limited the range of structural sizes that could be encompassed by experiment earlier this perhaps justified the somewhat rigid *R*-factor threshold. The larger dynamic range with the new instrumentation means that a much larger range of structural sizes can be encompassed by the experiment henceforth the *R*-factor

concept should also be made to accommodate this. To put things in perspective protein crystallographers are used to dealing with a large range of *R*-factors as being acceptable depending on the size of the structure. One can only question as to why small molecule crystallographers have not foreseen this. With the new Siemens SMART diffractometer at DTU it became possible for me to solve a series of difficult structures of the large floppy often solvent containing calixarene molecules as seen in *Chapter 3*. It was irritating that the structure could be solved and was well behaved but that the information could not be used for any serious scientific purpose because of a large *R*-factor. It should be pointed out that as the structural size grows so does the level of detail by which it can be scrutinised decrease. Rather than regarding this as a limitation it should be looked upon as a level of detail at which we are allowed to interpret and make use of the information obtained. Not to peoples surprise (people in this context are the referees that have rejected my contribution again and again for seemingly personal reasons) the *R*-factor increases with the structural size. If this is common knowledge why have no one made this study a long time ago and why are the large molecule structures still looked upon with the stringency normally imposed on small molecule structures. These questions are difficult to answer but at least the *R*-factor in terms of structural size or complexity can be examined.

4.1.3.2 The initial attempts

My belief was that the *R*-factor would increase in magnitude with increasing structural size or complexity (self evident perhaps). The way to show this is a different matter. The first attempt was to correlate the unit cell volume with the *R*-factor. The reason for this was that as the unit cell gets larger reciprocal space becomes more compressed and the intensity measurement and thereby the structure factors become less accurately determined. A clear picture was not obtained and it turned out that the number of independent atoms was a much better measure of the complexity of the structure. So for each number of independent atoms an average *R*-factor could be worked out. Attempts were made to include the compositional diversity of the structures i.e. a heavy atom containing structure for a given number of independent atoms would tend to give better data and a better *R*-factor than a corresponding light atom structure. It was however found to be most representative and general to take the entire lot. Particular sub-sets could be analysed at a later stage in an attempt to illuminate just one aspect. In the case of the heavy atom sub set it was found to depend on the definition of heavy as opposed

to light and a large dispersion of the average *R*-factor with an increasing number of heavy atoms and their atomic number. It was concluded that a clear picture was not easily presented.

4.1.3.3 What should be shown

Having found the right approach it was a question of how to plot the data to properly emphasise the points that were to be made. The most important part was to show how the *R*-factor increased with increasing structural complexity. However of interest would also be to evaluate the number of structures that would fall in a given range of *R*-factor and the number of structures that would fall in a given range of structural complexity. Finally a sub-set containing only the structures that had their disorder flag set (i.e. analogous to the error flag the disorder flag is set if a structure has one or more atoms subject to disorder). Since disordered structures are more difficult to model the *R*-factors for this sub-set was expected to be larger on the average. Also of interest would have been a sub-set containing solvent molecules although this last point was never pursued.

4.1.3.4 The R-factor and correlation with structural complexity

All was now set and the analysis could be done. The raw data was filtered and the programs run that could retrieve the wanted parameters. A complete plot is shown in figure 4.1. It is amazing how well the data correlate and it is not until the size of the structure exceeds four hundred independent atoms that the data points represent single structures. While the amount of data becomes scarce in the region with higher number of independent atoms they have been included for completeness and they seem to follow the trend set by the data below two hundred and fifty independent atoms. Above, the density of structures as found in the CCD for a given number of independent atoms is plotted and it is noteworthy that most reported structures contain less than one hundred independent atoms with a maximum below fifty independent atoms. The reason as to why this is, is partially of an experimental nature since data collection using a classical four circle diffractometer with a point detector increases drastically in time as the size of the structure grows. Therefore the one hundred independent atoms as a maximum is probably the reason. The structures that exist at higher numbers of independent atoms have either been very important or solved recently with more efficient instruments. It is also interesting to speculate as to the number of structures found in a given range of *R*-factors. Most structures are found below *R*-factors of 0.07 and the maximum is

around 0.04. It is clear that the higher the number of independent atoms the higher the *R*-factor on average. It is also interesting to speculate on whether a bias has been introduced by the *R*-factor criterion.

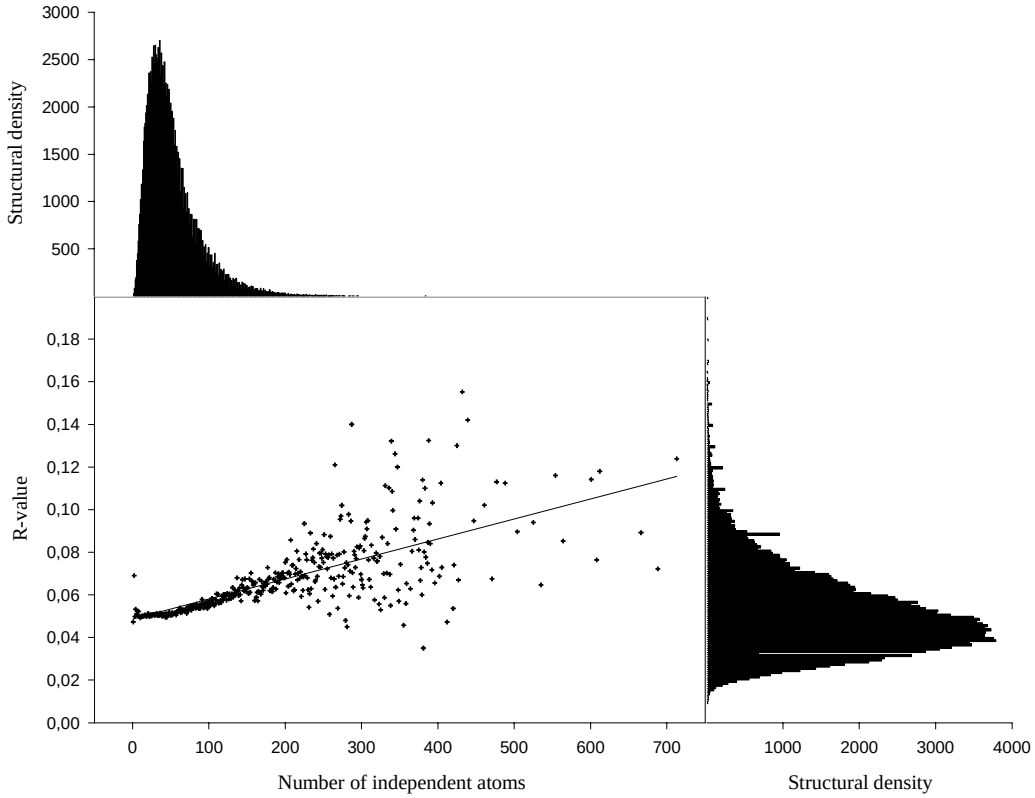

Figure 4.1. A plot of the average *R*-factor for all structures with the same number of independent atoms as a function of the number of independent atoms. Below 250 independent atoms the data points represent good averages, between 250 and 300 independent atoms the data points represent averages that are based on 5 – 10 structures and above 400 independent atoms the data points do not represent averages but correspond to single structures. All data points are however included for completeness. The line represents a linear fit to all data.

Interestingly the sub-set of disordered structures gave rise to a plot with the exact same properties as above but with the mean *R*-factor values displaced by about 0.005 towards higher values. My hope for this plot was that it would become or at least confirm the notion of how the *R*-factor is related to the structural complexity or size. For instance when having a structure like the superstructure of the helicene presented in *Chapter 1* and in *Appendix P4* the *R*-factor we obtained was 0.1 thus very high if looked upon with the stringency of the 0.05 or

0.07 criterion. But if considered in terms of the above plot it is not such a gravely unexpected *R*-factor i.e. it has 288 independent atoms and disorder. The typical and average *R*-factor for such a structure should lie around 0.085 as indicated by the plot making the obtained value of 0.1 more reasonable. It is not my intent with this plot to degrade the high standards set by crystallographers by using the average to judge the individual, however, it is my hope that the above plot could be used to see whether a reported *R*-factor is reasonable considering some other parameters and not just following some dogma like an archaic *R*-factor threshold. Furthermore I would like to express my disappointment with respect to the referees that I have had to examine this paper whilst submitting it to various journals. My opinion is (while biased) that it is an important scientific report which should reach a broad readership. The reasons for rejecting my contribution so far has been seemingly personal reservations and small minds. It is my sincere hope if I ever become respected within science that I will accept the thoughts of newcomers to a field and accept their contributions if scientifically sound and not because I personally do not like what I see. This work has been submitted several times and the current version of the manuscript which circulates the editorial offices around the world has been included in *Appendix P15* (should it come to never be accepted I hope it will haunt the minds of the people responsible for rejecting it).

4.2 Disappearing atropisomers

Some organic molecules with various degrees of intermolecular rotational freedom exhibit a kind of isomerism called atropisomerism. Atropisomeric molecules are molecules that can exist in two or more forms which can be interconverted (often through rotation). The rotational barrier is however so high that individual isomers can be isolated or distinguished. Atropisomers may have very different physical properties but of interest in this context was the influence on the outcome of a photochemical reaction as different atropisomers may give rise to different reaction products.

4.2.1 Taut polycyclic aromatic molecules

Interesting molecular conformations of polycyclic molecules arise when a preferred planar conformation can not be attained for steric reasons.

4.2.1.1 Examples of taut molecules

As we saw in *Chapter 1* the helicenes were good examples of molecules that could not adopt a planar conformation. The consequence was of course the non-planar alternative conformation. Several other examples of large polyaromatic molecules with a taut conformation are known and it would be appropriate to mention a few examples that are relevant as an illustration for this particular study on saddle shaped molecules.

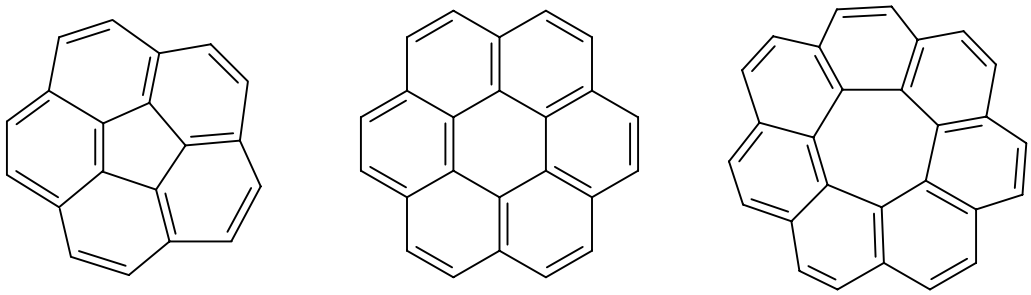

Figure 4.2. Three different polycyclic molecules all belonging to the circulene family. Only the middle one is planar (coronene). To the left corannulene which is bowl shaped and to the right [7]circulene which is saddle shaped.

The distinction to make here is that the helicenes become taut due to the steric demands of different parts of the same molecule that would ideally like to occupy the same region of space. In figure 4.2 it is the entire molecule which becomes taut and simply can not be arranged in a planar manner i.e. the atoms can be arranged in a two dimensional space but it is not a flat space.

4.2.2 Atropisomerism of precursors

Photochemical reactions where the reactants exhibit atropisomerism are interesting in that depending on the reactivity and the stability of the individual atropisomer different possible products may form some perhaps in excess and some not at all.

4.2.2.1 An example

The system of interest in this study were the 1,2-bis-naphthylbenzenes where the naphthyl substituent can exhibit hindered rotation around the benzene-naphthyl bond due to the adjacent naphthyl substituent. For the 1-naphthyl substituent only one possibility exist as we shall see in the following sub-section but the 2-naphthyl substituent can give rise to three

different products. The barrier for rotation around the benzene-naphthyl bond is however much lower for the 2-naphthyl derivative than for the 1-naphthyl derivative and it is questionable whether the different atropisomers can be isolated i.e. the compound does not exhibit real atropisomerism at room temperature. Interestingly their conformations range from planar to slightly taut to considerably taut. It would be of interest to understand these reaction mechanisms and if one product was favoured the reasons for it.

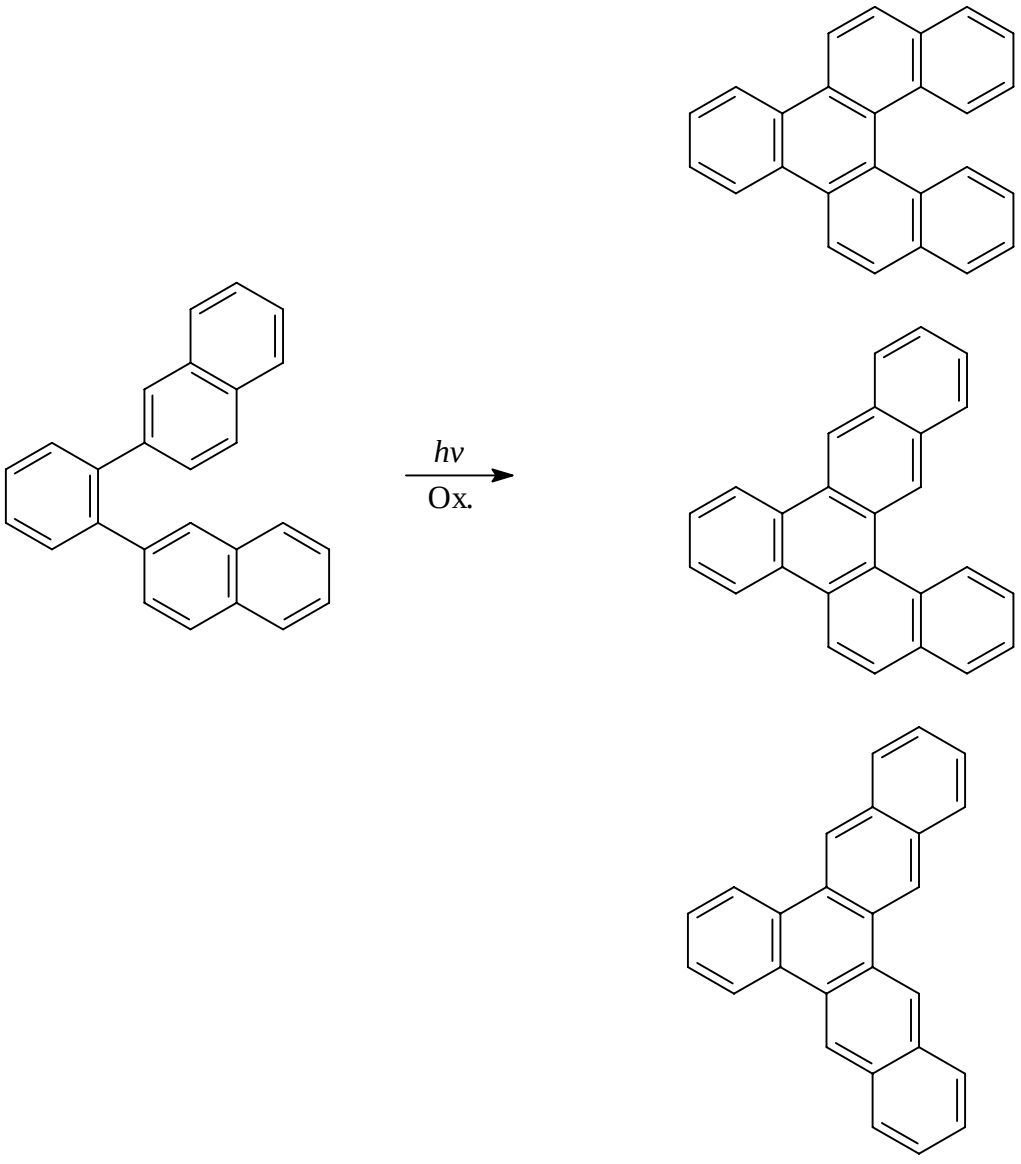

Figure 4.3. An illustration of the three possible products from an atropisomeric precursor molecule. The product at the top is a [5]helicene and will deviate significantly from planarity the middle product is a [4]helicene and will deviate slightly from planarity whereas the lower product will be planar.

4.2.2.2 The 1-naphthyl atropisomer

While the 1,2-bis-2-naphthylbenzene derivatives could in principle give rise to several products the 1,2-bis-1-naphthylbenzene products would if at all reacting give rise to only one product. The questions that were of interest to answer was whether both atropisomers could be crystallised since they were both found to exist in solution and the barrier of rotation was found to be significant. Also the planarity of the photochemical product had to be examined as propositions had been made as to the planarity of the product and suggestions had been made that the product itself might exhibit atropisomerism.

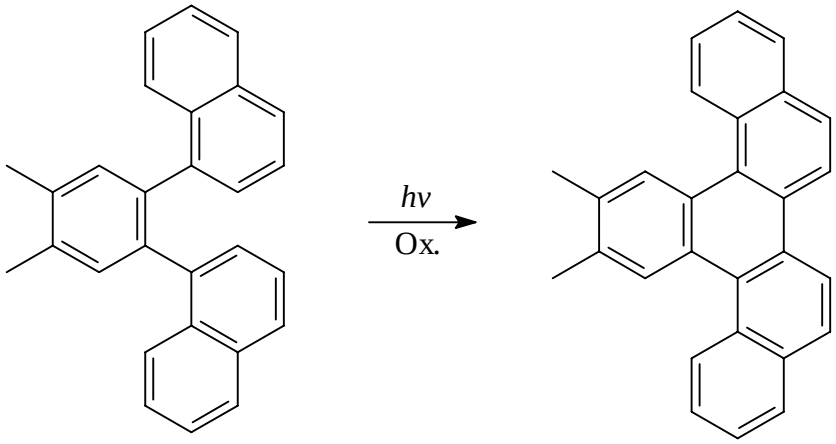

Figure 4.4. The molecules examined in this study. The atropisomeric precursor and the product which is a benzo[s]picene system.

In this case the atropisomerism of the precursor is not so important as the reaction can only proceed to give one product. This product however is a double [4]helicene and could in principle exhibit atropisomerism i.e. fix the dimethylbenzene group in the plane of the paper, the two benzene rings at each end of the picene system can either both be above or below the plane of the paper or one can be above and the other below. It is however appropriate to point out that the [4]helicenes normally are not very taut.

4.2.3 The saddle shape of double bay region containing molecules

We now turn to the results obtained on the compounds studied in this work namely 1,1'-bis(4,5-dimethyl-1,2-phenylene)naphthalene and 14,15-dimethylbenzo[*s*]picene.

4.2.3.1 The precursor

From NMR experiments it was found that both the *cis* and the *trans* atropisomer existed in solution. What about the solid state would it be possible to crystallise the molecules in an atropisomeric state ? There are three different atropisomers *meso*(*cis*), *R*(*trans*) and *S*(*trans*). Crystals were grown and it was found that only the *R*(*trans*) and *S*(*trans*) crystallised in a centrosymmetric space group.

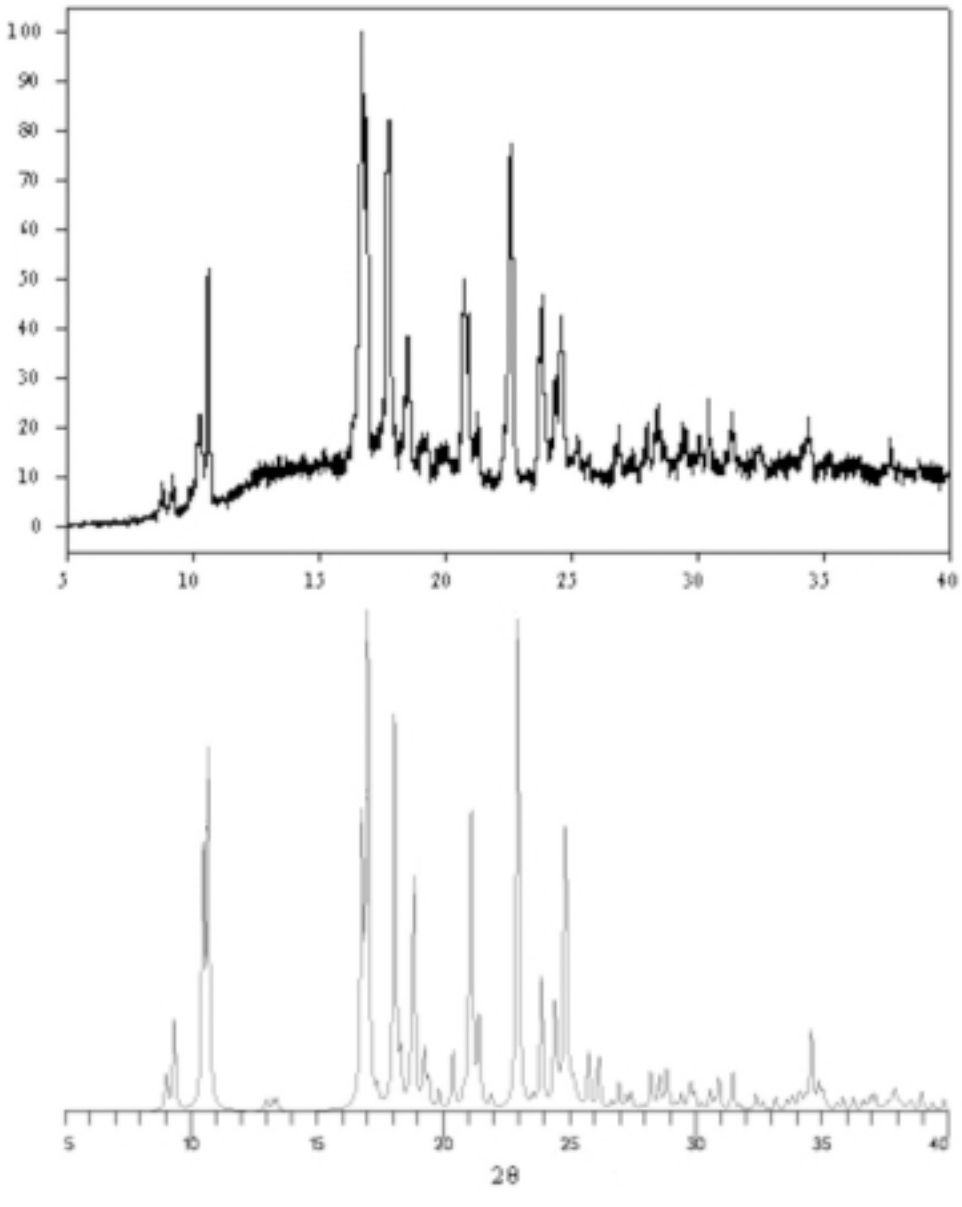

Figure 4.5. Observed powder diffractogram for a fully crystallised sample (above) and a calculated powder diffractogram for the *trans* compound (below, based on the single crystal data).

Our put differently the crystal that I chose was one containing only one atropisomer. If the different atropisomers have the same energy they should exist in a ratio of 1:1:1 and since the *trans* forms can not be distinguished by NMR a ratio of 1:2 should be observed an assignment made by Mikkel Jørgensen showed that the ratio was closer to 0.8:1 with the smaller component being the *cis* form. If a solution known to contain both *cis* and both *trans* forms were left to crystallise did the *cis* form at all crystallise and if it did could we find a *cis* crystal and determine the structure of the *cis* form. A powder diffractogram was recorded on such a fully crystallised sample and it was found that there is no significant amount of the *cis* form. Based on the powder diffractogram the *cis* form does not really form crystals as the powder diffractogram based on single crystal data for which a good model of the *trans* form exist accounts well for the observed powder diffractogram for the fully crystallised sample. The conclusion is thus that the *cis* form exists in solution but does not crystallise to any significant extent but converts through rotation of a naphthyl substituent to the *trans* form which then in turn crystallises.

4.2.3.2 The product

Molecules like the product, 14,15-dimethylbenzo[*s*]picene, obtained by the photochemical reaction of 1,1'-bis(4,5-dimethyl-1,2-phenylene)naphthalene has been subject to studies on carcinogeneity as they contain bay or fjord regions which are believed to be responsible for the carcinogenic nature of many of these polyaromatic compounds. 14,15-Dimethyl-benzo[s]picene is interesting in this context because it contains three bay regions.

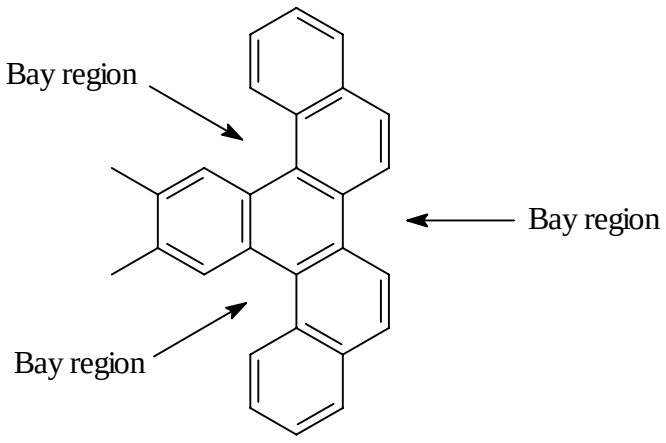

Figure 4.6. A drawing of 14,15-dimethylbenzo[s]picene with arrows indicating the bay regions.

While many of these polyaromatic molecules are known as well as their structures which have been determined the benzo[s]picene structure seems to have escaped peoples attention. The only similar compound for which the structure has been solved is β-tribenzopyrene.

4.2.3.3 The structures

While β-tribenzopyrene is also a non planar molecule it is a bit more constrained than benzo[s]picene system due to the extra benzene ring. The proposition that these molecules should be able to exhibit atropisomerism is unlikely to be true as the molecule would become exceptionally strained. The β-tribenzopyrene has a mirror plane passing through the molecule and is a little less strained than 14,15-dimethylbenzo[s]picene.

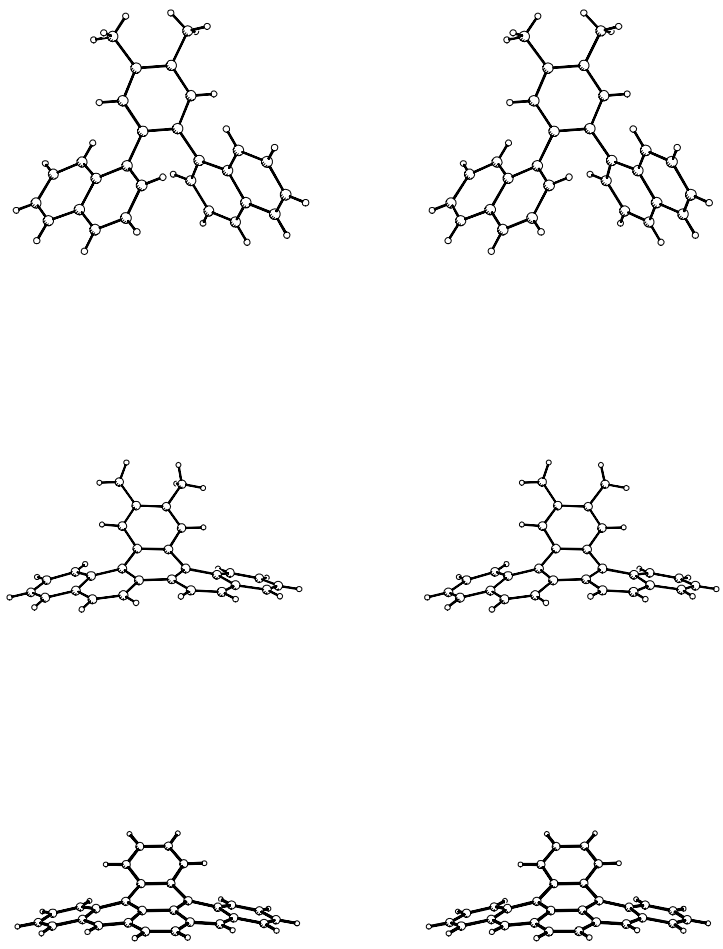

Figure 4.7. Stereoviews of the molecular conformation as obtained from the crystal structures for the three compounds. 1,1'-bis(4,5-dimethyl-1,2-phenylene)naphthalene (above), 14,15-dimethylbenzo[s]picene (middle) and β-tribenzopyrene (below, data taken from the CCD).

It is thus concluded that only the *trans* atropisomer of 1,1'-bis(4,5-dimethyl-1,2-phenylene)naphthalene crystallises while both the *cis* and the *trans* form co-exist in solution. Further the photochemical product 14,15-dimethylbenzo[s]picene is a non-planar taut polyaromatic compound with a saddle shape that does not exhibit atropisomerism. The results from this work have been published and can be found in *Appendix P16*.

4.3 A cryoprotectant for neutron studies

This last part of the trilogy is of a technical character and addresses the problem of making a cryoprotectant for neutron studies on solvent containing molecular organic crystals but also for neutron studies in general.

4.3.1 Use of cryoprotectants

Many of the crystal structures presented in *Chapter 1, 2* and *3* contained solvent molecules. In the X-ray studies of these a cryoprotectant was used.

4.3.1.1 X-ray cryoprotectants

Sometimes when organic molecules crystallise from a solvent a solvent molecule is included in the crystal. Most often this situation arises for molecules with a floppy nature or for molecules that do not fill space well when packed into a crystal. When crystals of organic molecules contain solvent molecules the solvent molecule may be either loosely bound or tightly bound. When tightly bound it is often a case of a high boiling solvent or some molecular interactions between the solvent molecule and the host molecule i.e. specific hydrogen interactions, charge transfer etc. In these cases the crystals are stable to the atmosphere and can be handled without any particular difficulty. In the case of loosely bound solvent molecules the crystals are often highly unstable outside the mother liquor and since they have to be removed from solution in order to collect data some way of prolonging their life outside the mother liquor has to be accommodated for. Normally data would be collected at low temperature i.e. 120 K so that once the crystal has been placed under the cold stream of the diffractometer it is stable for the duration of the data collection. I have in my time collected data on around fifty crystals that contained solvent. In some cases there probably were no need for a cryoprotectant but in most cases the crystal was stable for thirty seconds in air and five to ten minutes in the cryoprotectant which allowed time enough for selecting the

crystal, measuring its dimensions and mounting it on the goniometer head on the diffractometer. I have in a few cases experienced extreme sensitivity, in one case the selection had to be done in the mother liquor and subsequent mounting on the diffractometer had to be done in less than one minute. The dimensions of the crystal had to be measured after the data collection. The Cryoprotectant was in all instances a simple mineral oil consisting of saturated branched hydrocarbons which does not crystallise upon cooling i.e. it becomes a glass. The idea is then to suspend the crystals in the oil getting rid of the solvent which adheres to the surface of the crystal. Subsequent removal of the crystal from the oil leaves a thin protective layer of oil around the crystal and it can be mounted on a glass fibre on the goniometer with grease and quickly transferred to the cold stream of the diffractometer. The oil does not interfere with the experiment in a detrimental way but of course some diffuse scattering from the oil is observed.

4.3.1.2 Other cryoprotectants

The idea of cryoprotectants have been known for a while particularly within the field of bio-molecule crystallography where the often large solvent molecule content simply destroys the crystal upon cooling as it itself crystallises (solvent content may be as high as 50%). In these cases glycerol, glycols and dimethylsulphoxide have been employed which efficiently mix with the solvent molecules and prevents them from crystallising[100,101,102].

4.3.2 The need for a neutron cryoprotectant

Suppose that a neutron experiment on a solvent containing organic molecule or some other sensitive material which required a cryoprotectant had to be carried out.

4.3.2.1 The incoherent scattering problem

In the case of the mineral oil based cryoprotectant that has been of most relevance to this project there is the problem that it contains a lot of hydrogen and that hydrogen scatters incoherently (i.e. isotropic) and thus gives rise to a very high background. This would mean that a hydrogen based cryoprotectant would interfere and perhaps impair the measurements particularly of weak reflections. The obvious solution to the problem would be to obtain a

[100] Parkin, S.; Hope, H. *J. Appl. Cryst.* **1998**, *31*, 945.
[101] Walker, L.; Moreno, P. O.; Hope, H. *J. Appl. Cryst.* **1998**, *31*, 954.
[102] Kwong, P. D.; Liu, Y. *J. Appl. Cryst.* **1999**, *32*, 102.

mineral oil that contained no hydrogen but deuterium instead that does not scatter incoherently (or at least not to any significant level). Hydrogen containing mineral oils come in all sorts of grades and qualities. While some pure alkanes are available in a fully or partially deuterated form fully or partially deuterated mineral oil analogues can not be purchased at all. An alternative thus had to be found.

4.3.2.2 Desired properties of neutron cryoprotectants

As mentioned already of prime importance is a reduction of the incoherent scattering from the cryoprotectant and this basically involves the synthetic replacement of all hydrogen atoms for deuterium atoms. Of second priority is of course that the cryoprotectant does not crystallise when cooled. It should preferably form a glass and also the glass temperature should be well above the temperature of the experiment. Of third priority is a relatively easy way of achieving the substitution of hydrogen for deuterium i.e. an easy and preferably cheap synthetic route. Finally the viscosity of the synthetic cryoprotectant oil had to be similar to the mineral cryoprotectant oil used for X-rays. While in principle simple some trials would have to be made to get the viscosity right. It would perhaps be an advantage to have a slightly higher viscosity than the X-ray oil.

4.3.3 PEP-d as an easily synthesisable neutron cryoprotectant

Knowing what is required of the cryoprotectant it was just a matter of finding a suitable system. Polyethylenepropylene was a good candidate, it is branched and fully saturated.

4.3.3.1 The synthesis

The good thing about perdeuterated polyetylenepropylene (PEP-d) is that the polymer precursor is the well recognised polyisoprene. So the synthesis would be a question of catalytic deuteration of perdeuterated polyisoprene. Perdeuterated polyisoprene is made from isoprene and a good choice of polymerisation conditions would be anionic polymerisation where a good control of the chain length is achieved simply by adjusting the amount of catalyst or initiator for the polymerisation reaction. Isoprene-d_8 was thus required and while having been reported in the literature the methods available were either based on tedious exchange reactions or reactions where only some of the hydrogen atoms were exchanged for deuterium. An improved method for the preparation of isoprene-d_8 had to be developed. The

reaction avoids the use of any exchange reactions and the only expensive starting material is acetone-d_6 which is commercially available.

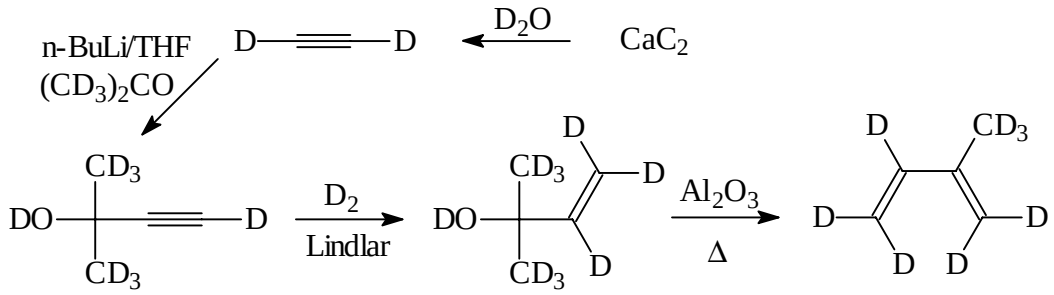

Figure 4.8. The improved synthesis of isoprene-d_8 using CaC_2 as a starting material.

The only other sources of deuterium is deuterium oxide and deuterium gas. One major problem in the earlier routes to isoprene-d_8 was the distillations which involves the separation of azeotropes formed between the product and deuterium oxide. A very important synthetic trick here was found to be the addition of exactly two equivalents of deuterium oxide after the addition of lithiumacetylide-d to acetone-d_6 thereby precipitating $LiOD \times D_2O$ fully and avoiding any azeotrope in the subsequent distillation of the product mebynol-d_8. The deuteration over the Lindlar catalyst was reported to give rise to some fully deuterated product. It was found that a high pressure reaction in this case gave a better product in very short time (less than 10 min.). The final dehydration step was found to be very critical with respect to temperature. But once the entire set-up had been worked out large amounts could be made in short time i.e. 50 grams per run of isoprene-d_8. In this way tangible quantities of the cryoprotectant oil could be made accessible.

4.3.3.2 The polymerisation

There are many different ways of making polymers. In this context only the methods pertaining to the polymerisation of alkenes are of interest. These can be divided into three broad categories (while several other sub-categories exist) according to the mechanism by which polymer chain elongation takes place namely radical, cationic, and anionic polymerisation. Disadvantages for methods involving the first two are various termination reactions that interfere with the control of the polymerisation reaction. The anionic polymerisation reaction has many distinct advantages and are often called living polymers

because the growing end of the polymer is alive i.e. does not terminate provided that impurities are kept out of the reaction.

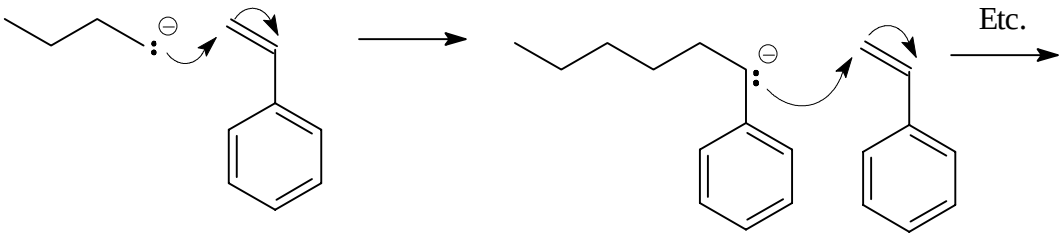

Figure 4.9. An illustration of the initiation of the polymerisation reaction for styrene by the *n*-butyl anion from i.e. *n*-butyllithium.

In mechanistic terms this can be illustrated by the anionic polymerisation of styrene initiated by the *n*-butyl anion i.e. from *n*-butyllithium in cyclohexane or some ether solvent like tetrahydrofurane (THF). It is noteworthy that the anion is stable when the reaction mixture becomes depleted of styrene at which point the reaction can be stopped or some more styrene can be added to continue the reaction or a different monomer can be added to continue the reaction but now giving rise to a polymer chain with two different polymer blocks. This forms the basis for the strength of the anionic polymerisation mechanism. In the case of isoprene the reaction is complicated by the fact that isoprene is a 1,3-diene. For this reason several different chain addition mechanisms exist.

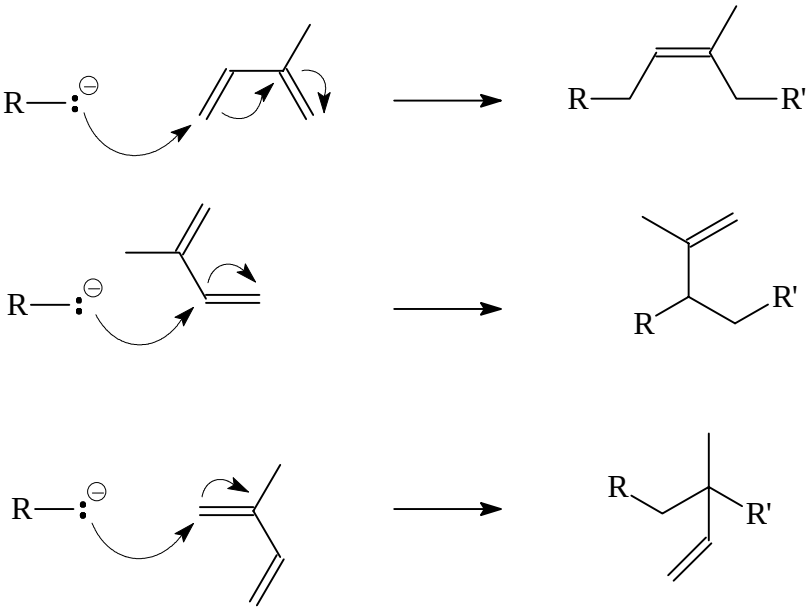

Figure 4.10. An illustration of some of the addition mechanism for isoprene leading to different polymer products (1,4 addition (above), 3,4 addition (middle) and 1,2 addition (below)).

The mode of addition can to a large extent be controlled by the reaction conditions and in our case using *n*-butyllithium in cyclohexane gives rise to mainly *cis*-1,4-addition. It was however of interest for this particular application that the polymer product was as disordered as possible with respect to the mode of addition since any crystalline behaviour was undesirable.

4.3.3.3 The final product

The final deuteration reaction was of course required to make the oil inert to most conditions like atmospheric oxygen and moderate heat. While high pressures and excessive use of catalyst (often 2-3 times the weight of the polymer) is required for hydrogenation/deuteration of unsaturated polymers it proved unnecessary in this case because the chain length of the polymer was relatively short.

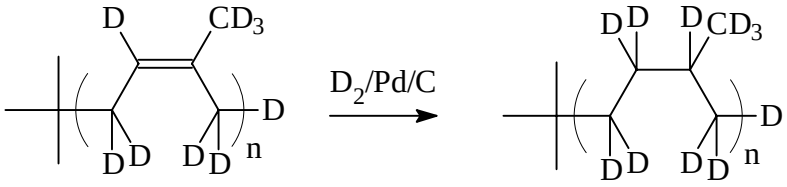

Figure 4.11. The final deuteration reaction using D_2 over Pd/C at low pressure giving a perdeuterated polymer.

Of importance were some of the physical properties of the polymer like the viscosity and glass temperature mentioned in the introduction. The viscosity of the mineral oil used for X-ray studies was measured to be 0.09 Pa s. A trial polymer was made using standard hydrogen containing isoprene to work out the required chain length and exact conditions of reaction. While isotope effects are known to be large for some polymers they were not that critical in this context. Initially a polymer consisting of 20 monomer units was attempted synthesised and thereafter analysed using MALDI-TOF MS and SEC (Matrix Assisted Laser Desorption Ionisation-Time Of Flight Mass Spectrometry and Solvent Exclusion Chromatography respectively). It was found that the chain length was very close to the intended chain length as seen in figure 4.12 and that the dispersity of the polymer was around 1.1. It was not possible to acquire MALDI-TOF data for the saturated polymer due to problems of ionisation. The viscosity of the PEP-h obtained using the trial polymer shown in figure 4.12 was 1.12 Pa s which was more than a factor of ten higher than the X-ray mineral oil.

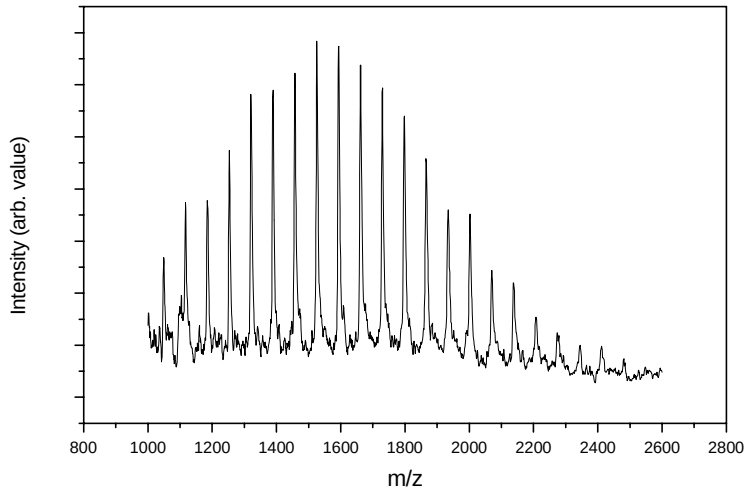

Figure 4.12. A MALDI-TOF mass spectrum of the hydrogen containing polyisoprene made as a test.

The deuterated polymer was thus made in roughly half the molecular weight and the viscosity was determined to be 0.62 Pa s which is desirable for the studies using it as a cryoprotectant.

4.3.3.4 The scattering properties

A final measurement of the neutron scattering properties were carried out as comparison between the PEP-h and PEP-d. The results are shown in figure 4.13.

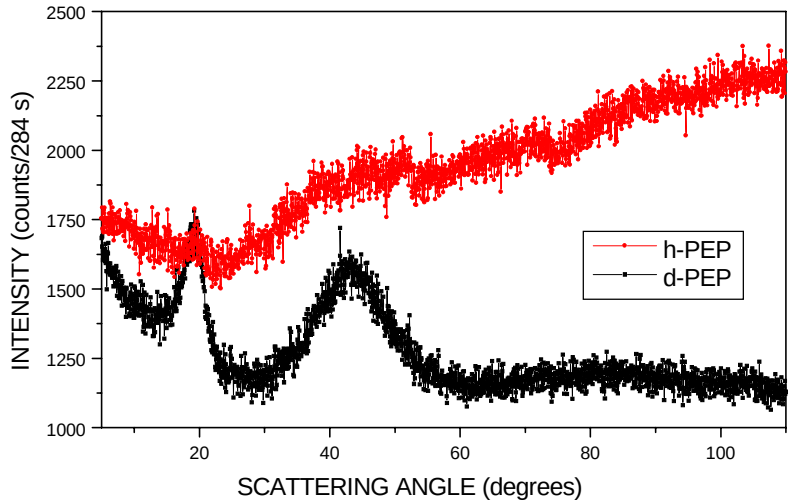

Figure 4.13. The neutron scattering properties of PEP-d as compared to PEP-h. It is noticeable that the background for PEP-d is generally lower than for PEP-h (incident wavelength 1.56 Å).

While the background is generally lower for PEP-d than for PEP-h as intended the difference is largest at higher scattering angles. Furthermore some scattering from the structure of the polymer glass can be seen for PEP-d whereas for PEP-h they are barely visible in the noise from the background. The experiment was carried out at 8K on five gram samples of the polymers on the Risø powder diffractometer facility at TAS 3. The results from this work has been published and can be found with further detail in *Appendix P17*.

Appendix E

The scattering instruments used during this work

In this chapter a brief description of the instruments used for the various scattering experiments are shown.

E1 Weissenberg camera

The Weissenberg camera at DTU was used in the beginning of the project for the general apprenticeship of a young crystallographer like myself.

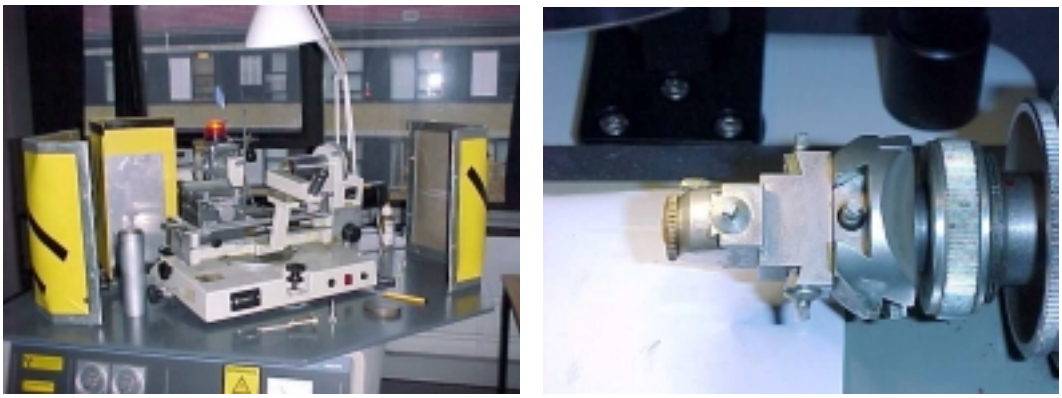

Figure E.1. Photographs of the Weissenber camera (left) and a goniometer under the microscope (right).

It was at later stages very useful in the study of the helicenes found in *Chapter 1* where the superstructure reflections could be seen clearly. In most cases it was found a lot quicker to just collect data as the Weissenberg technique is quite time consuming and useless if one is dealing with solvent containing molecules. So as a general conclusion to the Weissenberg technique it can be said that it is indispensable as a technique and unsurpassed in many ways but only for specific problems and not for routine work.

E2 Powder diffractometer

The powder diffractometer at DTU was used in a few cases most notably for the helicenes in *Chapter 1*, for the triphenylenes in *Chapter 2* and for the disappearing atropisomers in *Chapter 4*.

Figure E.2. The powder diffractometer at DTU used in a few instances for characterisational/analytical purposes.

E3 SMART diffractometer

The SMART diffractometer at DTU proved to be the workhorse of all the crystallographic experiments carried out during this project.

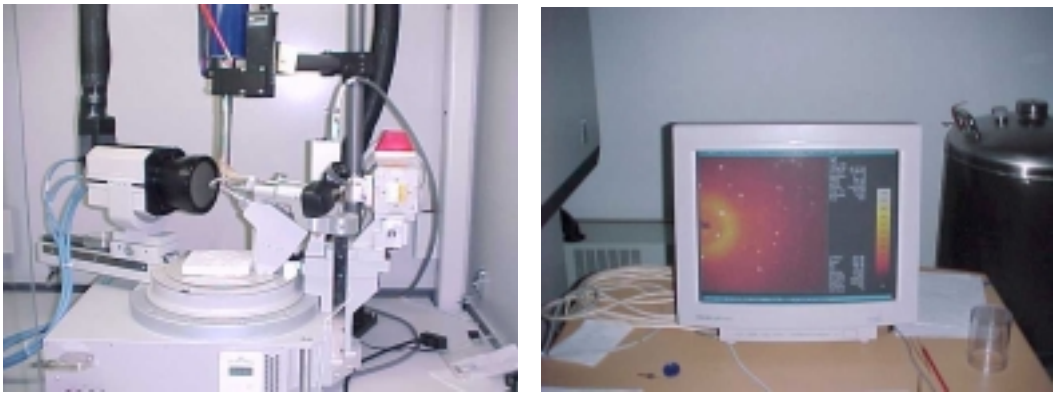

Figure E.3. The SMART diffractometer platform (left) with the cryogenic stream comming down from above. The detector is also seen and at the screen (right) an image of the diffracted intensity from the crystal can be seen.

E4 Synchrotron beam line D3 at HASYLAB

We (myself, André Faldt, Niels Thorup and Klaus Bechgaard) had the opportunity to visit HASYLAB and collect data on 7,8-dioxa[6]helicene to further investigate the superstructure *Chapter 2* and also for one of the calixarenes *Chapter 3*. I wrote the proposal for beamtime and made most of the arrangements for the trip to HASYLAB.

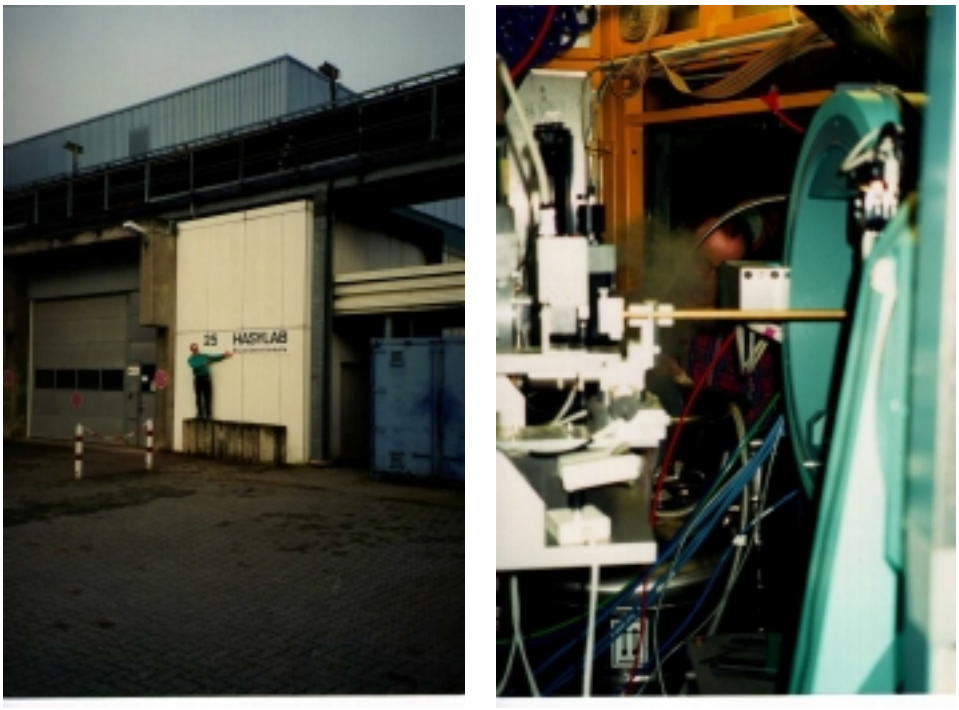

Figure E.4. The synchrotron facility HASYLAB in Hamburg (Germany) with the author presenting the entrance (left). To the right I am can be seen behind the equipment filling the dewar with liquid nitrogen. The horizontal brass tube in the middle is the direct beam and the chi-circle can also be seen to the right.

Figure E.5. A view of the diffractometer in the hut from the outside during an experiment (left). The direct beam, goniometer, cryostream and the edge of the detector (right).

Figure E.6. The author filling the dewar as seen from the outside of the hut (left). A monitor displaying a video image of the crystal on the coniometer (right) a very handy feature.

Figure E.7. A picture showing the SMART CCD detector and the goniometer (left) and the famous professor (right).

Figure E.8. The team being instructed in the use of shutters outside the hut Niels Thorup is just visible from the back Klaus Bechgaard and André Faldt are in profile (left). André Faldt doing some calculations in the computer room.

E5 TAS 3 neutron powder diffraction

The mounting of the sample differs a bit from the mounting normally employed in X-Ray powder diffraction. TAS 3 was used for phosphangulene in *Chapter 2* and for the cryoprotectant in *Chapter 4*.

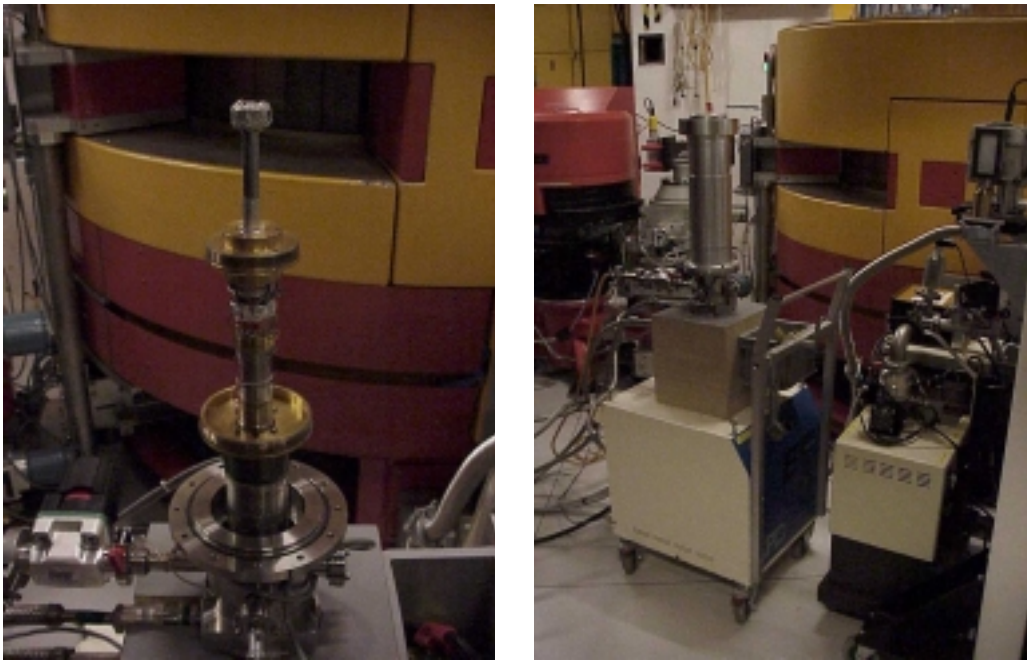

Figure E.9. The sample holder for TAS 3 mounted on the displex (left). The entire displex and sample assembly on the pumping trolley.

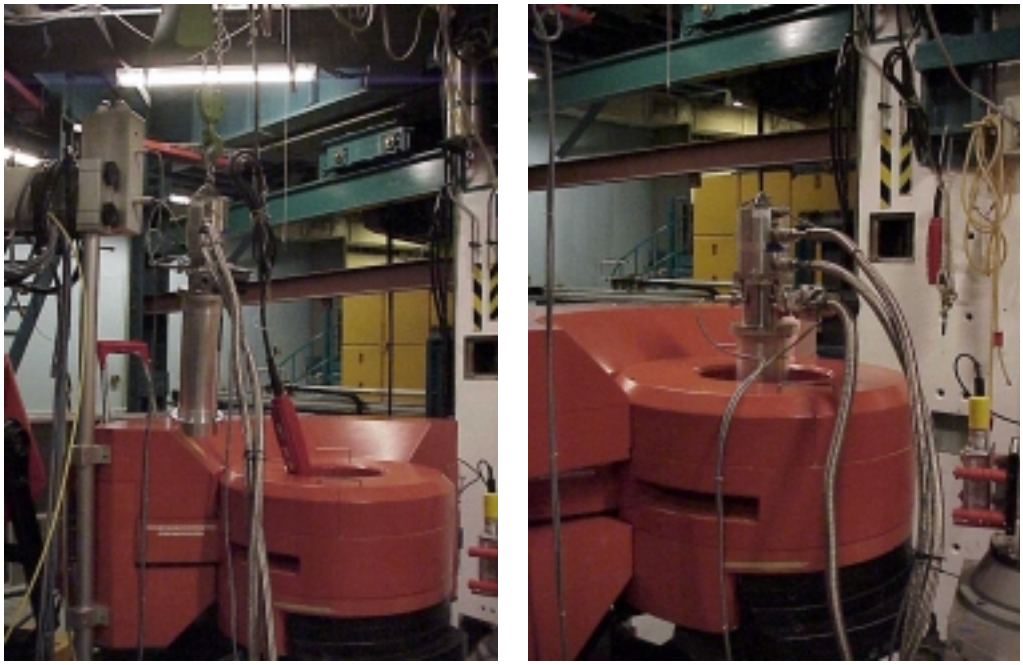

Figure E.10. The displex with the sample is being hoisted into the diffractometer (left) and finally the displex and sample has been mounted on the diffractometer (right).

Figure E.11. The diffractometer with displex and sample etc. has now been brought into position and counting can begin.

Appendix P

The list of the publications pertaining to this work

Chapter one

P1 – J. Chem. Soc. Perkin Trans. II	**1997**, 2219-2227.
P2 – Chem. Eur. J.	(Accepted, 11/10/99)
P3 – J. Org. Chem.	(Submitted, 05/10/99)
P4 – Cryst. Eng. Comm.	**1999**, *6*.
P5 – Acta Cryst. B	**1999**, *B55*, 410-423.
P6 – J. Am. Chem. Soc.	**1998**, *120*, 12255-12263.

Chapter two

P7 – Synthesis	**1997**, 1285-1290.
P8 – Acta Chem. Scand.	**1999**, *53*, 410-416.
P9 – Chem. Mater.	(Submitted, 10/11/99)

Chapter three

P10 – J. Org. Chem.	**1998**, *63*, 4420-4424.
P11 – J. Chem. Soc. Perkin Trans. II	**1999**, 1749-1757.
P12 – Tetrahedon Letters	(Submitted, 27/10/99)
P13 – J. Org. Chem.	**1998**, *63*, 9872-9879.
P14 – J. Chem. Soc. Perkin Trans. II	(Submitted, 23/08/99)

Chapter four

P15 – J. Appl. Cryst.	(Submitted, 15/07/99)
P16 – J. Org. Chem.	(Accepted, 11/10/99)
P17 – Polymer Bulletin	(Accepted, 18/10/99)

P1

Title: "Synthesis, Structure and Properties of Various Molecules Based on the 4,8,12-trioxa-4,8,12,12c-tetrahydrodibenzo[*cd,mn*]pyrene System With an Evaluation of the Effect Differing Molecular Substitution Patterns Has on the Space Group Symmetry"

Authors: André Faldt, Frederik C. Krebs* and Niels Thorup

Journal: *J. Chem. Soc. Perkin Transactions II*, (**1997**), 2219-2227.

P2

Title: "Evaluation of the Solid State Dipole Moment and Pyroelectric Coefficient of Phosphangulene by Multipolar Modeling of X-ray Structure Factors"

Authors: Georg K. H. Madsen*, Frederik C. Krebs, Finn K. Larsen and Bente Lebech

Journal: *Chem. Eur. J.* (Submitted, 04/08/99)

P3

Title: "Preparation and Properties of 7,8-Dioxa[6]helicenes and 7a,14c-dihydro-7,8-dioxa[6]helicenes"

Authors: Jørgen Eskildsen, Frederik C. Krebs, André Faldt, Peter Sommer-Larsen and Klaus Bechgaard*

Journal: *J. Org. Chem.* (Submitted 05/10/99)

P4

Title: "Arrested Handedness and Disordered Stacking in Crystals of the Prehelical Molecule 7,8-Dioxa[6]helicene"

Authors: Frederik C. Krebs, André Faldt, Niels Thorup and Klaus Bechgaard*

Journal: *Cryst. Eng. Comm.* (Submitted 31/08/99)

P5

Title: "The Geometry and Structural Properties of the 4,8,12-trioxa-4,8,12,12c-tetrahydrodibenzo[*cd,mn*]pyrene System in the Cationic State. Structures of a Planar Organic Cation with Various Monovalent- and Divalent anions."

Authors: Frederik C. Krebs*, Bo W. Laursen, Ib Johansen, André Faldt, Klaus Bechgaard, Claus S. Jacobsen, Niels Thorup and Kamal Boubekeur

Journal: *Acta Cryst.* (**1999**) *B55*, 410-423.

P6

Title: "2,6,10-Tris(dialkylamino)-trioxatriangulenium Ions. Synthesis, Structure, and Properties of Exceptionally Stable Carbenium Ions"

Authors: Bo W. Laursen*, Frederik C. Krebs, Merete F. Nielsen, Klaus Bechgaard, Jørn B. Christensen, and Niels Harrit

Journal: *J. Am. Chem. Soc* (**1998**), *120*, 12255-12263.

P7

Title: "Purification of 2,3,6,7,10,11-hexamethoxytriphenylene and Preparation of hexakiscarbonylmethyl and hexakiscyanomethyl derivatives of 2,3,6,7,10,11-hexahydroxytriphenylene"

Authors: Frederik C. Krebs, Niels C. Schiødt, Walther Batsberg and Klaus Bechgaard*

Journal: *Synthesis*, (**1997**), 1285-1291.

P8

Title: "Crystal Structure of Three Compounds Related to Triphenylene and Tetracyanoquinodimethane"

Authors: Thomas L. Andresen, Frederik C. Krebs, Mogens Larsen and Niels Thorup*

Journal: *Acta. Chem. Scand.* (**1999**), *53*, 410-416.

P9

Title: "Crystal structures of 2,3,6,7,10,11-oxytriphenylenes. Implications for columnar discotic mesophases"

Authors: Thomas L. Andresen, Frederik C. Krebs∗, Niels Thorup and Klaus Bechgaard

Journal: *Chem. Mater.* (Submitted, 10/11/99)

P10

Title: "Synthesis, Structure and Fluorescence Properties of 5,17-Distyryl-25,26,27,28-tetraproproxycalix[4]arenes in the *Cone* Conformation"

Authors: Mogens Larsen*, Frederik C. Krebs, Mikkel Jørgensen and Niels Harrit

Journal: *J. Org. Chem.* (**1998**), *63*, 4420-4424.

P11

Title: "Synthesis and Conformational Studies of a Series of 5,17-bis-aryl-25,26,27,28-tetrapropoxycalix[4]arenes: The Influence of π-π Interactions on the Molecular Structure."

Authors: Mogens Larsen, Frederik C. Krebs, Niels Harrit and Mikkel Jørgensen*

Journal: *J. Chem. Soc. Perkin Transactions II*, (**1999**), 1749-1757.

P12

Title: "Lithium-ion induced conformational change of 5,17-bis(9-fluorenyl)-25,26,27,28-tetrapropoxycalix[4]arene resulting in an egg shaped clathrate"

Authors: André Faldt, Frederik C. Krebs and Mikkel Jørgensen*

Journal: *Tetrahedron Letters* (Submitted, 27/10/99)

P13

Title: "Synthesis and Structural Properties of 5,17-Bis(N-methyl-N-arylaminocarbonyl)calix[4]arenes. Directing the Substituents toward the Cavity by Use of the *cis*-Generating Property of the N-Methylaminocarbonyl Linker"

Authors: Frederik C. Krebs*, Mogens Larsen, Mikkel Jørgensen, Pernille R. Jensen, Mia Bielecki and Kjeld Schaumburg

Journal: *J. Org. Chem.* (**1998**), *63*, 9872-9879.

P14

Title: "A Closer Look on the Conformational Behavior of Calix[4]arene Dicarboxylic Acids and their (Supramolecular) Interactions with Aliphatic Amines e.g. (-)-Ephedrine"

Authors: Frederik C. Krebs and Mikkel Jørgensen*

Journal: *J. Chem. Soc. Perkin Trans. II* (Submitted, 23/08/99)

P15

Title: "How the *R*-Factor Changes as Molecules Become Larger"

Author: Frederik C. Krebs*

Journal: *J. Appl. Cryst.* (Submitted, 15/07/99)

P16

Title: “On the Saddle Shaped Nature of 14,15-Dimethylbenzo[s]picene”

Authors: Frederik C. Krebs*, Mikkel Jørgensen and Mogens Larsen

Journal: *J. Org. Chem.* (Accepted, 08/09/99)

P17

Title: “Synthesis of Small Molar Mass Perdeuterated Polyethylpropylene (d-PEP) as an Auxiliary for Neutron Studies”

Authors: Frederik C. Krebs*, Mikkel Jørgensen, Bente Lebech, Kristoffer Almdal and Walther B. Pedersen

Journal: *Polymer Bulletin* (Submitted, 14/09/99)

Appendix S

Bibliographic Data Sheet Risø-R-1144(EN)

Title and authors

Initium Sapientiæ Timor domini, Ph.D. Thesis by Frederik Christian Krebs

ISBN	ISSN
87-550-2614-1; 87-550-2633-8 (Internet)	**0106-2840**

Department or group	Date
Condensed Matter Physics and Chemistry Department	**01/01/2000**

Groups own reg. number(s)	Project/contract No(s)

Pages	Tables	Illustrations	Refences
481	**1**	**155**	**102**

Abstract(max. 2000 characters)

This Ph.D. Thesis describes the synthesis, structure and properties of a series of organic molecules. The main effort has been placed towards the structural understanding of organic materials and the scattering techniques employed for this purpose has involved conventional X-rays, synchrotron X-rays and neutrons.

The report is divided into four *Chapters*. The first, *Chapter one*, is in three *Parts*. The first *Part* gives a brief but complete introduction to the dielectric properties of organic materials. The second *Part* describes the experimental work on synthesising organic dielectric materials and provides an understanding their structure and properties. The third *Part* describes some work on placing polar organic materials on surfaces under UHV (Ultra High Vacuum) conditions. *Chapter two*, is also in three *Parts* the first being a brief introduction to the subject of molecular liquid crystals with particular emphasis on discotic liquid crystals. The second *Part* describes the structural characterisation pertaining to triphenylene based discotic premesogens and their relation to the structural properties as found in the literature. The final *Part* is a critical discussion of the structure of discotic mesophases as presented in the literature and as implied by the results obtained from this work. *Chapter three* describes the work done on the structural characterisation of a particular type of macromolecule and is in three *Parts*. The first *Part* is a brief introduction to the subject while the second *Part* describes the synthesis and the structural characterisation of the conformational behaviour of these molecules. The third *Part* describes a statistical survey based on the CCD (Cambridge Crystallographic Database). *Chapter four* is the final *Chapter* and is also in three *Parts*. The first *Part* is a statistical survey of *R*-factors as found in the CCD. The second *Part* is a structural study of an atropisomeric organic molecule and the final *Part* describes the synthesis of a perdeuterated polymer for neutron studies.

Descriptors

SYNTHESIS, STRUCTURE, PROPERTIES, X-RAY, NEUTRON, SYNCHROTRON, SURFACES, LIQUID CRYSTALS, CALIXARENE, MACROMOLECULE, POLYMER, ISOTOPE LABELLING, DIPOLE MOMENTS, POLARISATION, DIELECTRIC, PIEZOELECTRIC, PYROELECTRIC, FERROELECTRIC

Available on request from Information Service Department, Risø National Laboratory,
(Afdelingen for Informationsservice, Forskningscenter Risø), P.O. Box 49, DK-4000 Roskilde, Denmark.
Telephone (+45) 4677 4004, Telefax (+45) 4677 4013